Universitat Autònoma de Barcelona

Role of PS/γ-secretase-mediated signaling during neuronal development and degeneration

Míriam Javier Torrent

Institut de Neurociències
Departament de Bioquímica i Biologia Molecular
Unitat de Bioquímica i Biologia Molecular,
Facultat de Medicina
Universitat Autònoma de Barcelona

Role of PS/γ-secretase-mediated signaling during neuronal development and degeneration

Míriam Javier Torrent

TESI DOCTORAL

Bellaterra, 2019

Institut de Neurociències
Departament de Bioquímica i Biologia Molecular
Universitat Autònoma de Barcelona

Role of PS/γ-secretase-mediated signaling during neuronal development and degeneration

Paper de la senyalització mediada per PS/γ-secretasa durant el desenvolupament neuronal i la degeneració

Memòria de tesi doctoral presentada per *Míriam Javier Torrent* per optar al grau de Doctor en Neurociència per la Universitat Autònoma de Barcelona.

Treball realitzat a la Unitat de Bioquímica i Biologia Molecular de la Facultat de Medicina del Departament de Bioquímica i Biologia Molecular i l'Institut de Neurociències de la Universitat Autònoma de Barcelona, sota la direcció del Doctor Carlos Saura Antolín.

El treball realitzat en aquesta tesi doctoral ha estat finançat pels projectes de recerca del Ministerio de Economía y Competitividad *Transcriptional mechanisms underlying memory loss in Alzheimer´s disease transgenic mouse models* (SAF2013- 43900-R) i *Transcriptional mechanisms of synaptic plasticity in memory circuits in a mouse mouse of neurodegeneration (MESYMEC)* (SAF2016-80027-R), pel Centro de Investigación Biomédica en Red de Enfermedades Neurodegenerativas (CIBERNED CB06/05/0042), per BrightFocus Foundation (Grant A2014417S) i la Generalitat de Catalunya (ICREA Academia and 2017 SGR749).

Bellaterra, 7 de Gener de 2019

Doctorand — Director de tesi

Míriam Javier Torrent — Carlos A. Saura Antolín

Als meus pares,
als meus avis
i a en Sergio

“From my rotting body
flowers shall grow
and I am in them
and that is eternity”

Edvard Munch

CONTENTS

ABBREVIATIONS

AD Alzheimer's disease
ADAM A desintegrin and metalloprotease
AICD APP intracellular domain
AMPA α-amino-3-hydroxy-5-methyl-4-isoxazolepropionic acid
APOE Apolipoprotein E
APP Amyloid precursor protein
Aph-1 Anterior pharynx-defective 1
Aß Amyloid ß peptide
BACE ß-site APP cleaving enzyme
BBB Blood-brain barrier
BDNF Brain-derived growth factor
BP Basal progenitors
BSA Bovine Serum Albumin
CA Constitutively active
CAM Cell adhesion molecule
cAMP Cyclic adenosine monophosphate
CFC Contextual fear conditioning
CKII Casein kinase II
cKO Conditional knockout
CNS Central nervous System
CP Cortical plate
CTF C-terminal fragment
DAPT N-[N-(3,5-Difluorophenacetyl)-L-alanyl]-S-phenylglycine t-butyl ester
DCC Deleted in colorectal carcinoma
DIV Days in vitro
DMSO Dimethyl sulfoxide
DNA Deoxyribonucleic acid
ECM Extracellular matrix
EGF Epidermal growth factor
EGFP Enhanced green fluorescent protein
ELC Essential light chain
E4ICD ErbB4 intracellular fragment
FAD Familial Alzheimer's disease
FN Fibronectin repeats
GE Ganglionic eminence
GAP GTPase activating protein
GBM Glioblastoma
GDP Guanosine diphosphate
GEF GTP exchange factor
GFP Green fluorescent protein
GPI Glucose-6-phosphate isomerase
GTP Guanosine triphosphate
HA Hemagglutinin molecule
HC Heavy chain
ICD Intracellular domain
IClip Intramembranous cleaving proteins
IGF Insulin-like growth factor
IPC Intermediate progenitor cell
IZ Intermediate zone
JM Juxtamembrane
LTD Long-term depression
LTP Long-term potentiation
MAP Microtubule associated proteins
MLCK Myosin light chain kinase
MLCP Myosin light chain phosphatase
MMP Matrix metalloprotease
MRCK Myotonic dystrophy-related Cdc42-binding kinase
NMIIA Non-muscle myosin IIA
NCAM Neural cell adhesion molecule
NGF Nerve growth factor
NGS Normal goat serum
NICD Notch intracellular domain
NMDA N-methyl-D-aspartate
Nrg Neuregulin
NTF N-terminal fragment
Pak p21-activated kinase
PAR Partioning-defective protein
PBS Phosphate-buffered saline
PCR Polymerase chain reaction
Pen-2 Presenilin enhancer 2
PI3K Phosphoinositide 3-kinase
PIP3 Phosphatidylinositol (3,4,5)-trisphosphate
PKA Protein kinase A
PKC Protein kinase C
PS Presenilin
PS1$^{-/-}$ PS1-deficient cells
PS1$^{+/+}$ PS1-expressing cells
PDS Postsynaptic density
RGS Radial Glial cells
RLC Regulatory light chain
RNA Ribonucleic acid
ROCK Rho kinase
SAD Sporadic Alzheimer's disease
SAM Sterile alpha motif
sAPP Soluble APP

shRNA Short hairpin RNA
SVZ Subventricular zone
TACE Tumor necrosis factor-α converting enzyme
TBS Tris-buffered saline
TM Transmembrane
TMD TM domain
VZ Ventricular zone
WT Wild type
∆**ICD** Deletion of intracellular domain
∆**LBD** Deletion of ligand binding domain
∆**PDZ** Deletion of PDZ-binding domain

ABSTRACT

Presenilin-1 (PS1), the catalytic component of γ-secretase that regulates the processing of multiple transmembrane proteins is mutated in the majority of cases of familial Alzheimer's disease (FAD). Recent evidence indicates that FAD-linked *PS1* mutations reduce the γ-secretase cleavage of several transmembrane proteins, suggesting a loss-of-function mechanism. Indeed, *PS1* inactivation during embryogenesis leads to morphological defects, whereas genetic inactivation of both *PS* in the adult brain causes age-dependent memory impairments and neurodegeneration. Moreover, the participation of PS in the proteolysis of signaling molecules involved in the development of nervous system, including ErbB4, suggest that these signaling pathways could contribute to neurodegeneration.

In this doctoral thesis we have studied the role of PS1/γ-secretase-dependent cleavage of EphA3 and Nrg1/ErbB4 signaling in neuronal development and neurodegeneration. Our results show that PS1/γ-secretase is required for axon growth in the developing brain. PS1/γ-secretase mediates axon elongation through the cleavage of EphA3 at Tyr560 resulting in the generation of an ICD fragment. EphA3 ICD regulates negatively RhoA, and interacts with and increases phosphorylation (S1943) of non-muscle myosin IIA (NMIIA) leading to filament disassembly and axon growth. In contrast to the classical ephrin/EphA3 signaling, PS/γ-secretase-dependent EphA3 signaling is independent of ligand. This result suggests for the first time opposite roles of EphA3 on inhibiting (ligand-dependent) and enhancing (PS/γ-secretase-dependent processing) axon growth in neurons. Second, we show that PS/γ-secretase regulates *Nrg1 type III* expression, mediates the processing of Nrg1 type III and ErbB4 and regulates negatively synaptogenesis through Nrg1. Taken together, our results show that PS1/γ-secretase regulates axon growth and synaptogenesis by regulating ligand-independent EphA3 signalling and Nrg1/ErbB4 processing/signalling, respectively. Our investigation paves the way for exploring new relationships between neurodevelopment and neurodegeneration, providing insights of the existence of a crosstalk among the signaling pathways involved in these processes.

RESUM

Presenilina-1 (PS1), el component catalític de γ-secretasa que regula el processament de múltiples proteïnes transmembrana, es troba mutada en la majoria de casos d'Alzheimer familiar (FAD). Evidències recents indiquen que mutacions en *PS1* lligades a FAD redueixen el processament de múltiples proteïnes transmembrana, suggerint un mecanisme de pèrdua de funció. De fet, la inactivació de *PS1* durant l'embriogènesi comporta defectes morfològics, mentre que la inactivació genètica d'ambdues *PS* en el cervell adult causa defectes en memòria dependents d'edat i neurodegeneració. A més, la participació de PS en la proteòlisi de molècules de senyalització implicades en el desenvolupament del sistema nerviós, incloent ErbB4, suggereix que aquestes vies de senyalització podrien contribuir a la neurodegeneració.

En aquesta tesi doctoral hem estudiat el paper del processament dependent de PS1/γ-secretasa d'EphA3 i de la senyalització Nrg1/ErbB4 en el desenvolupament neuronal i la neurodegeneració. Els nostres resultats mostren que PS1/γ-secretasa és necessària pel creixement axonal en el cervell en desenvolupament. PS1/γ-secretasa regula l'elongació axonal a través de l'escissió d'EphA3 en la tirosina 560 que resulta en la generació d'un fragment ICD. EphA3 ICD regula negativament RhoA, interacciona amb la miosina IIA no-muscular (NMIIA) i incrementa la seva fosforilació (S1943) produint el desmuntatge del filament i el creixement axonal. De manera contrària a la senyalització clàssica ephrin-EphA3, la senyalització d'EphA3 dependent de PS/γ-secretasa és independent de lligand. Aquest resultat suggereix per primer cop papers oposats d'EphA3 inhibint (dependent de lligand) o promovent (processament dependent de PS1/γ-secretasa) el creixement axonal en neurones. En segon lloc, mostrem que PS1/γ-secretasa regula l'expressió de *Nrg1 tipus III* i el processament de Nrg1 tipus III i ErbB4, i regula negativament la sinaptogènesi a través de Nrg1. En conjunt, els nostres resultats mostren que PS1/γ-secretasa regula el creixement axonal i la sinaptogènesi a través de la regulació de la senyalització d'EphA3 independent de lligand i del processament/senyalització de Nrg1/ErbB4, respectivament. La nostra investigació obre el camí a explorar noves relacions entre el neurodesenvolupament i la neurodegeneració, proporcionant evidències sobre l'existència d'una comunicació entre les vies de senyalització implicades en aquests processos.

INTRODUCTION

1. Neuronal development

Brain development and diseases share some cellular mechanisms regulating, among others, cell death, morphogenesis and regeneration. Understanding the common molecular mechanisms linking neuronal development and degeneration is crucial for a better knowledge of neurodevelopmental and neurodegenerative brain diseases.

During mammalian embryogenesis, the ectoderm develops into the neural plate giving raise to the neural tube at embryonic day 8.5 (E8.5) (Ikeuchi and Sisodia 2003). The neural tube, formed mainly by neuroepithelial cells, develops into transient structures: the prosencephalon (forebrain; that will be subdivided into the telencephalon and diencephalon), mesencephalon (midbrain) and rhomboencephalon (hindbrain). Later on, the dorsal telencephalon will form the adult cortex and hippocampus.

At early developmental stages, neuroepithelial cells form the ventricular (VZ) and the subventricular zones (SVZ). These cells derivate into radial glial cells (RGCs) and basal progenitors (BPs) at later stages (E13). RGCs also serve as scaffolding for neuronal migration to form the adult cerebral cortex patterning (Haubensak et al. 2004; Malatesta, Appolloni, and Calzolari 2008; Kriegstein and Noctor 2004; Noctor et al. 2004). In the developing cortex, excitatory neurons migrate radially to the cortical plate while inhibitory interneurons migrate tangentially into the cortex to their final destination (Tan and Shi 2013; O'Rourke et al. 1995) **(Fig. 1)**.

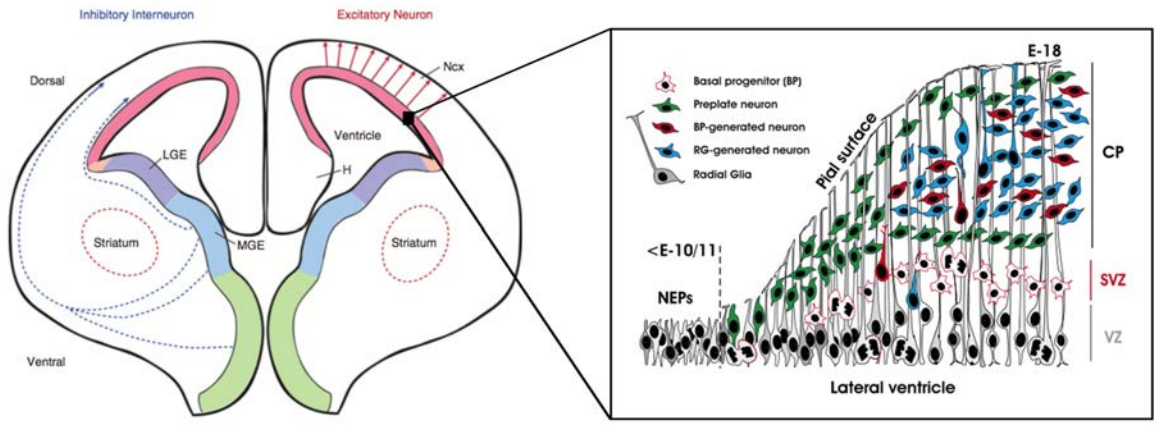

Figure 1. Schematic model of neuron generation and migration in the developing mouse cortex. BP and RGCs accumulate in the SVZ. There, both divide to generate mainly excitatory neurons, which migrate to the cortical layers through the radial glia (red arrows). By contrast, postmitotic neurons from the ganglionic eminence (GE), among others, migrate tangentially to the neocortex (blue arrows). BP: basal progenitor; CP: cortical plate; H: hippocampus; LGE: lateral GE; MGE: medial GE; Ncx: neocortex; RGC: radial glial cell; SVZ: subventricular zone; VZ: ventricular zone. Modified from (Tan and Shi 2013) and (Malatesta, Appolloni, and Calzolari 2008).

1.1. Stages of neuronal development

Neuronal development can be divided into at least five stages that were initially characterized in cultured hippocampal neurons (Dotti, Sullivan, and Banker 1988), and recently *in vivo* or *in situ* (Barnes and Polleux 2009; Hatanaka, Yamauchi, and Murakami 2012) (**Fig. 2**). In stage 1, immature postmitotic neurons with a spheroid shape develop lamellipodia and filopodia protrusions that start to grow leading to the emergence of multiple neurites (stage 2). In stage 3 (neuronal polarization) the symmetry of the neurites break when usually one of these neurites grow faster than the others, forming an axon. The axon continues growing as well as the remaining neurites, which constitute the different dendrites (stage 4). Finally, in stage 5, the axon and the dendrites continue spreading forming synapses (synaptogenesis) by developing dendritic spines and presynaptic elements, respectively (Govek 2005; Barnes and Polleux 2009; Flynn 2013).

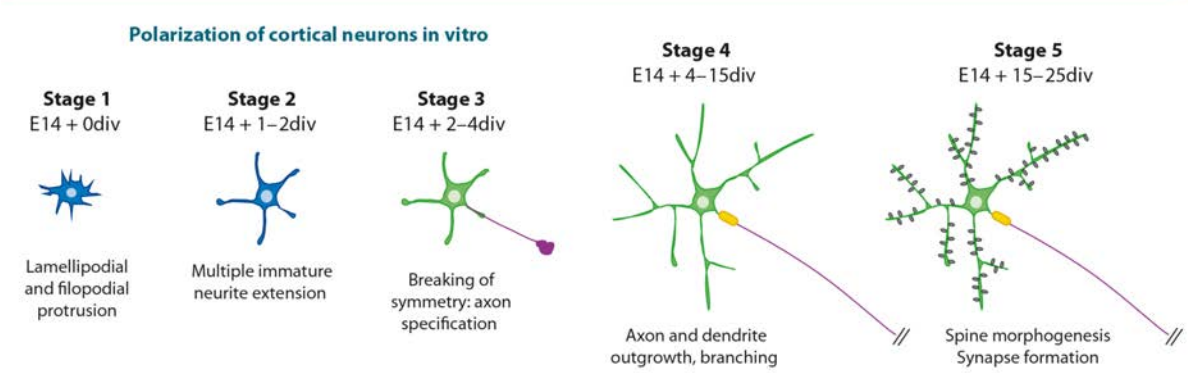

Figure 2. Stages of neuronal development in cultured neurons. Cultured hippocampal neurons start to form a lamellipodia and filopodia when they attach to the substratum (stage1). After few hours, multiple neurites start growing (stage 2) and the following day, one of the neurites starts to grow faster than the rest, establishing the axon (stage 3). After few days, the axon continues to grow and the neurites branch to form the dendrites (stage 4). Several days after, the axon and dendrites develop synapses. Modified from (Barnes and Polleux 2009).

In summary, neuronal development include three main processes, neuritogenesis, neuronal polarization and synaptogenesis, that are described next.

Neuritogenesis

Neuritogenesis is the initial stage of neuronal morphogenesis. The neurite initiation involve both intracellular and extracellular signals that lead to changes of cytoskeletal structures and dynamics, modifying the morphology of neurons from a spherical shape to a cell containing neurites (Edson, Weisshaar, and Matus 1993; Dent, Gupton, and Gertler 2011).

Neuritogenesis begins with the activation of membrane receptors by signals of the extracellular matrix (ECM), which modulate the tensile forces that are generated at the distal part of the cytoskeleton (Fass and Odde 2003; Tanaka et al. 2018). The ECM contains the adhesion molecules collagen, laminin and tenascins, the polysaccharide hyaluronan, the heparin-binding growth-associated molecule (HB-GAM), and the family of Slit proteins, which among others, modulate a wide variety of processes such as cellular adhesion, axonal growth and migration (Brose and Tessier-Lavigne 2000; Bovolenta 2000; Raulo et al. 1994). Binding of these ECM molecules to the appropriate membrane receptors as the integrin family or the cell adhesion molecule (CAM) induce changes both in the cytoskeleton and intracellular calcium influx leading to activation of multiple signaling pathways (Hu and Reichardt 1999; Da Silva and Dotti 2002; Walsh, Skaper, and Doherty 1994; Gomez 2001). Other proteins as the Rho family GTPases (Cdc42, Rac and Rho) also modulate neuritogenesis by mediating the formation of filopodia and lamellipodia (Hall 1994; Albertinazzi et al. 1998). Likewise, neuritogenesis can be also regulated by soluble molecules as the fibroblast growth factors FGF2 and FGF7, transforming growth factor-ß (TGF-ß), vascular endothelial-cell growth factor (VEGF), insulin-like growth factor (IGF) and neurotrophins (Tucker, Meyer, and Barde 2001; Williams, Furness, and Walsh 1994; Jin, Mao, and Greenberg 2006; Da Silva and Dotti 2002).

Neuronal polarization

Neuronal polarization is the second stage of neuronal development in which the formation of new axons (axonogenesis) and dendrites (dendritogenesis) takes place. Axons are a single long process that includes the axon terminals with multiple synaptic vesicles that store neurotransmitters. In contrast, dendrites are branched extensions with small protrusions called dendritic spines, which contain neurotransmitter receptors. The formation of these structures are responsible for electric transmission within the neuronal circuitry. Recent *in vivo* evidences show that neuronal polarization of both cortical and hippocampal neurons occurs during differentiation (Noctor et al. 2004). Although most neurons first develop the trailing process (nascent axons) and then the leading process (future dendrites), the coordination between them remains unclear (Takano et al. 2015; Namba et al. 2014). Several mechanisms including extracellular and intracellular signaling, local degradation of proteins, positive and negative feedbacks, vesicle trafficking and cell interactions are involved in both the establishment and the maintenance of neuronal polarity. The coordination of all these factors modulate cytoskeleton dynamics and neuronal polarization.

Extracellular cues, such as the cell adhesion molecules TAG-1 and L1, the extracellular matrices laminin and NgCAM, and extracellular molecules, including neurotrophins, netrins, integrins, the transforming growth factor β (TGF-β), Wnt, insulin-like growth factor 1 (IGF-1), sema3A and reelin, are involved in axon differentiation (Tahirovic and Bradke 2009; Funahashi et al. 2014; Guo et al. 2007; Moore et al. 2008; Esch, Lemmon, and Banker 1999).

Most of these factors regulate axon morphogenesis through Rho-GTPases. The Rho-family GTPases, which includes Rac1, Cdc42 and RhoA, plays a key role in the modulation of actin cytoskeleton. Indeed, the coordination of this family with multiple signalling pathways is essential for neurites to become polarized (Fukata, Nakagawa, and Kaibuchi 2003). The PI3K/Akt/GSK-3ß/CRMP-2 and the Cdc42/Par complex/Rac1 cascades are two main signaling pathways involved in neuronal polarization. Thus, activation of PI3K/Akt/GSK-3ß/CRMP-2 signaling regulates axon specification. Once glycogen synthase kinase 3β (GSK-3ß) becomes phosphorylated and inactivated, the microtubule associated proteins (MAPs) are activated (Gärtner 2006). Recently it has been described that GSK-3ß also regulates negatively CRMP-2 activity reducing its binding ability to tubulin (Yoshimura et al. 2006). On the other hand, the activation of Par complex (Par6-Par3-aPKC) by Cdc42 mediates the axon formation through the activation of Rac1. The activation of this cascade is highly regulated since Rac1 activates PI3K which in turn regulates Cdc42 activity (Arimura and Kaibuchi 2007; Shi, Jan, and Jan 2003; Nishimura et al. 2005). The activation of Par complex also regulates negatively MARK2 activity, preventing the phosphorylation of MAP and promoting microtubule assembly (Y. M. Chen et al. 2006).

Synaptogenesis

Synaptogenesis is the last stage of neuronal polarization. This process allows the flow of electrical information between a presynaptic neuron, which contains neurotransmitters that will be released into the synaptic cleft after a depolarizing action potential, and postsynaptic neuron that contains neurotransmitter receptors. These events are essential for multiple brain physiological events, including learning and memory processes. Synaptogenesis consists in the formation of synapses and their stabilization over time. During this process, both axon and dendrites continue developing and the postsynaptic dendritic spines appear and presynaptic terminals mature. Dendritic spine morphogenesis is tightly regulated by cell adhesion proteins, EphA3/ephrin signaling, Rho and Rhas

family GTPases, actin-binding and regulatory proteins and calcium responses (Hering and Sheng 2001).

However, for a synapse to occur, pre- and post-synaptic membranes must interact. This contact arises at the active zone of presynaptic neurons, formed by the fusion of synaptic vesicles to the cellular membrane (Shapira et al. 2003). In contrast, the postsynaptic neuron contains the postsynaptic density (PSD) that appears by the gradual accumulation of neurotransmitter receptors, voltage-gated ion channels, hundreds of proteins and various second-messenger signaling molecules (Bresler 2004). One of the most well characterized postsynaptic scaffolding proteins is PSD-95, which in turn recruits glutamate receptors. This transynaptic communication is closely regulated by cell adhesion molecules as well as multiple proteins involved in growth cone guidance as netrins, semaphorins and ephrinA (Pascual et al. 2004; Shamah et al. 2001). Likewise, molecules produced by both neurons and glial cells also have been reported to be involved in this "targeting" process (Farhy-Tselnicker and Allen 2018; Ullian, Christopherson, and Barres 2004). Once the synapses are formed and established, neuronal activity can modulate its stability or elimination (Ehlers 2003).

1.2. Cytoskeletal organization during axon growth

Neuronal polarization requires constant changes in the dynamics of the cytoskeleton. Neuron cytoskeleton is composed by microfilaments, composed of actin, microtubules and intermediate filaments. Thereby, axon outgrowth occurs trough the modulation of cytoskeletal dynamics of growth cones that leads to multiple extension and retraction processes over the coordination of both "pushing" (microtubules) and "pulling" (actomyosin filaments) forces (Letourneau, Shattuck, and Ressler 1987). The distal part of axon growth cones present three main domains involved in the regulation of axonal outgrowth: the central (C) domain, the T zone and the more distal P domain. The distal part contains two transient structures: filopodium and lamellipodium. In this region, actin filaments are assembled and retrogradely transported by myosin II in the T zone, where they are recycled and disassembled (Lin and Forscher 1995; Lin et al. 1996). As a matter of fact, the accepted model of axonal growth comprise three stages: protrusion, in which the membrane of the growth cones is extended out by F-actin polymerization; engorgement, in which microtubules mediated-transport of vesicles and organelles to the C domain; and consolidation, in which actin retrograde flow is reduced, resulting in the stabilization of growth cones (Dent, Gupton, and Gertler 2011) **(Fig. 3).**

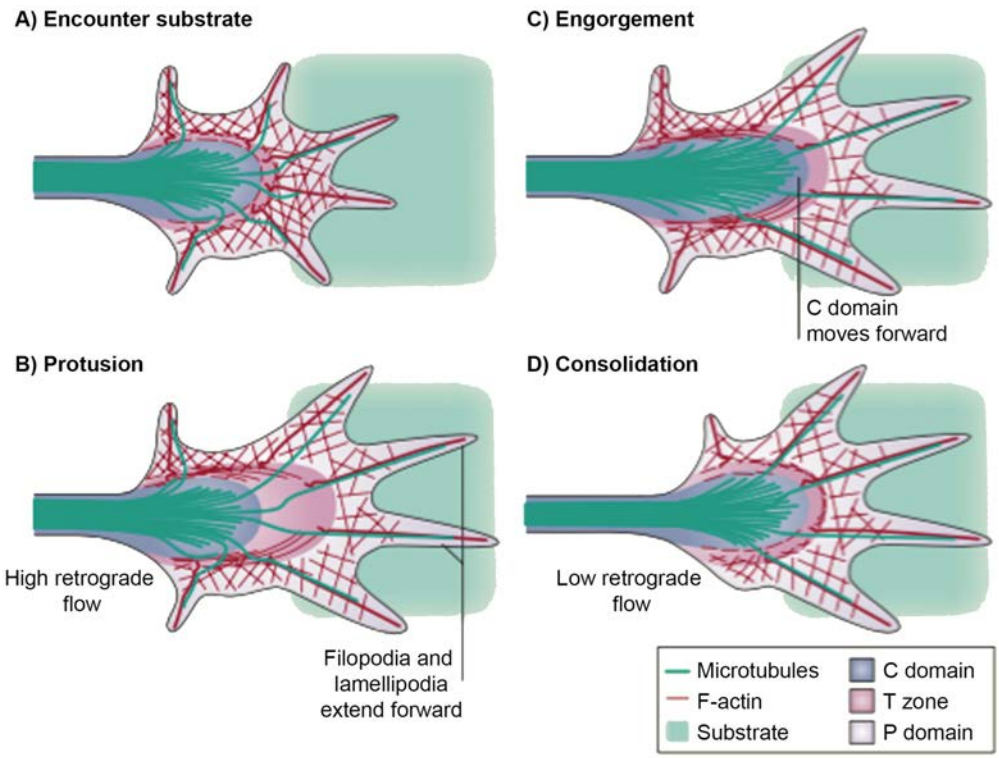

Figure 3. Stages of axonal growth cone. A) F-actin is assembled at the leading edge and moves to the central domain (retrograde flow). Axon growth cones are constantly looking for substrates and the distal end is characterised for having a high F-actin retrograde flow. B) During protrusion, F-actin binds to the substrate, decreasing the F-actin retrograde flow and allowing filopodia and lamellipodia to move forward to the P domain. C) During engorgement: F-actin arcs guide microtubules in the C domain to initiate a forward movement towards the site of growth. D) Consolidation occurs when the myosin II-containing actin arcs keep the microtubules into the C domain, F-actin is depolymerized in the neck of the growth cone and filopodia retracts, resulting in the elongation of the axon shaft. Modified from (Lowery and Vactor 2009).

1.2.1. Non-muscle myosin IIA

The superfamily of myosin proteins contains over 18 types, including conventional and non-conventional myosins. In neurons the main expressed isoforms are the conventional myosin II and the non-conventional myosins I, V, VI, IX and X (Wylie and Chantler 2003). Classically, non-muscle myosin II has been the most studied protein since their similarities with its muscular analogous. In humans, there are three isoforms of non-muscle myosin II (A, B and C) that are encoded by three different genes: MYH9, MYH10 and MYH14 (Simons et al. 1991; Golomb et al. 2004). The expression and function of these isoforms depends on both the cell type and the stage of development. Thus, whereas all neurons express isoforms IIA and IIB, developing hippocampal neurons do not express myosin IIC

(Kollins et al. 2009). Interestingly, myosin IIA is distributed over the C domain and the periphery of the axon growth cone (Rochlin et al. 1995; Brown and Bridgman 2003).

Myosin IIA (NMIIA) is a mechanoenzyme that regulates contractile activity through the interaction with actin filaments. NMIIA molecules consist of three pairs of domains: two heavy chains (HCs, 230 kDa), two regulatory light chains (RLCs, 20 kDa) and two essential light chains (ELCs; 17 kDa) (**Fig. 4**). Therefore, NMIIA consists of two globular heads that contain ATP- and actin-binding sites and a long coiled-coil tail. The globular head allows myosin to use Mg-ATP hydrolysis to generate mechanical movement and move forward over the microfilaments (toward "+" end). The rod coil contains a region that allows the self-assembly of myosin II molecules responsible for the assembly of bipolar filaments.

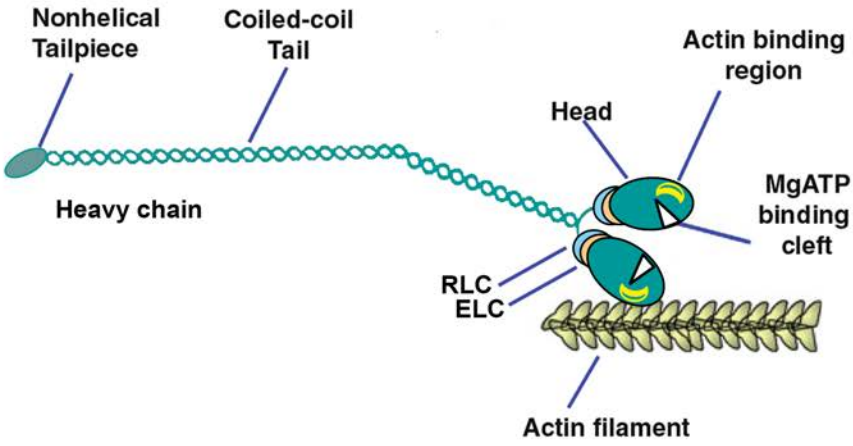

Figure 4. Representation of the molecular organization of non-muscle myosin IIA. NMIIA consists of two heavy chains that contain the globular head, a coiled-coil tail and a C-terminal non-helical tailpiece. The head domain binds to actin filaments and catalyzes Mg^{2+}-ATP hydrolysis leading to force generation. Following the head, in the neck domain, there are the essential (ELC) and the regulatory (RLC) light chains. The ELC stabilizes the neck domain while the RLC also contains several phosphorylation sites that modulate the activation of NMIIA. The coiled-coil tail contains a dimerization sequence that allows the homodimerization of NMIIA molecules. The non-helical tailpiece contains multiple phosphorylation sites that regulate NMIIA filament assembly. Modified from (Chantler et al. 2010).

NMIIA play important roles in a wide range of physiological functions. In fact, NMIIA knockout mice are embryonic lethal due to defects in cell adhesion (Conti et al. 2004; Wylie and Chantler 2001; Vicente-Manzanares et al. 2009). Other important functions in which NMIIA is involved are cell motility (Dulyaninova et al. 2007; Even-Ram et al. 2007), brain morphogenesis (Gutzman, Sahu, and Kwas 2015), neuronal guidance (Kubo et al.

2008; Cai et al. 2006), neurite retraction (Chantler and Wylie 2003; Wylie and Chantler 2003; Gallo 2006), oxidative stress-induced neuronal apoptosis (Wang et al. 2017) and trafficking of sodium pumps (Dash, Dib-Hajj, and Waxman 2018).

1.2.2. Role of non-muscle myosin IIA in neurite extension

NMIIA acts as a downstream effector of Rho GTPase signaling pathway during neurite retraction (Gallo 2006). Neurite retraction is responsible of the growth cone collapse phenomenon, and this event is directly regulated by either extracellular or intracellular signals that impact on Rho signalling. It is known that myosin RLC phosphorylation by myosin light chain kinase (MLCK) leads to the activation of NMIIA. Likewise, Rho activates its effector ROCK, which in turn phosphorylates the myosin binding subunit (MBS, also called MYPT1) of myosin light chain phosphatase (MLCP), causing its inhibition and allowing NMIIA to continue phosphorylated (Kimura et al. 1996). However, all three members of Rho-family GTPases, Rac, Cdc42 and RhoA modulate the phosphorylation of NMIIA and therefore its activation (**Fig. 5A**). Hence, NMIIA has an

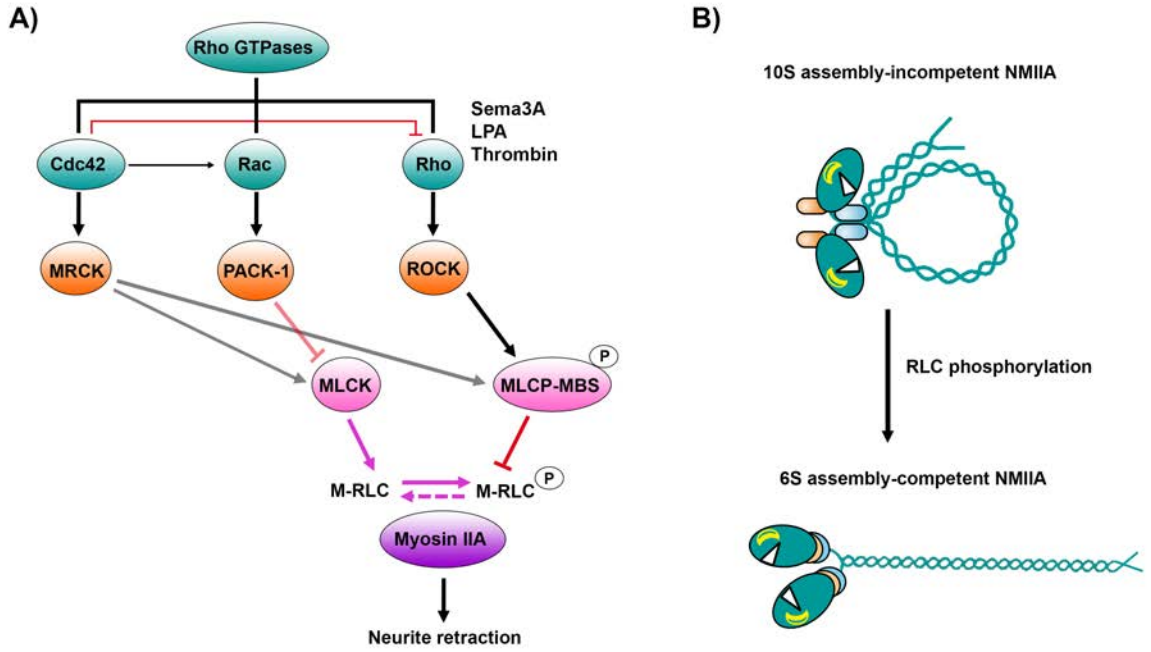

Figure 5. Activation of NMIIA by Rho-family GTPases. A) Downstream effectors of Rho Family GTPases regulate NMIIA activity by phosphorylation of the myosin RLC. **B)** Conformation of 10S assembly-incompetent and 6S assembly-competent NMIIA. When, RLC is not phosphorylated the head and the tail domain interact, allowing to 10S conformation to be stable. On contrary, when

RLC is phosphorylated at Ser19, NMIIA becomes assembly-competent leading to activation of the motor activity and the assembly of NMIIA into bipolar filaments.

assembly-incompetent form (10S) until RLC phosphorylation takes place. When RLC is phosphorylated (Ser19) occurs, NMIIA becomes assembly-competent (6S) and then the Mg^{2+}-ATPase activity increases and motor activity is induced leading to the interaction and assembly of actin filaments (Scholey, Taylor, and Kendrick-Jones 1980) (**Fig. 5B**).

1.2.3. Regulation of non-muscle myosin IIA

Regulation of non-muscle myosin IIA activity not only occurs through the phosphorylation of its light-chains (**Fig. 5**) but also through phosphorylation of the heavy-chains, protein interactions or calcium binding (Chantler and Wylie 2003) (**Fig. 6**). As described above, RLC phosphorylation by ROCK (which is activated by RhoA) and by MLCK (which is activated by Ca^{2+}-calmodulin) on Ser19 increases the Mg^{2+}-ATPase activity of NMIIA (Hathaway and Adelstein 1979). Moreover, theses kinases can also phosphorylate NMIIA at Thr18. When both phosphorylations happen, a further increase of the Mg^{2+}-ATPase activity occurs (Ikebe, Koretz, and Hartshorne 1988). Additionally citron Rho-interacting kinase (CRIK) that is also activated by RhoA, leucine zipper interacting kinase (ZIPK) and myotonic dystrophy-related Cdc42-binding kinase (MRCK) that acts downstream of Cdc42 can also phosphorylate Ser19 and/or Thr18 residues of RLC-NMIIA (Yamashiro et al. 2003; Murata-Hori et al. 1999; Komatsu and Ikebe 2004; Unbekandt and Olson 2014). Whereas the above kinases play an activating role, protein kinase C (PKC) has an opposite function. PKC phosphorylates RLC-NMIIA on Ser1, Ser2 and Thr9 leading a decrease of NMIIA activity (Nishikawa et al. 1984).

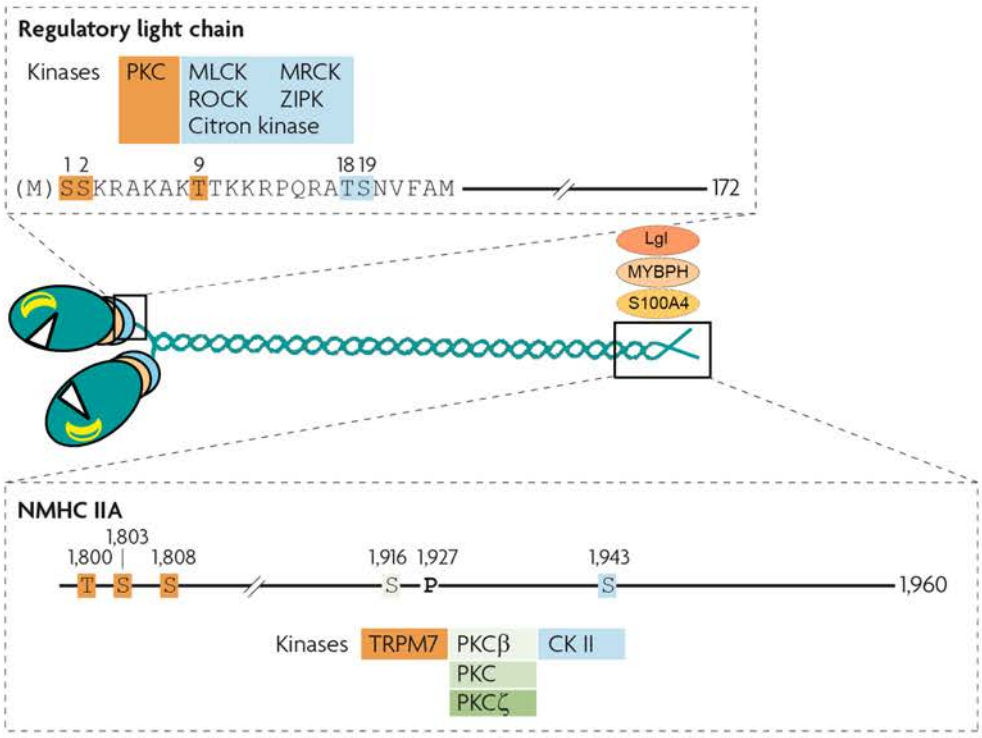

Figure 6. Phosphorylation-dependent regulation of non-muscle myosin IIA. The phosphorylation sites and the kinases responsible for the phosphorylation are indicated in the same colour. CKII: casein kinase II; Lgl: lethal(2) giant larvae; MLCK: myosin light chain kinase; MRCK: myotonic dystrophy kinase-related CDC42-binding kinase; MYBPH: myosin binding protein H; PKC: protein kinase C; ROCK: Rho-associated protein kinase; S100A4: S100 calcium-binding protein A4; TRPM7: transient receptor potential melastatin-7; ZIPK: leucine zipper interacting kinase. Modified from (Vicente-Manzanares et al. 2009).

Interestingly, while RLC phosphorylation regulates positively the formation of NMIIA filaments, phosphorylation events of NMIIA heavy chains (NMHC IIA) promote their dissociation or decrease filament formation. The main three kinases responsible for NMHC IIA phosphorylation are: PKC, casein kinase II (CKII) and transient receptor potential melastatin-7 (TRPM7). PKC phosphorylates NMHC IIA at Ser1916 and Ser1917 (Conti et al. 1991). Similarly, CKII induces Ser1943 phosphorylation causing NMIIA filament disassembly and cytoskeleton rearrangement. Additionally, phosphorylation at both sites, Ser1917 and Ser1943 prevent the assembly of NMIIA into filaments (Dulyaninova et al. 2005). Finally, TRPM7 phosphorylates NMIIA at Thr1800, Ser1803 and Ser1808 sites. In addition to decreasing filament formation, these phosphorylations were recently described to affect NMIIA subcellular localization (Clark et al. 2008).

Recent evidences point out that some protein interactions with NMIIA can also regulate NMIIA activity. In fact, these interactions could be a mechanism for maintaining activated monomeric filaments of NMII since all the NMII-binding proteins that have been identified to date promote the disassembly of filaments. The identified proteins so far are: lethal(2) giant larvae (Lgl), myosin binding protein H (MYBPH) and S100 calcium-binding protein A4 (S100A4, also called MTS1). Lgl binds to NMIIA interfering with its filament assembly and its distribution. This interaction is negatively regulated by PKC phosphorylation (Dahan et al. 2012). MYBPH play a dual role in the inhibition of NMIIA filament assembly since it not only interacts with ROCK leading to the inhibition of the RLC phosphorylation but also binds directly to NMHC IIA (Hosono et al. 2012a; Hosono et al. 2012b). Finally, the binding site of S100A4 protein is located within PKC- and near the CKII-phosphorylation sites and its function is to prevent the filament formation. Notably, when CKII phosphorylates NMIIA, S100A4 cannot bind to NMIIA, thereby protecting against inhibition of filament assembly (Li et al. 2003; Dulyaninova et al. 2005).

1.3. Signaling pathways in axon growth

Neuronal growth cones are constantly looking for and interpreting attractive and repulsive cues that allow them to reach their targets. The main signaling pathways involved in regulation of axon growth are: ephrins, netrins, semaphorins and slits (**Fig. 7**). I will describe next the involvement of the last three molecules on axon growth since one entire section will be dedicated to ephrins.

Netrins

Netrin-1 was the first axon guidance molecule to be characterized (Serafini et al. 1994). The main netrin functions in the nervous system are modulation of axon guidance and cell migration during development, axon branching and synaptogenesis and oligodendroglia development and maturation (Sun, Correia, and Kennedy 2011; Finci et al. 2015). Netrins are characterized for being bi-functional because they can produce both attractive and repulsive responses depending on the binding receptor. In mammals, the receptors for netrin are deleted in colorectal carcinoma (DCC), Neogenin, UNC5 and Down syndrome cell adhesion molecule (DSCAM) (Keino-Masu et al. 1996; Leonardo et al. 1997; Ly et al. 2008). I will specifically focus here on the interaction between Netrins and DCC and UNC5.

The structure of both receptors and netrin is very important for their binding. Netrin structure consists in a laminin-like domain (LN), three EGF repeats (E1-E3) and a C-terminal netrin-like domain (NTR). Further, the structure of UNC-5 consists in 2 Ig-like domains, 2 thrombospondin type I domains and a very large cytoplasmic tail. Finally, the structure of DCC receptor contains 4 IG-like domains in the N terminal region, 6 fibronectin type III domains (FN1-6), a transmembrane segment (TM) and 3 P motifs within the cytoplasmic tail. This cytoplasmic tail has a key role in downstream signal transduction pathways.

The chemoattraction effect of netrin depends on the interaction with the DCC receptor. The intracellular domain of DCC is constitutively bound to Nck1 and to focal adhesion kinase (FAK; PTK2). When the interaction between netrin and DCC occurs (in the FN4 and FN5 domains of the extracellular region of the receptor), it triggers the homodimerization of the receptor leading to FAK autophosphorylation and phosphorylation of the intracellular domain of DCC (Stein 2001; Ren et al. 2004). All these events converge in the activation of multiple intracellular signaling pathways involved in the modulation of axon attraction. The main intracellular signaling events involved are: 1) Activation of FYN, a member of Src family of kinases (SFK), that regulates the activity of Rho GTPases by the activation of Rac1 and Cdc42 and by the inhibition of RhoA (Guofa Liu et al. 2004; Li et al. 2004); 2) Activation of Trio and Dock180 which are guanine nucleotide exchange factors (GEFs) for Rac1 that regulate activation of RhoA GTPases (Briançon-Marjollet et al. 2008; Li et al. 2008); 3) Activation of some downstream effectors of Cdc42: p21-activated kinase Pak1 (which is also a downstream effector of Rac1), Enabled/vasodilator-stimulated phosphoprotein (ENA/VASP) and neuronal Wiskott-Aldrich syndrome protein (N-WASP) (Lebrand et al. 2004; Shekarabi 2005); 4) Activation MAPK (ERK) signaling cascade (Forcet et al. 2002); and 5) Promotion of the synthesis and hydrolysis of phosphoinositide phosphatidylinositol (4,5) bisphosphate (PIP_2), which results in the production of phosphatidylinositol (3,4,5) trisphosphate (PIP_3) and the activation of PKC, respectively (Huang 1989; Xie et al. 2006).

On the other side, the chemorepulsion effect depends on the binding of netrin to UNC5 receptor. Moreover, this binding differs depending whether the repulsion effect has a short-range (mediated by UNC5 signaling) or long-range (mediated by UNC5-DCC signaling) (Keleman and Dickson 2001). In the short-range effect, netrin binds to Unc-5 that results phosphorylated by tyrosine kinases as Src1. Likewise, netrin induces the recruitment of the tyrosine phosphatase SHP2 into the cytoplasmic domain of Unc-5. By contrast, the long-range response requires the interaction between the cytoplasmic tails of

DCC and Unc5, leading to the formation of the DCC-Unc5 complex. In this case, netrin induces the DCC-dependent phosphorylation of Unc5 trough Src1 and FAK, leading to the binding of SHP2 to Unc5 (Tong et al. 2001; Killeen et al. 2002; Li 2006). Unfortunately, signaling mechanisms that regulate this chemorepulsion effect are unknown.

Semaphorins

Semaphorins (Semas) are a large family of secreted, transmembrane and GPI-linked proteins. All semaphorins have a large extracellular domain called Sema domain and a PSI domain (also called cysteine rich domain, CRD). On contrary, some other motifs as Ig-like domain or thrombospondin are only present in some members. Although most of semaphorins mediate chemorepulsive responses (Sema3A has been the most studied), some semaphorins can induce an attraction effect on certain neuronal populations too (for example Sema3E) (Bagnard et al. 1998). Thus, both the expression of semaphorins and their binding to the receptors will determine which type of function will perform. There are two main semaphorin receptors: Neuropilins (Nrpn) and Plexins (Plex).

Neuropilins (Nrpn) are the receptors for secreted semaphorins. There are two types: NRP1 and NRP2. The structure of neuropilins consists in a large extracellular moiety, a transmembrane domain and a short cytoplasmic tail. In order to become active, and so semaphorin can bind, neuropilins have to dimerize and form homo- or heterodimers (Pellet-Many et al. 2008). Then, once the dimers are formed, Sema binds to Nrpn, which in turn will bind to Plex. This binding with Plex, which in turn is the receptor of transmembrane semaphorins, ensures signal transduction through its cytoplasmic domain (Rohm et al. 2000).

On the other hand, Plexins (Plex) are the receptors for transmembrane semaphorins. The family of Plexins consists in 4 members that are divided into 4 families (PlexA-D). Plexins are transmembrane proteins with an extracellular domain that comprises the Sema domain, the PSI and IPT domains; and the intracellular region that contains the SEX protein (SP) domain and the PDZ-binding motif. Plexins can also form homo- or heterodimers, and these dimers may regulate its own activation (Tamagnone et al. 1999; Takahashi and Strittmatter 2001; Usui et al. 2003; Kong et al. 2016).

Therefore, semaphorin-mediated signaling depends on the cytoplasmic domain of plexins, which in some cases have intrinsic RasGAP activity. Moreover, some small GTPases can bind directly to plexin's cytoplasmic domain, as well as regulators of GTPase activity as

guanine-nucleotide exchange factors (GEFs) and (GTPase activating protein) GAPs. Accordingly, the signaling pathways related to semaphorins are Rho GTPases (RhoA and Rac1), the PI3K/Akt, cyclin dependent kinase 5 (Cdk5) and GSK-3ß kinases and MAP kinases, among others (Jin and Strittmatter 1997; Liu and Strittmatter 2001; Pasterkamp and Kolodkin 2003).

Slits

The Slit family of glycoproteins (Slit1-3) mediates axon repulsion through their Roundabout (Robo) receptors (Brose et al. 1999). The structure of slit consists in four leucine-rich repeat (LRR) domains, seven to nine EGF-like domains, a laminin G domain (ALPS) and a cysteine rich C-terminal region. Slit is proteolytically processed within its EGF domain to generate an active N-terminal fragment allowing its binding to Robo. Robo is a transmembrane receptor with an ectodomain that consists in five Ig domains and three fibronectin repeats; a transmembrane domain; and a long cytoplasmic tail that contains four conserved cytoplasmic (CC0-CC3) sequences. The binding between Slit and Robo occurs through the second LRR and the first two Ig domains, respectively (Zhe Liu et al. 2004; Howitt, Clout, and Hohenester 2004).

The interaction between Slit and Robo, increases the amount of Dock, which binds to Robo's cytoplasmic domain, leading to a stimulation of Rac activity through the recruitment of Pak (Fan et al. 2003). 09/01/19 18:52Moreover, srGAP1 and srGAP2 can also bind to the cytoplasmic domain of Robo, inhibiting Cdc42 (Wong et al. 2001). Additionally, there are multiple proteins that have been described as binding partners of Robo as the tyrosine kinase Abelson (Abl) and its substrate Enabled (Ena). Interestingly, both can bind to the cytoplasmic domain of Robo but Ena join to transduce its repulsive signal, while Abl plays an opposing role (Bashaw et al. 2000).

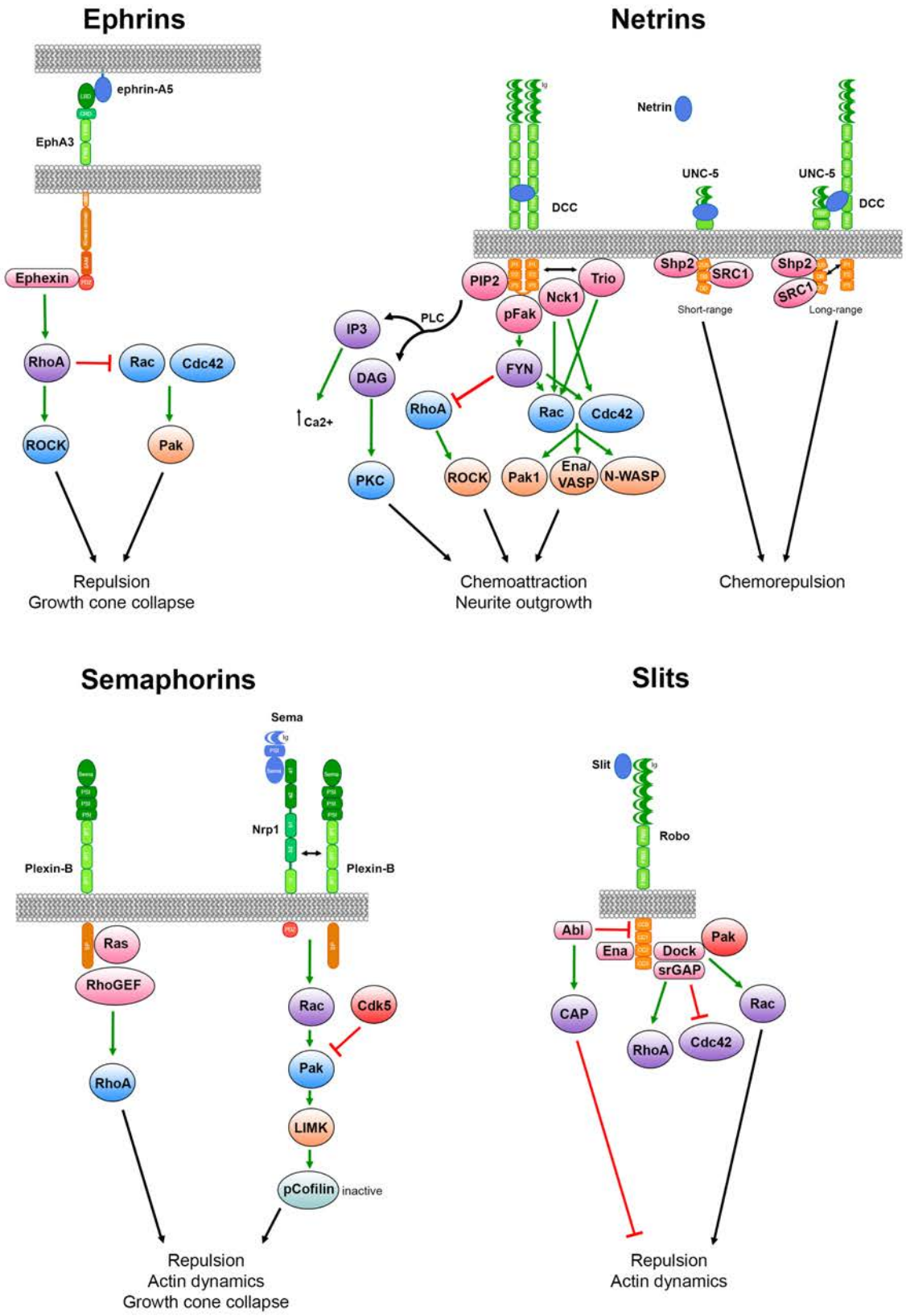

Figure 7. Signalling pathways involved in axon growth activated by the four main axon guidance cues and their receptors. Extensive description of ephrins, netrin, semaphorins and slits and acronyms are in the main text.

2. Ephrin receptors

2.1. Eph-ephrin family

The mammalian family of tyrosine kinase Ephrin receptors (Eph) consists of fourteen members that are divided in two classes: EphA (EphA1-A8 and EphA10) and EphB (EphB1-B4 and EphB6). Their ligands, the ephrins, are divided also in two subclasses: ephrin-A (ephrinA1-A5) that are characterised for having a glycosylphosphatidylinositol (GPI) domain as an anchorage to the membrane; and ephrin-B (ephrinB1-B3) that have a transmembrane domain followed by a PDZ-binding domain (Flanagan and Vanderhaeghen 1998). Normally, ephrin-A ligands bind to EphA, whereas ephrin-B interacts EphB receptors, except for EphA4 and EphB2 that are able also to bind ephrin-B and ephrin-A5 ligands, respectively (Himanen et al. 2004; Pasquale 2004).

The structure of Eph receptors consists of an extracellular region, containing a globular domain, the ligand-binding domain (LBD), a cysteine rich region; and two fibronectin-type III repeats, the transmembrane region and the cytoplasmic domain. The cytoplasmic region contains a juxtamembrane domain (JM) where two tyrosine residues are located, which are necessary for phosphorylation and therefore activation of the receptor; a tyrosine kinase domain that contains an ATP-binding pocket; a sterile alpha motif (SAM) responsible of oligomerization; and a PDZ-binding domain (**Fig. 8**) (Himanen and Nikolov 2003). Interestingly, a recent study shows that the SAM domain plays also a regulatory role over the catalytic function, by acting together with JM and Kinase domains (Kwon et al. 2018).

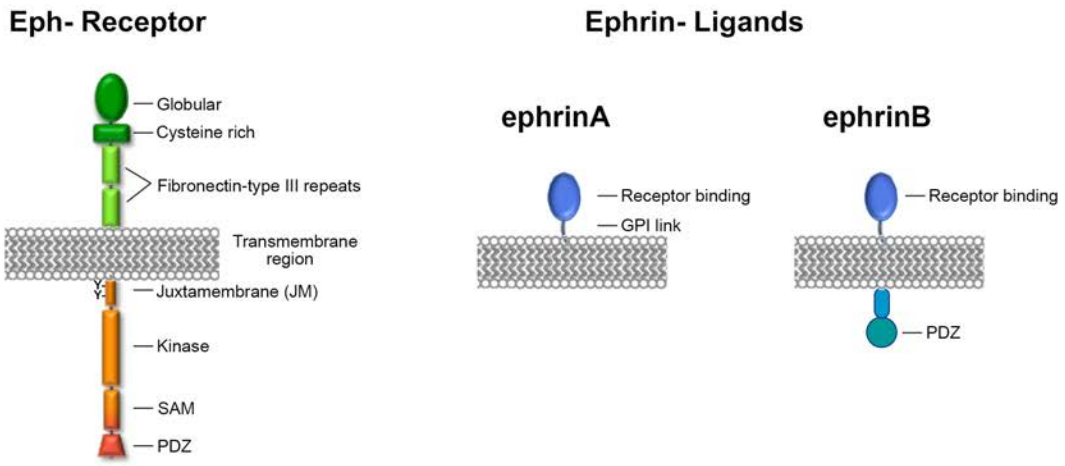

Figure 8. Structural domains of Eph receptors and ephrin ligands. Description of molecular domains and functions are indicated in the main text. Adapted from (Charmsaz 2013).

Eph receptors and ephrins have a widespread expression during CNS development. The expression of each isoform differs between neuronal cell types and the stage of development. Moreover, during development each region of the brain will have a different combination of Eph expression members. Specifically, EphA3, EphA4, EphA5, EphA6 and EphA7 show high expression levels in the hippocampus of developing mouse brain, suggesting a potential role in the formation of the hippocamposeptal topographic map (Yue et al. 2002). During corticogenesis, EphA4 is the most expressed isoform. During this process, both EphA4 and EphA7 are expressed in most zones, whereas EphA3 and EphA5 are expressed mainly in SVZ and intermediate zone (IZ), whereas EphA6 is more restricted to the CP. The expression pattern of these receptors suggest that these EphA receptors could be involved in cortical lamination (Yun et al. 2003). In addition to their role on structure patterning in the developing nervous system, this family of tyrosine kinase receptors is also involved in regulating axon growth, neuronal migration and other neuronal, including synaptogenesis and synaptic plasticity (**Table 1**). Importantly, recent evidences demonstrate that Eph receptors are involved in actin-myosin polymerizations events (Krupke and Burke 2014).

Table 1. Function of most expressed EphA receptors in hippocampus and cortex of mice.

Receptor	Ligand	Function	References
EphA3	ephrin-A5 ephrin-A2	Axon guidance retinotectal patterning	(Cheng et al. 1995; Connor, Menzel, and Pasquale 1998)
	ephrin-A5	Somitogenesis and organization of MHB	(Oates et al. 1999)
	ephrin-A5	Thalamocortical projections	(Mackarehtschian et al. 1999)
	ephrin-A5	Regulation of cell morphology and adhesion	(Lawrenson et al. 2002)
	-	Motor-sensory organization	(Gallarda et al. 2008)
	-	Inhibition of cell migration and process outgrowth	(Hu et al. 2009)
	ephrin-A5	Callosal axon guidance	(Nishikimi et al. 2011)
	ephrin-A5	Growth cone collapse in a kinase-dependent manner	(Brennaman, Moss, and Maness 2014)
EphA4	ephrin-A5	Thalamocortical projections	(Mackarehtschian et al. 1999)

	ephrin-A3	Spine morphology and glial glutamate transport	(Murai 2003; Carmona et al. 2009)
	-	Motor-sensory organization	(Gallarda et al. 2008)
	ephrin-B3	Formation of LTP in amygdala	(Deininger et al. 2008)
	ephrin-A3	Formation of LTP in amygdala and hippocampus	(Filosa et al. 2009)
	-	Spinal motor axon guidance	(Gatto et al. 2014)
	ephrin-A5	Modulation of neurogenesis and angiogenesis	(Shu et al. 2014)
	ephrin-A5	Modulation of IPC generation in cortical layers	(Gerstmann et al. 2015)
	-	Long-term CFC memory formation in a kinase-independent manner	(Dines et al. 2015)
	ephrin-B2	Dendritic spine formation/maintenance, memory function and consolidation	(Abate et al. 2018)
	ephrin-A1	Contribution to BBB damage following ischemic stroke through Rho/ROCK signaling	(Chen et al. 2018)
EphA5	ephrin-A2	Hippocamposeptal projection organization	(Gao et al. 1996)
	ephrin-A5	Thalamocortical projections	(Gao et al. 1998; Mackarehtschian et al. 1999)
	-	Retinotectal patterning in mice	(Brown et al. 2000)
	ephrin-A5	Regulation of synaptogenesis	(Akaneya et al. 2010)
	ephrin-A5	Modulation of targeting of the 5-HT serotonin receptor to neurons	(Teng et al. 2017)
EphA6	-	Retinotectal patterning in mice	(Brown et al. 2000)
EphA7	ephrin-A5	Dendritic spine formation and maturation	(Clifford et al. 2014)
	ephrin-A5	Maintenance of GABAergic synapses	(Beuter et al. 2016)
	ephrin-A5	Formation of LTP and hippocampus-dependent learning	(Beuter et al. 2016)
	ephrin-A5	Modulation of cortical neuronal migration and corticothalamic axon guidance	(Son et al. 2016)

BBB: blood-brain-barrier; CFC: contextual fear conditioning; IPC: intermediate progenitor cell; MHB: Midbrain/Hindbrain boundary ; LTP: long-term potentiation.

2.1.1. EphA3 receptor

According to the Human Protein Atlas project, the highest EphA3 mRNA expression and protein levels are found in the cerebral cortex and caudate nucleus in humans. The mouse genome database (MGD) (*Mouse Genome Informatics website*), that compiles all works that have reported EphA3 expression during the different stages of development, indicates that EphA3 is expressed in brain during development and remains constant until adulthood in mice. Interestingly, the distribution between mRNA and protein levels of EphA3 differs in the developing forebrain. Whereas EphA3 protein levels are found in hippocampus at around E16 and in the IZ during all stages, EphA3 mRNA is located in the dorsal thalamus and in the cortical IZ during the early stages (E13-E15) and in cortical plate during the late stages (E18) (Dufour et al. 2003; Kudo et al. 2005). However, EphA3 expression is critical during development processes not only in the CNS. Interestingly, it has been recently shown that EphA3 ectodomain antagonizes the role of EphA4 forward signaling and decreases EphA4 signaling pathway (Fiore et al. 2018). Indeed, EphA3 is involved in multiple processes such as cell adhesion, cytoskeletal organization, growth cone collapse, cell migration, heart development, retinotectal mapping of neurons and segregation of motor-sensory axons (see **Table 1**) (Stephen et al. 2006).

The most accepted theory of EphA3 signaling activation consists of the receptor clustering model, which initiates with high concentrations of a ligand. Although EphA3 can bind to all ephrin-As ligands, it has a high preference for ephrin-A5. Indeed, the binding of ephrin-A5 to EphA3, changes the inclination between the two molecules, bringing near both contact superficies, and leading to an increase of binding affinity (Forse et al. 2015). Then, an elevated amount of ligand causes the accumulation of the receptor in that region, which leads to receptor dimerization through SAM domain of EphA3 from opposite cells. This brings closer the two kinase domains, and stimulates the kinase activity causing the phosphorylation and activation of each other (Lackmann et al. 1998). The activation of the kinase domain is related to the two tyrosine residues in the JM region that seems that interact with the active site of the kinase, modulating the kinase activity (Davis et al. 2008). In 2015, it was proposed a new model of EphA3 activation: the “pre-formed dimer”. According to this model, EphA3 dimerizes in the absence of ligand. Then, the SAM domain stabilizes the interaction between the unliganded receptors. This unliganded dimers are autophosphorylated and allows a rapid activation of other receptors when the ligand concentration increases (Wimmer-Kleikamp et al. 2004; Singh et al. 2015).

An important aspect of EphA3 signaling is its regulation. Regulation of EphA3 signaling can occur mainly by: proteolysis, phosphatases or binding proteins. At high ligand levels, for instance when EphA3/ephrin-A5 clusters are formed, EphA3 suffers conformational changes in its cytoplasmic domain that promote the recruitment of the metalloproteinase ADAM10, which can recognize this complex and cleaves ephrin-A5 binding, leading to separation of cells in contact (Janes et al. 2005; Janes et al. 2009). At present, effects of ADAM10 or other metalloproteases on EphA3 processing have not been so far reported. On the other hand, two protein phosphatases regulate EphA3: PTP-PEST and PTP1B. PTP-PEST modulates negatively activation of EphA3 by two different ways: 1) by preventing EphA3 endocytosis; and 2) EphA3-ephrin-A5 binding increases caspase-3 activity, which proteolyzes PTP-PEST leading to the generation of an N-terminal product that reduces EphA3 phosphorylation (Wimmer-Kleikamp et al. 2008; Mansour et al. 2016). In the case of PTP1B, regulation of EphA3 occurs through the control of receptor internalization and trafficking (Nievergall et al. 2010). Finally, some EphA3 binding proteins also affect EphA3 signaling. One of these is the binding of Nck1 within the JM domain of EphA3, whose interaction is enhanced by EphA3-ephrin-A5 binding. Thus, Nick1 seems to act as a key player in downstream signaling, probably by interacting with other proteins such as PAK1 or WASPs (**Fig. 9**) (Hu et al. 2009).

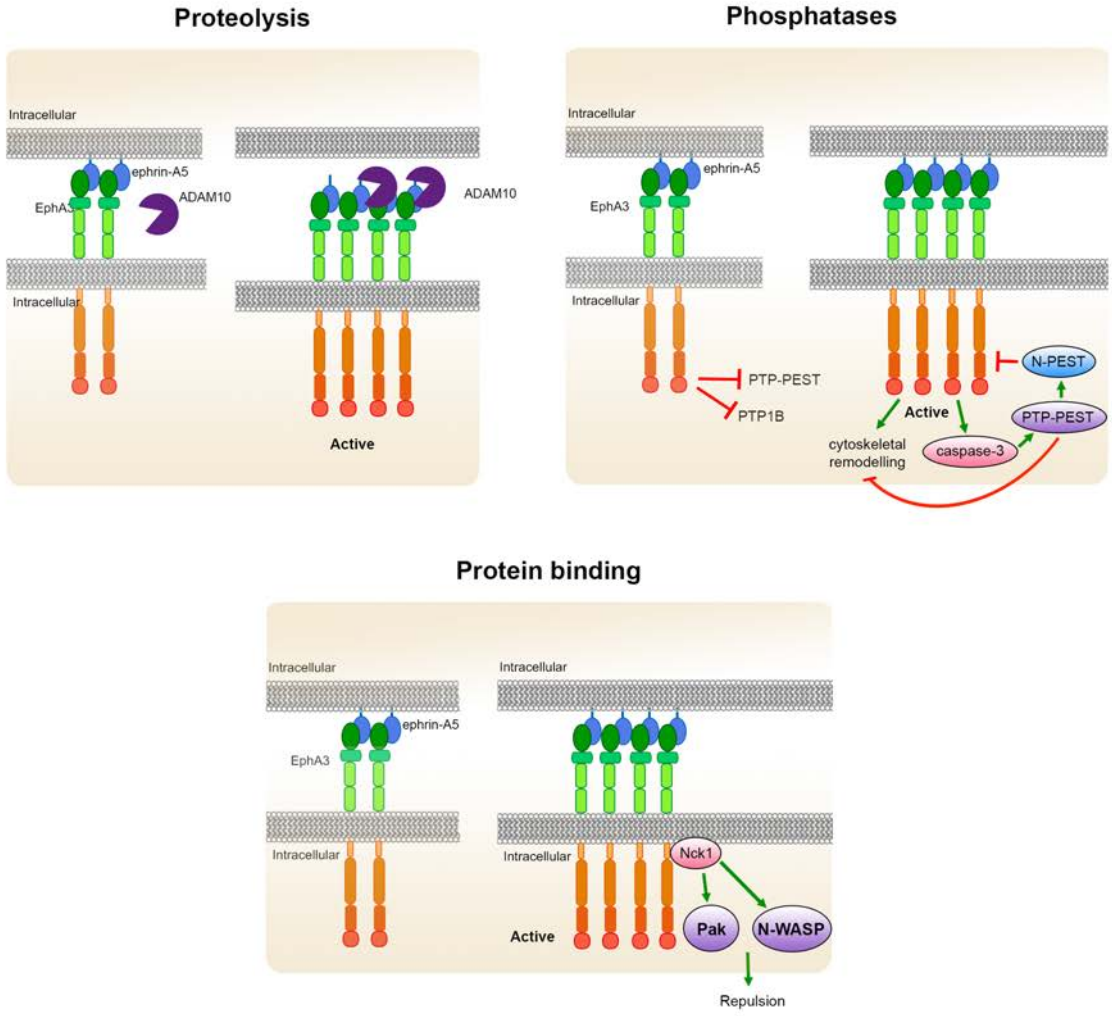

Figure 9. Regulation of EphA3 activity. The presence of high ligand levels induces receptor clustering and kinase activity. The EphA3 activity can be then downregulated by the recruitment of the metalloprotease ADAM10, which will cleavage ephrin-A5 and disrupt cell-cell interaction; or by enhancing the activity of phosphatases PTP-PEST or PTP1B. In addition, some proteins, such as Nck1, are recruited by active EphA3 and promote cytoskeleton remodelling and repulsion events.

2.2. Eph receptor signaling

Eph-mediated signaling is very diverse, not only because of the high number of Eph members, but also because each Eph cluster can contain more than one type of receptor. Eph receptors can interact in *cis* with other receptors of the cluster, and also with ligands that are located within the same cell. Furthermore, as the Eph-ephrin *cis* interaction is independent of the globular domain, the receptor can also be bound in *trans* with another ligand, leading to a bidirectional signaling. Therefore, two types of signaling that can occur simultaneously depending on where occurs the signal transduction: in the cell that contains

the Eph receptor (forward signaling) or in the cell that contains the ephrin ligand (reverse signaling) (**Fig. 10**) (Egea and Klein 2007).

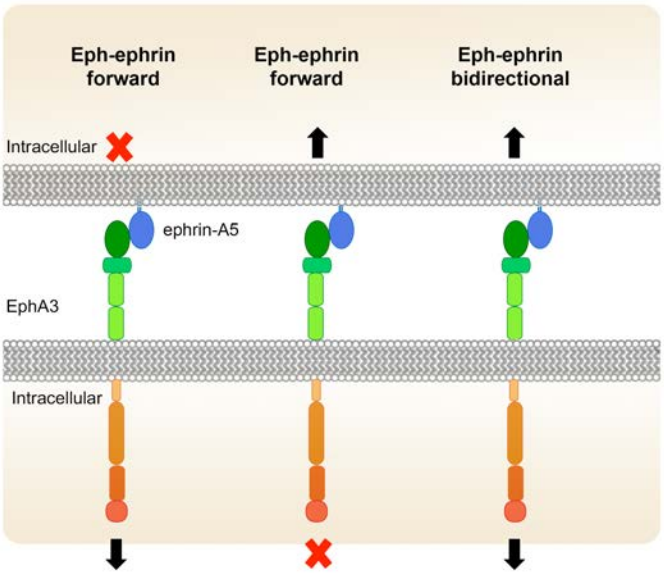

Figure 10. Types of Eph-ephrin signaling. Forward signaling: signaling in the cell where the receptors are located. Reverse signaling: signalling in the cell where the ligand is located. Bidirectional signaling: signal transduction occurs simultaneously in cells containing the receptors and ligands. Adapted from (Kania and Klein 2016).

Eph-ephrin forward signaling

The forward signaling starts with the binding of the ephrin ligand to the Eph receptor with a 1:1 stoichiometry. Then, Eph-ephrin binding causes the receptor clustering that leads to the activation of the kinase domain, inducing the autophosphorylation of the receptors within the JM domain (residues Tyr596 and Tyr602) (Binns et al. 2000; Shi, Yue, and Zhou 2010). This phosphorylation events promote the binding of SH2 domain-containing proteins that together with the phosphorylation of target proteins propagates the signaling to downstream pathways (Pasquale 2005).

The molecules that acts downstream of Eph receptor are: SH2-domain containing proteins as Nck1 or Nck2, PI3K, Src family kinases and GEFs proteins such as kalirin, Vav (that also contains SH2 domain) and ephexin (Kania and Klein 2016). These molecules are related to Rho GTPAses, which raise cytoskeleton rearrangements that cause changes in cell morphology, growth cone collapse and dendritic spine remodelling (Murai and Pasquale 2005). Rho GTPases are molecular switches that can change from inactive (GDP-bound) to

active (GTP-bound) conformations to trigger downstream effectors. In neurons, activated Eph receptors recruit GEF proteins that exchange bound GDP for GTP leading the activation of RhoA, and GAPs that facilitate GTP hydrolysis to GDP, inhibiting Rho family members as Rac. Interestingly, each GEF can modulate the Rho GTPase activity in several ways. In absence of ephrins, Ephs are constitutively bound to ephexin, which is not phosphorylated leading to activation of RhoA, Rac1 and Cdc42 promoting axon outgrowth. When, ephrin binds to EphA, ephexin is phosphorylated and RhoA is activated, promoting axon growth cone collapse (Shamah et al. 2001). On the contrary, Vav binds to activated Eph receptors, which causes the phosphorylation of Vav2 enhancing Rac-1 dependent endocytosis of Eph-ephrin complex, and leading to a repulsion effect (Cowan et al. 2005).

Eph-ephrin forward signaling also involves the Ras-MAPK pathway. Usually, Ephrin-ephrin signaling inhibits Ras-MAPK pathway through the action of p120Ras-GAP that inactivates H-Ras (Minami et al. 2011). p120Ras-GAP also inhibit R-Ras, causing a reduction in the integrin activity and facilitating the retraction process (Dail et al. 2006). In other cases, Eph-ephrin signaling can abrogate the activation of Ras-MAPK pathway through the action of other kinases. For example, in neurons, the BDNF-TrkB signaling stimulates MAPK activity, whereas the Eph-ephrin signaling supress this activity by inhibiting its phosphorylation, leading to growth cone collapse (Meier, Anastasiadou, and Knöll 2011). Finally, it has been also reported that Eph receptors can activate Ras-MAPK pathway (Vindis et al. 2003; Xiao et al. 2012).

In addition, Eph-ephrin forward signaling also regulates negatively the Akt pathway leading to the inactivation of mTORC1, which is involved in cell cycle and migration. Although normally Eph-ephrin signaling inhibits Akt activation by inducing a rapid dephosphorylation of T308 and S473 residues, which are responsible for its activation, this signaling can also be involved, in some circumstances, in the Akt activation. Moreover, Akt can also regulate Eph receptors through feedback loop mechanisms (Miao et al. 2009; Maddigan et al. 2011; Yang et al. 2011).

Eph-ephrin reverse signaling

Eph-ephrin interaction can also cause the activation of the reverse signaling. Due to the fact that the structure of ephrinA and ephrinB ligands is different, the regulation this signaling is also different. Ephrin-B reverse signaling can be dependent or independent of phosphorylation. In the first case, EphB binding to ephrinB causes a rapid binding of SFK,

that phosphorylates the cytoplasmic domain of the ligand. Similarly, Grb4 is also recruited and acts as a downstream effector of ephrin-B binding to other proteins involved in the modulation of cytoskeleton dynamics as Abi-1, CAP and Axin (Cowan and Henkemeyer 2001). On the other hand, ephrin-B reverse signaling can also be mediated by the interaction between ephrin-B and PDZ-containing proteins. The best characterized example of PDZ-binding protein is PTP-BL, which inhibits both ephrin-B phosphorylation and Src activity (Palmer et al. 2002). Ephrin-A reverse signaling, on contrary is poorly understood. On example is ephrinA2 reverse signaling, which is activated by EphA7 and inhibits cell proliferation and neurogenesis (Holmberg 2005).

Finally, there are two mechanisms that regulate negatively EphA-ephrinA5 signaling: the proteolysis (in *cis* or in *trans)* of the ligands and the endocytosis. The *cis* cleavage occurs when ephrin is bound to ADAM10 within the same cell and before the contact with the opposing cell; then EphA join the complex and ADAM10 can cleavage the ectodomain of Ephrin, leading to a repulsive effect. On contrary, the *trans* cleavage mechanism occurs when EphA3 receptor is constitutively associated with ADAM10 and when Ephrin-A5 contact occurs, ADAM10 is able to cleavage ephrinA5, leading the same effect than before. It is not clear whether one or both mechanisms occur *in vivo* (Janes et al. 2005). In addition, the forward signaling is also negatively regulated by endocytosis, where EphB-ephrin-B complexes are internalised via bi-directional trans-endocytosis, that is from one cell containing the receptor or the ligand to the opposing cell (Zimmer et al. 2003; Egea and Klein 2007). Moreover, ephrin-A5 binding to EphA3 also triggers the rapid internalization of the receptor-ligand clusters into endosomes but not into lysosomes (Vearing et al. 2005; Nievergall et al. 2010). Of interest, based on this concept, EphA3 antibody therapies have been developed. Specifically, an EphA3 monoclonal antibody that binds to the globular domain of EphA3 causing the internalization of EphA3/ephrin-A5 clusters showed an anti-tumour response in glioblastoma (Offenhäuser et al. 2018).

2.3. Role of Eph-ephrin signaling in human diseases

Eph family kinases are involved in a wide range of diseases from multiple types of cancer, neurological disorders including Alzheimer's disease, and nerve degeneration. Moreover, Ephrin-ephrin signaling can play both protective or damaging roles in these diseases.

Classically, EphA2, EphB2 and EphB4 have been the most involved receptors in tumour development, although recent evidences show that EphA3 is also implicated. EphA2

expression is found to be elevated in breast cancer and melanoma (Udayakumar et al. 2011; Bian et al. 2017). Moreover, the EphA2 ligand-dependent signaling has a protective role, inhibiting the migration of glioma and prostate cancer cell, whereas EphA2 ligand-independent signaling promotes cell migration. EphA2 can also act as a can also act as a substrate of Akt which is related to brain tumour progression (Miao et al. 2009). Similarly, the kinase activity of EphB2 has been related to cell proliferation in adenoma cancers, whereas in prostate and colorectal cancers, this receptor plays a protective role against uncontrolled growth. Additionally, some EphB2 mutations in prostate cancer cells destabilize its mRNA or transcripts, leading to inactivation of EphB2 function (Huusko et al. 2004; Batlle et al. 2005; Genander et al. 2009). EphB4 expression is also increased in breast cancer (Wu et al. 2004). Indeed, the ligand-dependent EphB4 signaling is associated with a protective role as it inhibits tumour progression and migration, whereas the ligand-independent signaling has a more tumour promoter role (Noren et al. 2004; Noren et al. 2006). EphA3 expression is upregulated in breast, lung, colorectal, gastric, prostate and hematological cancers and also in melanoma, sarcoma, mesenchymal subtype of glioblastoma (GBM) where a high number of EphA3 mutations have been identified (Dottori et al. 1999; Bardelli 2003; Fox, Tabone, and Kandpal 2006; Singh et al. 2008; Valsesia et al. 2011; Day et al. 2013; Ross et al. 2014). Interestingly, EphA3 activation in GBM inhibit tumour growth, role that could be mediated by inactivating somatic mutations or by epigenetic modifications that lead to EphA3 silence (Vail et al. 2014). On contrary, EphA3 expression has been found to be downregulated in esophageal squamous cell carcinoma (ESCC) (Chen et al. 2008).

Eph-ephrin signaling play essential roles during development of CNS and therefore it is also involved in neurological disorders. In mouse models of Alzheimer's disease (AD), the expression of EphB2 and EphA4 genes is downregulated in the hippocampus (Simón et al. 2009). Indeed, both EphB2 and EphA4 are substrates of Presenilin (PS)/γ-secretase. The PS/γ-secretase-dependent processing of EphB2 and EphA4 leads to the generation of intracellular domains that play roles in cell sprouting and spine formation, respectively (Inoue et al. 2009; Haapasalo and Kovacs 2011). Noteworthy, mutations in PS genes account for the majority of cases of Familial AD (FAD). Interestingly, it seems that EphB2 could have also a protective role in LTP and memory impairments (Cissé et al. 2011). EphA4 expression is also involved in amyotrophic lateral sclerosis (ALS) pathogenesis, as its expression inversely correlates with disease survival (Van Hoecke et al. 2012). On the other hand, EphB2 has been also related with anxiety disorders (Attwood et al. 2011). Additionally, EphB1 expression has been related a genetic risk for Parkison's disease (Lin

et al. 2009). Interestingly, mutations in EphA3 have been recently linked to autism, major depressive disorder and schizophrenia (Casey et al. 2012; Castellani et al. 2014; Chang et al. 2014).

Ephs have been also involved in traumatic brain injury (TBI) and spinal cord injury (SCI). EphA4 expression is upregulated after TBI and it seems to be involved in the BBB damage after ischemic injury (Goldshmit and Bourne 2010; Frugier et al. 2012; Chen et al. 2018). EphA4 also seems to inhibit nerve regeneration after SCI, through its interactions with their ligands ephrin-B2 and ephrin-B3 (Duffy et al. 2012; Ren et al. 2013). However, SCI increases the expression of several EphA and EphB genes (Willson et al. 2002).

In summary, the involvement of Eph and ephrins in such a range of human diseases suggests their use as potential therapeutic targets. Indeed, the current main therapeutic EphA strategies are: monoclonal antibodies against Eph receptors, soluble Eph fusion proteins, multi-targeted kinase inhibitors, vaccines and siRNAs (Boyd, Bartlett, and Lackmann 2014).

3. Nrg1/ErbB4 signaling

3.1. Neuregulins

Neuregulins (NRGs) belong to the family of proteins structurally related to the epidermal growth factor (EGF) that regulate cell-cell interactions in multiple organs including the nervous system. Neuregulin 1-4 proteins encoded by *Nrg* genes (*Nrg1*-4) contain an EGF-like domain that is necessary for the binding and activation of their ErbBs receptors (Carraway III et al. 1997; Gassmannl and Lemke 1997; Zhang et al. 1997; Harari et al. 1999). There are several Nrg isoforms for each gene generated by alternative splicing. The best characterized subtype is Nrg1, which has a broad expression in both embryonic and adult tissues, including the nervous system where is expressed in neurons and glial cells. On contrary, Nrg2 and Nrg3 are expressed mainly in adult nervous system whereas Nrg4 is expressed in adult pancreas and skeletal muscle (Busfield et al. 1997; Zhang et al. 1997; Harari et al. 1999). Their structural and patterning expression differences, suggest that they can perform similar or complementary physiological functions. For instance, Nrg1-3 regulate neuronal migration and plasticity by modulating the expression of neurotransmitter receptors (Anton et al. 1997; Rio et al. 1997; Sandrock Jr. et al. 1997; Zhao and Lemke 1998).

Nrg1, the most studied Nrg subtype, encodes six different proteins (I-VI) comprising at least 31 different isoforms in humans. Notably, neuronal activity regulate differentially the expression of each Nrg1 isoform (Liu et al. 2011). In humans, the most abundant Nrg1 types I, II and III contain the EGF-like domain but they differ in their N-terminal region. Nrg1 isoforms are synthesized as membrane associated proteins that are proteolyzed to become mature. Nrg1 type I and II contain an Ig-like domain and a single cleavage site leading to the generation of a soluble and mature Nrg1 that acts in an autocrine/paracrine manner. By contrast, type III Nrg1 contains a cysteine-rich domain (CRD) within its second transmembrane domain, which is processed to generate a N-terminal fragment (NTF) that remains anchored to the membrane allowing the juxtacrine signaling (Cabedo et al. 2002). A second cleavage is responsible of the EGF-like domain release that acts in a paracrine signaling manner, similar as Nrg1 types I and II (Fleck et al. 2013). Specifically, the processing of Nrg1 type III consists of a first cleavage by BACE1 and ADAM10/17 proteases that generates two fragments named CTF and NTF that remain anchored to the membrane, called as CTF and NTF. The Nrg1 type III CTF is then proteolyzed by PS/γ-secretase, resulting in a soluble Nrg1-ß fragment that is released into the luminal space, and an intracellular ICD fragment. Otherwise, the Nrg1 type III NTF is processed by the signal peptide peptidase-like (SPPL) proteases resulting in the release of a soluble EGF-like

domain (responsible of paracrine signaling), a C-peptide and a N-ICD (Fleck et al. 2016) (**Fig. 11**).

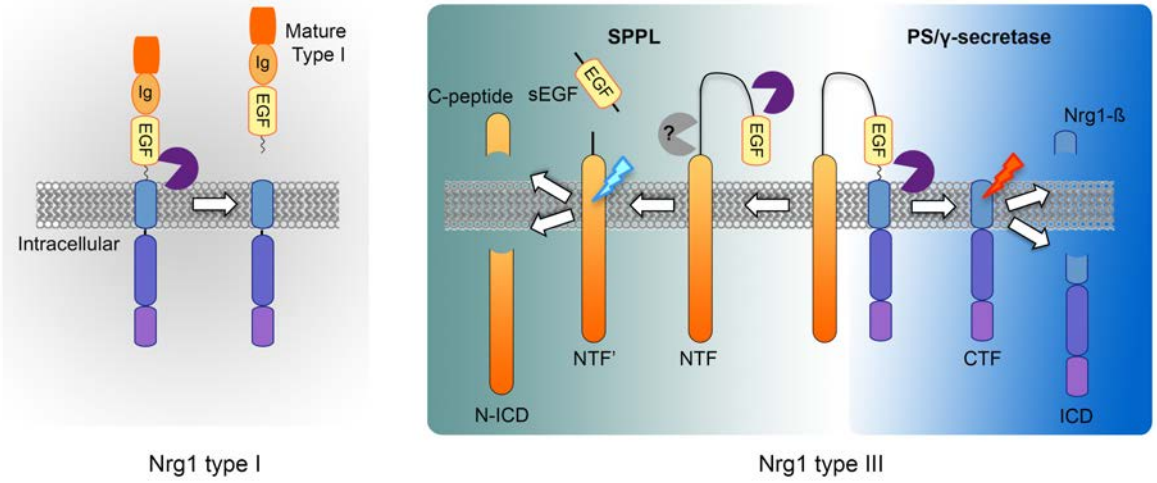

Figure 11. Schematic representation of Nrg1 type I and III structure and processing. Description of molecular domains and Nrg1 processing are explained in detail in the main text.

3.2. ErbB receptors

Neuregulin receptors belong to the family of type I tyrosine kinase receptors ErbB (ErbB1-4), which are structurally related to the epidermal growth factor receptor (EGFR). Nrg1 can bind and activates ErbB3 and ErbB4. On contrary, ErbB1 binds to other ligands as the growth factor EGF whereas ErbB2 is known as a orphan receptor since has no known ligand domain (Burden and Yarden 1997).

The structure of ErbB receptors consists of an ectodomain with two ligand binding domains (also known as cysteine-rich domains), two Furin-like domains, a single TM domain, and a cytoplasmic tail that contains the tyrosine kinase domain and the pseudo kinase domain. Noteworthy, ErbB3 lacks the kinase domain whereas ErbB4 is the only Nrg-bound receptor that can act as an homodimer (Junttila 2000; Holbro and Hynes 2004). Furthermore, ErbB2 is the preferred partner for heterodimerization once ErbB3 and/or ErbB4 are Nrg1-bound (Graus-Porta 1997) (**Fig. 12**).

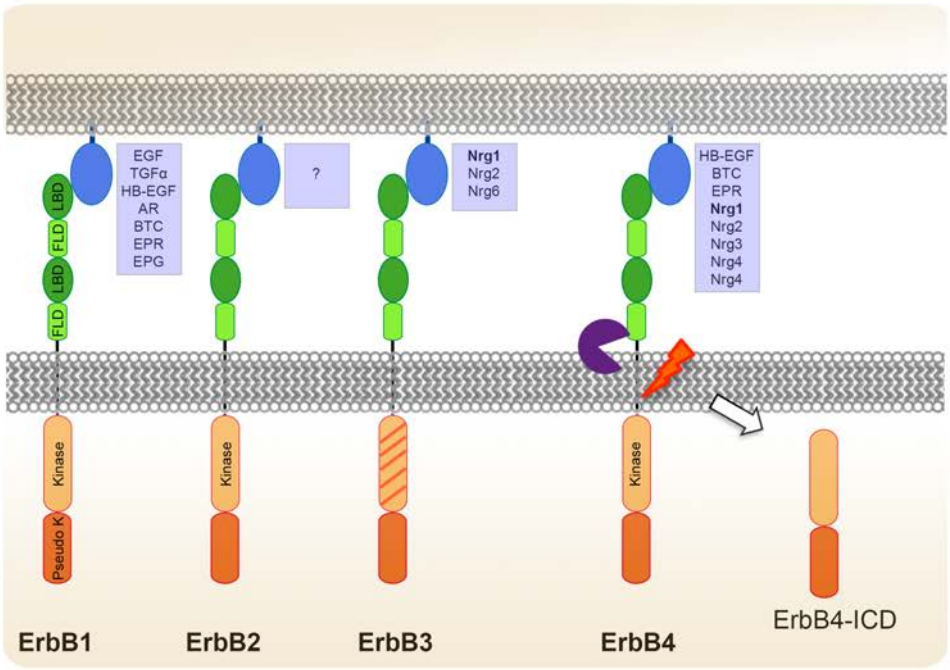

Figure 12. Structure of ErbB1-4 receptors. The scheme also shows the proteolytic processing of ErbB4 JM-a by TACE (represented by a Pacman drawing) and by PS/g-secretase (indicated by the lightning).

Interestingly, ErbB4 undergoes alternative splicing in both the JM and cytoplasmic (Cyt) domains. Regarding the JM domain, the most abundant isoforms in brain are JM-a and JM-b as a result of alternative splicing in exons 16 and 15b, respectively. When ErbB4 JM-a is bound to a ligand, is cleaved first by TNF-α converting enzyme (TACE) and then by the γ-secretase complex, generating the ErbB4-ICD. This ICD can translocate to the nucleus where it regulates the transcription of certain genes involved in astrogenesis, cell differentiation and proliferation, and apoptosis (Vidal et al. 2005; Naresh et al. 2006; Sardi et al. 2006; Sundvall et al. 2010). Moreover, alternative splicing in the exon 26 give rise to the ErbB4 Cyt1 and Cyt2 isoforms (Zeng et al. 2009; Veikkolainen et al. 2011).

All ErbB receptors are present in germinal zones of the developing rodent brain and their expression is reduced in the adulthood (Seroogy et al. 1995; Kornblum et al. 2000). However, the expression of each receptor type differs in the brain region and the cellular type, indicating that they may play distinct roles during the brain development and adulthood (**Table 2**) (Iwakura and Nawa 2013).

Table 2. Region- and cell type-specific ErbB1-4 expression in the brain and their functions. Adapted from (Iwakura and Nawa 2013)

Receptor	Tissue	Cell Type	Function
ErbB1	Subventricular zone	Neural stem cell	Proliferation/ migration
	Midbrain	Dopaminergic neuron	Survival/ development
	Cortex, hippocampus	GABAergic neuron	Regulation of synaptic function
		Astrocyte	Proliferation/ differentiation
	Cerebellum	Purkinje cell Granule cell, Astrocyte	Development/ proliferation
	Pituitary gland	Lactotroph	Production/release of cortisol and prolactin
ErbB2	Cerebellum, cortex, hippocampus, midbrain, etc.	Oligodendrocyte Astrocyte Radial glia	Proliferation/ differentiation
ErbB3	Cortex, hippocampus, etc.	Oligodendrocyte	Maturation/ myelination
ErbB4	Cortex, hippocampus	GABAergic neuron	Attenuates synaptic function
		Astrocyte Oligodendrocyte	Proliferation/ differentiation
	Cerebellum	Granule cell	Regulation of synaptic function
	Midbrain	Dopaminergic neuron	Survival, attenuates synaptic function

The binding of Nrgs to ErbB3 and ErbB4 induce its homo- (in the case of ErbB4) or heterodimerization, leading to the phosphorylation of the partner receptor and transduction of signaling pathways that are modulated by positive and negative signals. In fact, ligand binding to ErbB receptors usually causes down-regulation of these receptors by endocytosis or lysosomal degradation (Cao et al. 2007; Omerovic et al. 2007), although it seems that down-regulation mechanisms are more specific of ErbB4 (Sundvall et al. 2008).

3.3. Nrg1-ErbB4 signaling pathway

The Nrg1-ErbB4 signaling can also be retrograde (when it is transduced in the cell containing the Nrg1, as a result of the proteolytic processing of this ligand) or forward (when the signal it is transduced to the cell containing the ErbB receptors). Classically, Nrg1-ErbB4 transduces the signal by activating PI3K/Akt and Ras/MAPKs cascades but also can interact with PDZ-containing proteins or ubiquitin ligases (**Fig. 13**). In schwann cells, the activation of PI3K/Akt signaling induces the expression of myelin protein zero (P0) (Suzhen Chen et al. 2006), activates several transcription factors involved in myelinization like Oct6 (Leimeroth et al. 2002) and induces cholesterol and fatty acid biosynthesis pathways (Porstmann et al. 2005). In addition, the activation of MAPK cascade induces cell proliferation by the regulation of c-fos gene expression (Eto et al. 2010). As an alternative signalling, binding of Nrg1 to ErbB4 not only activates downstream pathways but also cleaves the ErbB4 receptor generating the ErbB4-ICD that upon nuclear translocation regulates transcription.

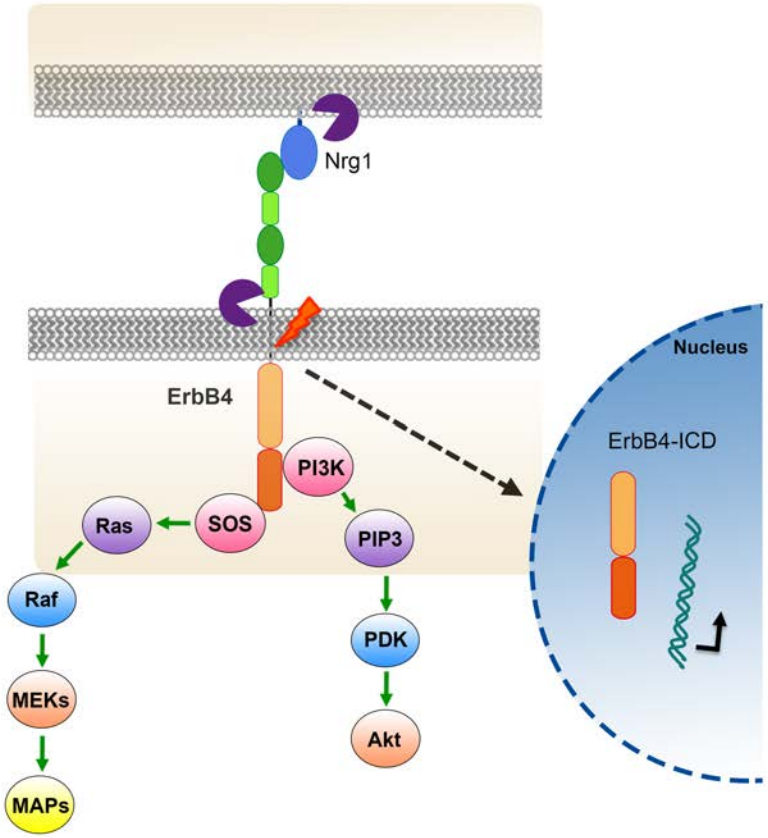

Figure 13. Nrg1-ErbB4 signaling pathways. The scheme shows the two main signaling pathways (i.e, PI3K and Ras) downstream of Nrg1-ErbB4 activation. Alternatively, PS/g-secretase

dependent-cleavage of ErbB4 generates the ErbB4-ICD, which translocates to the nucleus to regulate gene expression.

In neurons, the main cellular responses activated by Nrg1-ErbB4 signaling are related to myelination, regulation of proliferation, migration, and synaptogenesis.

Nrg1-ErbB pathway differentially regulates the myelination process in both the peripheral nervous system (PNS) and the CNS. In the PNS, Nrg1-ErbB4 pathway plays an essential role in cell survival, proliferation and differentiation of Schwann cells. Schwann cells, which are the main glial cell in the PNS, form the myelin sheath around the axons. The two main Nrg1-ErbB-dependent signaling pathways involved in Schwann cells functions are MAPK and PI3K. Thus, the balance between them determines the level of differentiation of Schwann cells (Michailov 2004; Jessen and Mirsky 2005; Taveggia et al. 2005; Stassart et al. 2013). In addition, it has been recently reported that cAMP increases the expression of ErbB receptors in Schwann cells leading to maintained activation of Nrg1-dependent signaling (Monje, Bartlett Bunge, and Wood 2006). On the other hand, oligodendrocytes in the CNS carry out the myelination process. Interestingly, Nrg1 is also involved in development and maturation of oligodendrocytes and myelination, although is not clear whether regulates myelin sheath thickness (Schmucker et al. 2003; Sussman 2005; Roy et al. 2007; Taveggia et al. 2008; Brinkmann et al. 2008).

The Nrg1-ErbB4 pathway is also involved in neuron development and migration. First, Nrg1 promotes neurite growth and regulates motoneuron survival (Mòdol-Caballero et al. 2018). Nrg1-ErbB4 modulates dendritogenesis by affecting RhoGTPase activity (Van Aelst and Cline 2004; Rieff and Corfas 2006; Cahill et al. 2013). Moreover, Nrg1-ErbB4 signaling plays a role during the migration of cortical interneurons along radial glial cells (Flames et al. 2004; Li et al. 2012).

Finally, Nrg1-ErbB4 signaling regulates glutamatergic synaptic transmission at both presynaptic and postsynaptic levels (Zhong et al. 2008; Jiang et al. 2013; Zhong et al. 2017). It induces the expression of GABA, NMDA and acetylcholine (ACh) receptors (Ozaki et al. 1997; Rieff et al. 1999; Liu et al. 2001). Thus, the activation of Nrg1-ErbB4 signaling reduces the NMDAR-mediated currents through the PLC/IP_3R/Ca^{2+} and Ras/Mek/ERK signaling, which in turns modulate the endocytosis of NMDAR in an actin-dependent manner (Gu 2005). Other studies show that Nrg1-ErbB4 signaling has a negative impact on LTP by reducing AMPAR expression and favouring GABA release (Kwon 2005; Chen et al. 2010; Wen et al. 2010). Moreover, Nrg1-ErbB4 signaling also

contributes to the maturation and plasticity of glutamatergic synapses and regulates cognition (Li et al. 2007; Krivosheya et al. 2008; Ledonne et al. 2018). A recent study using specific genetic deletion of ErbB4 in interneurons indicates that Nrg1-ErbB4 signaling is also involved in the excitatory synaptogenesis on cortical interneurons (Ting et al. 2011). Interestingly, Nrg1-ErbB4 signaling also participates in the regulation of GABAergic synaptic transmission through presynaptic ErbB4 receptors and is required for maintaining GABAergic activity in the amygdala (Woo et al. 2007; Lu et al. 2014).

3.4. Role of Nrg1/ErbB4 signaling in pathogenesis

Nrg1-ErbB4 signaling has been related to multiple disorders of the nervous system (Corfas, Roy, and Buxbaum 2004; Mei and Xiong 2008; Shamir et al. 2012; Mei and Nave 2014; Zhang et al. 2017). First, several mutations in the Nrg1 and ErbB4 genes are linked to schizophrenia, as the V322L mutation in Nrg1 type III, which reduces the generation of both Nrg1-ß peptide and ICD (Yang et al. 2003; Norton et al. 2006; Walss-Bass et al. 2006; Marballi et al. 2014). Similarly, BACE1$^{-/-}$ mice exhibit a reduction in the binding of ErbB4 to postsynaptic density protein 95 (PDS95) and a schizophrenia-like behaviour, suggesting that alterations in the BACE1-dependent Nrg1/ErbB4 signaling are related to the pathogenesis of schizophrenia (Savonenko et al. 2008; Hu et al. 2016). Indeed, several studies performed in schizophrenia post-mortem brains, show altered Nrg1 processing and increased Nrg1-ErbB4 signaling that attenuates the NMDAR-mediated response (Hahn et al. 2006; Marballi et al. 2012).

Since Nrg1-ErbB4 signaling has an essential role controlling synaptic functions, an imbalance in this signaling has been proposed to contribute to Alzheimer's disease pathogenesis. In fact, single nucleotide polymorphisms (SNPs) have been related to an increased risk of AD (Go et al. 2005). Indeed, ErbB4 levels are increased in AD brains compared to controls (Woo et al. 2011). Interestingly, a recent study reported that Nrg1 improves synaptic loss in an Alzheimer's disease mouse model (Xu et al. 2016).

Other studies have also reported a relationship between altered Nrg1-ErbB4 signaling and Parkinson's disease (Depboylu et al. 2012), bipolar disorder (Thomson et al. 2007; Goes, Sanders, and Potash 2008; Prata et al. 2009; Zuliani et al. 2011), epilepsy (Zhu et al. 2017) and amyotrophic lateral sclerosis (Takahashi et al. 2013).

4. Presenilin/γ-secretase

Presenilins (PS) are the founding members of the family of intramembranous aspartyl proteases. In humans, the *PSEN1* (chromosome 14) and *PSEN2* (chromosome 1) genes encode for PS1 and PS2 proteins, respectively. The amino acid sequence and structure of PS1 and PS2 are very similar. The main accepted model for PS structure was based on eight-TM topology with 8-10 hydrophobic domains, although a seven-TM topology was also proposed. However, in 2005, it was proposed a nine-TM domain model, where the hydrophilic N terminus is located in the cytosol and the C terminus in the lumen of the endoplasmic reticulum. In this model, in the hydrophobic domains TM6 and TM7 are located two catalytic residues, Asp 257 and Asp 385 that lead to the catalytic site of presenilins (Wolfe et al. 1999; Laudon et al. 2005). Although, PS are synthesized as precursor proteins of 50 kDa, to become active they undergo endoproteolytic cleavage within the cytoplasmic loop between TM6 and TM7, resulting in a N terminal fragment (NTF) of 27-28 kDa and a C terminal fragment (CTF) of 17-18 kDa that remain associated between them (Thinakaran et al. 1996; Saura et al. 1999) (**Fig. 14**).

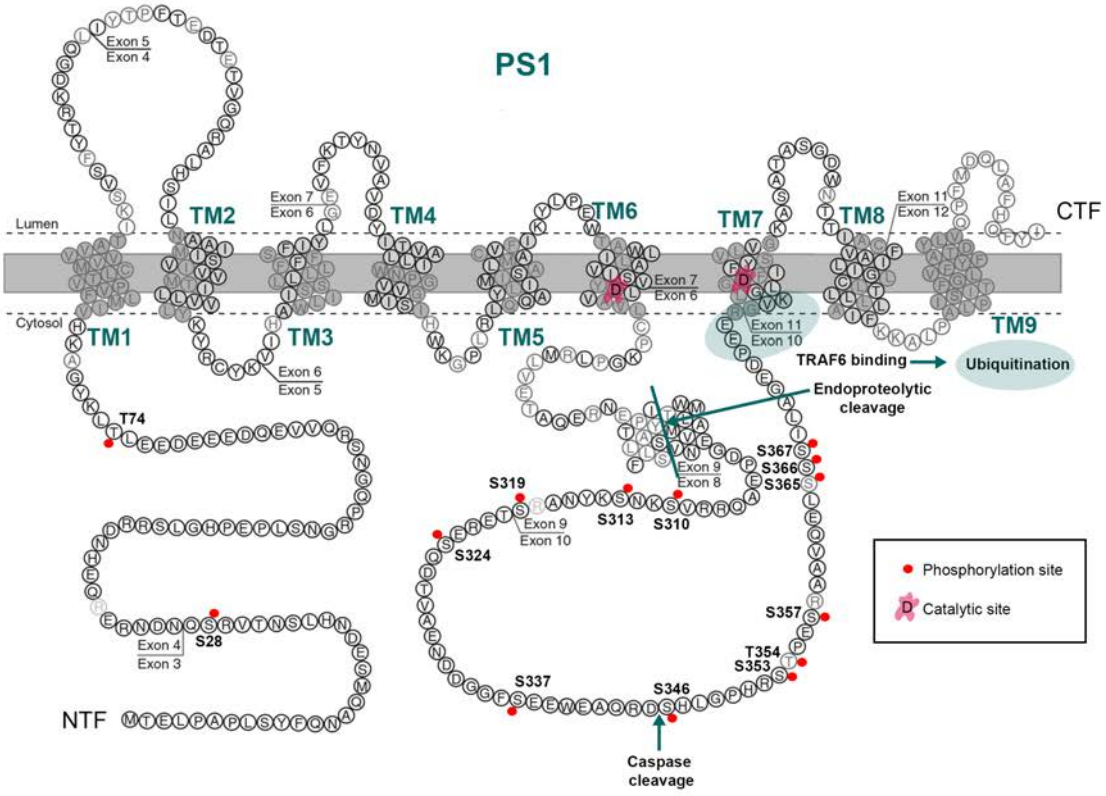

Figure 14. Presenilin structure and post-translational modifications. Nine-TM domain model for PS1. Asp-257 and Asp-358 are represented in pink and phosphorylation sites with a red point. Modified from (De Strooper, Iwatsubo, and Wolfe 2012).

Besides endoproteolysis, multiple post-translational modifications as caspase cleavage, phosphorylation and ubiquitination have been shown to modulate the function of presenilins (Duggan and McCarthy 2016). It has been reported that presenilins are phosphorylated by protein kinase A (PKA), PKC, GSK-3ß, c-Jun N-terminal kinases (JNK) and Cdk5 (Kirschenbaum et al. 2001; Lau et al. 2002; Fluhrer et al. 2004; Matz et al. 2015). Interestingly, the role of phosphorylation in Ser367 is controversy since both increase and reduction of Aß levels have been reported (Bustos et al. 2017; Maesako et al. 2017). Additionally, it has recently described that PS1 can be polyubiquinitated through its binding with TRAF6, leading to PS1 stabilization and regulation of Ca^{2+} release (Powell et al. 2009; Yan, Farrelly, and McCarthy 2013).

4.1. γ-secretase complex and substrates

PS are the catalytic subunit of the γ-secretase complex, which belongs to the family of intramembrane cleaving protesases (IClips). For γ-secretase complex to become mature, is required the recruitment in the complex of anterior pharynx-defective-1 (Aph-1), presenilin enhancer-2 (Pen-2) and nicastrin (Nct) with 1:1:1:1 stoichiometry, plus the endoproteolytic cleavage of PS. Taking into account that both PS and Aph-1 have two isoforms (PS1/PS2 and Aph-1a/Aph-1b) and that Aph-1 can also suffer alternative splicing, six different γ-secretase complexes with different biological functions exist (Lai et al. 2003; Shirotani et al. 2004). Pen-2 is a small hairpin-like protein of ~12 kDa with three-TMD, although the first two only crosses half the membrane (Zhang, Yu, and Sisodia 2015). Recent evidences show that Pen-2 is necessary for endoproteolysis of PS to takes place (Ahn et al. 2010; Takasugi et al. 2003). Aph-1, in turn, is a ~25 kDa protein with seven-TMD that seems involved in presenilin stabilization and γ-secretase activity (Takasugi et al. 2003). Finally, nicastrin is a type I membrane glycoprotein of ~130 kDa that seems to act as a scaffold for the γ-secretase complex and as substrate-recognizing subunit (Shah et al. 2005; Zhang et al. 2012) (**Fig. 15**).

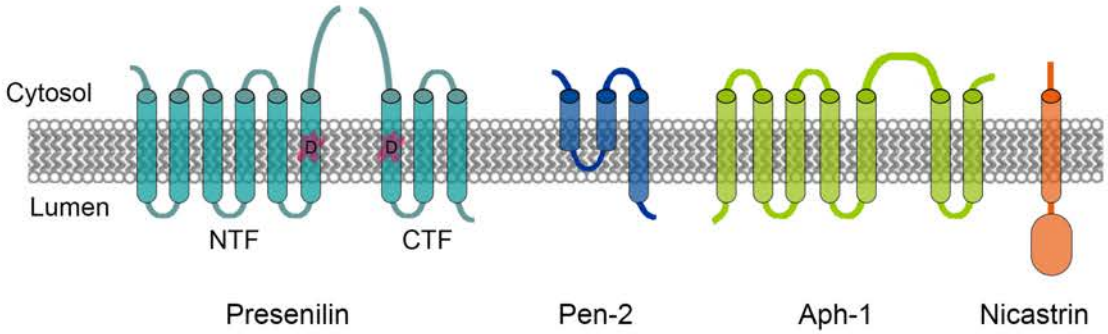

Figure 15. Representation of PS/γ-secretase complex structure. Catalytic Asp residues in Presenilin are indicated in pink.

Assembly of PS/γ-secretase complex occurs in a three-step sequential recruitment of the above-mentioned proteins. The first subcomplex begins with the binding of nicastrin and Aph-1. Then, presenilin binds to this complex, and finally, Pen-2 joins to it, turning the complex active. While, the formation of the complex seems to occurs in the ER, growing evidences show that the activation takes places in vesicles of the Golgi apparatus (Kim et al. 2007). Interestingly, the composition of the lipid bilayer plays a role in the activation of γ-secretase complex and also in its proteolytic function (Osenkowski et al. 2008; Aguayo-Ortiz, Straub, and Dominguez 2018). Modulation of γ-secretase activity occurs through interaction with GSAP and Hif-1a proteins (He et al. 2010; Villa et al. 2014). Furthermore, some groups have reported that gender also influences γ-secretase activity. In particular, in mice, the γ-secretase activity is much higher in females than males in aged brains (Placanica, Zhu, and Li 2009). Finally, some molecular mechanisms as ligand-binding or calcium influx may affect also the PS/γ-secretase-dependent processing of some substrates (Mumm et al. 2000; Litterst et al. 2007).

Once the γ-secretase complex is assembled and become active, it can then initiate the catalytic processing activity. The amyloid precursor protein (APP), which generates the amyloid-ß peptide that accumulates in AD brain, was the first PS/γ-secretase reported substrate. Currently, more than 90 substrates have been identified (Lleó and Saura 2011). Despite the fact that there is no identical consensus cleavage sequence, these proteins share several features: 1) they are type-I transmembrane proteins; 2) prior to the γ-secretase activity, their ectodomain must be shed, usually by a disintegrin and metalloprotease (ADAM) enzyme resulting in the generation of CTFs; 3) γ-secretase-dependent cleavage must occurs near the border of the transmembrane; 4) PS/γ-secretase processing leads to the generation of an intracellular domain fragment (ICD), which is degraded by the proteasome and/or translocates into the nucleus; and 5) the

inactivation of PS/γ-secretase complex leads to accumulation of CTFs and prevents the generation of ICD (Haapasalo and Kovacs 2011). In summary, the process that involves the PS/γ-secretase processing consists in a previous cleavage of the ectodomain by a metalloprotease-like proteinase as ADAM-10/17 (also called TACE) or ß-secretase (BACE). This ectodomain is usually released from the cell surface as a soluble protein and a CTF fragment remains anchored to the membrane. Then, the PS/γ-secretase complex is able to process the CTF on the cellular membrane or in endosomes (Urra et al. 2007). Accordingly to the most accepted model PS/γ-secretase complex proteolyzes sequentially the substrates in multiple sites of the TMD, resulting finally in the release of an intracellular domain (ICD) fragment. In some substrates, the presence of this multiple cleavage sites, results in various cleaved products.

Among the already identified substrates of PS/γ-secretase complex are the following: APP or Amyloid precursor-like proteins (APLP); Notch receptors and their ligands; Low Density Lipoprotein (LDL) Receptor-related proteins as ApoER2; and cell adhesion proteins as cadherins, Ephs and ephrins, and ErbBs. Unfortunately, the physiological function of many of the resulting cleavage products is still largely unknown (**Fig. 16**) (Lleó and Saura 2011).

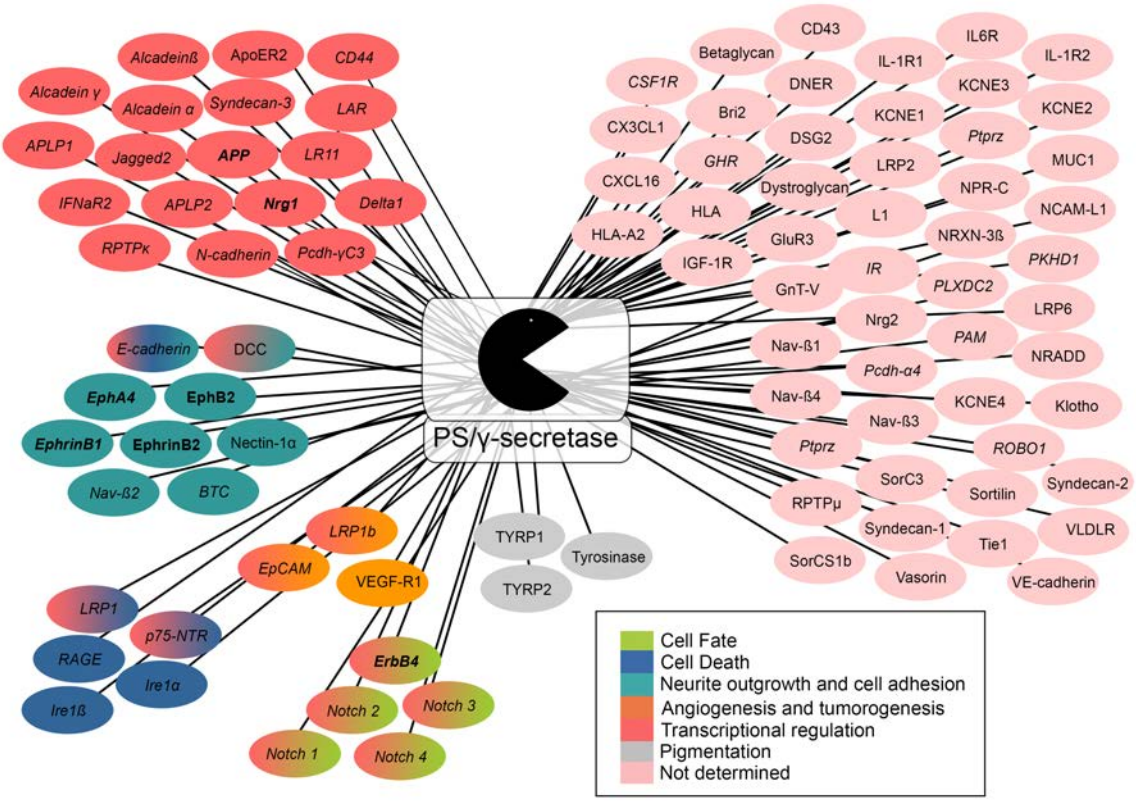

Figure 16. Identified PS/γ-secretase substrates classified according to their function. Those substrates whose γ-secretase cleavage products are found in the nucleus are indicated *in italics*.

Abbreviations: APLP, amyloid-protein precursor-like protein; ApoER2, apolipoprotein E receptor 2; APP, amyloid precursor protein; BTC, betacellulin; CSF1R, colony-stimulating factor 1 receptor; CX3CL1, fractalkine; DCC, deleted in colorectal cancer; DNER, delta/notch-like EGF repeat containing; DSG2, desmoglein 2; EpCAM, epithelial cell adhesion molecule; GHR, growth hormone receptor; GluR3, glutamate receptor; GnT-V, N-acetylgluco-saminyltransferase V; HLA, human leukocyte antigen; IFN, interferon; IGF, insulin-like growth factor; IL, interleukin; IR, insulin receptor; Ire1, inositol requirement 1; KCNE, voltage-gated potassium channel -subunit; LAR; leukocyte-common antigen related; LRP, low-density lipoprotein receptor; MUC1, mucin 1; Na_V, voltage-gated sodium channel; NPR-C, natriuretic peptide receptor C; NRADD, neurotrophin receptor alike death domain protein; NRXN, neurexin; NTR, neurotrophin receptor; PAM, peptidylglycine-amidating monooxygenase; Pcdh, protocadherin; PKHD1, fibrocystin; PLXDC2, plexin domain-containing protein 2; Ptprz, protein tyrosine phosphatase, receptor type z; RAGE, receptor for advanced glycation end products; ROBO, roundabout; RPTP, receptor-like protein tyrosine phosphatase; SorCS, sortilin-related VPS10 domain containing receptor; Tie1, Tyrosine kinase with immunoglobulin-like and EGF-like domains 1; TYRP, tyrosinase-related protein; VEGF, vascular-endothelial growth factor; VLDLR, very low density lipoprotein receptor.

In particular, the PS/γ-secretase-dependent processing of APP occurs through two different pathways depending whether Aß is generated (amyloidogenic pathway), or not (non-amyloidogenic pathway). The amyloidogenic pathway starts with the initial processing of APP through ß-secretase, which releases a soluble fragment (sAPPß) and an intramembranous APP carboxy-terminal fragment (APP-CTF). Then, this APP-CTF is cleavage by PS/γ-secretase in the ε site (residues 48-49, the closest region to cytoplasmic membrane), releasing the APP ICD (AICD) into the cytosol, which can then translocate to the nucleus. Similarly, PS/γ-secretase also proteolyzes the remaining substrate every three amino acids from ζ site (residues 45-46) to the γ site (residues 40-43), leading to the generation of Aß peptides of different lengths. On the other hand, APP can also be proteolyzed by α-secretase through the non-amyloidogenic pathway resulting in the generation of two fragments: APPsα and α-CTF. Then, PS/γ-secretase cleaves the α-CTF to generate two fragments: the P3 peptide and the AICD (Gu et al. 2001; Sastre et al. 2001; Weidemann et al. 2002; Zhao et al. 2004).

4.2. Biological functions of presenilin/γ-secretase

4.2.1. PS/γ-secretase-dependent cell signaling

The full length proteins and the cleavage products resulting from the PS/γ-secretase processing usually perform different functions. In many cases the ICDs translocate to the

nucleus where regulate gene transcription. Some reported examples are: AICD (APP), CD44-ICD, DCC-ICD, Notch-ICD, E and N-cadherin-ICD, receptor-like protein tyrosine phosphatases (RPTP), leukocyte-common antigen related (LAR) and ß-subunits of the voltage-gated sodium channels (Na_vß) among others (Haapasalo and Kovacs 2011).

PS/γ-secretase signaling is also involved in the regulation of cell fate. In this context, the PS/γ-secretase-dependent processing of Notch leads to the release of Notch-ICD, which regulate gene transcription pathways involved in cell differentiation and maintenance of stem cell populations (Strooper et al. 1999). Similarly, the ErbB4 ICD (E4ICD) regulates cell fate determination in the brain, specifically regulates the maturation of oligodendrocytes and astrogenesis (Lai and Feng 2004; Sardi et al. 2006). Furthermore, the generation of E4ICD is also implicated in the regulation of tumorigenesis, since it has pro-apoptotic activity and it increases the levels of the anti-apoptotic protein p53 (Arasada and Carpenter 2005; Vidal et al. 2005).

The p75 neurotrophin receptor ($p75^{NTR}$), which usually mediates cell survival, is also a substrate of PS/γ-secretase complex. By contrast, the generation of the p75-ICD is involved in apoptotic events in neurons, through the ubiquitination and nuclear translocation of neurotrophin receptor interacting factor (NRIF) (Kenchappa et al. 2006).

Some Ephs and ephrins have been also reported to be PS/γ-secretase substrates, and their cleavage products are involved in the regulation of neurite outgrowth and cell adhesion. Binding of ephrin-B2 to EphB2 results in the PS/γ-secretase-dependent processing of the ligand. This consists in a initial cleavage of the ectodomain by a metalloprotease, generating a membrane bound CTF1 that is then proteolyzed by PS/γ-secretase, producing a soluble CTF2. This processing is related to Src activation, which is involved in the rearrangement of cytoskeleton and the modulation of neuritogenesis and migration (Georgakopoulos et al. 2006). EphB2, in turn, can also be proteolyzed by PS/γ-secretase. In this case, the signaling derived of this processing will differ depending on whether it is ligand-dependent or -independent. In the first case, the ectodomain cleavage occurs in the endosomes, which stimulates the ubiquitination of EphB2 receptors and its degradation. In contrast, the ligand-independent processing of EphB2 takes place in the plasma membrane and depends on the calcium influx and NMDA activation (Litterst et al. 2007). Finally, PS/γ-secretase-dependent processing of EphA4 is regulated by synaptic activity. The generated EphA4-ICD fragment then translocates to the nucleus contributing to the formation and maintenance of dendritic spines (Inoue et al. 2009).

4.2.2. Presenilin-1 in neuronal development

PS1 is ubiquitously expressed in most tissues, including developing and adult brain, although the expression is higher in embryonic than adult brain. In the developing brain, PS1 is mainly expressed in the ventricular zone, whereas in the adult brain, the higher levels are found in the hippocampus and entorhinal cortex (Lee et al. 1996).

The lack of PS1 expression during brain development causes a loss of neural progenitor cells, first in the ventricular zone and then in the subcortical region, leading to a reduction in the number of neurons through the regulation of neuronal differentiation (Shen et al. 1997; Handler, Yang, and Shen 2000). In fact, *PS1* knockout mouse embryos develop shortened tails and rostro-caudal body axes, as well as cranial hemorrhages that contribute to their unviability and subsequent premature death (Shen et al. 1997). Additionally, PS1 is also involved in the regulation of neuronal migration and morphogenesis of the cerebral cortex and radial glial generation (Louvi 2004). Thus, PS1 inactivation in the postnatal forebrain also causes deficits in long-term spatial memory (Yu et al. 2001). Similarly, the inactivation of both PS also in the postnatal forebrain leads to impairments in hippocampal synaptic plasticity and memory and neurodegeneration, which worsen with aging in a PS dose-dependent manner (Saura et al. 2004a; Watanabe et al. 2014). All these results indicate that PS1 play essential roles in both the developing and adult brain by regulating different physiological, differentiation and survival mechanisms.

In addition, PS1 also regulates Notch signalling during neuronal development (Strooper et al. 1999). Notch-1 is an immature type I transmembrane protein that needs to be cleaved by a furin-like convertase (FLC) at the cleavage site 1 (S1) in the Golgi during its trafficking to the cell surface in order to become mature (Logeat et al. 1998). Then, when ligand binding occurs, the region next to the membrane is susceptible to be cleaved by an ADAM metalloprotease at the S2 site. This ectodomain shedding generates a C-terminal fragment (NEXT) that is then proteolyzed by PS/γ-secretase complex at the S3 site, leading to the generation of a NICD fragment. NICD translocates to the nucleus where it acts as a transcriptional factor involved in regulation cell fate during development (Louvi and Artavanis-Tsakonas 2006). In turn, the activity of NICD can be regulated through the action of ubiquitin ligases that control the state of Notch signalling to continue the signal or to undergo proteosomal degradation (Guruharsha, Kankel, and Artavanis-Tsakonas 2012). The transduction of downstream signalling pathways involves the interaction between NICD and CSL DNA-binding proteins. In basal conditions, the DNA-binding

adaptor CSL, interacts with some proteins as histone deacetylases (HDACs) favouring a more condensed chromatin conformation that prevents the transcription. In contrast, when NICD translocate to the nucleus, NICD binds to CSL and other proteins as histone acetyltransferases (HATs), which relax the chromatin, allowing the transcription of target genes (Kopan and Ilagan 2009; Kopan 2012). The family of HES proteins (HES1 and HES5 in mammals) are crucial effectors of Notch signalling pathway. Indeed, HES transcription factors regulate the expression of genes involved in cell-fate decision, as apoptosis, proliferation and differentiation (Kageyama and Ohtsuka 1999). Interestingly, the Notch ligands Delta-like and Jagged are substrates of PS/γ-secretase, adding an additional level of regulation of Notch signalling (Ikeuchi and Sisodia 2003).

4.2.3. Role of PS/γ-secretase in Alzheimer's disease

Alzheimer's disease (AD) is the most common cause of dementia worldwide. There are two forms of AD: sporadic (SAD), that accounts for most of the cases and appears in people after age of 65; and familial (FAD), that represents less than 5 % of all cases and affects people younger than 65 years (Holtzman, Morris, and Goate 2011). FAD is an inherited autosomal dominant disease where mutations in APP and PS genes account for most cases. To data, a total of 230 mutations have been described for *PSEN1* and 39 for *PSEN2 (Alzheimer Disease and Frontotemporal Dementia Mutation Database).*

PS/γ-secretase cleaves APP, leading to the generation of Aβ of different length, mainly Aβ40. These mutations normally cause a partial loss of PS function, enhancing the generation of Aβ42 peptides or favouring the ratio of Aβ42 to Aβ40. Aβ42 is more easily to aggregate into amyloid plaques that are present in the brains of AD patients (Scheuner et al. 1996). Although it is still unclear how Aβ induces neurodegeneration, growing evidences indicate that the soluble aggregated Aβ forms rather than the amyloid plaques are the major cause of synaptic dysfunction in AD (Danysz and Parsons 2012). It is thought that Aβ inhibits long-term potentiation (LTP) and favours long-term depression (LTD) in hippocampal neurons (Walsh et al. 2002; Shankar et al. 2007; Li et al. 2009). These defects also correlate with loss of dendritic spine density (Hsieh et al. 2006; Shankar et al. 2008). In addition, some FAD mutations are related to a disruption of Ca^{2+} signalling since they can affect the generation of the AICD which in turn regulates the transcription of some genes involved in Ca^{2+} homeostasis (Hamid et al. 2007). For these reasons, several preclinical studies are focus on developing therapies based on γ-secretase inhibitors. Although they

usually are very toxic and none of them have resulted successful to date, the development of these compounds is still one of the main therapeutically strategies used against AD. Notably, it has been recently described that γ-secretase inhibition causes an increase in PS1 as a rebound effect, indicating that this and other considerations has to be carefully taken into consideration when using these therapies (Sogorb-Esteve et al. 2018).

Besides the well established role of PS/γ-secretase on APP cleavage in AD pathology, the relevance of this processing in other substrates in AD are currently still unknown.

OBJECTIVES

The objectives of this doctoral thesis are:

Objective 1: To study the mechanisms of EphA3 processing by PS/γ-secretase and metalloproteases

Objective 2: To investigate the biological role of the EphA3 intracellular domain (ICD) on axon growth in cultured neurons and brain

Objective 3: To identify EphA3 ICD interacting proteins that modulate axon growth

Objective 4: To analyse PS/γ-secretase-dependent Nrg1/ErbB4 signaling in the brain

MATERIALS AND METHODS

1. Mouse models

Mouse colonies were maintained at the Animal Core facility of the Universitat Autònoma de Barcelona, on a 12 h light/dark cycle with food and water available ad libitum conditions. Animal experimental procedures were conducted according to the Animal and Human Ethical Committee of the Universitat Autònoma de Barcelona (protocol CEEAH 2896; DMAH 8787) following the European Union guidelines (2010/63/EU).

1.1. PS1 knockout mice

$PS1^{-/-}$ mice were generated in the laboratory of Dr. Susumu Tonegawa at Harvard Medical School as previously described (Shen et al., 1997). The genetic background of all mice was C57BL6/129 hybrid. As the absence of *PS1* is embryonic lethal due to CNS haemorrhages, we only used $PS1^{-/-}$ hippocampal or cortical neurons for *in vitro* experiments. The $PS1^{-/-}$ neurons were obtained by crossing heterozygous ($PS1^{+/-}$) mice. The phenotypic differences between the $PS1^{-/-}$ (cerebral haemorrhages and shortened tails) and the $PS1^{+/+}$ and/or $PS1^{+/-}$, allows us to differentiate them. However, the genotype of cultured neurons was further confirmed by PCR.

1.2. Brain-specific *PS* conditional double knockout (PS cDKO) mice

To overpass the lethality of $PS1^{-/-}$ mice we use the PS cDKO mice. These animals were generated in the laboratory of Dr. Jie Shen at Harvard Medical School as previously described (Saura et al., 2004). Briefly, PS cDKO mice were generated by crossing *PS1* floxed/floxed;CaMKIIα-Cre *(PS1* cKO) and $PS2^{-/-}$ mice (Steiner et al., 1999; Yu et al., 2001). The inactivation of PS1 is restricted to excitatory neurons of the postnatal forebrain starting at P18 since Cre-recombinase is mainly expressed under the CaMKIIα promoter. The genetic background of these mice is C57BL6/129 hybrid. PS cDKO mice develop impairments of hippocampal-dependent memory and synaptic plasticity, and age dependent neurodegeneration (Saura et al., 2004).

2. Cell culture

2.1. Cell lines

Human embryonic kidney cell lines (HEK293T) that express the SV40 T-antigen were maintained in supplemented DMEM at 37°C in a humidified 5% CO_2 incubator. Monolayer cultures were washed with PBS pre-warmed at 37°, treated with 0.25% trypsin-EDTA and incubated for 3 min at 37°C. Trypsinisation was stopped by adding supplemented DMEM which was also pre-warmed at 37°C. Cells were spin at 1,000 rpm for 5 min and seeded in the supplemented cultured medium at the required cell density.

Cell culture media and buffers:

Supplemented Dulbecco's Modified Eagle's Medium: DMEM (Sigma Aldrich D5796) supplemented with 10% of fetal bovine serum (FBS; Invitrogen-Gibco 10106-169) and penicillin/streptomycin (5000 U/mL, Life Technologies 15070-063)

Phosphate-buffered saline (PBS) 1X: 136.8 mM NaCl, 2.5 mM KCl, 0.8 mM Na_2HPO_4, 1.47 mM K_2HPO_4, pH 7.4

Tripsin-EDTA, Methyl sulfoxide (DMSO; Sigma)

2.1.1. Transfection of cell lines

HEK 293T cells were cultured at $1.2 \cdot 10^6$ cells in 60 mm dishes or $2.2 \cdot 10^6$ cells in 100 mm dishes. Transfection was performed 24 h after plating using the technique based on the formation of liposomes (Lipofectamine 2000; Invitrogen 11668-019). The DNA-liposome complexes were formed by incubating DNA with Lipofectamine in a 1:2 ratio (for each 1 µg of DNA, 2 µg of Lipofectamine) for 20 min at room temperature in OptiMEM (Invitrogen, 31985-062) supplemented with glutamine (2 mM). Cells were washed with PBS 1X and the plating media was replaced by OptiMEM/glutamine. After the incubation, the DNA-liposome complexes were added into each plate. Transfection media were maintained for 2-3 h at 37°C, and then replaced with regular culture medium (DMEM supplemented with 10% FBS). All cells were lysed 48 h after transfection.

NOTE: the transfection protocol used before MALDI-TOF is explained in detail in section *3.5.1. of Material and Methods.*

2.1.2. Pharmacological treatments

HEK293T cultured cells were treated directly to the medium with γ-secretase, ß-secretase and broad-spectrum metalloprotease inhibitors as indicated in **Table 3**. In the case of combined treatments, DAPT was applied 3h after the metalloprotease inhibitors.

Table 3. Inhibitors of γ-secretase, ß-secretase and broad-spectrum metalloprotease used in this study. The specific targets and used doses are indicated.

Inhibitor	Target	Company (catalog #)	Dose (µm)
N-[N-(3,5-Difluorophenacetyl)-L-alanyl]-S-phenylglycine t-butyl ester (DAPT)	γ-secretase	Sigma (D5942)	5 (alone); 1 (mixed)
(5S)-(tert-Butoxicarbonilamino)-6-fenil-(4R)- hidroxi-(2R)-benzilhexanoil)-L-leuci-L-fenilalaninamida (L-685,458)	γ-secretase	Tocris (2627)	5
Galardin, Ilomastat, N-[(2R)-2-(Hydroxamidocarbonylmethyl)-4-methylpentanoyl]-L-tryptophan methylamide (GM-6001)	MMPs: 1, 2, 3, 7, 8, 9, 12, 14, 26	Enzo (BML-EI300-0001)	25
MMP9/13	MMPs: 1, 3, 7, 9 and 13	Calbiochem (444252)	10
EGCG	ß-secretase	Tocris (4524)	20
SB-3CT	MMPs: 1, 2, 3, 7 and 9. ADAM17/ TACE	Enzo (BML-EI325)	25
1,10-Phenanthroline (1,10-PNT)	ADAMs: 10, 12 and 28	Sigma (131377)	83
Marimastat	MMPs: 1, 2, 7, 9 and 14	Tocris (2631)	20

2.2. Primary neuron culture

Coverslips were previously treated with poly-D-lysine and incubated at 37°C for 24 h. Previous to neuron culture, coverslips were washed twice with PBS. For immunofluorescence experiments, neurons were seeded in 12 mm coverslips (24-well plates) previously treated with 150 µg/ml poly-D-lysine (Sigma; P7658). For biochemical assays, neurons were seeded in 100 mm plates, previously treated with 50 µg/ml poly-D-lysine.

Cortical and hippocampal neurons were obtained from E15.5 $PS1^{+/+}$ and $PS1^{-/-}$ mouse embryos (C57BL6/129 background) obtained from $PS1^{+/-}$ heterozygous crossings. Embryos were placed in a 100 mm diameter dish containing cold PBG. As $PS1^{-/-}$ embryos are slightly smaller, have a defect in the tail development and present cerebral hemorrhages (Shen et al., 1997), we classified the embryos as $PS1^{-/-}$ or controls ($PS1^{+/+}$ or $PS1^{+/-}$). The genotypes of both groups were further confirmed by PCR (Section 4.1.2 of *Materials and Methods*). *Wild-type* neurons were obtained from C57BL/6J inbred mice. Then, brains were extracted, both hemispheres separated and the meninges removed. The dissected cortices and hippocampi were transferred to a tube containing 10 ml of Solution 1 and centrifuged (300 x *g*, 1 min). The pellet was incubated in Solution 2 (trypsin-containing solution) at 37°C for 10 minutes, agitating every 2 minutes. The trypsin reaction was stopped by adding Solution 3 (containing trypsin-inhibitor) and by centrifugation (300 x *g*, 1 min). The pellet that contains the digested tissue was resuspended in the Solution 4 and disrupted using a Pasteur pipette. The cell suspension was filtered with a nylon mesh of 40 µm pore size. Finally, the cell suspension was mixed with Solution 5 and centrifuged (250 x *g*, 5 min). The cell pellet was resuspended in Complete DMEM medium. Cells were stained with trypan blue and counted in a Neubauer chamber. Trypan blue positive cells were excluded from the total. For immunofluorescence experiments, hippocampal neurons were seeded in 24-well plates at $1.5 \cdot 10^4$ cells/cm^2 density, whereas for biochemical assays, hippocampal or cortical neurons were seeded in 35 mm diameter dishes (62,500 cells/cm^2), 6-well dishes (75,000 cells/cm^2) or 60 mm diameter dishes (95,238 cells/cm^2). In all cases, neurons were incubated at 37°C with 5% CO_2 for 2 h. Then, the plating medium was replaced by B27/glutamine-supplemented Neurobasal medium. When neurons were maintained for more than 5 DIV, the culture medium was changed every 4 days by half of the conditioned medium plus fresh medium.

Cell culture media and buffers:

Solution 1: Krebs buffer supplemented with 0.3% bovine serum albumin and 0.03% Mg2SO4

Solution 2: solution 1 supplemented with 0.0025% trypsin

Solution 3: solution 1 supplemented with 0.0056% trypsin inhibitor, 0.008% DNAse and 0.03% MgSO4

Solution 4: solution 1 plus 16% solution 3

Solution 5: solution 1 supplemented with 0.03% MgSO4 and 0.0014% CaCl2

Krebs buffer: 120 mM NaCl, 4.8 mM KCl, 1.2 mM KH2PO4, 25 mM NaHCO3, 14.3 mM Glucose

Complete Dulbecco's Modified Eagle's Medium (DMEM; Sigma Aldrich D5796) supplemented with 10% FBS, 2 mM L-glutamine, 0.6% of glucose and 0.25 mg/ml of penicillin/streptomycin. This medium was only used as plating media.

Neurobasal / B-27: Neurobasal medium (Gibco 211103.049) supplemented with B-27 (Invitrogen; 17504-044), 2 mM L-glutamine, 0.6% glucose and 0.25 mg/ml penicillin/streptomycin. This medium was used for the maintenance of primary neurons.

PBG: PBS (1x) supplemented with 0.6% glucose and 0.25 mg/ml penicillin/streptomycin.

2.2.1. Pharmacological treatments

γ-secretase inhibitor: N-[N-(3,5-Difluorophenacetyl)-L-alanyl]-S-phenylglycine t-butyl ester (DAPT) (250 nM; Sigma #D5942) was added to the B27/glutamine-supplemented Neurobasal medium at 0 DIV. DAPT treatment was renewed at 2 DIV, directly added over the conditioned media.

(±)-Blebbistatin: active blebbistatin inhibitor (20 μM; Calbiochem #203390). Hippocampal neurons were treated at 2 DIV, directly adding *(±)-Blebbistatin* to the cultured medium.

(-)-Blebbistatin: Inactive blebbistatin inhibitior (20 μM; sigma #B0560). As a control, hippocampal neurons were treated at 2 DIV, directly adding the *(-)-Blebbistatin* enantiomer to the cultured medium.

rhNRG1: recombinant Human Neuregulin-1 (rhNRG1; 100 ng/ml). Hippocampal neurons were treated at 6 DIV and 11 DIV directly adding to the cultured medium.

2.2.2. Neuronal transfection

Primary hippocampal neurons were plated in 24-well dishes at density of $3 \cdot 10^4$ cells/well. Transfection was performed 48 h after plating using the technique based on the formation of liposomes (Lipofectamine 2000; Invitrogen 11668-019). The cDNA-liposome complexes were formed by incubating cDNA with Lipofectamine 2000 (in a ratio of 1:0.7, that is for each µg of DNA, 0.7 µg of Lipofectamine 2000) for 20 min at room temperature. In order to preserve the viability of neurons, half of the conditioned medium was kept in a tube at 37°C, and neurons remained with half of conditioned medium plus half of OptiMEM (Invitrogen, 31985-062) supplemented with glutamine (2 mM) during the incubation with the DNA-liposome complexes. Transfection medium was maintained for 1:15 h, and then, discarded. Cells were incubated with culture medium composed of 50% of conditioned culture medium and 50% of fresh culture medium. Hippocampal neurons were fixed and immunolabeled (Section 5.1 of *Material and Methods*).

2.2.3. Lentiviral transduction of neurons

Primary hippocampal neurons were transduced with lentivirus at 1 DIV (for axon growth analysis experiments) or 2 DIV (for biochemical assays). At the moment of the viral transduction, half of the conditioned medium was kept and the neurons were transduced overnight using 2 infective particle/cell. Next day, the medium was replaced by half of the conditioned medium plus fresh Complete Neurobassal medium.

2.2.4. Ephrin-A5-Fc treatment

In order to activate EphA3 receptor, we used the chimera protein ephrin-A5 Fc (R&D Systems; 374-EA). Prior to the treatment, ephrin-A5 Fc ligands were clustered by the incubation of the ligands with an antibody against the human Fc (Jackson Immunoresearch; 109-001-008), following a 1:10 molar ratio (ligand:antibody) for 20 min in agitation at room temperature. The ephrin-A5-IgG clusters were added directly to the cells at 0.18 ng/mm^2 (Lawrenson et al., 2002) for 30 min prior to the cell lysis.

3. Biochemical methods

3.1. Immunoprecipitation and co-immunoprecipitation

For immunoprecipitation (IP) and co-immunoprecipitation (Co-IP) experiments from embryonic brain, the tissue was homogenized in 10 volumes of CHAPS lysis buffer. HEK293T cells were cultured in 100 mm plates ($3{,}5 \cdot 10^4$ cells/cm^2) and transfected with EphA3 (4 µg / plate) 48 h before the lysis. Cells were washed twice with cold PBS in order to remove the remnants of culture medium and mechanically lysed (Potter-Elvehjem glass-Teflon) in CHAPS lysis buffer supplemented with protease and phosphatase inhibitors (Roche). Finally, the pellet was discarded and the supernatant was transferred into a clean tube. Protein concentration was determined with the Pierce™ BCA Protein Assay Kit (Pierce #23225) and the Co-IP assays were performed on the same day, to avoid the freezing of samples and losing protein interactions. The lysates (1.50 µg/µl in a final volume of 500 µl) were incubated with the antibody of interest (1-3 µg) overnight at 4°C in rotation. Next day, the magnetic beads (Dynabeads Protein G) were washed in CHAPS lysis buffer according to the manufacturer's instructions (20 µl/sample). The cleared beads were incubated with the mixture containing the sample plus antibody for 15 min in rotation at room temperature. Then, the tubes were placed in the magnet, the supernatant was discarded and the magnetic bead-antibody-antigen complex was washed (4x, 500 µl *CHAPS lysis buffer).* The last wash was done with only 100 µl of CHAPS lysis buffer and the samples were transferred into a clean tube. Finally, samples were eluted in 30 µl of sample buffer 2X and heated for 5 min at 95°C.

Reagents and Buffers:

CHAPS lysis buffer: HEPES 50 mM pH 7.4, NaCl 100 mM, EDTA 0.1 mM, 1% CHAPS (supplemented with protease and phosphatase inhibitors, and PMSF).

Dynabeads Protein G: # 10004D; LifeTechnologies

3.2. Nuclear fractionation

Whole mouse cortex was washed with PBS in order to eliminate the blood and mechanically homogenized (Dounce-glass) in 2 ml of Buffer A. To separate the cytosolic and membrane fractions (supernatant) from the nuclear pellet, the homogenates were centrifuged (3,000 x *g*, 15 min, 4°C). The pellet was resuspended and homogenised with

the pippete in 400 µl of NHB. Nuclei were obtained by a sucrose gradient that was prepared freshly from Gradient Buffer. The order of sucrose gradients was (from bottom to top): 2 ml of 2.2 M, 2 ml of 2 M, 2 ml 1.8 M, 2 ml of sample 1.6 M (adding 2.2 M sucrose up to 2ml) and 2 ml of 1.4 M. The gradient was ultra-centrifuged (75,000 x *g*, 35 min, 4°C) in a Beckman swing SW41 rotor in a Sorvall Discovery 90 ultracentrifuge. The sucrose gradients were aspirated and the nuclear pellet was resuspended in 125 µl of lysis buffer. Finally, the nuclei were sonicated (15 sec, 4°C) and stored at -80°C.

Buffers:

Buffer A: 10 mM Hepes pH 7.5, 1.5 mM $MgCl_2$, 10 mM KCl, 0.5 mM PMSF, 1 mM $NaVO_4$, 200 mM Sucrose, 25 mM NaF (supplemented with protease inhibitor and PNT)

Gradient buffer (pH 7.4): 10 mM TEA, 10 nM Acetic acid, 1 mM $MgCl_2$, 0.5 mM $ZnCl_2$

Lysis buffer: 150 mM NaCl, 25 mM Tris HCl, 1% NP40, 10% Glycerol (supplemented with 1mM PMSF and protease inhibitor)

NHB: 250 mM Sucrose, 10 mM TEA, 10 nM Acetic acid, 1 mM $MgCl_2$, 0.5 mM $ZnCl_2$ (supplemented with protease inhibitor)

3.3. In vitro γ-secretase assay

This protocol has been described elsewhere (Sastre et al., 2001). Prior to γ-secretase assay, HEK293T cells were cultured in 100 mm plates ($3{,}5 \cdot 10^4$ cells/cm^2) and transfected using Lipofectamine 2000 with EphA3-HA cDNA (4 µg / plate) 48 h before the lysis in hypotonic lysis buffer. Cells were washed twice with PBS and mechanically lysed (Dounce Homogenizer) in hypotonic lysis buffer (500 µl / plate). Cell lysates were centrifuged (1000 x *g*, 15 min, 4°C) and the pellets were discarded. Supernatants were centrifuged (16.000 x *g*, 20 min, 4°C) and pellets (non-purified membrane fraction) were resuspended in assay buffer. The membrane fraction, incubated with vehicle (DMSO) or DAPT (1 µM) at 37°C for 0 – 2h in an Eppendorf ThermoMixer (500 rpm). Then, the tubes were ultra-centrifuged (100,000 x *g*, 1h, 4°C) obtaining the soluble (supernatant, called S100) and the non-soluble (pellet, P100) fractions.

Buffers:

Hypotonic lysis buffer: 10 mM MOPS pH 7.0, 10 mM KCl, supplemented with protease inhibitors

Assay buffer: 150 mM Sodium citrate pH 6.4, supplemented with protease inhibitors

3.4. Electrophoresis and Western blotting

3.4.1. Cell and brain lysis and protein quantification

Mice were euthanized by cervical dislocation and the brain was dissected on ice. For mice embryo brains, embryos were extracted and the brain was obtained. Cortices, hippocampi or whole brain were mechanically homogenized (Dounce-glass) in low-detergent lysis buffer containing protease and phosphatase inhibitors. 1200 µl lysis buffer was used for 1/2 cortices, 400 µl lysis buffer was used for 1/2 hippocampi and 10 volumes of lysis buffer to 1 brain weight for whole embryonic brain. Cells were washed twice with cold PBS in order to remove the remnants of culture medium. Cells were mechanically lysed (Potter-Elvehjem glass-Teflon) in low-detergent lysis buffer supplemented with protease and phosphatase inhibitors (Roche). Cell lysates were incubated on ice for 30 min to solubilize the proteins, and then pre-cleared by centrifugation (10,000 rpm, 10 min, 4°C). Finally, the pellet was discarded and the supernatant was transferred into a clean tube. Protein concentration was determined with the Pierce™ BCA Protein Assay Kit (Pierce #23225). For ectoshedding studies, conditioned media was recollected after 48h of EphA3 transfection and treated with protease inhibitor PMSF (1 mM). Then, cells were removed by centrifugation (1.000 rpm, 5 min, RT) and proteins were concentrated using Amicon® Ultra 10K filters (EMD Millipore; #UFC501024), according to the manufacturer's instructions.

Buffers:

Lysis buffer: 50 mM Tris HCl, pH 7.4, 150 mM NaCl, 2 mM EDTA, 1% NP40, 1 mM PMSF

Protease inhibitor cocktail tablets: #11836145001; Roche

Phosphatase inhibitors: #04906837001; Roche

3.4.2. SDS-PAGE and Western blotting

Same amount of total protein was diluted in Laemmli loading buffer (3x) and heated at 95°C for 5 min and loaded to the polyacrylamide gels (PAGE) (8-12.5%). A molecular weight marker was added in order to identify the proteins of interest. Electrophoresis was

performed at room temperature (20 mA, maximum voltage) in *Running buffer* (1X) and proteins were transferred into a PVDF membrane (Bio-Rad), previously activated with methanol (110V, 500mA; *Transfer buffer* 1X). Lastly, membranes were stained with Ponceau S (Fluka) to verify the presence of protein, which was eliminated with a few washes of distilled water and Tris-buffered saline plus 0,1% Tween (TBS-T).

PVDF membranes were incubated with blocking buffer for 1 hour and washed with TBS-T (3 x 10 min). Membranes were incubated with primary antibody diluted in antibody buffer overnight at 4°C in orbital agitation. Membranes were washed with TBS-T (3 x 10 min) and incubated with secondary antibody conjugated to horseradish peroxidase (HRP; 1:3,000; Pierce) diluted in BSA-blocking buffer (phosphorylated antibodies) or complete blocking buffer (non-phosphorylated antibodies), at room temperature for 45 min and in orbital agitation. Finally, membranes were washed three times for 10 min with TBS-T. Proteins of interest were detected by Chemidoc (Bio-Rad) by a chemiluminescent reaction using luminol (Sigma) and the signal was quantified by Image Lab software (Bio-Rad). If necessary, membrane was stripped in stripping buffer at room temperature for 20 min, washed in TBS-T (10 min x3), blocked in blocking buffer and re-blotted.

Reagents:

Antibodies: List of antibodies used (**Table 4**)

Antibody solution: TBS, 0.1% bovine serum albumin (BSA), 0.02% thimerosal

BSA-blocking buffer: TBS-T, 5% BSA

Complete blocking buffer: TBS-T, 5% skimmed milk powder, 0.1% BSA

Loading buffer (1x): 62.5 mM Tris HCl (pH 6.8), 10% glycerol, 2% SDS, 5% β-mercaptoethanol, 0.01% bromophenol blue

Ponceau S solution: Sigma 81462

Protein Benchmark: 10748-010; Invitrogen

Precision Plus Protein All Blue Standards: 161-0373; Bio-Rad

Running buffer for SDS-PAGE (10x): 250 mM Tris base, 2 M glycine, 1% SDS, pH 8.3

Stripping solution: 0.1 M Glycine pH2.3

TBS (1X): 20 mM Tris base, 137 mM NaCl, pH7.4

Transfer buffer (20x): 200 mM Tris base, 2 M glycine, pH 8.3

Table 4. Primary antibodies used for Western blotting (WB), immunoprecipitation (IP) and immunofluorescence (ICC). - : Not tested.

Antibody	Company	Ref	Host	Application and dilution		
				WB	IP	ICC
Alexa Fluor 488	Invitrogen	A11039	Chicken	-	-	1:300
Alexa Fluor 568	Invitrogen	A11031 A11036	Mouse Rabbit	-	-	1:300
Alexa Fluor 594 Phalloidin	Invitrogen	A12381	F-actin	-	-	1:50
Alexa Fluor 647	Invitrogen	A32728 A32733	Mouse Rabbit	-	-	1:300
ß-actin (AC-15)	Sigma	A1978	Mouse	1:60,000	-	-
ß-tubulin (SAP.4G5)	Sigma	T7816	Mouse	1:20,000	-	-
ErbB4 N terminal	Invitrogen	PA5-14637	Rabbit	1:1000	-	-
ErbB4 C-18	Sta. Cruz	sc-283	Rabbit	1:1000	-	-
EphA3 C19	Sta. Cruz	sc-919	Rabbit	1:1000	-	-
EphA3 L18	Sta. Cruz	sc-920	Rabbit	1:1000	-	-
EphA3 Receptor	Invitrogen	37-3200	Mouse	1:1000	5 µg	-
Flag-Tag	Abcam	125243	Mouse	-	25 µg	-
GAPDH	Ambion	Am4300	Mouse	1:100,000		
GFP	Abcam	13970	Chicken	-	-	1:1000
HA-probe (F-7)	Sta. Cruz	sc-7392	Mouse	1:1000	-	-
HA-tag	Cell signaling	#2362	All species	1:1000	-	-

HA-Tag (Oct-A)	Sta. Cruz	Sc-807	Rabbit	-	-	1:50
HA-Tag Sepharose	Cell signaling	#3956S	Rabbit	-	4.5 µl	-
Hoescht	Invitrogen	34580	Nuclei	-	-	1:10000
Myc-Tag	Cell signaling	2276	Mouse	1:1000	2 µg	-
MYH9 H-40	Sta. Cruz	sc-98978	Rabbit	1:5000	-	1:100
MYH9 3F7.1	Merck Millipore	MABT164	Mouse	1:1000	-	-
Nrg1 H-210	Sta. Cruz	sc-28916	Rabbit	1:1000	-	-
Nrg1 C-20	Sta. Cruz	sc-348	Rabbit	1:1000	-	-
Nrg1-C19	Sta. Cruz	sc-1791	Goat			
p-ErbB4 (Y1284)	Cell signaling	4757	Rabbit	1:1250	-	-
p-EphA3 (Y779)	Cell signaling	8862	Rabbit	1:3000	-	-
p-MYH9 (S1943)	Merck Millipore	AB2974	Rabbit	1:1000	-	1:100
PSD95	Cell signaling	3450	Rabbit	-	-	1:200
SMI 312	Covance	SMI-312R	Mouse	-	-	1:500
Synaptophysin	Abcam	SY38	Mouse	-	-	1:500

3.5. Proteomic assays

3.5.1. MALDI-TOF MS

The proteomic identification of EphA3 ICD-interacting proteins is based on a previous protocol (Free, Hazelwood, & Sibley, 2009). HEK293T cells were cultured in 100 mm plates ($7{,}1 \cdot 10^4$ cells/cm^2) and transfected with pcDNA3.1-3xFlag or EphA3 ICD-3xFlag (50 µg/plate) vector with a commercial $CaCl_2$ method (CalPhos Mammalian Transfection kit). In order to increase the transfection efficiency, the culture medium was supplemented with 25 µM Chloroquine prior to transfection. 48 h after transfection, cells were treated with EBBS supplemented with 5 mM EDTA (10 min, 37°C, 5% CO_2). Then, cells were recollected and centrifuged (200 x *g*, 10 min) and the supernatant was discarded. Pellets were resuspended in 1000 µl of lysis buffer supplemented with protease and phosphatase inhibitors. In order to solubilize the proteins, the tubes were incubated (1h, 4°C) in an orbital shaker and centrifuged (20,000 x *g*, 40 min, 4°C). The pellets containing cell debris were discarded and the supernatant transferred into a clear tube. Then, the lysates were immunoprecipitated using the antibody against the Flag-Tag (DYKDDDDK). In this case, we pre-cleared the lysate before to add the antibody to the samples. The beads of sepharose (100 µl/condition) were washed with 1000 µl of lysis buffer, centrifuged (1500 x *g*, 1 min, 4°C), and resuspended again with 200 µl of lysis buffer. Then, the beads were incubated with the samples for 3h at 4°C in rotation. After this, Protein G pellets were discarded by centrifuging (2,000 x *g*, 5 min, 4°C) and the supernatant was transferred to a clean tube, where the Flag-Tag antibody was added (25 µg). Then, 100 µl of Protein G were washed once with lysis buffer and incubated with the sample for 3h at 4°C in rotation. The bead-antibody-antigen complex was centrifuged (1500 x *g*, 5 min, 4°C) and washed with washing buffer (3 x times). Finally, pellets were resuspended with 50 µl of Sample Buffer 2X and heated at 95°C for 5 min.

The co-immunoprecipitation result was resolved by an 8.5% SDS-PAGE gel, which was stained by Colloidal Comassie reagent overnight. After, extensive washes, samples were in-gel digested with trypsin automatically (DigestPro MS, Intavis). This involves reduction with dithiothreitol (DTT), derivatization with iodoacetamide (IAA), and enzymatic digestion with trypsin (37°C, 8h). The resulting peptide mixture was analysed by MALDI-TOF/TOF mass spectrometer (Bruker Daltonics Ultraflex TOF/TOF; ProteoRed-ISCIII) and by the database search (Mascot, Matrix Science) with a significance threshold of the MOWSE score of $P < 0.05$. The results were manually validated. SwissProt database restricted to *Homo sapiens* taxonomy was used for peptide identification.

Reagents and buffers:

CalPhos Mammalian Transfection kit: #631312; Clontech

Cloroquine: #C6628; LifeTechnologies

Earle's Balanced Salt Solution (EBBS): #14155063; LifeTechnologies

Lysis buffer: 50 mM Tris HCl, pH 7.4, 150 mM NaCl, 2 mM EDTA, 1% NP40, 1 mM PMSF supplemented with protease and phosphatase inhibitors

Washing buffer: 50 mM Tris HCl, pH 7.4, 300 mM NaCl, 2 mM EDTA, 1% NP40, 1 mM PMSF supplemented with protease and phosphatase inhibitors

3.5.2. LC-MS/MS analysis

We first used bioinformatics tools to predict the potential cleavage site in EphA3 by sequence alignment of EphA3 and known PS1/γ-secretase substrates using the ClustalW2-EMBL platform. To identify the exact PS/γ-secretase-mediated cleavage site in EphA3, we perform liquid chromatography-tandem mass spectrometry (LC-MS/MS) analysis. The main limitation of this type of study is the amount of protein needed, which is approximately 10 times of the amount required for protein detection by Western blotting. For this reason, we perform 10 times the *in vitro* γ-secretase assay described in the 3.3 section of *Materials and Methods*. The 10% of the soluble fractions (S100) were resolved on 8.5% SDS-PAGE followed by Western blot analysis and serves as a control, and the remaining 90% was also resolved on 8.5% SDS-PAGE but stained using silver staining. Bands (~47-49 kDa) were excised and in-gel digested with trypsin automatically (DigestPro MS, Intavis), and peptides were extracted in MeOH/H2O (2:1), 0.1% TFA. Samples were evaporated and reconstituted in 5 µl of 5% MeOH, 0.5% TFA and loaded into the chromatographic system. The LTQ XL Orbitrap was operated in the positive ion mode with a spray voltage of 1.8 kV. The spectrometric analysis was performed in a data dependent mode acquiring a full scan followed by 5 LC-MS/MS scans of the 5 most intense signals from an inclusion list. The inclusion list included all the theoretical peptides generated after MS-digestion (ProteinProspector) (**Table 5**). Moreover, we confirmed the presence of EphA3 ICD in our sample, by looking for the most suitable (detectable) peptides before (NILINSNLVcK) and after (QFAAVSITTNQAAPSPVLTIK) the PS/γ-secretase predicted cleavage site in ESI-LC-MS/MS analysis by PeptideRank software (http://wlab.ethz.ch/peptiderank/) (underlined in **Fig. 17**).

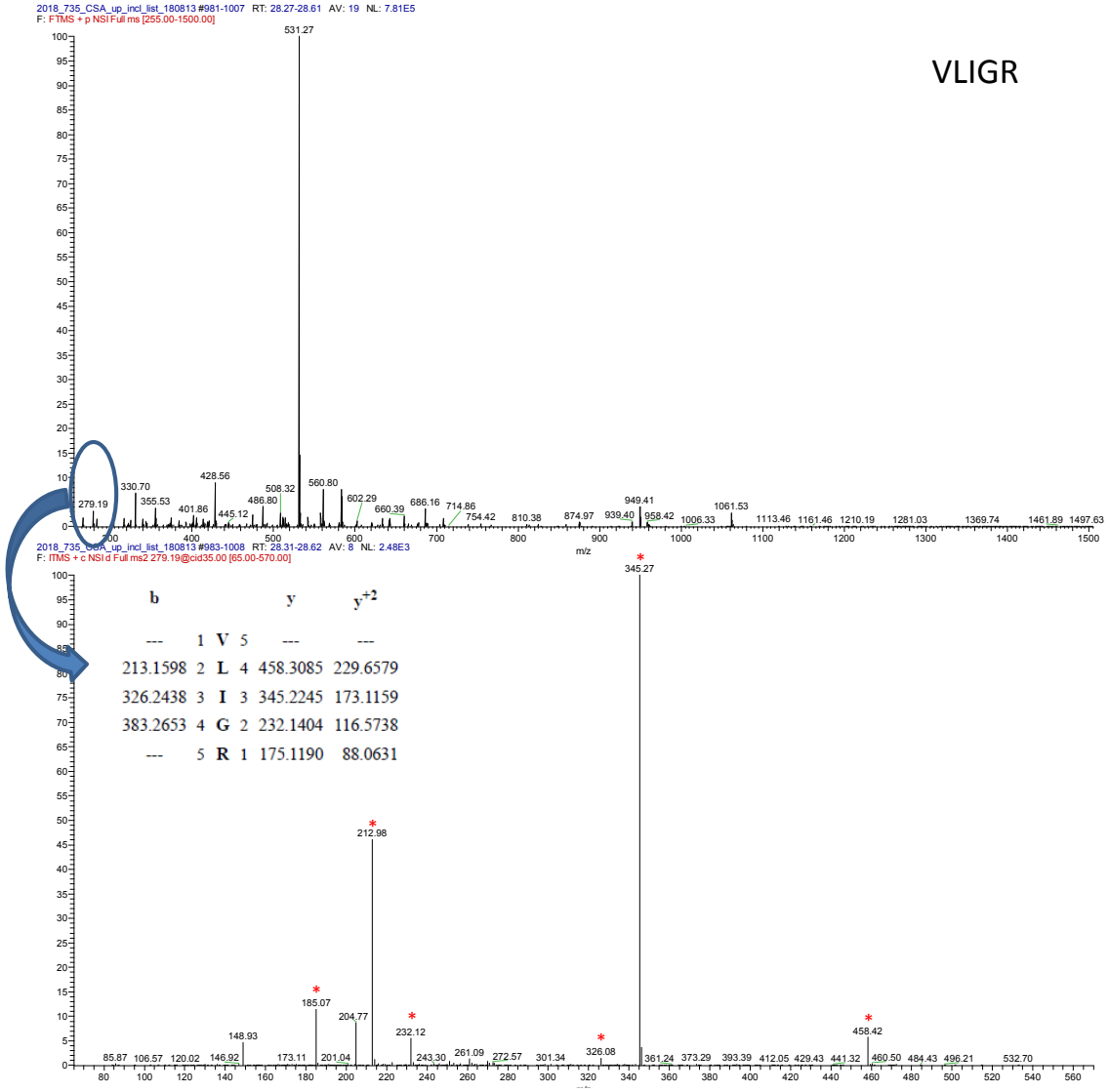

Figure 17. VLIGR identified peptide. The full MS spectra of the trypsin-digested band (~47-49 kDa) (top spectra) and specific MS/MS spectra obtained for peptide VLIGR showing the mass/charge (m/z) values (bottom spectra) are shown below. Detected signals corresponding with theoretical ions are labelled with red asterisks.

Table 5. Theoretical peptides generated from different secretase cleavage sites. For all these peptides m/z was calculated taking into account charges +1, +2 and +3

Sequence	z1	z2	z3
VLIGR	557.377	279.1921	186.4638
YVLIGR	720.4403	360.7238	240.8183
IYVLIGR	833.5243	417.2658	278.513
VIYVLIGR	932.5928	466.8	311.5358
VVIYVLIGR	1031.661	516.3342	344.5586
TVVIYVLIGR	1132.709	566.8581	378.2411
LTVVIYVLIGR	1245.793	623.4001	415.9358
LLTVVIYVLIGR	1358.877	679.9421	453.6305
ILLTVVIYVLIGR	1471.961	736.4842	491.3252
IILLTVVIYVLIGR	1585.045	793.0262	529.0199
AIILLTVVIYVLIGR	1656.082	828.5447	552.6989
VAIILLTVVIYVLIGR	1755.151	878.079	585.7217
AVAIILLTVVIYVLIGR	1826.188	913.5975	609.4008
AAVAIILLTVVIYVLIGR	1897.225	949.1161	633.0798
SAAVAIILLTVVIYVLIGR	1984.257	992.6321	662.0905
ISAAVAIILLTVVIYVLIGR	2097.341	1049.174	699.7852
AISAAVAIILLTVVIYVLIGR	2168.378	1084.693	723.4642
IAISAAVAIILLTVVIYVLIGR	2281.462	1141.235	761.1589
mIAISAAVAIILLTVVIYVLIGR	2428.498	1214.753	810.1709
MIAISAAVAIILLTVVIYVLIGR	2412.503	1206.755	804.8391
VmIAISAAVAIILLTVVIYVLIGR	2527.566	1264.287	843.1937
VMIAISAAVAIILLTVVIYVLIGR	2511.571	1256.289	837.8619
VVmIAISAAVAIILLTVVIYVLIGR	2626.635	1313.821	876.2165
VVMIAISAAVAIILLTVVIYVLIGR	2610.639	1305.823	870.8847
QVVmIAISAAVAIILLTVVIYVLIGR	2754.693	1377.85	918.9027
QVVMIAISAAVAIILLTVVIYVLIGR	2738.698	1369.853	913.5709
SQVVmIAISAAVAIILLTVVIYVLIGR	2841.725	1421.366	947.9134
SQVVMIAISAAVAIILLTVVIYVLIGR	2825.73	1413.369	942.5815
SSQVVmIAISAAVAIILLTVVIYVLIGR	2928.758	1464.882	976.924
SSQVVMIAISAAVAIILLTVVIYVLIGR	2912.762	1456.885	971.5922
ESSQVVmIAISAAVAIILLTVVIYVLIGR	3057.8	1529.404	1019.938
ESSQVVMIAISAAVAIILLTVVIYVLIGR	3041.805	1521.406	1014.606
GESSQVVmIAISAAVAIILLTVVIYVLIGR	3114.822	1557.914	1038.945
GESSQVVMIAISAAVAIILLTVVIYVLIGR	3098.826	1549.917	1033.614
SGESSQVVmIAISAAVAIILLTVVIYVLIGR	3201.854	1601.43	1067.956
SGESSQVVMIAISAAVAIILLTVVIYVLIGR	3185.858	1593.433	1062.624
ISGESSQVVmIAISAAVAIILLTVVIYVLIGR	3314.938	1657.972	1105.651
ISGESSQVVMIAISAAVAIILLTVVIYVLIGR	3298.942	1649.975	1100.319

4. Molecular biology

4.1. DNA extraction and analysis

4.1.1. DNA amplification and purification

Bacterial transformation

Bacterial transformation allows introducing plasmid DNA into a bacterial cell using heat shock. For each plasmid, 50 µl of DH5α Competent cells (Invitrogen) were thawed on ice for 10 min. Then, 1 µg of purified plasmid DNA or 10 µl of ligation reaction (section 4.1.3. of *Materials and Methods*) were incubated with the competent cells at 4°C for 15 min. After this time, bacteria got a heat shock at 42°C for 45 s and immediately after, incubated at 4°C for 5 min. Then, 950 ul of S.O.C. medium (Invitrogen) were added to the bacteria and incubated at 37°C, 250 rpm for 1 h in agitation. The transformed bacteria were seeded onto a LB agar plate containing 100 µg/ml of ampicillin (50 µg/ml, in the case of ligations) and incubated overnight at 37°C. Next day, only those colonies that have incorporate the plasmid will be resistant to ampicillin, and thus, they grow. We selected a positive colony and added into 5 ml of LB medium containing ampicillin (100 µg/ml of ampicillin) at 37°C in orbital agitation overnight.

Miniprep

Miniprep allows obtaining plasmid DNA at low quantities (up to 20 µg). We used Minipreps for cloning (to perform digestions with restriction enzymes or to amplify by PCR). 3ml of bacterial cultures were centrifuged (10,000 x *g*, 2 min, 4°C). Then, the pellet that contains the plasmid DNA was isolated using the QIAprep Spin Miniprep Kit (Qiagen), according to the manufacturer's instructions. The Purified DNA was resuspended in sterile MilliQ H_20 or TE, and stored at -20°C.

Maxiprep

Maxiprep is aimed for large-scale DNA purifications, and allows obtaining high quantities of plasmid DNA (~850 µg). In this case, 3 ml of bacterial culture were transferred into 250-500 ml of LB medium containing ampicillin (or the indicated resistance) and allowed to growth overnight at 37°C in agitation (250 rpm). Next day, bacterial cultures were centrifuged (4000 × g for 10 minutes) and plasmid DNA was obtained using PureLink™ HiPure Plasmid Filter Maxiprep Kit, according to the manufacturer's instructions.

Depending on the future application, the purified DNA was resuspended in TE or PBS 1X. Finally, an aliquot was stored at -20°C for short-term use, and the remaining volume was stored at -80°C.

Material used in bacterial culture:

Luria Broth (LB): #12795027; Invitrogen

LB Agar: #22700025; Invitrogen

S.O.C. medium: #15544034; Invitrogen

QIAprep Spin Miniprep Kit: # 27104; Qiagen

PureLink™ HiPure Plasmid Filter Maxiprep Kit: #K210017; Invitrogen

4.1.2. Genotyping

For genomic DNA extraction, approximately 2 mm fragment of the tail was digested in lysis buffer containing proteinase K (0.1 mg/ml; Roche) overnight at 56°C in orbital agitation. Tubes were centrifuged (9250 x *g*, 15 min, 25°C) and the genomic DNA (supernatant) was precipitated in 2-propanol (Baker) and centrifuged (9250 x *g*, 10 min, 25°C). Then, pellets were washed with 70% EtOH and centrifuged (15,000 x *g*, 10 min, 25°C). Finally, the precipitate was resuspended in TE buffer at 65°C for 2h.

The purified DNA was amplified by Polymerase Chain Reaction (PCR). The final volume of the reaction was 25 µl and included 2 µl of purified genomic DNA, 2.5 µl of 10X PCR buffer (Biotools), 0.5 µl dNTP (10 mM; Biotools), 0.5 µl MgCl2 (50 mM; Biotools), 0.2 µl Taq DNA polymerase (5 U/ml; Biotools) and forward and reverse primers (0.5 µM; Life Technologies).

During the amplification we checked the presence of *PS1* and *Cre* (PCR 1), and *PS2* (PCR 2) in two independent PCRs, as indicated in (**Table 6**). All sequences of the primers used in these PCRs are shown in **Table 6.**

Reagents and buffer:

Lysis buffer: 100 mM Tris HCl pH 8.5, 5 mM EDTA, 0.2% SDS, 200 mM NaCl

TE buffer: 10 mM Tris HCl pH 8.5, 1 mM EDTA

Table 6. Primers and PCR conditions used for mouse genotyping

Gene	Primer	Sequence (5'-3')	PCR
PS1	P139	GGTTTCCCTCCATCTTGGTTG	94°C, 4 min 94°C, 1 min 60°C, 1 min 72°C, 1 min 72°C, 7 min **40 cycles**
	P140	TCAACTCCTCCAGAGTCAGG	
	P158	TGCCCCCTCTCCATTTTCTC	
Cre	P156	GCCTGCATTACCGGTCGATGCAACGA	
	P157	GTGGCAGATGGCGCGGCAACACCATT	
PS2	P162	CATCTACACGCCCTTCACGG	94°C, 4 min 94°C, 1 min 65°C, 1 min 72°C, 1 min 72°C, 7 min **35 cycles**
	P163	CACACAGAGAGGCTCAAGATC	
	P164	AAGGGCCAGCTCATTCCTCC	

4.1.3. Cloning

EphA3 vectors

EphA3 ICD and EphA3 ΔICD cDNAs were subcloned into a pCAGIG vector using the ligation procedure, which consists on joining two segments of DNA to generate a single circular molecule (**Fig. 18)**. The codifying sequence of EphA3 ICD was included in a pCMV-HA vector between KpnI and EcoRI restriction sites. Specific oligonucleotides were designed to include a XhoI restriction site on 5' to facilitate the insertion of DNA into the pCAGIG vector. These oligonucleotides also contained a start codon (ATG) and the Myc-tag sequence (CATGAGCAGAAGCTGATCAGCGAGGAAGATCTG). After sequential digestion of EphA3 ICD (pCMV) with ApaI and EcoRI enzymes (1.5 h each at 37°C), the digested plasmid was checked by agarose gel electrophoresis and purified with QIAquick Gel Extraction Kit. Then, the oligonucleotides (**Table 7**) were annealed in annealing buffer (Reaction: 4 min at 90°C, 10 min at 70°C, and then 10°C) and ligated to the lineal

digested plasmid. The ligation product was transformed into DH5α competent cells and purified by Miniprep. The ligated-plasmid was digested with XhoI and NotI (1.5 h each, at 37°C), and then separated by agarose gel electrophoresis and purified as before. The recipient plasmid (pCAGIG) was also sequentially digested with XhoI and NotI and dephosphorylated with calf intestinal alkaline phosphatase (CIAP) (5 min, 50 °C). The digestion was checked by agarose gel electrophoresis and purified as before. Finally, the EphA3 ICD-pCAGIG vector was obtained by the ligation of the insert (oligonucleotides-ICD) with the pCAGIG-opened vector with TAKARA kit, following the manufacturer's instructions. 10 µl of ligation product were transformed into DH5α competent cells and from several positive colonies the insert was verified and purified with Maxiprep.

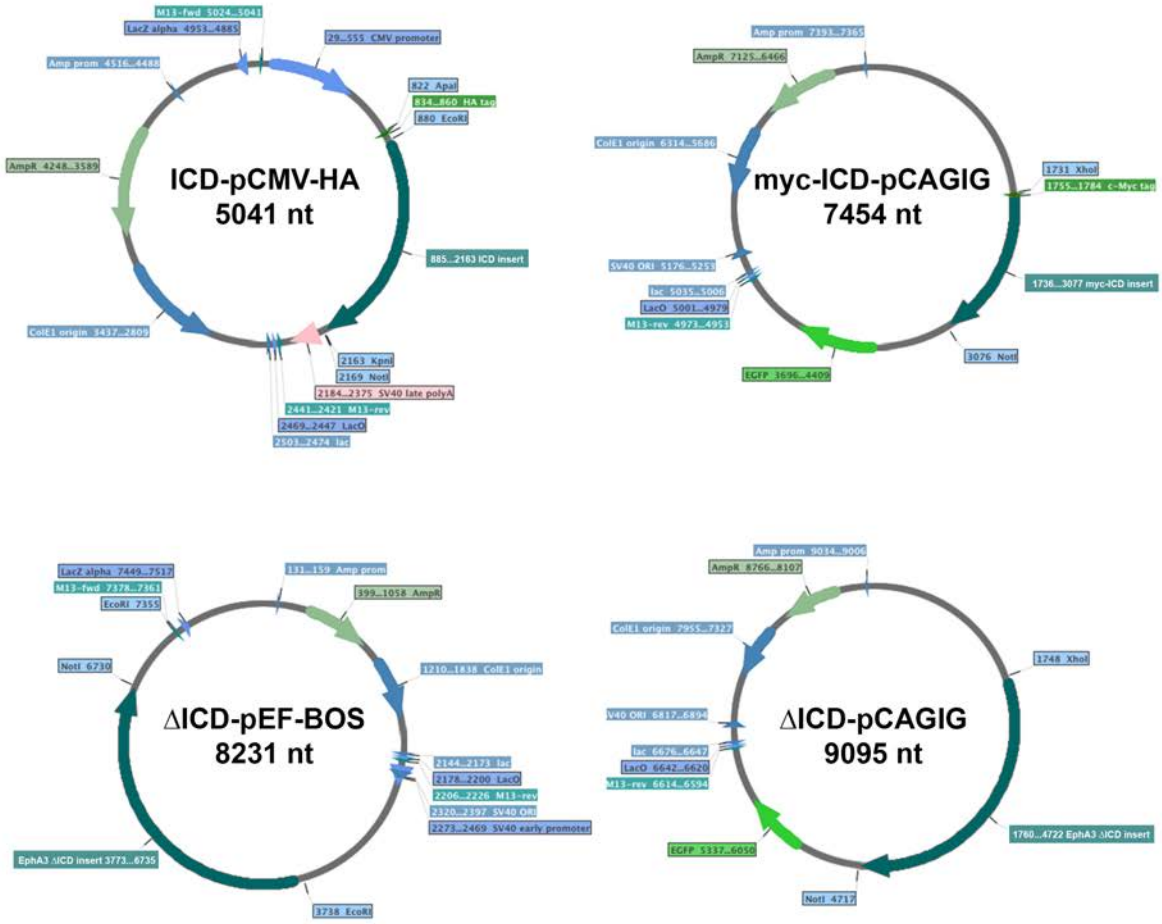

Figure 18. Maps from EphA3 cloning vectors

Table 7. Oligonucleotides used for EphA3 ICD subcloning.

Primer	Sequence (5'-3')
Forward	CCCGCTCGAGCGGATGTCACCAGGT**CATGAGCAGAAGCTGATCAGCGA GGAAGATCTG**CG
Reverse	AATTCG**CAGATCTTCCTCGCTGATCAGCTTCTGCTCATG**ACCTGGTGACA TCCGCTCGAGCGGGGGCC

Underlined are indicated the XhoI restriction site, and in bold, the Myc-tag sequence.

In the case of EphA3 ΔICD, the sequence was included in a pEFBOS vector between BstXI and NotI restriction sites. EphA3 ΔICD was sequential digested with EcoRI and NotI enzymes (1.5 h each at 37°C), the digestion was checked by agarose gel electrophoresis and the 3,200 bp fragment that corresponds to the digested plasmid, was purified with QIAquick Gel Extraction Kit. Then, the EphA3 ΔICD insert was ligated to the previously digested pCAGIG recipient plasmid (EcoRI and NotI: 1.5 h each at 37°C) with TAKARA kit, following the manufacturer's instructions. 10 µl of ligation product were transformed into DH5α competent cells and from several positive colonies the insert was verified and purified with Maxiprep.

pWPI vector

For biochemical analysis of gene overexpression in primary neuron cultures, EphA3 ICD (1500 bp) and ErbB4 cyt1A1 (4000 bp) sequences were cloned into the pWPI lentiviral vector that contains an EGFP marker (**Fig. 19)**. This procedure was performed using the In-Fusion HD Cloning kit according to the manufacturer's instructions.

First, we designed oligonucleotides containing the sequence of interest flanked by 15 pb before and after the PmeI restriction site of the recipient vector (pWPI) (**Table 8**). Then, the inserts were amplified by PCR in a 50 µl of reaction that included: 10 µl of 5X SuperFi Buffer, 10 µl of 5X SuperFi GC Enhancer, 1 µl dNTPs (10 mM; Biotools); 0.5 µl Platinum SuperFi DNA Polymerase (5 U/ml; Invitrogen), 2.5 µl forward and reverse primers (10 µM) (**Table 8**). The amplified inserts were check by agarose gel electrophoresis and purified with QIAquick Gel Extraction Kit. Simultaneously, the recipient plasmid pWPI was digested with the restriction enzyme PmeI (1 h at 37°C) and 100 ng of PCR product were

incubated with 50 ng of lineal vector and 2 ul of 5X In-Fusion HD Enzyme premix (15 min at 50°C). Finally, 2.5 ul of the In-Fusion reaction mixture were transformed into Stellar competent cells (Takara), and the insert was verified from several positive colonies and purified with Maxiprep.

Then, the generation and titration of lentiviral particles was performed as in Section 4.1.4. of *Material and Methods*.

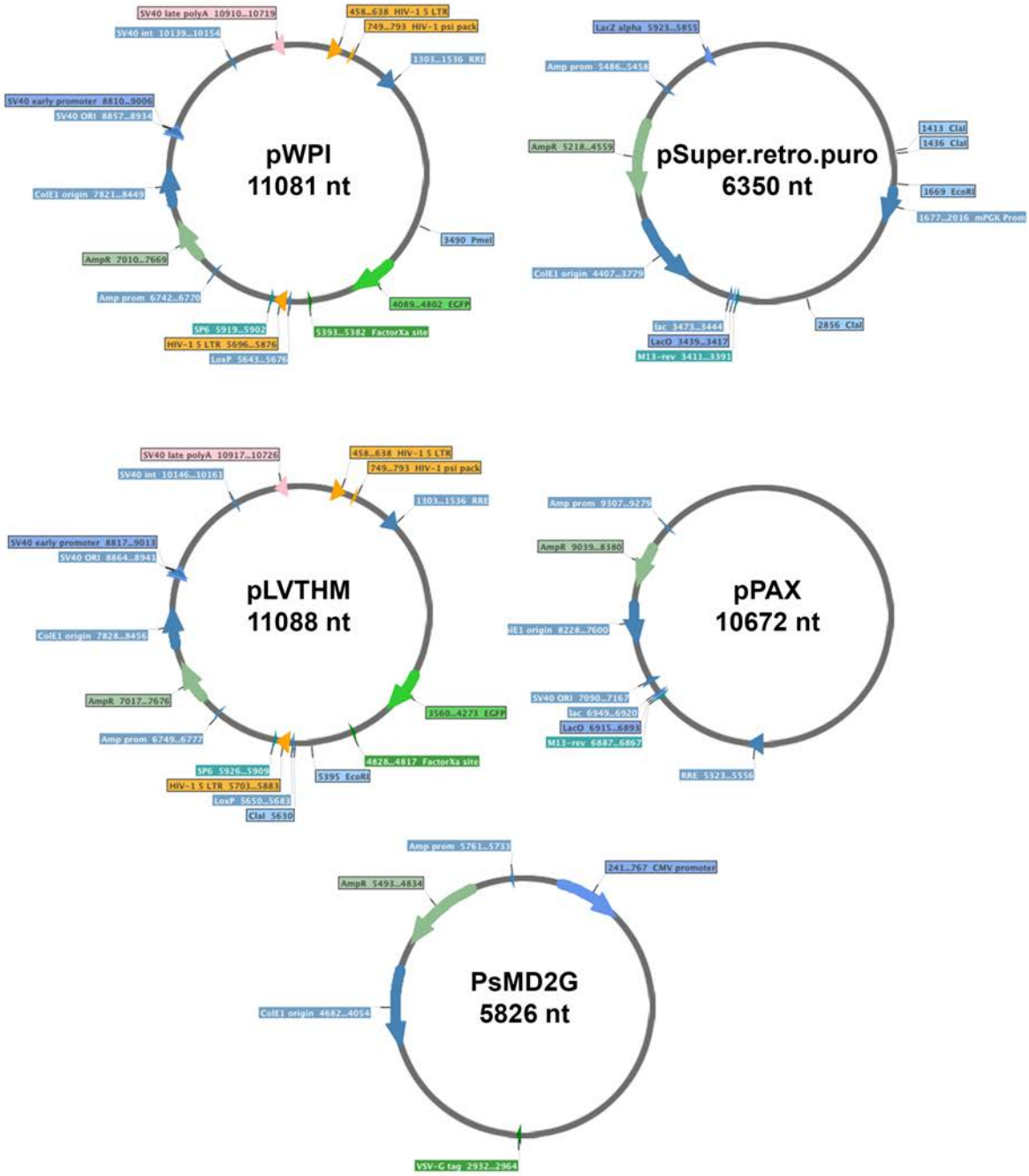

Figure 19. Maps of lentiviral vectors used to generate lentiviral particles

Table 8. Oligonucleotides and PCR conditions used for lentiviral cloning. Capital letters indicate the sequence of the gene and *italics* the 15 pb sequence before (*ctagcctcgaggttt*) and after (*tgcagcccgtagttt)* the PmeI restriction site.

Primer	Sequence (5'-3')	PCR
ICD Fw	*ctagcctcgaggttt*CTCGAGCGGATGTCACCAGG	94°C, 4 min 94°C, 15 sec 55°C, 30 sec 68°C, 90 sec **35 cycles** 4°C, ∞
ICD Rv	*tgcagcccgtagttt*GCGGCCGCGGGTACCCCTTA	
ErbB4 Fw	*ctagcctcgaggttt*GCTAGCCAAAAATGAAGCTG	98°C, 30 sec 98°C, 10 sec 72°C, 60 sec **35 cycles** 72°C, 5 min 4°C, ∞
ErbB4 Rv	*tgcagcccgtagttt*GCGGCCGCCAGTGTGATGG	

Reagents and buffers:

Annealing buffer: 50 mM HEPES pH 7.4, 100 mM NaCl

CIAP: #18009027; Invitrogen

In-Fusion HD Cloning kit: # 121416; Takara

Platinum SuperFi DNA Polymerase: #12351010; Invitrogen

QIAquick Gel Extraction Kit: #28115; Qiagen

Stellar competent cells: # 636766; Takara

Table 9. List of constructs used in this study

Construct	Specie	Vector	Resistance	Source
EGFP C1	-	-	kanamycin	Clontech
EphA3 WT	H	pEFBOS	ampicillin	Dr. M. Lackmann
EphA3 ICD	H	pCMV	ampicillin	Dr. S. Marco
EphA3 ΔICD	H	pEFBOS	ampicillin	Dr. M. Lackmann
EphA3 ΔICD-pCAGIG	H	pCAGIG	ampicillin	M. Javier
Myc-EphA3 ICD	H	pCAGIG	ampicillin	M. Javier
Myc-EphA3 ICD	H	pWPI	ampicillin	M. Javier
ErbB4 cyt1A1	H	pIRES puro2	ampicillin	Dr. G. Gambarotta
ErbB4 cyt1A1	H	pWPI	ampicillin	M. Javier
NMIIA WT	R	pEGFP-C3	ampicillin	Dr. A.R. Bresnick
NMIIA S1943A	R	pEGFP-C3	ampicillin	Dr. A.R. Bresnick
RhoA Q63L	H	pCEFL-HA	ampicillin	Dr. P. Crespo

H: Human, R: rat.

4.1.4. Generation of short-hairpin RNA

In order to inactivate non-muscle myosin IIA (NMIIA) gene expression, we design multiple short-hairpin RNA (shRNA) molecules based on the RNA interference (RNAi) technology. First of all, we design the sequence of RNAi trough the siDESIGN Center tool (https://dharmacon.horizondiscovery.com/design-center/; Dharmacon). Four potential siRNAs of *mus musculus* NMIIA gene (GenBank, NM_022410) of 19 nucleotides of length were selected taking into account that the ORF was the region of interest and that the minimum and the maximum of G/C percentage were 30% and 64%, respectively. We also designed a negative control called “scrambled” that consists in a random nucleotide sequence. After checking that the chosen sequences did not interfere with any other gene in *mus musculus*, for each shRNA sequence a pair or primers (forward and reverse) were

design adding the short-hairpin structure, specific restriction sites and a stop codon (**Table 10**).

The final recipient plasmid is the long-size pLVTHM vector (**Fig.19**). Since the shRNA are very short fragments, the shRNA primers were annealed in *annealing buffer* (Reaction: 4 min at 90°C, 10 min at 70°C, and then 10°C) and inserted into the medium-size pSuper.Retro.Puro vector (**Fig. 19**). To do that, the pSuper.Retro.Puro was sequentially digested with BglII and HindIII restriction enzymes (1 h each at 37°C). After checking the digestion and purifying the digested plasmid with the QIAquick Gel Extraction Kit, the shRNA oligonucleotides and the digested pSuper vector were ligated using the T4 DNAse ligase (Invitrogen). 10 µl of ligation product were transformed into DH5α competent cells and from several positive colonies the insert was verified and purified with Miniprep. Then, the shRNA-pSuper and the pLVTHM plasmids were sequentially digested with ClaI and EcoRI restriction enzymes (1.5 h each at 37°C). We checked the digestion of the shRNA-pSuper vector and purified a band of 300 bp of length that corresponds to the shRNA sequence bound to H1 promoter (300 bp). Then, the opened pLVTHM and the shRNA+H1 promoter sequence were ligated with the T4 DNAse ligase (Invitrogen). Finally, 10 µl of ligation product were transformed into DH5α competent cells and the insert was verified from several positive colonies and purified with Maxiprep.

In order to generate the lentiviral particles, we transfected HEK293T cells using the Calphos Mammalian Transfection Kit (Clontech) based on calcium phosphate transfection, following the manufacturer's instructions. In summary, the DNA solution including 30 µg of pLVTHM-shRNA, 15 µg of a plasmid containing the viral genes of packaging (psPAX2) and 10 µg of a plasmid containing the viral genes of envelope (pM2D.G) were mixed with 250 mM $CaCl_2$ and H_2O. Then, 1.5 ml of the DNA solution was added to the HBS buffer (adding 1/8 each time), softly mixed and incubated for 20 min at room temperature. During this time, the medium of HEK293T was replaced by transfection medium. Then, 1 ml of the transfection mix was added to the HEK293T cells, which were incubated for 7-8 h at 37°C in 5% CO_2. HEK293T cells were washed with PBS 1X and maintained in supplemented DMEM at 37°C in 5% CO_2. After 48h, the culture medium was recollected and centrifuged (100,000 x *g*, 4°C, 2h) and the pellet (containing the viral particles) was resuspended in 100 µl of sterile PBS 1X in agitation overnight at 4°C. Finally, the lentiviral particles were aliquot and stored at -80°C.

Since the pLVTHM-shRNA plasmid contain a GFP-expressing cassette, lentiviral particles were tittered by flow cytometry. HEK293T cells were cultured in 24-well plates ($1.5 \cdot 10^4$

cells/cm^2) and 24h later, transduced with lentiviral particles (range of dilutions: 2 µl, 1 µl, 0.5 µl, 0.25 µl, 0.125 µl, 0.062 µl and 0.031 µl) overnight in half of the culture medium. Next day, we added 1 ml of culture medium, and HEK293T cells were maintained for 48 h at 37°C in 5% CO_2. Finally, cells were washed twice with PBS 1X, trypsinized, recollected and centrifuged (10,000 rpm, 3 min). The pellet containing the cells, were washed twice with PBS and the GFP fluorescence of 10,000 cells was measured in a flow cytometer (Cytomics FC 500, Beckman Coulter). The final titer in infective particles i.p./ml was calculated according to the following formula: (nº of GFP-positive cells x 1000 x nº of cells at the moment of transduction) / (100 x viral dilution).

Reagents and buffers:

Annealing buffer: 50 mM HEPES pH 7.4, 100 mM NaCl

Calphos Mammalian Transfection Kit: # 631312; Clontech

Supplemented DMEM: DMEM (Sigma Aldrich D5796) supplemented with 10% of fetal bovine serum (FBS; Invitrogen-Gibco 10106-169) and penicillin/streptomycin (5000 U/mL, Life Technologies 15070-063)

T4 DNAse ligase: #15224-017; Invitrogen

Transfection medium: DMEM supplemented with 25 µM of Chloroquine

Table 10. Oligonucleotides used in NMIIA silencing.

Primer	Sequence (5'-3')
sh1 Fw	**GATC**CCCGACAAAGGTTCGAGAGAAA*TTCAAGAGA*TTTCTCTCGAACCTTTGTCTTTTT
sh1 Rv	**AGCT**AAAAAGACAAAGGTTCGAGAGAAA*TCTCTTGAA*TTTCTCTCGAACCTTTGTCGGG
sh2 Fw	**GATC**CCCGAGCAGACGAAGCGGGTAA*TTCAAGAGA*TTACCCGCTTCGTCTGCTCTTTTT
sh2 Rv	**AGCT**AAAAAGAGCAGACGAAGCGGGTAA*TCTCTTGAA*TTACCCGCTTCGTCTGCTCGGG
sh3 Fw	**GATC**CCCGTGCCAACATTGAGACTTA*TTCAAGAGA*TAAGTCTCAATGTTGGCACTTTTT
sh3 Rv	**AGCT**AAAAAGTGCCAACATTGAGACTTA*TCTCTTGAA*TAAGTCTCAATGTTGGCACG

	GG
sh4 Fw	**GATC**CCCGGAGTAGGCACAAGAGTTT*TTCAAGAGA*AAACTCTTGTGCCTACTCCTT TTT
sh4 Rv	**AGCT**AAAAAGGAGTAGGCACAAGAGTTT*TCTCTTGAA*AAACTCTTGTGCCTACTCC GGG
sc Fw	**GATC**CCCGAACGAACGATAGAGATAG*TTCAAGAGA*CTATCTCTATCGTTCGTTCTTT TT
sc Rv	**AGCT**AAAAAGAACGAACGATAGAGATAG*TCTCTTGAA*CTATCTCTATCGTTCGTTCG GG

In **bold** are indicated BglII (GATC) and HindIII (AGCT) restriction sites; underlined, the RNAi (sense) and RNA (reverse complementary) shRNA sequences; and in *italics*, the hairpin structure. Fw: forward; Rv: reverse; Sc: Scramble; Sh: shRNA.

4.2. RNA extraction and analysis

4.2.1. RNA extraction and reverse transcription

Mouse hippocampal neurons were cultured for 7 DIV and the RNA isolated using the PureLink RNA Mini Kit according to the manufacturer's instructions (Ambion, Life Technologies, USA). Once RNA was obtained, the RNA Integrity Number (RIN) was measured with the Agilent RNA 6000 Nano Kit in a 2100 Bioanalyzer instrument (Agilent Technologies, USA).

Purified RNA (500 ng; RIN 9.0) was reverse-transcribed (RT-PCR) in 50 µl of a mix containing 1 µM Oligo(dT) primers, 1 µM random hexamers, 0.5 mM dNTPs, 0.45 mM DTT, 10 units of RNaseOut and 200 units of SuperScript™ II reverse transcriptase.

PCR program: 25°C for 10 min → 42°C for 60 min → 72°C for 10 min

Reagents and buffers:

dNTPs: REF; Life technologies

DTT: REF; Life technologies

Oligo(dT) primers: REF; Life technologies

PureLink RNA Mini Kit: # 12183018A; Ambion, Life Technologies, USA

Random hexamers: REF; Life technologies

RNAseOut: REF; Life technologies

SuperScript™ II reverse transcriptase: REF; Life technologies

4.2.2. RNA analysis by quantitative real time qPCR

The cDNA obtained by RT-PCR was amplified and analysed by quantitative real-time PCR (qPCR) according to (Bustin et al., 2009), using the Power SYBR Green PCR Master Mix (LifeTechnologies) in the Applied Biosystems 7500 Fast system. qPCR reactions were performed in duplicate using 2.5 µl of 1:100 pre-diluted cDNA and 7.5 µl of a mix containing custom designed primers (400 nM; **Table 11**) and SYBR Power SYBR Green Master Mix. Prior to the real analysis, the specificity of the primers was verified by detecting a single melting point in the melt curve. Amplification data was acquired using the 7500 Software v2.0.6 (Applied Biosystems) and the analysis of data was performed by the comparative ΔCt method using the Ct values and the average value of PCR efficiencies obtained from LinRegPCR software (Ruijter et al., 2009). For each experiment, the stability of Glyceraldehyde 3-phosphate dehydrogenase (*Gapdh*), hypoxanthine guanine phosphoribosyl transferase-1 (*Hprt1*), peptidylprolyl isomerase A (*Ppia*), b-actin (*Actb*) and TATA box binding protein (*Tbp*) genes was evaluated by the NormFinder algorithm (Andersen, Jensen, & Ørntoft, 2004) and gene expression was normalized using the geometric mean of the most stable genes.

Reagents:

Power SYBR Green PCR Master Mix: #4367659; Invitrogen

Table 11. List of used primers in q-PCR and their sequences.

Gene		Sequence (5'-3')
EphA1	Forward	CACCAGTTTCCAGAAGCCTG
	Reverse	*CATAAATCCCGATCAGCAGAGC*
EphA2	Forward	TCCAAGTCAGAACAACTAAAGC
	Reverse	GGTCTTCGTAAGTGTGAGGA

EphA3	Forward	CTAGCCCAGACTCTTTCTCC
	Reverse	CGGAAATAGCAATCATCACCA
EphA4	Forward	GAGAGTTCCAGACCAAACAC
	Reverse	ACTACAGCAGAGAATTCAGGG
EphA5	Forward	TCCGCACACTTATGAAGATCC
	Reverse	TCACCAAATTCACCTGCTCC
EphA6	Forward	TGATCCAGACACCTATGAAGAC
	Reverse	CAAATTCACCTGCTCCAATCAC
EphA7	Forward	GCATTTCTCAGGAAACACGA
	Reverse	ACCTCTCAACATTCCTACCA
EphA8	Forward	TCTAGCCTATGGTGAACGAC
	Reverse	CTGATGACATCCTGGTTGGT
EphA10	Forward	TCCTGAGACTCTACAGTTTGG
	Reverse	GCCTTGATTACATCTTGTCCAG

5. Cellular biology

5.1. Immunofluorescence of cultured neurons

Hippocampal neurons were seeded (30,000 cells/well) in 24-wells plates containing coverslips previously treated with poly-D-lysine. Cells at 4-16 DIV were washed twice with PBS and fixed with 4% of paraformaldehyde solution (PFA) diluted in PBS (Electron Microscopy Sciences) for 15 min at room temperature.

Depending on the protein of interest, we used two different immunofluorescence protocols based on the type of detergent used for permeabilising the cells: the first, use Saponin that does not permeabilize the nuclear membrane, and the second use Triton, which permeabilizes all lipid bilayers. Briefly, both consist in: permeabilization, blockage, incubation with primary antibody, incubation with secondary antibodies, nuclear staining

and coverslip mounting using FluorSave Reagent (Calbiochem) (see in detail in **Table 12**).

Table 12. Comparison of saponin and triton-based immunofluorescence staining protocols.

<table>
<tr><th></th><th>Saponin</th><th>Triton</th></tr>
<tr><td>Washing</td><td colspan="2">3 x PBS (10 min, 25°C in agitation)</td></tr>
<tr><td>Permeabilization</td><td>SOL. 1: 0.02% saponin, PBS 1X (7 min, 25°C)</td><td rowspan="3">2% NGS, 0.2% Tx-100, PBS 1X (30 min, 25°C)</td></tr>
<tr><td rowspan="2">Blocking</td><td>SOL. 2: 0.01% saponin, 10 mM Glycine, PBS 1X (15 min, 25°C)</td></tr>
<tr><td>SOL. 3: 0.01% saponin, 10 mM Glycine, 5% BSA, PBS 1X (30 min, 25°C)</td></tr>
<tr><td>Primary antibody</td><td>Diluted in SOL. 4: 0.01% saponin, 1% of NGS, PBS 1X (overnight, 4°C)</td><td>Diluted in 1.5% NGS, 0.1% Tx-100, PBS 1X (overnight, 4°C)</td></tr>
<tr><td>Washing</td><td colspan="2">3 x PBS (10 min, 25°C in agitation)</td></tr>
<tr><td>Secondary antibody</td><td>Diluted in SOL. 4: 0.01% saponin, 1% of NGS, PBS 1X (overnight, 4°C)</td><td>Diluted in PBS 1X (45 min, 25°C)</td></tr>
<tr><td>Washing</td><td colspan="2">3 x PBS (10 min, 25°C in agitation)</td></tr>
<tr><td>Nuclear Staining (Hoechst)</td><td colspan="2">Hoechst (1 µg/ml) diluted in PBS (10 min, 25°C in agitation)</td></tr>
<tr><td>Washing</td><td colspan="2">3 x PBS (10 min, 25°C in agitation)</td></tr>
<tr><td>Mounting of coverslips</td><td colspan="2">5 ul of FluorSave Reagent / coverslip</td></tr>
</table>

In all cases, when the protein of interest was phosphorylated, the PBS 1X was replaced by TBS 1X. *BSA*: bovine serum albumin, *NGS*: normal goat serum, *Tx-100*: Triton X-100.

Reagents:

FluorSave: REF; Calbiochem

Hoechst 33258: REF; LifeTechnologies

5.1.1. Analysis of axon growth

Hippocampal neurons were fixed at 4 DIV and stained (saponin-based protocol) with mouse anti-SMI312, chicken anti-GFP, phalloidin-Alexa594 and Hoechst 33258. Images were captured with a Zeiss LSM700 laser-scanning microscope and analyzed with FilamentTracer tool from Imaris 8.1 Software (Bitplane, South Windsor, CT, USA). Neurons were traced using semi-automated FilamentTracer tool. After defining the starting point, the filaments were defined by moving the mouse over the axon until the end.

5.1.2. Analysis of colocalization

Hippocampal neurons (4 DIV) were fixed and stained (saponin-based protocol) with rabbit polyclonal anti-pNMIIA and chicken polyclonal anti-GFP antibodies, phalloidin-Alexa594 and Hoechst 33258. For synaptogenesis experiments, hippocampal neurons (16 DIV) were fixed and stained (triton-based protocol) with mouse monoclonal anti-synaptophysin, rabbit polyclonal PSD95 and chicken polyclonal anti-GFP antibodies and Hoechst 33258. Images were captured with a Zeiss LSM700 laser-scanning microscope and colocalization between pNMIIA and F-actin was determined using the tool ImarisColoc from Imaris 8.1 Software (Bitplane, South Windsor, CT, USA). Results are expressed as percentage of colocalized spots relative to total spots. Quantitative immunofluorescence of pNMIIA of the axon was measured by ImageJ software (Institute Jacques Monod, Service Imagerie, France) and expressed as area integrated intensity.

5.1.3. Analysis of growth cone morphology

Hippocampal neurons (4 DIV) were fixed and stained (saponin-based protocol) with rabbit polyclonal pNMIIA, chicken polyclonal anti-GFP, phalloidin-Alexa594 and Hoechst 33258. Images were captured with a Zeiss LSM700 laser-scanning microscope and axon growth cones were manually classified as collapsed, those that have no lamellipodia and no more than 2 filopodia or as non-collapsed (the remaining) (**Fig. 20**) (Chitsaz, Morales, Law, & Kania, 2015).

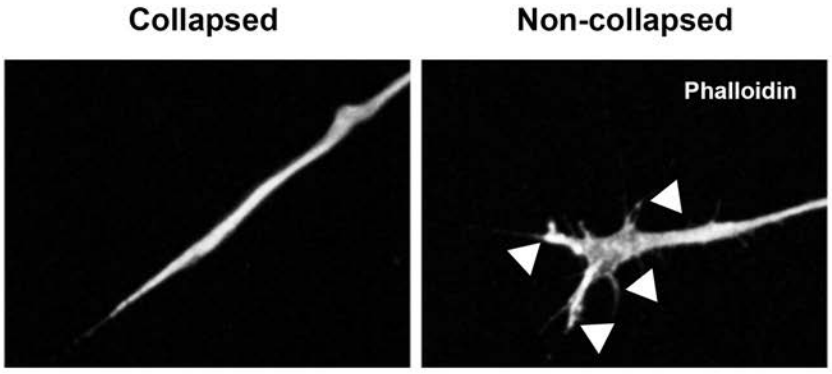

Figure 20. Morphological classification of axon growth cones. Arrowheads Indicate individual filopodia. Adapted from (Chitsaz et al., 2015).

5.2. Fluorescent Immunohistochemistry staining

5.2.1. Intracardial perfusion and tissue processing

Mouse embryos (E15.5) were perfused intracardially with 4% PFA (pH 6.9 Histology grade, Merck) solution. Next, whole heads were submerged in 5ml of 4% PFA overnight at 4°C, washed in PBS and maintained in 70% ethanol before inclusion. Before the paraffin embedding, heads were dehydrated in graded series of ethanol and xylene. Coronal sections (5 µm) were cut in a microtome (Leica RM 2255) and mounted on microscope glass slides (Fisher Superfrost).

5.2.2. Fluorescent immunohistochemistry

Coronal sections (5 µm) were cut in a microtome (Leica RM 2255) and mounted on microscope glass slides (Fisher Superfrost). Sections were heated at 60°C for 2 h, further deparaffinised with two incubations with xylol (5 min) and rehydrated with graded series of ethanol of 3 min: 100%, 100%, 96%, 70% and 50%. For antigen retrieval, sections were microwave-heated with citrate buffer for 8 min. Then, the slices were washed with TBS (3 x 5 min) in orbital agitation and blocked in blocking buffer for 30 min at room temperature. Sections were incubated with antibodies against neurofilament (SMI312) overnight at 4°C. Next day, the sections were washed in TBS and incubated with the secondary AlexaFluor-488-conjugated goat IgGs antibody diluted in TBS for 2 h at room temperature. Then, the sections were washed again in TBS (3 x 5 min) and the nuclei were stained with Hoechst

(30 min, room temperature). Finally, the slides were mounted with FluorSave Reagent. Images were examined with a Zeiss LSM700 laser-scanning microscope (20x).

For axonal quantification in tissue, a 3D reconstruction picture of ventricular zone was generated from multiple stacks of each section. Axons were semi automatically tracked using Filament Tracer tool from Imaris Software (Bitplane Inc). In total, 5 axons of each section (10-15 sections/animal) were quantified from 3-4 animals/genotype.

Reagents and buffers:

Blocking buffer: 1% BSA, 0.1% Tx-100, TBS 1X.

Citrate buffer pH 6: 10 mM sodium citrate (#71405; Sigma), 0.1% Tween-20, TBS 1X.

6. Contextual Fear Conditioning (CFC)

Before starting CFC experiments, mice were handled individually during 3 consecutive days before. Mice were placed in the conditioning chamber (15.9 cm x 14 cm x 12.7 cm; Med Associates Inc.) for 3 min allowing them to develop a representation of the context by exploration before the onset of the unconditioned stimulus (footshock, 1s/1mA). Mice were maintained in the chamber for 2 additional minutes, allowing the association of the context with the shock. The conditioning chamber was cleaned using 70% ethanol before each animal. Contextual fear memory was tested 2 h after training (short-term memory test), when mice were re-exposed to the same chamber. For biochemical analysis, mice were sacrified by cervical dislocation 2 h after training. Conditioning was tested by freezing response, which was automatically measured using the Video Freeze Software (Med Associates Inc.). The CFC experiments were performed by Meng Chen.

7. Statistical analysis

Statistical analysis was performed essentially by one- or two-way analysis of variance (ANOVA) followed by Bonferroni *post hoc* test using GraphPad Prism (GraphPad Software, La Jolla, USA). Values identified as outliers by Grubbs' test were not included in the analysis ($p < 0.05$). Each experiment was performed using, at least, three independent experiments. Values represent mean ± SD or SEM. Value differences were considered significant when $p < 0.05$.

RESULTS

CHAPTER 1:

PS1/γ-SECRETASE MEDIATES EPHA3 PROCESSING

CHAPTER 1: PS1/γ-SECRETASE REGULATES EPHA3 PROCESSING

1. EphA expression during neuronal polarization

EphA comprises a large family of ephrin receptors involved in axon differentiation and growth (Hu et al., 2009; Shu et al., 2014; Son, Hashimoto-Torii, Rakic, Levitt, & Torii, 2016).To better understand the role of EphA receptors in neuronal polarization we first examined the transcript levels of *EphA1-8* in cultured hippocampal neurons from mouse embryos (E15.5). Neurons were cultured at 2, 4 and 7 DIV and mRNA was extracted and quantified by RT-qPCR. Quantitative analysis of mRNAs showed that *EphA1, -A3, -A4, -A7 and -A8* are expressed in cultured neurons at 2 DIV and then are significantly reduced as neuronal differentiation progresses. By contrast, levels of EphA2, -A5, -A6 and -A10 mRNAs do not change during differentiation stages. Interestingly, levels of EphA3, -A4, –A7 and –A8 decline progressively between 2 DIV and 4-7 DIV suggesting a potential role of these receptors in the initial stages of neuronal polarization, that is when neurite extension and axon growth occur (**Fig. 21**).

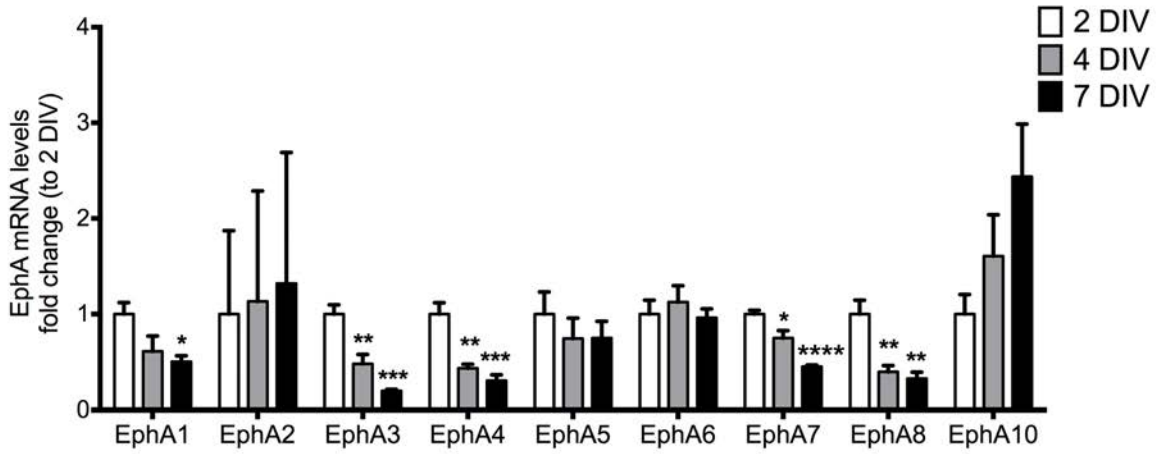

Figure 21. Analysis of *EphA* levels at different stages of neuronal polarization. Cultured hippocampal neurons from WT mice (E15.5) were seeded at high density (62,500 cells/cm^2) in p35 dishes for 2-7 DIV. RNA was extracted and analysed by RT-qPCR. 2-, 4- and 7 DIV mRNA levels were normalized to GAPDH and HPRT1 at the same DIV. Values represent mean ± SEM of 4 independent experiments (n= 4 independent cultures). *$p < 0.05$, **$p < 0.01$, ***$p < 0.001$, compared to 2 DIV as determined by one-way ANOVA followed by Bonferroni *post hoc* test.

Since EphA3 signaling regulates axon growth in callosal axons (Nishikimi, Oishi, Tabata, Torii, & Nakajima, 2011), we next examined EphA3 protein levels in hippocampal neurons. Western blot results show high levels of EphA3 at 2 DIV and then progressively

declines at 4 and 7 DIV in cultured hippocampal neurons (**Fig. 22**). These results suggest that EphA3 receptor is highly expressed at early differentiation stages (2 DIV) and then progressively declines as axon elongation ends.

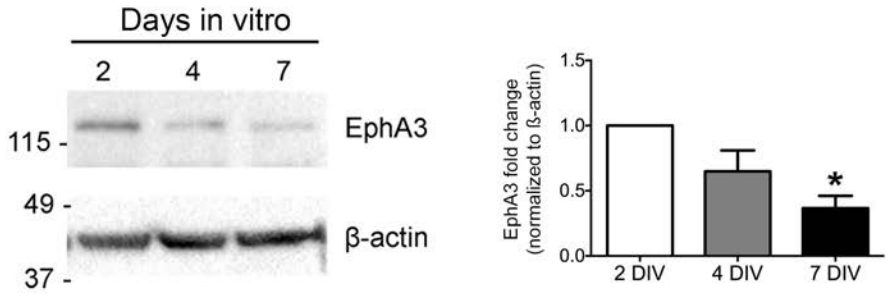

Figure 22. EphA3 protein levels at different stages of neuronal polarization. Biochemical analysis of EphA3 in cultured hippocampal neurons at 2, 4 and 7 DIV. Western blot of hippocampal neuron lysates at 2, 4 and 7 DIV using a C-terminal EphA3 antibody (5E11F2). Data represent mean ± SEM (n= 4 experiments). *p < 0.05, normalized to 2 DIV, as determined by one-way ANOVA followed by Bonferroni *post hoc* test.

2. PS1 regulates EphA3 processing

2.1. PS/γ-secretase-dependent EphA3 processing

Previous results from our lab showed that EphA3 and PS1 colocalize in axons and in growth cones of hippocampal neurons, and they interact in HEK 293T cells overexpressing EphA3, suggesting that EphA3 could be a binding protein and a substrate of PS/γ-secretase complex (Martín, 2013). To examine whether EphA3 is a *bona fide* PS/γ-secretase substrate we analyzed EphA3 C-terminal derived fragments (CTFs) accumulation in PS/γ-secretase-deficient cells. For typical PS/γ-secretase substrates, the metalloprotease-mediated ectodomain shedding of the substrate generates soluble NTF, membrane-attached CTFs, which are then cleaved by γ-secretase. The accumulation of CTF fragments indicates that the PS/γ-secretase is not able to cleave it to generate the ICD fragments, resulting in the accumulation of CTFs. We first tested this idea in $PS1^{-/-}$ mouse embryos (Shen et al., 1997). Using a specific anti-EphA3 C-terminal antibody (C-19), we detected the presence of an EphA3 CTF-derived specie of ~49 kDa in brain homogenates from $PS1^{-/-}$ embryos (**Fig. 23A**). The accumulation of EphA3 CTF is significantly higher in $PS1^{-/-}$ (2 fold) compared to $PS1^{+/+}$ (1 fold) embryos. To investigate whether inhibition of γ-secretase was responsible for the accumulation of EphA3 CTF, we analysed EphA3 processing in human

EphA3-transfected HEK293T cells, a cell line that do not express endogenous EphA3. 24 hours after transfection, cells were incubated with the reversible pharmacological γ-secretase inhibitor DAPT for an additional 24 h, before lysis and analysis by Western blot using a monoclonal CTF antibody (5E11F2). The results show a band of a ~110 kDa corresponding to exogenous hEphA3 and an additional ~49 kDa band, likely corresponding to EphA3 CTF since it was significantly increased after DAPT treatment (**Fig. 3B**). These results demonstrate that EphA3 could be a substrate of PS/γ-secretase.

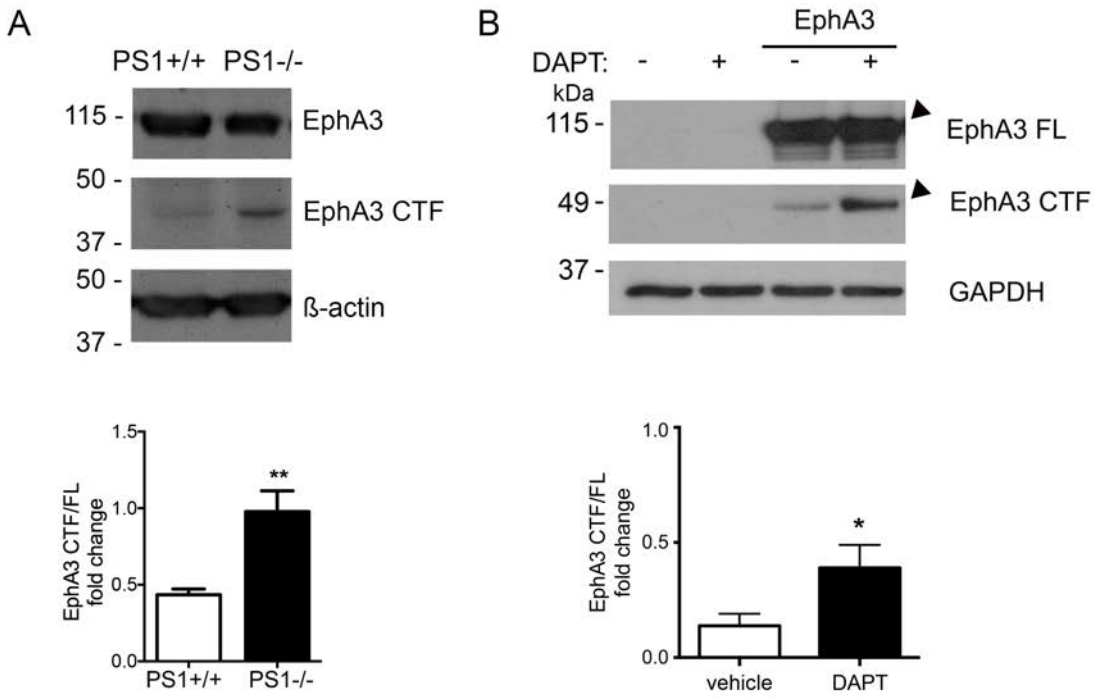

Figure 23. PS1/γ-secretase is required for EphA3 CTF processing in mammalian cells A) Biochemical analysis of brain lysates from $PS1^{+/+}$ and $PS1^{-/-}$ mouse embryos (E15.5) show the accumulation of EphA3 CTF in mouse brains lacking PS1 (C-19 antibody). **B)** EphA3 CTF accumulates in HEK293T cells overexpressing human EphA3 and treated with the γ-secretase inhibitor DAPT (5E11F2 antibody). Values represent mean ± SEM (n= 4 brains and n= 3 independent experiments); Unpaired two-tailed Student's *t* test: $*p < 0.05$, $**p < 0.01$.

We next study the possible metalloproteinase involved in the processing of EphA3. We tested the effect on EphA3 CTFs processing by incubating hEphA3-transfected HEK293T with several γ-secretase and metalloprotease inhibitors (48 h). Biochemical analysis showed that two potent γ-secretase inhibitors (DAPT and L-685,458) induced the accumulation of EphA3 CTFs. Treatment of cells with DAPT plus GM-6001 (MMPs: 1, 2, 3, 7, 8, 9, 12, 14, 26) did not affected CTFs accumulation. Thus, treatment of cells with

DAPT plus EGCG (ß-secretase), SB-3CT (MMP-1, 3, 7 and 9), 1,10-PNT (ADAMs: 10, 12 and 28) or Marimastat (MMPs: 1, 2, 7, 9 and 14) increases the accumulation of EphA3 CTFs subtly. By contrast, inhibitor MMP9/13, which is specific for MMP-1, 3, 7, 9 and 13, reduced significantly EphA3 CTFs (**Fig. 24**). This result show that the metalloproteinases involved in the EphA3 cleavage prior to PS/γ-secretase could be MMP-1, 3, 7, 9 and 13. (**Fig. 24**). Compared with the rest of inhibitors, and considering that MMP9/13 is the only that inhibits MMP13, it is likely that MMP13 could be the metalloproteinase involved in the EphA3 cleavage prior to PS/γ-secretase.

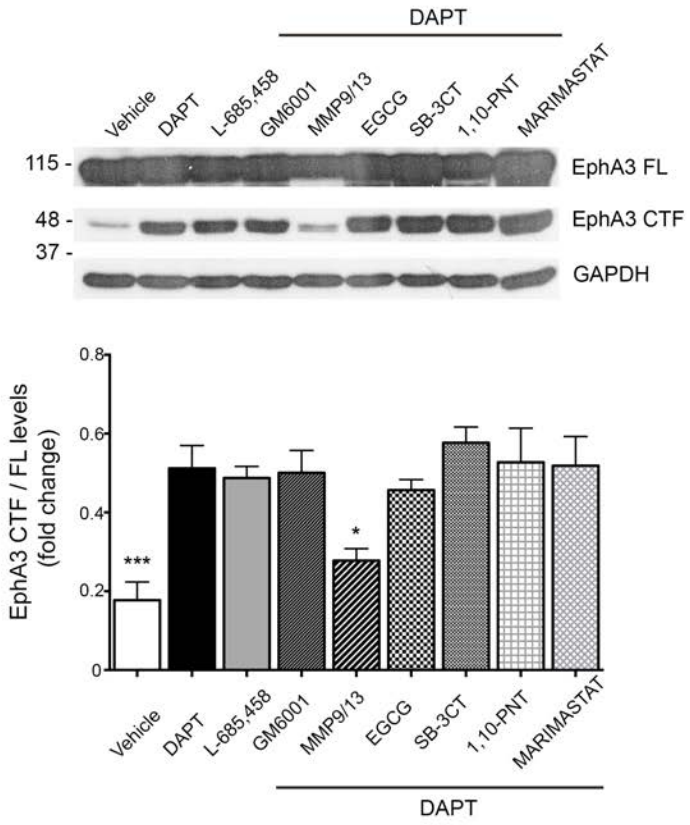

Figure 24. The ADAM/metalloprotease inhibitor MMP9/13 abrogated EphA3 CTF accumulation caused by DAPT in HEK293T cells. HEK 293T cells were transiently transfected with EphA3 for 48 h and treated with several γ-secretase and metalloprotease inhibitors. Western blot analysis (5E11F2 antibody) reveals a reduction in EphA3 CTF accumulation after the combined treatment of DAPT and MMP9/13. Data are mean ± SEM (n=6 independent experiments). One-way ANOVA followed by Bonferroni *post hoc* test: **p* < 0.05, ****p* < 0.0001, compared to DAPT treatment.

The inhibition of the metalloproteinase cleavage of EphA3 combined with the inhibition of the γ-secretase scission should reduce the release of the NTF into the extracellular medium. To analyse the presence of soluble EphA3 NTF in the extracellular medium,

HEK293T cells were transfected with hEphA3 and 24h after they were treated with MMP9/13 (10 μM) and DAPT (1 μM), or only treated with DAPT (5 μM). They were maintained in serum-free medium to avoid the interference of albumin in the detection of the NTF 48h after transfection. As above, DAPT treatment causes the accumulation of the EphA3 CTF fragment, whereas MMP9/13 inhibitor abrogated the accumulation of EphA3 CTFs (5E11F2 antibody; **Fig. 25A**). To analyse the release of EphA3 NTFs, the cultured mediums were filtered and concentrated. Western blot analysis (anti N-terminal EphA3 L-18 antibody) revealed a band of ~75 kDa corresponding to a soluble EphA3 NTF fragment. The released of this NTF is reduced with treatment with MMP9/13 inhibitor, indicating that MMP13 cleaves first EphA3 to generate a NTF (~75 kDa) and a CTFs (~49 kDa) that is then processed by PS/γ-secretase (**Fig. 25B**).

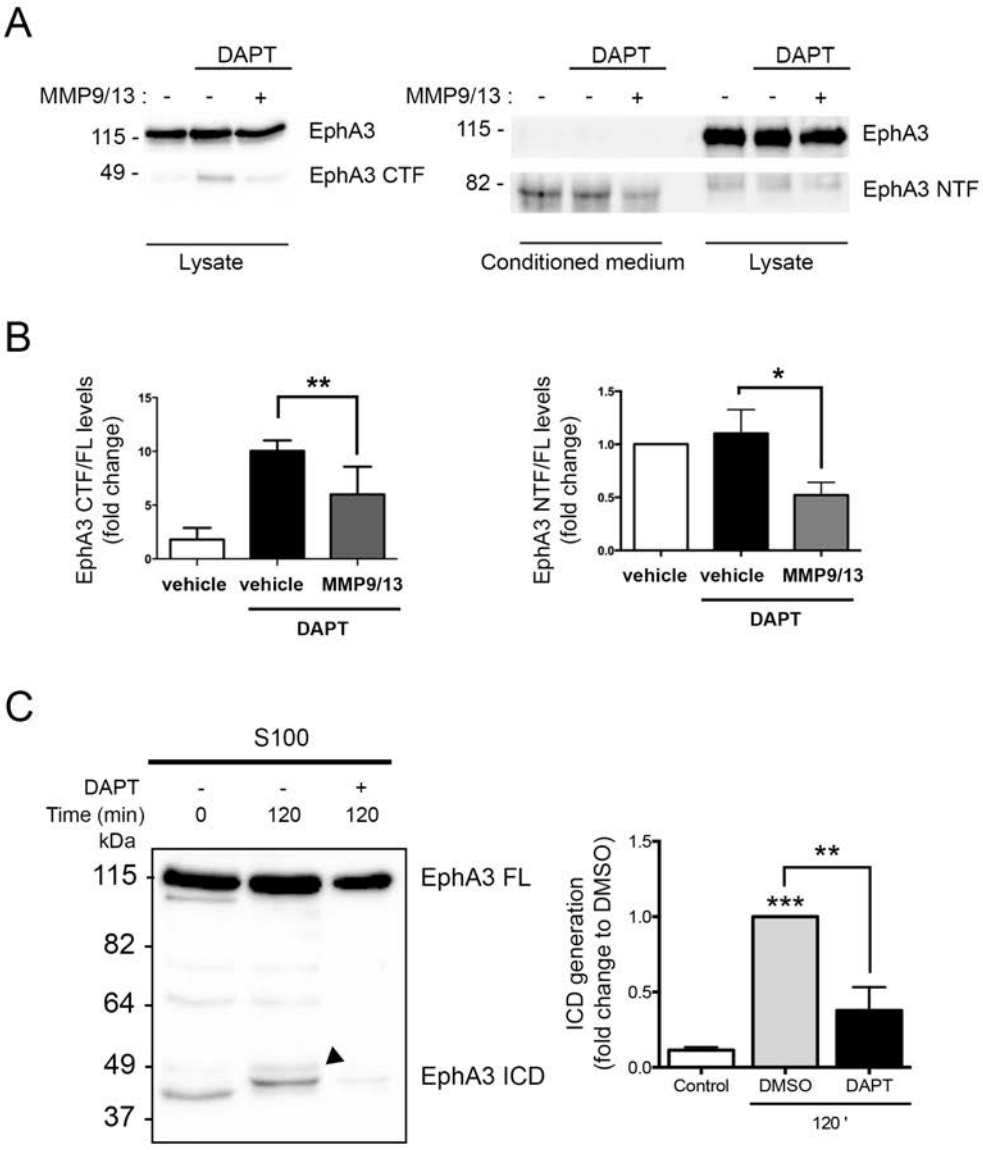

Figure 25. MMP9/13 treatment inhibits the ectoshedding of EphA3 in HEK293 cells. MMP9/13 reduces significantly EphA3 CTF accumulation induced by DAPT in lysates (5E11F2 antibody;

panel **A)** and EphA3 NTF in conditioned medium (L-18 antibody; panel **B)** of EphA3-overexpressing HEK293T cells. Data are mean ± SD (n= 5 experiments). Statistics was tested by one-way ANOVA followed by Bonferroni *post hoc* test: *$p < 0.05$, **$p < 0.01$, compared to vehicle or control or the indicated group. **C)** Cell-free γ-secretase assay showing generation of EphA3 ICD (arrowheads) in soluble fractions (S100) of EphA3-expressing HEK293 cells using a HA antibody. Data are mean ± SEM (n= 3 experiments). Statistics was tested by one-way ANOVA followed by Bonferroni *post hoc* test: **$p < 0.01$, ***$p < 0.001$, compared to control or the indicated group. *Indicates a reduction of ICD generation due to DAPT treatment.

PS/γ-secretase-mediated cleavage of CTF generates an intracellular domain (ICD) fragment that in most cases has independent functions from the non-processed receptor (Haapasalo & Kovacs, 2011). To further characterize the γ-secretase cleavage of EphA3, we examined the presence of an EphA3 ICD by an *in vitro* γ-secretase assay (Sastre et al., 2001). HEK293T were transiently transfected with EphA3-HA and 48 h later membrane fractions were purified. Membrane fractions were incubated with vehicle (DMSO) or DAPT at 37°C for 2h and ultracentrifuged for 1h at 100,000 x *g*. Finally, the soluble fractions (supernatant) were analysed by Western blotting using C-terminal EphA3 (C-19) antibody. The results show that incubation of membrane fractions at 37°C causes the generation of a fragment of ~45 kDa, most likely corresponding to EphA3 ICD. Moreover, the inhibition of PS/γ-secretase by DAPT abrogated EphA3 ICD generation, indicating that the presence of this ICD fragment depends on PS/γ-secretase (**Fig. 25C**).

2.2. PS/γ-secretase cleaves EphA3 at Y560

The cleavage of PS/γ-secretase usually occurs in the transmembrane domains of the type I protein. The transmembrane domain of EphA3 comprises amino acids 542-564, and the alignment by ClustalW of EphA3 with EphB2, a PS/γ-secretase substrate, predicted the EphA3 cleavage site at residues I559 and Y560 (**Fig. 26**) (Litterst et al., 2007; Martín, 2013).

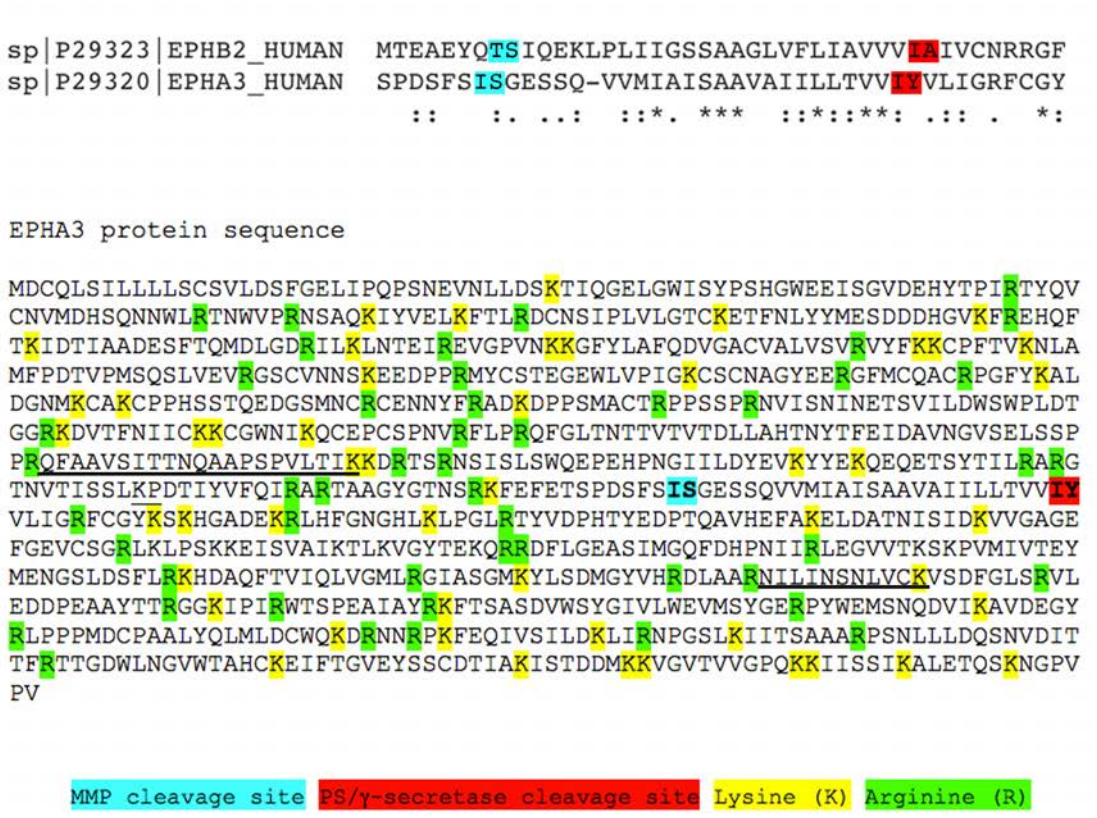

Figure 26. Potential cleaved sites in EphA3. Upper panel, alignment of EphA3 and EphB2 sequences by ClustalW. Lower panel, cleavage sites by MMP (in blue) and PS/g-secretase (in red) are indicated in the human EphA3 protein sequence. Trypsin cleavages at lysines (K; yellow) and arginines (R; green) are also shown. Underlined the sequences checked by mass spectrometry.

To confirm the predicted PS/γ-secretase cleavage site in EphA3 we used a proteomic approach based on sequential *in vitro* γ-secretase and anti-HA immunoprecipitation assays in EphA3-HA expressing HEK293T cells. Soluble fractions (S100) from the purified membranes were obtained and then immunoprecipitated proteins (anti-HA antibody) of each condition were split into 10% and 90% of the total of the volume. The immunoprecipitated proteins were resolved on 8.5% SDS-PAGE and analyzed in parallel: the 10% fraction was analyzed by Western blot and served as intern control of EphA3 ICD generation, whereas the remaining 90% was stained using silver staining and analysed using liquid chromatography-tandem mass spectrometry (LC-MS/MS). As, we could not identify a unique band around 45 kDa, the region of interest was excised and in-gel digested with trypsin. Finally, we could confirm the presence of EphA3 in the sample. We focused on the two most suitable (detectable) peptides prior (QFAAVSITTNQAAPSPVLTIK) and after (NILINSNLVCK) the predicted PS/γ-secretase cleavage site in LC-MS/MS analysis by using PeptideRank software (http://wlab.ethz.ch/peptiderank/). Interestingly, the detection of the

NILINSNLVCK peptide but the lack of detection of QFAAVSITTNQAAPSPVLTIK peptide confirmed the presence of a C-terminal fragment likely comprising EphA3 ICD (Fig. 27). Indeed, if PS/γ-secretase cleavages EphA3 at I559-Y560, we should detect a peptide from the expected cleavage site Y560 to R565 (the Arg where trypsin cleaves). Interestingly, the spectrometric analysis identifies the peptide **VLIGR**, confirming that PS/γ-secretase cleavages EphA3 at Y560 (**Figs. 26 and 27**).

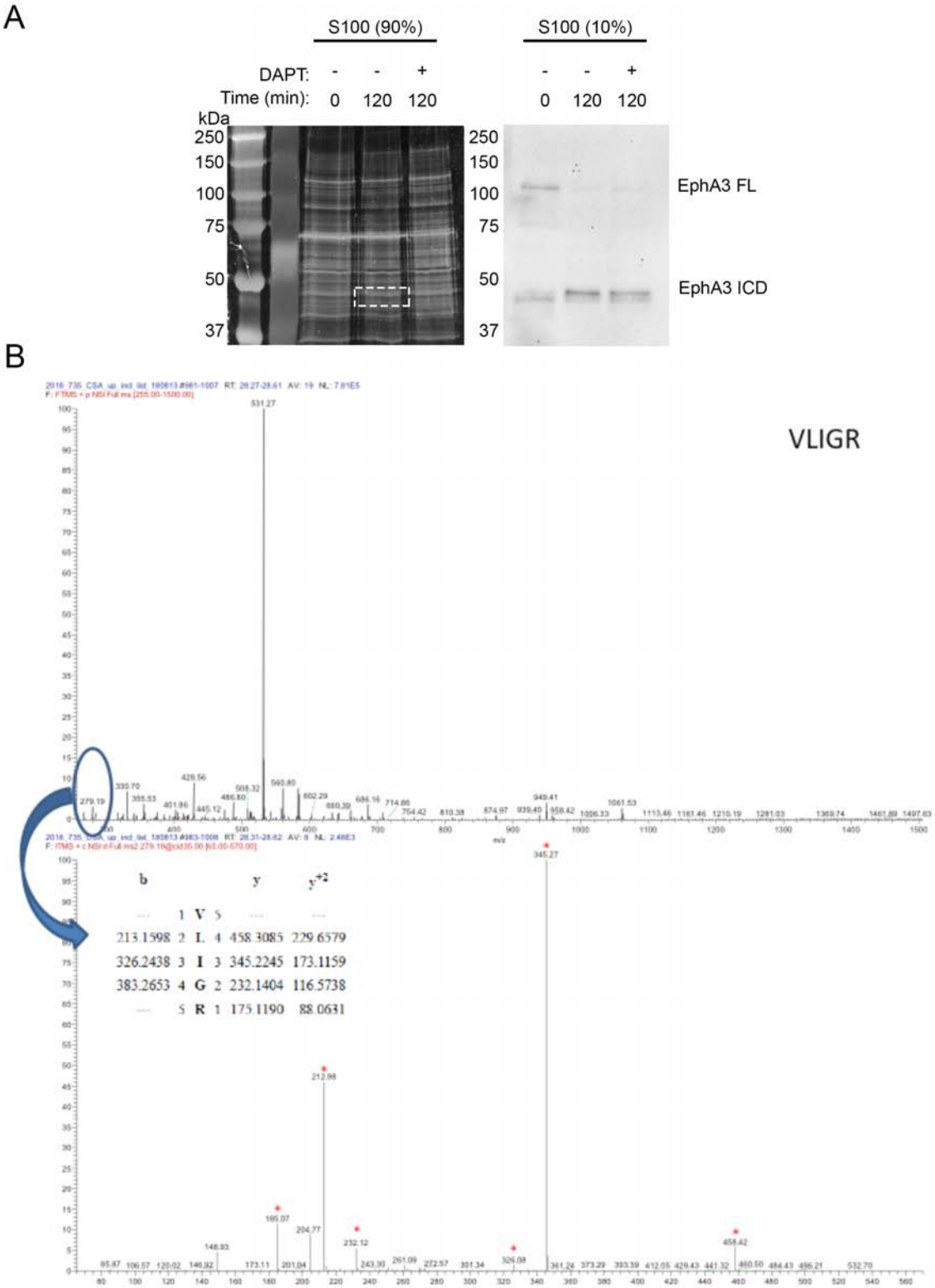

Figure 27. Identification of the PS/γ-secretase cleavage site in EphA3. A) Immunoprecipitated proteins were resolved on 8.5% SDS-PAGE (left). Western blot detecting EphA3 ICD after γ-secretase and immunoprecipitation assays (right). The white box indicates the in gel digested region. **B)** The full MS spectra of the trypsin-digested band of the gel region indicated in A (~47-49 kDa) (top spectra) and specific MS/MS spectra obtained for peptide VLIGR showing the mass/charge (m/z) values (bottom spectra). Detected signals corresponding with theoretical ions are labelled with red asterisks.

Taken together, these results demonstrate that EphA3 is a substrate of PS/γ-secretase. According to our results, EphA3 is first processed by the metalloprotease MMP13 causing the release of the soluble ectodomain EphA3 NTF to the extracellular space and generation of the EphA3 CTF that remains anchored to the membrane. EphA3 CTF is then cleaved at Y560 by PS/γ-secretase, leading to the generation of an EphA3 ICD (**Fig. 28**).

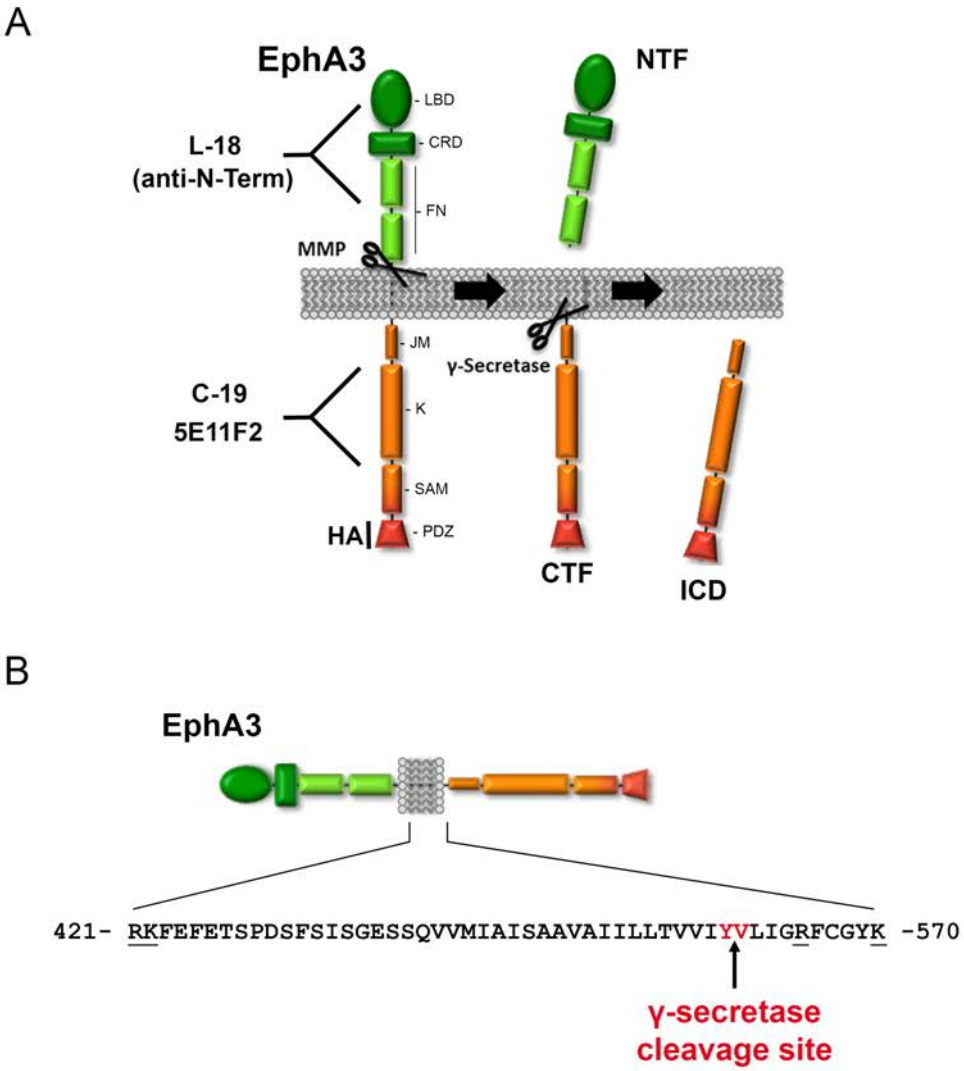

Figure 28. Proposed schematic model of EphA3 processing by PS/γ-secretase. A) EphA3 structural domains (colored boxes) and epitopes detected by antibodies used in this study are indicated. **B)** Schematic representation of PS/γ-secretase cleavage site of EphA3. LBD, ligand binding domain; CRD, cysteine-rich domain; FN, fibronectin repeats; JM, juxtamembrane domain; K, kinase domain; SAM, Sterile alpha motif; PDZ, PDZ-binding domain; MMP, matrix metalloproteinase protein; CTF, C- terminal fragment; ICD, Intracellular domain.

2.3. Ligand-independent EphA3 processing by PS/γ-secretase

The classical activation of tyrosine kinase receptors occurs through the binding to their ligands. However, growing evidences show that ligand-independent signaling can also occur (Boyd & Lackmann, 2001; Inoue et al., 2009). To examine whether PS/γ-secretase-dependent EphA3 cleavage was dependent on ligand binding, we cultured cortical neurons 3 h after seeding with vehicle or DAPT (250 nM). At 5 DIV, cells were incubated (30 min) with clustered ephrin-A5, a high affinity ligand (Janes et al., 2005). As expected from previous studies (Lawrenson et al., 2002), ephrin-A5 treatment enhanced EphA3 phosphorylation at Tyr 779. Interestingly, DAPT treatment did not affect EphA3 phosphorylation induced by ephrin-A5, and it did not change apparently the levels of EphA3 CTFs in cortical neurons (**Fig. 29**). This result suggests that EphA3 processing by PS/γ-secretase seems to occur independently of ligand binding.

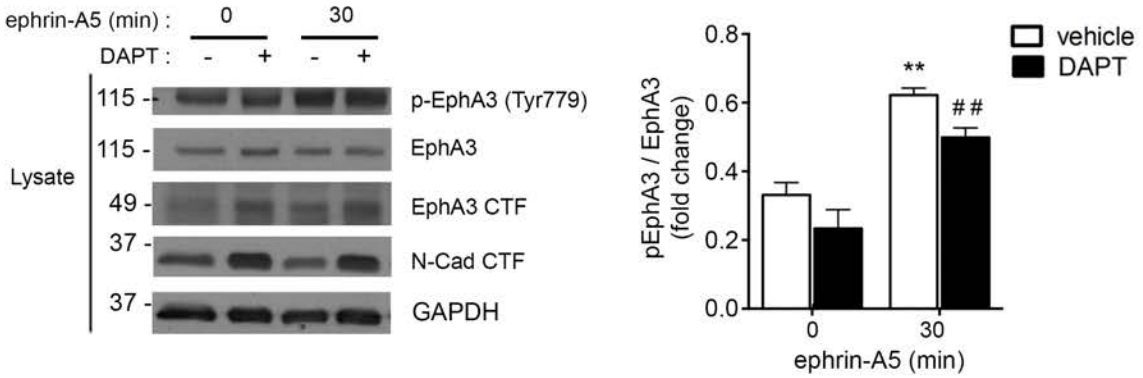

Figure 29. Inhibition of PS1/γ-secretase does not affect EphA3 phosphorylation. Biochemical analysis of total and phosphorylated (Tyr779) EphA3 and EphA3 CTFs in cortical cultured neurons (5 DIV) treated with vehicle (-) or the γ-secretase inhibitor DAPT (+) in the absence or presence of clustered ephrin-A5 (normalized to GAPDH). Data are mean ± SEM (n= 3-5 independent experiments). Two-way ANOVA followed by Bonferroni *post hoc* test: $^{**}p < 0.01$, compared with control (non-stimulated) and, $^{\#\#}p < 0.01$, compared to DAPT (non-stimulated).

To further confirm the previous results, we next studied the PS/γ-secretase-dependent processing of truncated EphA3 mutants. We used EphA3 WT (control), EphA3 lacking the ligand-binding domain (EphA3-ΔLBD) and EphA3 lacking the PDZ-binding domain (EphA3-ΔPDZ). HEK293T cells were transiently transfected with EphA3 constructs and treated with vehicle or DAPT for 48h. Western blotting using EphA3 C-19 antibody revealed the accumulation of EphA3 CTFs in all DAPT treated cells. The accumulation of EphA3 CTFs in cells expressing the EphA3 LBD mutant indicates that this domain is dispensable for PS/γ-

secretase-mediated cleavage, and that the binding of ligand is not required for metalloprotease and γ-secretase cleavages. Similarly, the absence of PDZ binding domain does not affect the PS/γ-secretase-mediated EphA3 processing (**Fig. 30**).

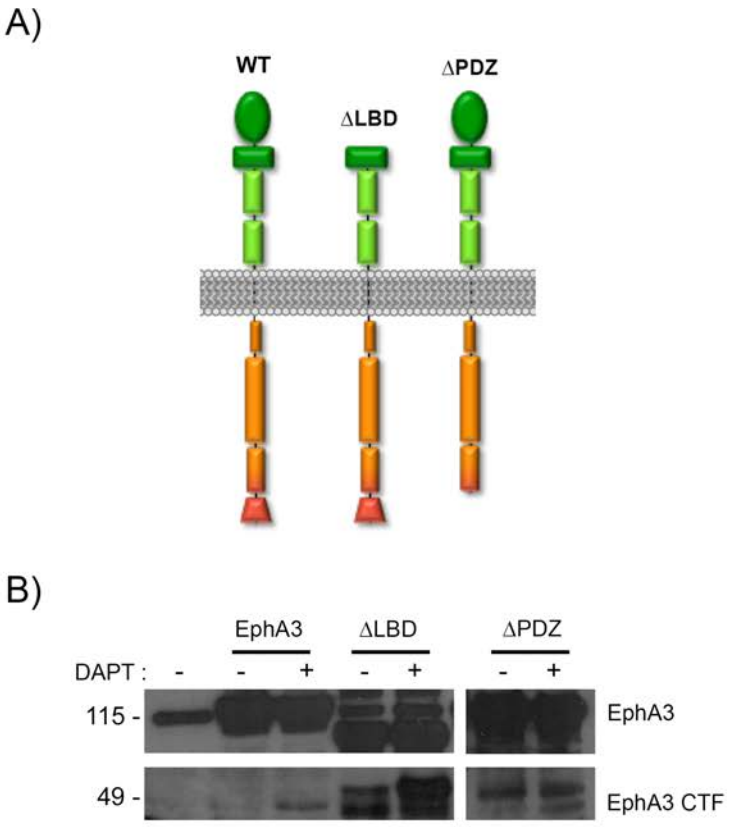

Figure 30. PS/γ-secretase processing of EphA3 truncated mutants. A) Schematic structure of EphA3 WT and truncated mutants. **B)** The deletion of ΔLBD and ΔPDZ does not affect EphA3 CTF accumulation induced by DAPT in HEK293T cells (5E11F2 antibody). ΔLB: EphA3 lacking ligand-binding domain; ΔPDZ: EphA3 lacking PDZ domain.

3. PS/γ-secretase-dependent EphA3 processing regulates axon growth and axon growth collapse

3.1. PS1/γ-secretase is required for axon length *in vitro* and *in vivo*

Expression of PS1 is essential during the development of CNS. Among their several reported functions is the regulation of neuronal migration and morphogenesis (Louvi, 2004; Shen et al., 1997). Here, we investigated if the processing of EphA3 by PS/γ-secretase is involved in axonal growth, which is critical event during the formation of neuronal

connections in the developing nervous system. We first performed an immunohistochemical analysis of the axon length of control ($PS1^{+/+}$) and $PS1^{-/-}$ embryonic mouse brains (E15.5) using the mouse anti-SMI312 antibody. This antibody provides a specific marker for axons since it recognizes phosphorylated axonal epitopes on neurofilaments of medium and high molecular weights. Confocal microscope images revealed regular axon morphology extending to the outer layer of the hippocampal formation and ventricular zone in $PS1^{+/+}$ embryos (**Fig. 31**). Notably, the intensity and length of SMI312-stained axons are apparently reduced in $PS1^{-/-}$ embryos. Quantitative Imaris analyses show that axon length is reduced in $PS1^{-/-}$ brains compared to controls (*$p < 0.05$) (**Fig. 31**). In agreement to this, similar axon length defects are observed in 4 DIV cultured hippocampal neurons treated with γ-secretase inhibitor DAPT (**Fig. 33A, C**), suggesting that PS/γ-secretase activity is required for axon growth in hippocampal neurons.

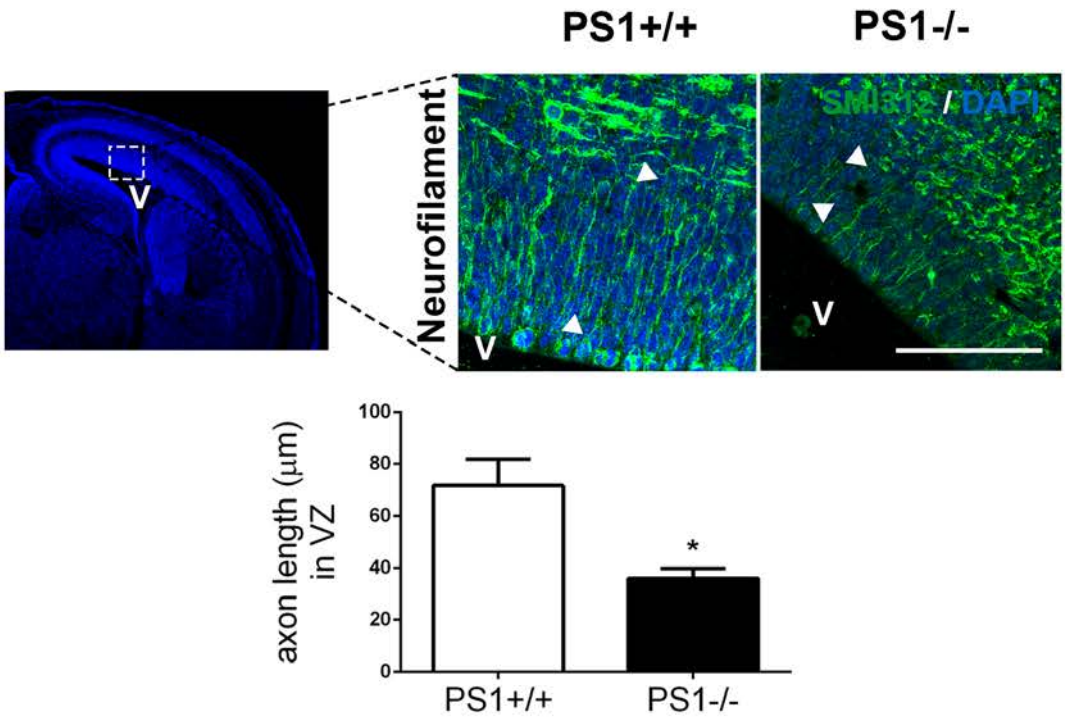

Figure 31. Reduced axon length in embryonic $PS1^{-/-}$ brains. Confocal microscope images (left) and quantitative analysis (right) showing reduced axon length in the ventricular zone of $PS1^{-/-}$ mouse brains (E15.5). Axons (green) are labeled with neurofilament (SM312 staining) and hoechst staining is shown in blue. Insets show magnified regions marked by dotted lines. Multiple neurofilament stained-axons (n=5 axons/section; 10-15 sections/embryo) were analyzed and quantified. Scale bar, 50 μm. Data are mean ± SEM (n=3-4 embryos/genotype). Unpaired two-tailed Student's *t* test: *$p < 0.05$, compared to $PS1^{+/+}$.

We next investigated the role of PS/γ-secretase-dependent EphA3 processing on axon elongation. We generated an EphA3 ICD mutant, which comprises aminoacids 561-983 plus a HA-tag, and ΔICD, which contains a stop codon at Y570 (**Fig. 32A**). Western blot results using the C-terminal EphA3 (C19) and the N-terminal EphA3 (L18) antibodies show the correct expression of EphA3 ICD (~47 kDa) and EphA3 ΔICD (~75 kDa) bands, respectively (**Fig. 32B**).

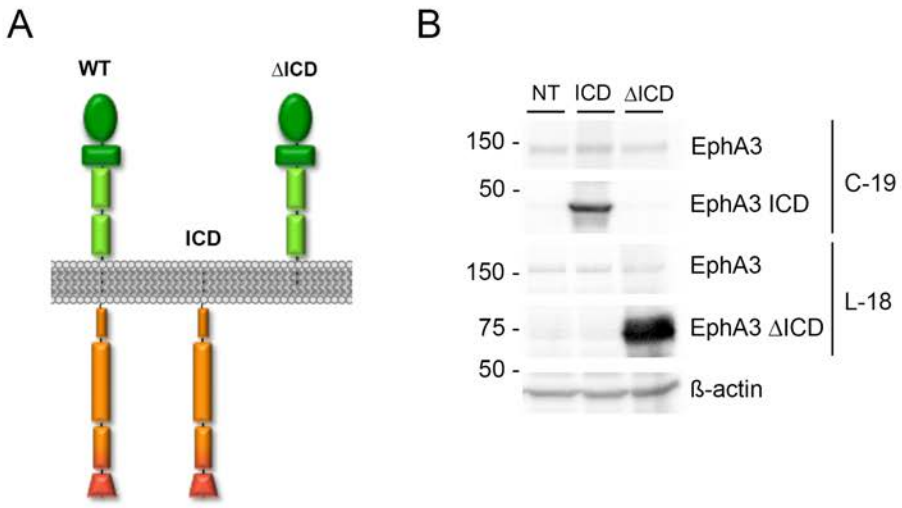

Figure 32. Expression of EphA3 mutants in HEK293T cells. A) Schematic representation of the generated EphA3 ICD and ΔICD constructs. **B)** HEK 293T cells were transiently transfected with EphA3 ICD and ΔICD for 48 h. Biochemical analysis by Western blotting shows exogenous EphA3 ICD (C-19 antibody) and ΔICD (L-18 antibody).

Previous results from our lab showed that the EphA3 ICD rescued the axonal length defects caused by γ-secretase inhibition in cultured neurons **(Martín, 2013) (Fig. 33A,C).** To further characterise the EphA3 structural domains involved in axon growth, we examined the effect of overexpressing the EphA3 ICD and the EphA3 ΔICD, which lacks the entire intracellular domain. Immunofluorescence analysis using the monoclonal anti-SMI312 antibody shows that EphA3 ICD efficiently reversed axon deficits in DAPT-treated neurons (**Fig. 33A, B)**. By contrast, the EphA3 fl and EphA3 ΔICD are not able to reverse the axon length defects in DAPT-treated hippocampal neurons (**Fig. 33B, C**). These results indicate that the EphA3 ICD generated by PS/γ-secretase-dependent EphA3 processing mediates axon elongation in hippocampal neurons.

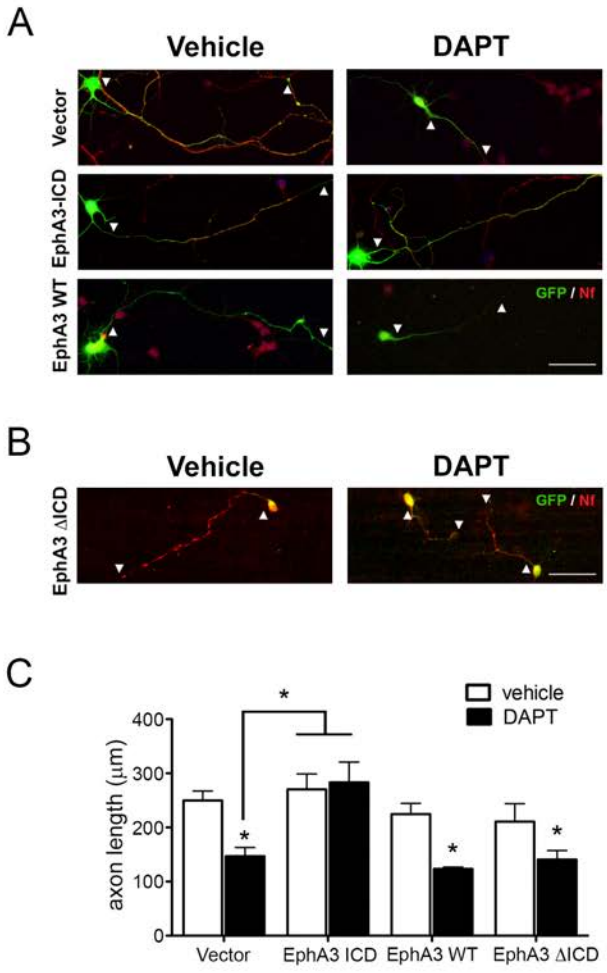

Figure 33. EphA3 ICD reverses axon defects in neurons lacking PS/γ-secretase. A-B) EphA3 ICD (GFP, green) reverses axon defects in PS/γ-secretase-deficient neurons, but not EphA3 WT or ΔICD (GFP, green). Axons were stained with SMI312 (red) and arrowheads indicate axon length. Scale bar, 50 μm. Panel A) has been obtained from (Martín, 2013). **C)** Quantitative analysis. Data represent mean ± SEM of at least three independent experiments (n = 3-6 coverslips, n= 30 neurons/coverslip). Two-way ANOVA followed by Bonferroni *post hoc* test: **p* < 0.05, compared to vector (control) or the indicated group.

3.2. PS/γ-secretase regulates axon growth through RhoA

EphA-ligand dependent signaling induces the growth cone collapse in a RhoA/ROCK-dependent manner, although the mechanisms of RhoA activation remains unknown (Noren & Pasquale, 2004; Shamah et al., 2001). We hypothesized that one possible mechanism underlying the control of axon elongation by PS/γ-secretase-dependent cleavage of EphA3, could be through the negative regulation of RhoA signaling. Previous experiments from our lab showed that the inhibition of RhoA efficiently reduced axon length defects in PS1-

deficient neurons and that the presence of EphA3 ICD significant reduced RhoA activity in neuronal cells (Martín, 2013). To further confirm that EphA3 ICD acts upstream of RhoA, we investigated the role of EphA3 ICD under conditions of RhoA signaling activation. We used a constitutive active RhoA mutant that contains a glutamine to leucine substitution at residue 63 (RhoA Q63L). Axon length imaging analysis shows that the overexpression of RhoA Q63L avoided the axon growth in control and DAPT-treated hippocampal neurons (**Fig. 34**). Thus, the constitutive activation of RhoA prevents the rescue effect of EphA3 ICD on axon length in DAPT-treated hippocampal neurons (**Fig. 34**). Taken together, these results confirm that EphA3 cleavage mediates axon elongation by regulating negatively RhoA signaling.

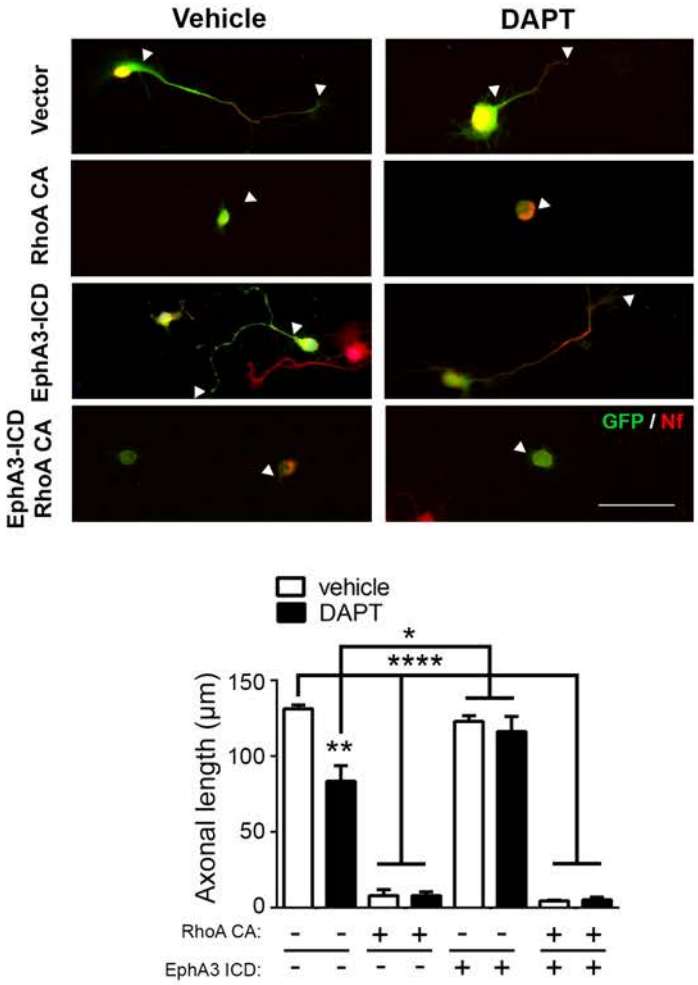

Figure 34. RhoA inhibits axon growth in hippocampal neurons. Immunofluorescence images (top) stained for GFP (green) and neurofilament (SMI312, red) and quantitative analysis of axon length (bottom). Neurons were transfected with GFP (vector), EphA3-ICD and/or a RhoA constitutive active (CA) mutant (RhoA Q63L) and treated with vehicle or DAPT at 2 DIV and fixed

and analyzed at 4 DIV. Scale bar, 50 μm. Data are mean ± SEM of three independent experiments (n=40-80 total neurons/group). *p < 0.05, **p < 0.01, ****p < 0.0001.

3.3. EphA3 ICD regulates growth cone collapse

Another measure to evaluate the effect of EphA3 ICD in axon growth is the rate of axon growth collapse. It is widely accepted that growth cone collapse is a motility-inhibiting mechanism underlying repulsive axon guidance (Luo, Raible, & Raper, 1993). On the contrary, growth cones with a non-collapsed morphology are active motile and related to axon elongation. We then examined the effect of EphA3 ICD in axon growth cone morphology in $PS1^{+/+}$ (control) and $PS1^{-/-}$ cultured hippocampal neurons. Hippocampal neurons were immunolabeled with chicken anti-GFP (green) and phalloidin-Alexa594 (white) and axon growth cones were manually classified as: collapsed, those that have no lamellipodia and no more than two filopodia, and the remaining axons were classified as non-collapsed. Interestingly, immunofluorescence analysis shows that the percentage of collapsed growth cones is significantly different between genotypes (****p < 0.0001). Indeed, there is an interaction effect between genotypes and EphA3 ICD expression (***p < 0.001) (**Fig. 35**). $PS1^{-/-}$ neurons show a percentage of collapsing growth cones similar to $PS1^{+/+}$ (**Fig. 35**). The presence of EphA3 ICD in $PS1^{-/-}$ neurons induces a decrease on the rate of collapsing growth cones, indicating that, in the absence of PS, EphA3 ICD promotes non-collapsed axon morphology (*p < 0.05). In contrast, EphA3 ICD does not affect the percentage of collapsed growth cones in $PS1^{+/+}$ (**Fig. 35**). These results are in agreement with the fact that EphA3 ICD induces axon elongation in $PS1^{-/-}$ hippocampal neurons.

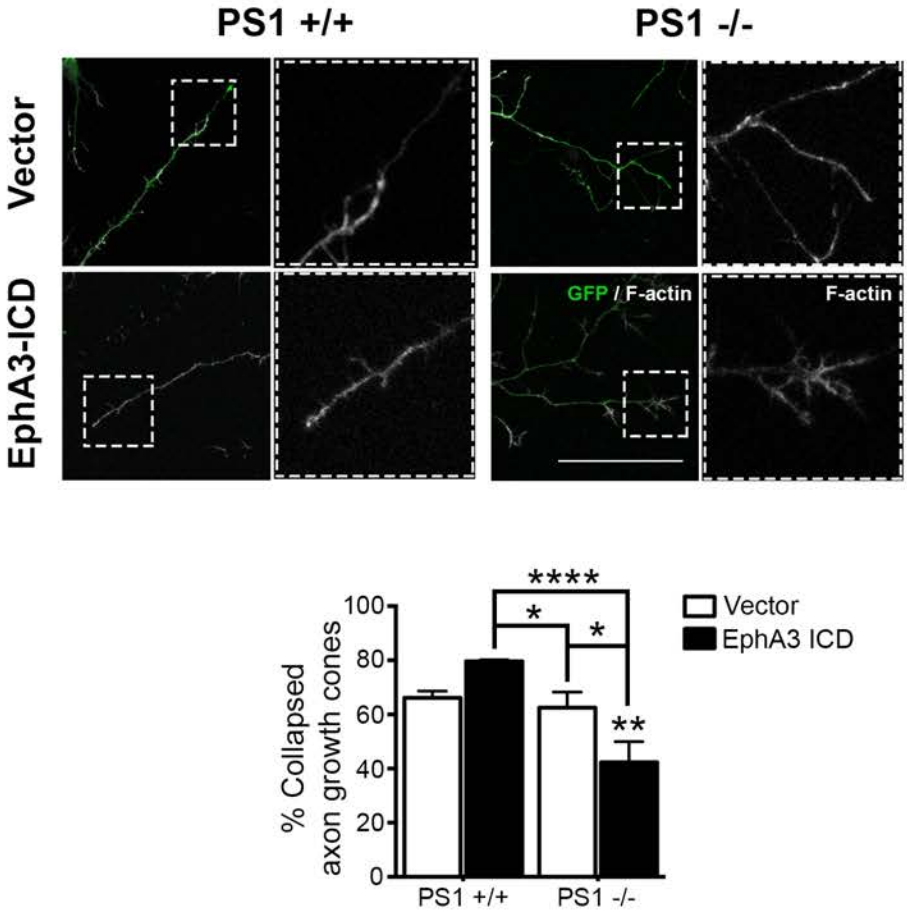

Figure 35. EphA3 ICD regulates growth cone collapse. Hippocampal neurons from $PS1^{+/+}$ (control) and $PS1^{-/-}$ embryo mice (E15.5) were transfected with vector (pWPI-GFP) or EphA3 ICD-GFP (green) at 2 DIV. Cultured neurons were fixed and stained with GFP (green) and F-actin (white) at 4 DIV. The two-way ANOVA analysis showed a genotype-dependent and an interaction effect between the two factors (genotype and ICD expression) ****p < 0.0001 and ***p < 0.001, respectively. N=26-33 neurons/group. The specific differences among groups were determined by Bonferroni *post hoc* test. *p < 0.05, **p <0.01, ****p <0.0001, compared to controls (PS1+/+, vector) or to the indicated group. Scale bar, 50 μm.

CHAPTER 2:

EPHA3 ICD REGULATES AXONAL GROWTH THROUGH NON-MUSCLE MYOSIN IIA

CHAPTER 2: EPHA3 ICD REGULATES AXONAL GROWTH THROUGH NON-MUSCLE MYOSIN IIA

The above results show that PS/γ-secretase-dependent cleavage of EphA3 modulates axon elongation and growth cone collapse in hippocampal neurons. At that point, we wonder if this modulation of axon dynamics could also be explained through the interaction of EphA3 ICD with actin cytoskeleton proteins.

1. EphA3 ICD interacts with NMIIA

To identify EphA3 ICD interacting proteins that could be relevant for axon outgrowth, we performed co-immunoprecipitation assays in HEK 293T cells overexpressing vector-Flag or EphA3 ICD-Flag followed by a proteomic analysis of immunoprecipitated proteins (Free, Hazelwood, & Sibley, 2009). Immunoprecipitated proteins were resolved on 8% acrylamide gel and stained with colloidal comassie. Three prominent protein bands of ~85 (band 3), ~200 (band 2) and ~250 kDa (band 1) were specifically present in the ICD-Flag immunoprecipitates compared with control immunoprecipitations (**Fig. 36A**). The three bands were excised and in-gel digested with trypsin and identified by Peptide Mass Fingerprinting (MALDI-TOF) as: heat shock protein (HSP), clathrin heavy chain 1 and non-muscle myosin IIA heavy chain (NMIIA) (**Table 13**).

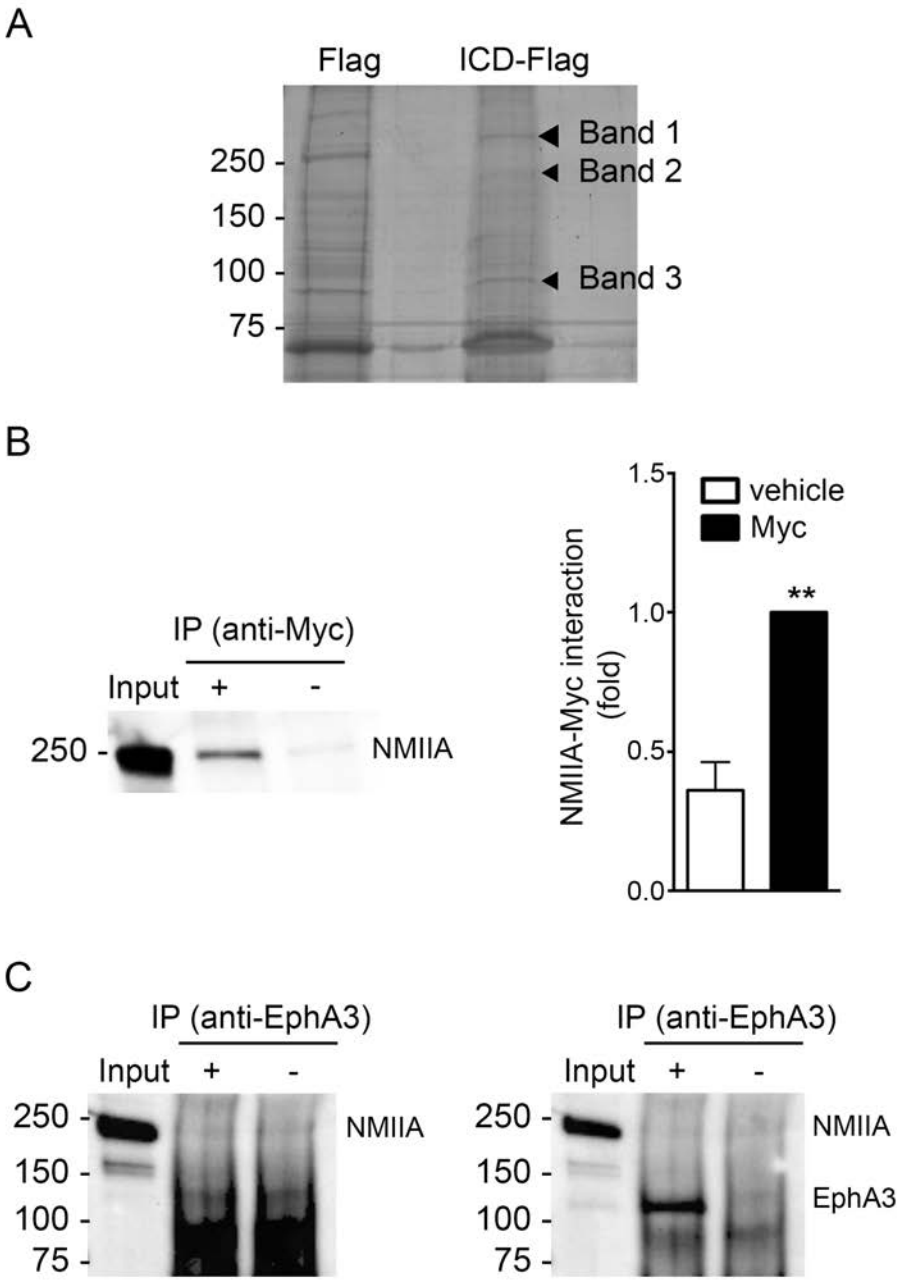

Figure 36. Proteomic analysis of EphA3 binding proteins. A) HEK293T cells transfected with vector (Flag) or EphA3 ICD-Flag (ICD-Flag) were immunoprecipitated with anti-Flag antibody. Proteins were resolved by SDS-PAGE and stained with colloidal comassie. Specific proteins corresponding to bands 1, 2 and 3 were identified by MALDI-TOF/TOF mass spectrometry. Band 1 corresponds to NMIIA. **B)** Binding of myc-EphA3 ICD to NMIIA. Coimmunoprecipitation (IP) of endogenous NMIIA and overexpressed myc-EphA3 ICD in HEK293T cells. Data are mean ± SEM of three independent immunoprecipitations. Unpaired two-tailed Student's *t* test: $^{**}p < 0.01$. **C)** Non-processed EphA3 does not bind to NMIIA. Coimmunoprecipitation (IP) of endogenous NMIIA and EphA3 in embryo brain homogenates (left panel) and detection of EphA3 by Western blot as a control that IP worked well (right panel). N = 2 independent experiments.

Table 13. List of EphA3 binding proteins identified by MALDI-TOF. Protein score is -10*Log(P), where P is the probability that the observed match is a random event. Protein scores > 56 are significant (*p < 0.05)*.

Protein identified	Protein description	Protein Score	Protein Mass (Da)
P35579 MYH9_HUMAN	Myosin-9 OS=Homo sapiens GN=MYH9 PE=1 SV=4	78	227646
Q00610 CLH1_HUMAN	Clathrin heavy chain 1 OS=Homo sapiens GN=CLTC PE=1 SV=5	76	193260
P07900 HS90A_HUMAN	Heat shock protein HSP 90-alpha OS=Homo sapiens GN=HSP90AA1 PE=1 SV=5	134	85006
P08238 HS90B_HUMAN	Heat shock protein HSP 90-beta OS=Homo sapiens GN=HSP90AB1 PE=1 SV=4	96	83554

The MALDI-TOF spectra obtained for each protein were interpreted by database search (Mascot, Matrix Science). Then, all the identified peptides were manually validated by the SwissProt Database restricted to *Homo sapiens* taxonomy (**Table 14**). We focused further on NMIIA/MYH9 since is a protein that regulates contractile activities through its interaction with cytoskeleton actin filaments and is involved in the regulation of neurite retraction (Gallo, 2006; Pecci, Ma, Savoia, & Adelstein, 2018). The Mascot score of NMIIA was 78.

Table 14. Identified peptides from NMIIA protein. *ppm is the deviation of the measured mass from the theoretical mass of the peptide

Start - End	Sequence	Molecular Mass (Observed)	Error (ppm*)
144 - 165	HEMPPHIYAITDTAYRSMMQDR	2663.2180	0.63
187 - 199	VIQYLAYVASSHK	1478.7799	-13.7
273 – 289	TFHIFYYLLSGAGEHLK	1996.0469	7.13
290 -301	TDLLLEPYNKYR	1524.7963	-6.13
328 - 341	IMGIPEEEQMGLLR	1615.8153	-1.76
374 – 387	VSHLLGINVTDFTR	1571.8421	-7.58
541 - 555	SFVEKVMQEQGTHPK	1744.9110	24.3
566 - 580	ADFCIIHYAGKVDYK	1799.9290	28.1

618 – 637	IIGLDQVAGMSETALPGAFK	2034.0428	-7.26
663 -678	NTNPNFVRCIIPNHEK	1953.0276	26.5
746 – 755	ALELDSNLYR	1193.6135	-2.10
1175 - 1181	TLEEEAK	819.4100	0.72
1393 - 1404	DLEGLSQRHEEK	1440.7017	-4.15
1755 – 1770	ANLQIDQINTDLNLER	1869.9816	8.09
1816 – 1830	IAQLEEQLDNETKER	1815.9179	5-31
1899 – 1912	ELEDATETADAMNR	1565.7169	26.9
1924 – 1933	GDLPFVVPRR	1155.6697	5.54

After the identification of NMIIA as a possible EphA3-ICD binding protein, we next validated this interaction by co-immunoprecipitation assays using the anti-myc antibody (9B11; Cell Signaling) in vector- and myc-EphA3 ICD expressing HEK293T cells. Immunoprecipitated proteins were analyzed by Western blot using an anti-NMIIA antibody (H-40). Biochemical results show the EphA3 ICD interacts physically with endogenous NMIIA in HEK293T cells (*$p<0.01$) (**Fig. 36B**).

We next wondered whether PS/γ-secretase-dependent processing of EphA3 was required for the interaction with NMIIA or, on the contrary, the non-processed EphA3 receptor could bind to NMIIA. To answer this question, we decided to change our study model since the endogenous levels of EphA3 in HEK293T are not detectable by Western blot. On contrary, in embryo brain lysates the amount of EphA3 as well as NMIIA are very high and easily detectable by Western blot. Embryonic brain homogenates were co-immunoprecipited using mouse anti-EphA3 antibody (5E11F2) and immunoprecipitated proteins were detected by Western blot using rabbit anti-NMIIA antibody (H-40). Biochemical results show no detection of binding of endogenous EphA3 to NMIIA in embryonic brains. Moreover, the presence of EphA3 FL band after re-blotting the membrane using an anti-rabbit EphA3 antibody (C-19), demonstrates efficient EphA3 immunoprecipitation (**Fig. 36C**). Taken together, these results indicate that the cleavage of EphA3 by PS/γ-secretase-dependent seems necessary for binding to NMIIA.

2. EphA3 ICD increases NMIIA phosphorylation at Ser1943

Next, we hypothesized that the effect of EphA3 ICD mediating the axonal growth occurs at least in part, by its interaction with NMIIA, preventing its binding to actin and allowing axon elongation. To test whether EphA3 ICD also induces changes in NMIIA activity, we analyzed levels of NMIIA phosphorylation (Ser1943), which is mediated by casein kinase II (CKII). Notably, Ser1943 phosphorylation inhibits NMIIA assembly and promotes disassembly of myosin/F-actin/microtubule filaments (Dulyaninova, House, Betapudi, & Bresnick, 2007), but the physiological role of this phosphorylation in neurons is still unknown

To investigate whether the EphA3 ICD affects the phosphorylation of NMIIA at S1943. We generated lentiviruses containing EphA3 ICD sequence (myc-EphA3 ICD pWPI) in order to express EphA3 ICD into cortical neurons. Virus transduction method avoids the low efficiency rates due to transfection problems in cortical neurons. Western blot analysis of cultured cortical neurons transduced with lenti-vector or -EphA3 ICD shows that the levels of pNMIIA (S1943) are higher in the presence of EphA3 ICD (p <0.05*)* (**Fig. 37**), suggesting that EphA3 ICD expression increases pNMIIA levels and likely myosin/F-actin/microtubule filament dissasembly.

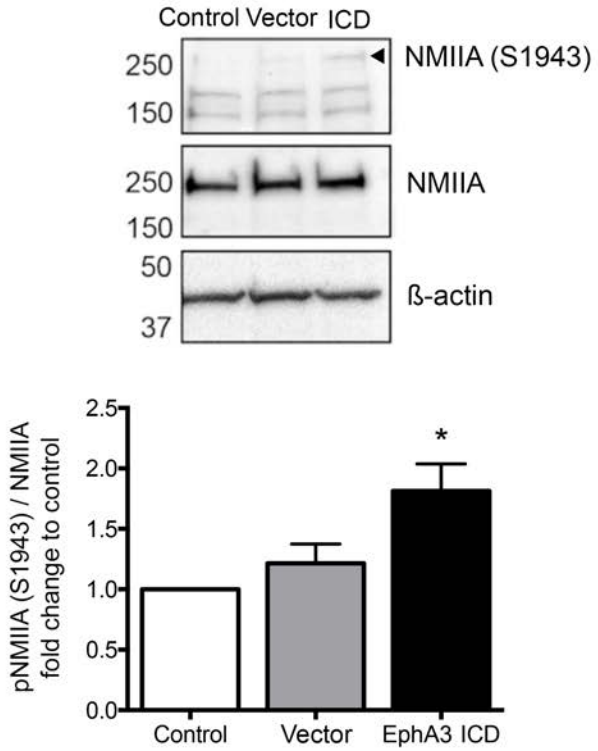

Figure 37. EphA3 ICD increases the phosphorylation levels of NMIIA. Cortical neurons were transduced with empty (pWPI) or EphA3 ICD (myc-EphA3 ICD pWPI) lentiviral vectors at 2 DIV and analysed by Western blotting at 4 DIV. Biochemical analysis show that EphA3 ICD increases pNMIIA

(S1943) levels. Data are mean ± SEM of three independent neuronal cultures. Statistics were tested by one-way ANOVA (*p = 0.05), followed by Bonferroni *post hoc* test. * p < 0.05, compared with control neurons.

Since EphA3 ICD generation depends on PS/γ-secretase activity, we next examined if *PS* expression could affect phosphorylated NMIIA. Cultured hippocampal neurons expressing vector or EphA ICD from $PS1^{+/+}$ (controls) and $PS1^{-/-}$ embryo mice at E15.5 were stained using chicken anti-GFP (Ab13970) and with rabbit anti-pNMIIA (Ser1943) (Ab2974). Images captured by confocal microscopy were analyzed by ImageJ software. Immuncytochemical analysis indicates that the intensity of pNMIIA (S1943) is reduced in the $PS1^{-/-}$ neurons, although this reduction is only significant compared to $PS1^{+/+}$ neurons expressing EphA3 ICD (p<0.01). Interestingly, EphA3 ICD increases significantly the levels of pNMIIA (S1943) in $PS1^{-/-}$ neurons, which were similar to the levels in $PS1^{+/+}$ neurons (**Fig. 38**). This result suggests that EphA3 ICD recovers the phosphorylated NMIIA levels in $PS1^{+/+}$ neurons.

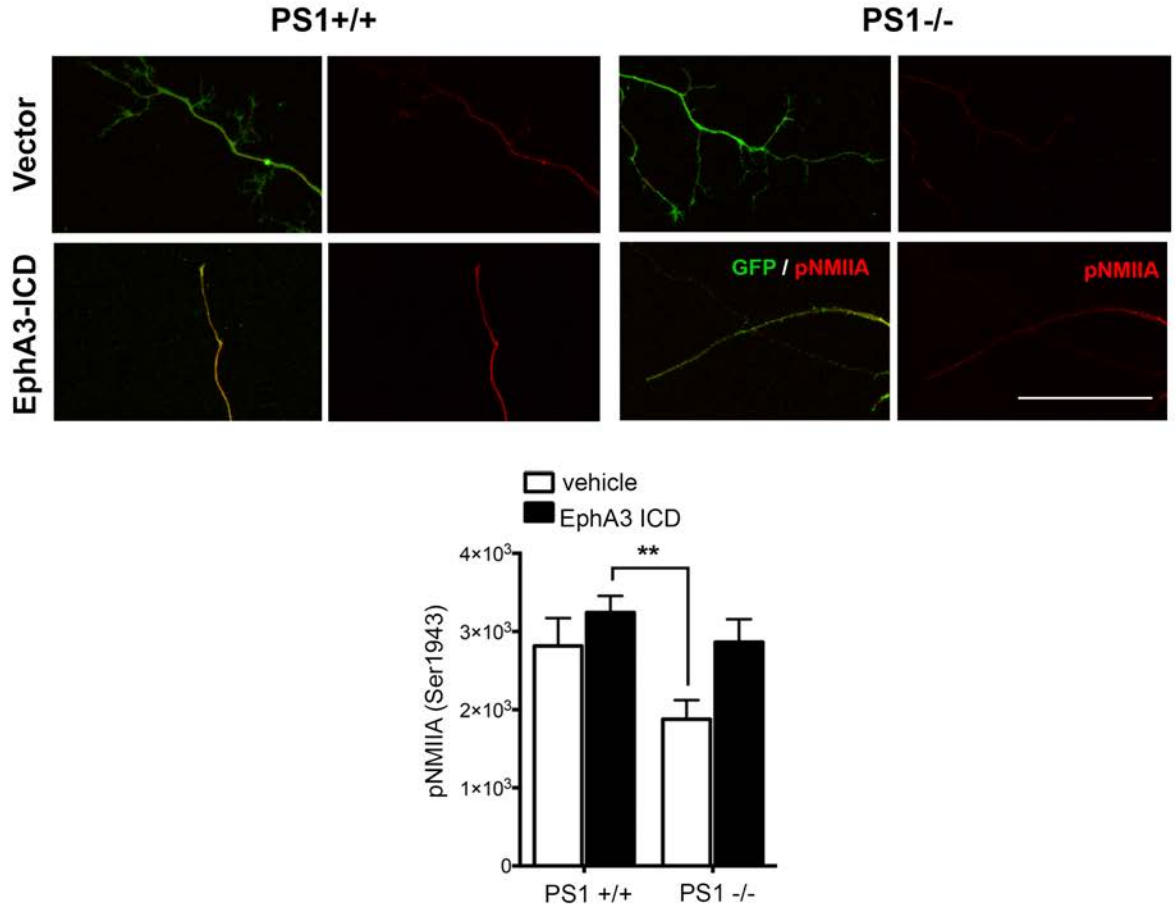

Figure 38. Reduced pNMIIA in axons of PS1-deficient neurons. Immunofluorescence staining (top) and quantitative analysis (bottom) of phosphorylated NMIIA heavy chain (S1943) (in red) in axons of $PS1^{+/+}$ and $PS1^{-/-}$ neurons. Cultured hippocampal neurons (E15.5) from $PS1^{+/+}$ (controls) and $PS1^{-/-}$

embryos were transduced with control (pWPI) or EphA ICD (myc-EphA3 ICD pWPI) lentivirus at 1 DIV and analysed at 4 DIV. PS1-lacking neurons show reduced axonal pNMIIA intensity that is reversed by expressing EphA3 ICD (GFP, green) Scale bar, 50 µm. Data are mean ± SEM of three independent experiments (n=25-33 total neurons/group). Two-way ANOVA indicates a significant genotype- and ICD-transduction effect (*$p < 0.05$). Bonferroni *post hoc* test indicates the intergroup differences **$p < 0.01$.

3. PS1/γ-secretase regulates NMIIA phosphorylation and NMIIA/actin colocalization

We next examined the levels of phosphorylated NMIIA in cortical neurons treated with the γ-secretase inhibitor DAPT. Biochemical analysis of protein lysates with the rabbit anti-NMIIA antibody (H-40; Sta. Cruz), allows the detection of two bands that probably correspond to insoluble (upper band) and soluble (lower band) forms of NMIIA. Interestingly, DAPT treatment causes an increase of insoluble NMIIA whereas the soluble forms are reduced. However, the levels of total NMIIA, considered as soluble plus insoluble forms, remain unchanged (**Fig. 39**). Moreover, DAPT decreased significantly pNMIIA (S1943) levels compared to vehicle-treated neurons (**Fig. 39**).

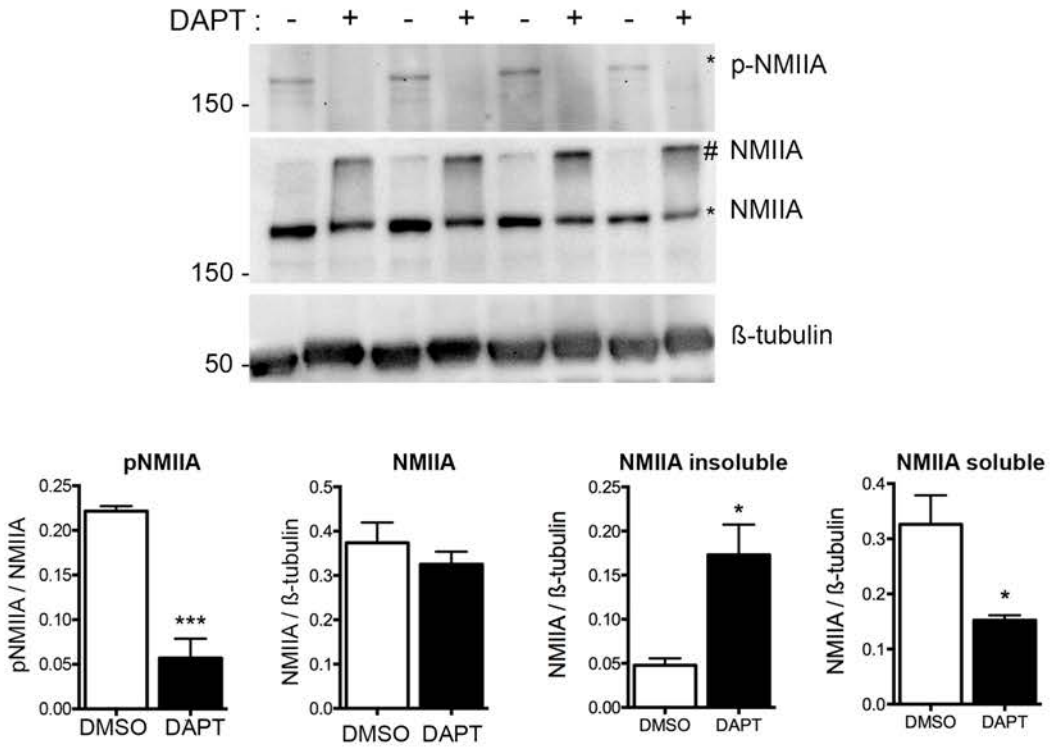

Figure 39. Inhibition of PS/γ-secretase activity reduces phosphorylated NMIIA levels. Cultured cortical neurons were treated with DAPT from 0 DIV and analysed at 4 DIV. Western blot results show

that DAPT treated cortical neurons show reduced pNMIIA (S1943) and soluble NMIIA (*), increased insoluble/aggregated NMIIA (#) and unchanged total NMIIA. Multiple independent cultures are shown. Data are mean ± SEM of four independent neuronal cultures. Unpaired two-tailed Student's *t* test: ***p = 0.001.

These results indicate that PS1/γ-secretase-dependent EphA3 processing maintains active phosphorylated NMIIA. Since phosphorylation of NMIIA at S1943 increases cytoskeleton filament assembly, we next studied whether γ-secretase activity could modulate actin cytoskeleton rearrangement by regulating NMIIA/actin interaction in growth cones. Hippocampal neurons transduced with empty or EphA3 ICD GFP lentiviral vectors were stained with chicken anti-GFP (Ab13970; Abcam) to detect transduced neurons, rabbit anti-pNMIIA (S1943) (Ab2974; MerckMillipore) and phalloidin-Alexa594 (Invitrogen). Colocalization of pNMIIA and F-actin was analysed in confocal microscopy images using the tool ImarisColoc from Imaris 8.1 Software. Immunocytochemical analysis show that the percentage of actin/phosphorylated NMIIA colocalization is decreased in axon growth cones of PS1-deficient hippocampal neurons (genotype-dependent effect, $p<0.05$) (**Fig. 40**). In addition, EphA3 ICD has no effect in control neurons but it increases significantly actin/pNMIIA colocalization and the percentage of colocalizing actin/pNMIIA spots to control levels in $PS1^{-/-}$ neurons (EphA3 ICD transduction-dependent effect, $p<0.01$) (**Fig. 40**). Otherwise, taking into account all the colocalizing spots (that is actin spots colocalized with pNMIIA together with pNMIIA spots colocalized with actin), the genotype-dependent effect is lost, whereas the EphA3 ICD transduction-dependent effect is maintained, $p<0.01$ (**Fig. 40**). Taken together, these results strongly suggest that PS1/γ-secretase-mediated EphA3 cleavage generates an EphA3 ICD peptide that maintains active phosphorylated NMIIA to inhibit assembly or to promote disassembly of cytoskeleton filaments at the growth cone.

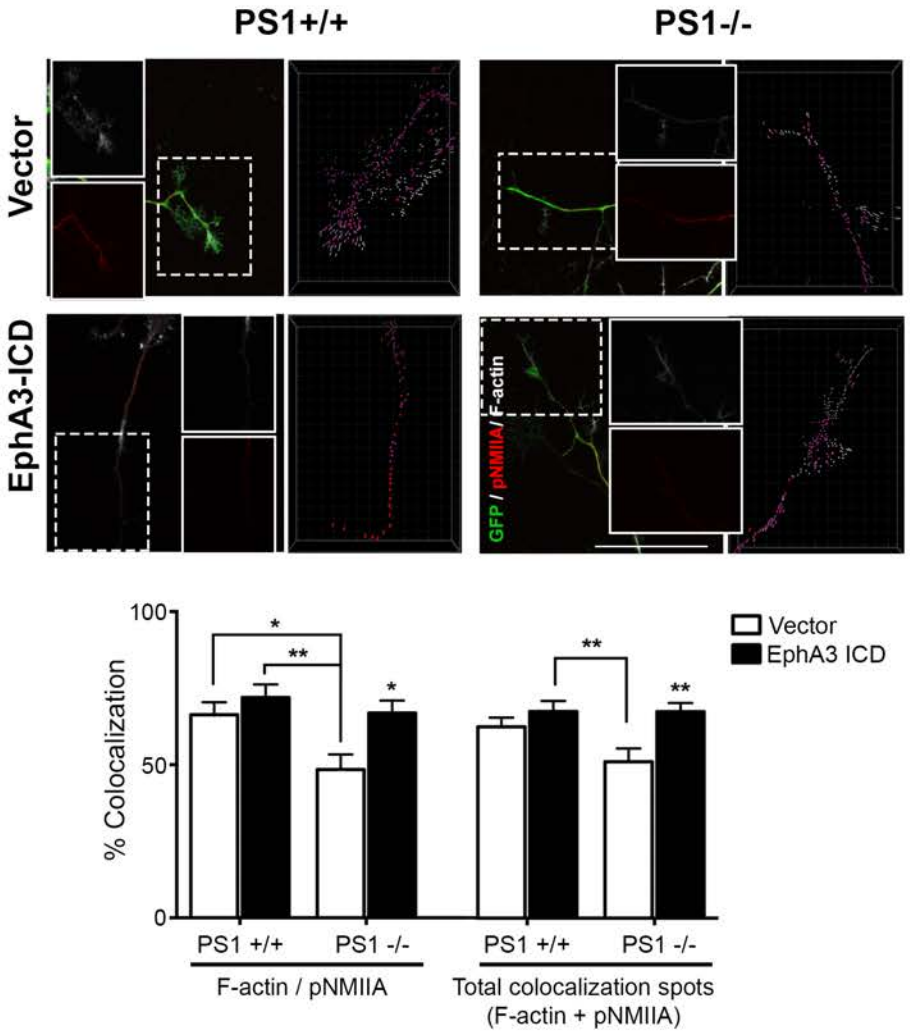

Figure 40. Colocalization of pNMIIA and F-actin at growth cones. Cultured hippocampal neurons from PS1$^{+/+}$ or PS1$^{-/-}$ were transduced with control (pWPI) or EphA ICD (myc-EphA3 ICD pWPI) viral vectors at 1 DIV and analysed at 4 DIV. The presence of EphA3 ICD increases the percentage of pNMIIA spots colocalized with F-actin at growth cones. Statistics was tested by two-way ANOVA followed by Bonferroni *post hoc* test. ** $p < 0.01$, as indicated and compared with vector transfected PS1$^{-/-}$ neurons. Data are mean ± SEM of 3 experiments (n=26-33 neurons/group). Scale bar, 50 µm.

4. NMIIA activity regulates axon growth

When NMIIA is active (ADP bound state), the head can interact strongly with actin, whereas when ADP-Pi binds to the catalytic domain, the affinity between myosin and actin is extremely low. Interestingly, the pharmacological inhibitor blebbistatin, binds to the myosin-ADP-Pi complex maintaining NMII in an actin-detached state (Kovács, Tóth, Hetényi, Málnási-

Csizmadia, & Sellers, 2004).The previous results suggest that PS/γ-secretase and EphA3 ICD could modulate NMIIA activity by regulating NMIIA phosphorylation. Our hypothesis was that NMIIA acts as downstream effector of PS/γ-secretase/EphA3 ICD-mediated axon growth. Interestingly, we found that the pharmacological inhibition of NMII by blebbistatin increased axon length in DAPT-treated hippocampal neurons, mimicking the effect of EphA3 ICD (**Fig. 41**). This effect was not observed when using the inactive blebbistatin enantiomer. Taken together, the results show that EphA3 ICD interacts with NMIIA and regulates its phosphorylation, that PS1/γ-secretase activity regulates NMIIA phosphorylation and NMIIA/actin colocalization and that NMIIA activity regulates axon growth, indicating that the effect of PS/γ-secretase on axon growth is mediated through NMII activation.

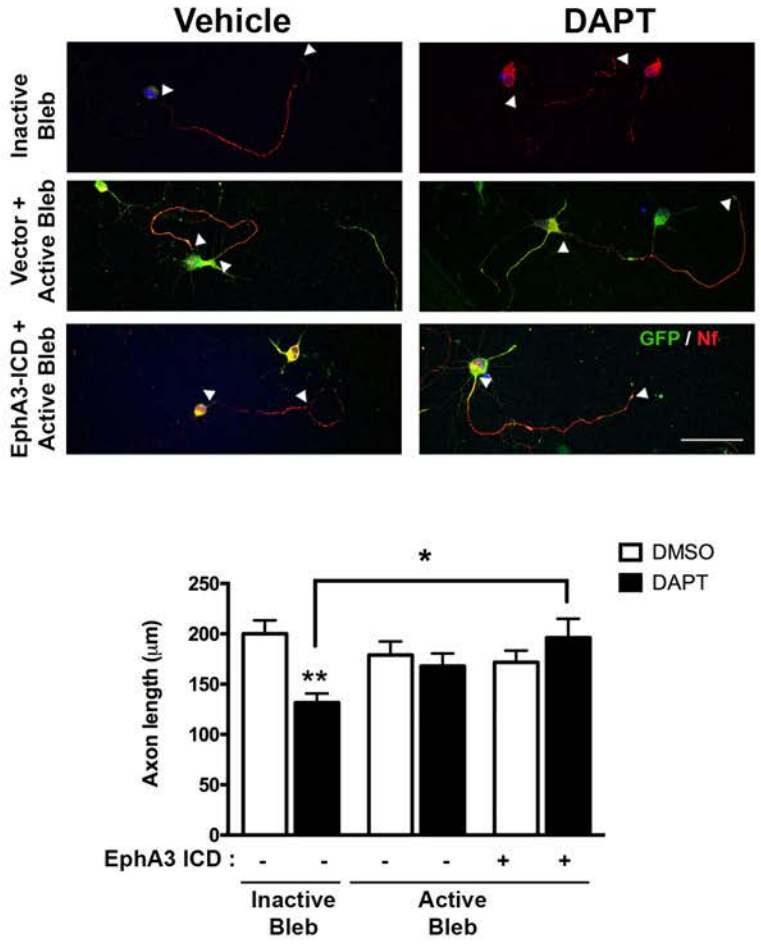

Figure 41. Pharmacological inhibition of NMII rescues the defects in axon length in DAPT-treated neurons. Cultured hippocampal neurons were transduced with control or EphA3 ICD lentiviral vectors at 1 DIV, and treated with active or inactive blebbistatin (20 μM; Calbiochem) at 2 DIV. Immunofluorescence images of hippocampal neurons stained for GFP (EphA3-ICD or vector-positive neurons; green) and neurofilament (SMI312, red). Scale bar, 50 μm. Data are mean ± SEM of 3 experiments (n=44-56 neurons/group). Two-way ANOVA indicates a significant DAPT treatment x

ICD/ blebbistatin interaction (**$p < 0.01$). Bonferroni *post hoc* test shows differences among groups. *$p < 0.05$, **$p < 0.001$ as indicated and compared to vector non-treated neurons.

One of the limitations of blebbistatin is that besides NMIIA can inhibit other myosin isoforms. To try to overcome this, we designed two interference RNA sequences of NMIIA inserted in a short-hairpin (shRNA) structure and a non-interference control sequence (scramble), which was used as a control of the lentivirus transduction. We tested the efficacy of shRNA NMIIA in cultured cortical neurons transduced from 0 DIV to 4 DIV. The RT-qPCR results show that sh3-NMIIA reduces the expression of *NMIIA* mRNA around 50% (**Fig. 42A)**. Likewise, the infection with the same shRNA, decreases the amounts of NMIIA protein more than 50% (**Fig. 42B**). Therefore, for the next experiment we used the scramble and sh3-NMIIA lentiviral particles.

Next, we analyzed the effect of silencing NMIIA in axon growth. Immunochemical analysis of cultured hippocampal neurons transduced with scramble and sh3-NMIIA show that the silencing of NMIIA has not any effect on axon growth (**Fig. 42C**). However, since NMIIA is a very abundant in neurons, we cannot exclude the possibility that ~50% NMIIA silencing of is not enough to produce any effect. Another possibility could be that since NMIIA is part of the actin cytoskeleton, its function could be compensated by other cytoskeleton proteins including other myosin isoforms.

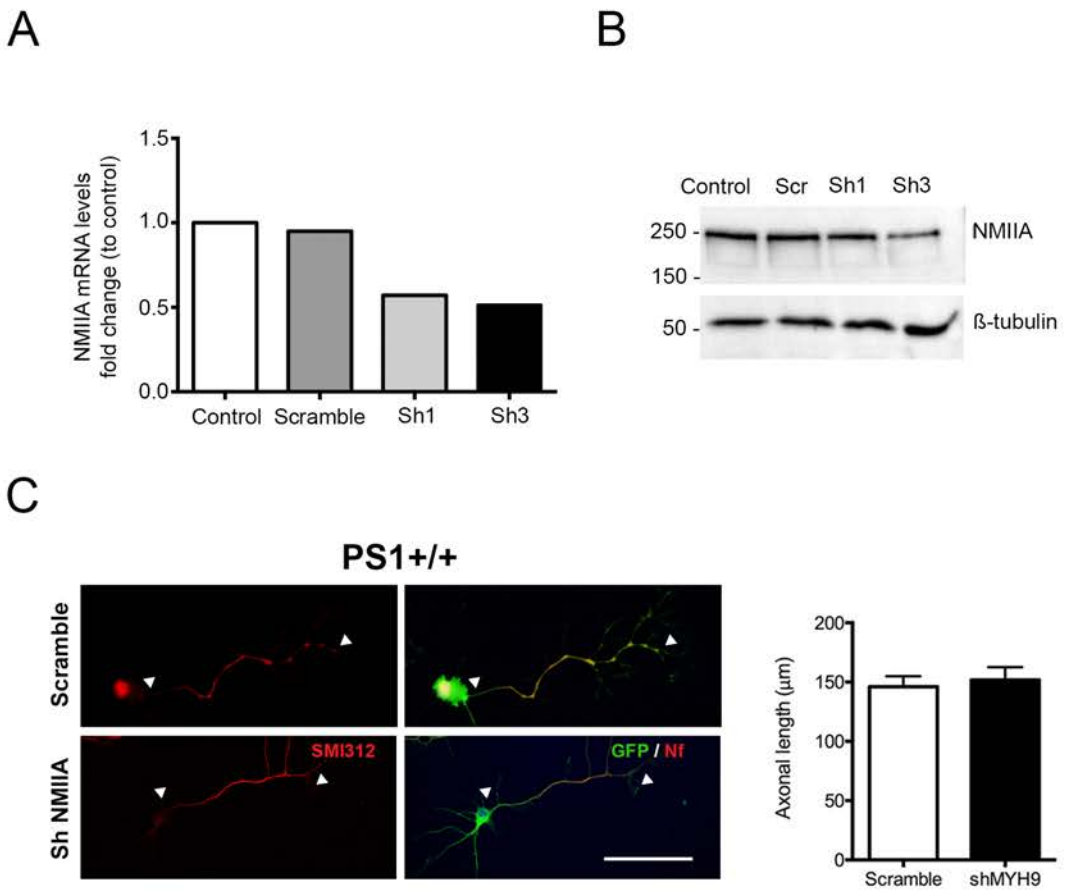

Figure 42. NMIIA silencing does not affect axon length in cultured hippocampal neurons. Cortical neurons were transduced at 0 DIV with scramble or shRNA against NMIIA and analysed at 4 DIV. **A)** Analysis by RT-qPCR shows a reduction in *NMIIA* expression in neurons infected with NMIIA-shRNA3 (Sh3) or NMIIA-shRNA1 (sh1), but not with scramble (Scr). **B)** Western blot results show a reduction in EphA3 protein levels in in neurons infected with NMIIA-shRNA3 (Sh3), but not with NMIIA-shRNA1 (sh1) neither scramble. **C)** NMIIA shRNA3 does not alter axon length of cultured hippocampal neurons.

To try to decipher the effect of myosin IIA in axon growth, we move to an overexpression strategy. We test the effect of a construct containing the NMIIA sequence (NMIIA WT) and a non-phosphorylated S1943A NMIIA mutant (NMIIA S193A) containing a GFP tag in cultured hippocampal neurons. Interestingly, immunocytochemical analysis shows that both NMIIA and NMIIA S1943A mutant cause a drastic reduction in axon length compared to vector-transfected control neurons (**Fig. 43**). This result shows that NMIIA is critically involved in the regulation of axon retraction. Indeed, this result agrees with the reduction of phosphorylated NMIIA founded in $PS1^{-/-}$ neurons (**Fig. 38**). Taken together, our results strongly suggest that EphA3 acts upstream of NMIIA either promoting disassembly or preventing assembly of NMIIA/actin filaments in axons.

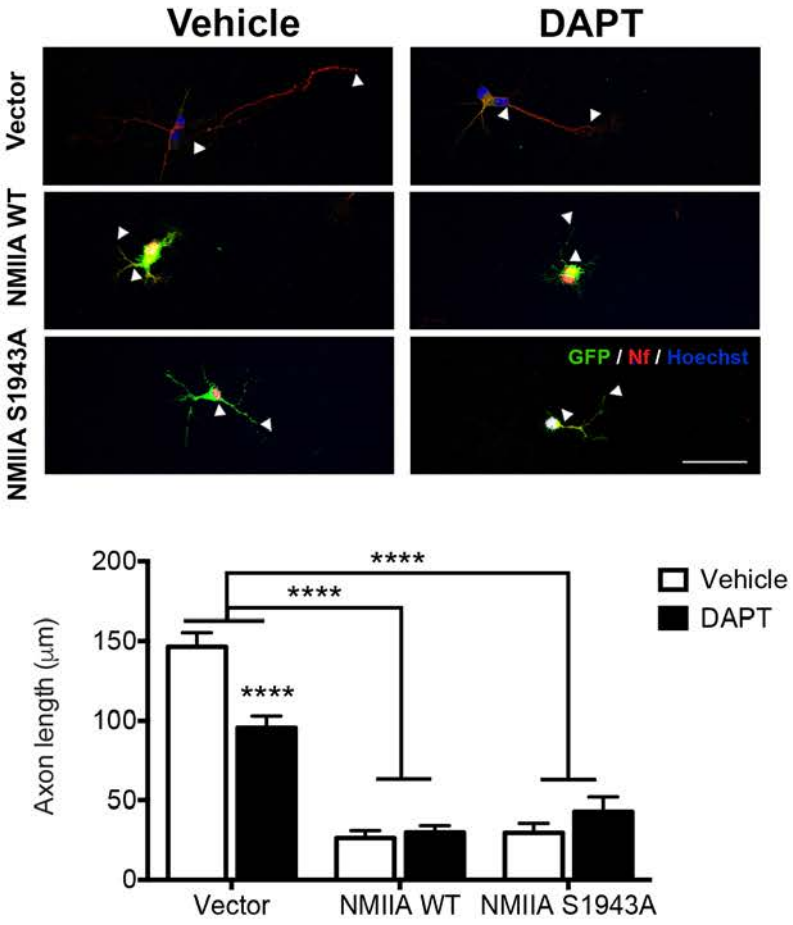

Figure 43. NMIIA and NMIIA S1943A induce axon retraction in hippocampal neurons. Hippocampal neurons were transfected with empty vector, NMIIA-GFP and NMIIA S1943A-GFP vectors at 2 DIV, treated with vehicle or DAPT and fixed at 4 DIV. Immunofluorescence analysis with GFP (green) and neurofilament (SMI312, red) show that NMIIA and NMIIA S1943A cause a reduction in axon length. Scale bar, 50 μm. Statistical analysis, tested by two-way ANOVA, indicates a significant NMIIA effect and DAPT treatment x NMIIA interaction. Data are mean ± SEM of 3 experiments (n=24-41 neurons/group). Bonferroni *post hoc* test shows differences among groups. ****p <0.0001 as indicated

CHAPTER 3:

NRG1-ERBB4 SIGNALING IS ALTERED IN PS-DEFICIENT MICE

CHAPTER 3: NRG1-ERBB4 SIGNALING IS ALTERED IN PRESENILIN-DEFICIENT MICE

1. Nrg1/ErbB4 signaling is disrupted in *PS* cDKO mice

PS/γ-secretase participates in the proteolysis of signaling molecules involved in the development of the nervous system, suggesting that alteration of these signaling pathways may also contribute to neurodegeneration (Crone & Kuo-Fen, 2002; Crone & Lee, 2002). Since disruption of Nrg1/ErbB4 signaling has been related to multiple neurodegenerative disorders, we decided to study whether PS contributes to neurodegeneration by affecting this signaling pathway. To do that, we used the forebrain-specific *PS* conditional double knockout (*PS* cDKO) mice model (Saura et al., 2004) since they present age-dependent neurodegeneration that leads to memory impairments and synaptic plasticity.

To address the role of Nrg1/ErbB4 processing and signaling, we first examined the transcript levels of *Nrg1* in the cortex of *PS* cDKO mice at 6, 9 and 12 months of age. Expression analyses by RT-qPCR show a significant reduction of *Nrg1 type I* mRNA during aging (***$p < 0.001$) although no significant differences were found between genotypes. In contrast, *Nrg1 type III* mRNA was significant reduced in frontal cortex of *PS* cKO mice compared to control at 6-12 months (*$p < 0.05$) (**Fig. 44**). These results suggest that *PS* can regulate the expression of *Nrg1 type III* during aging.

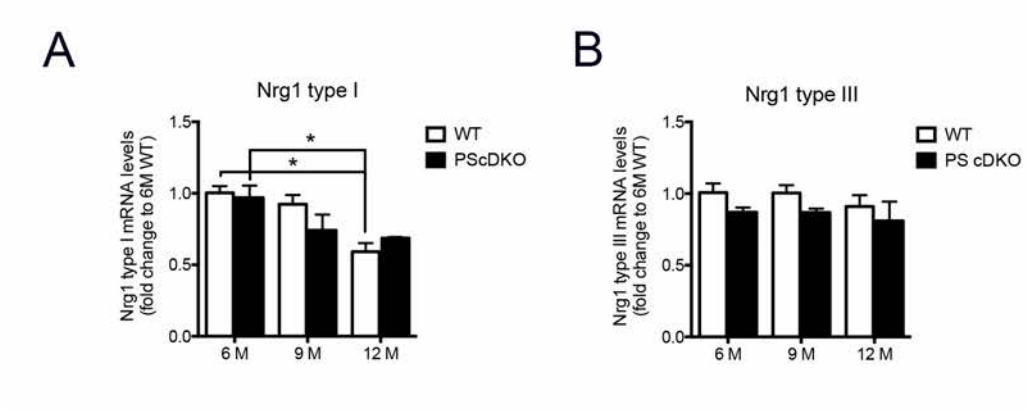

Figure 44. Expression levels of *Nrg1* type I and III isoforms. **A)** Analysis by RT-qPCR of *Nrg1* type I in frontal cortex of control (WT) and *PS* cDKO mice at 6-12 months of age, shows that *Nrg1* type I levels decrease with aging (***$p < 0.001$). **B)** Analysis by RT-qPCR of *Nrg1* type III in frontal cortex of control (WT) and *PS* cDKO mice at 6-12 months of age, reveals reduced *Nrg1* type III mRNA levels in *PS* cDKO mice compared to WT, showing a genotype-dependent effect (*$p <$ 0.05). Levels of mRNA were normalized to *Gapdh.* Values represent mean SEM (n=3-4

mice/group). Statistics was tested by two-way ANOVA followed by Bonferroni *post-hoc* test; *p < 0.05 as indicated.

1.1. Nrg1 type III and ErbB4 processing are regulated by PS/γ-secretase

We next studied if changes in *Nrg1 type I and type III* mRNAs correlated with protein levels. Western blot analysis showed similar levels of Nrg1 type I protein (115 kDa) in the cortex of control and *PS* cDKO mice (**Fig. 45A, B**). By contrast, the amount of a ~75 kDa band, likely corresponding to Nrg1 type III protein was reduced in PS cDKO mice at 6-12 months (***p < 0.001) (**Fig. 45A,C**). During the maturation, Nrg1 type III is processed first by metalloproteases generating NTFs and a CTF that in turn is proteolyzed by PS/γ-secretase. Interestingly, biochemical results showed the accumulation of a C-terminal-derived Nrg1 type III fragment (Nrg1 CTFs; ~65 kDa) in *PS* cKO mice at 6-12 months of age (genotype effect: ****p < 0.0001; **Fig. 45A,C-D**). These results indicate that Nrg1 type III is a substrate of PS/γ-secretase.

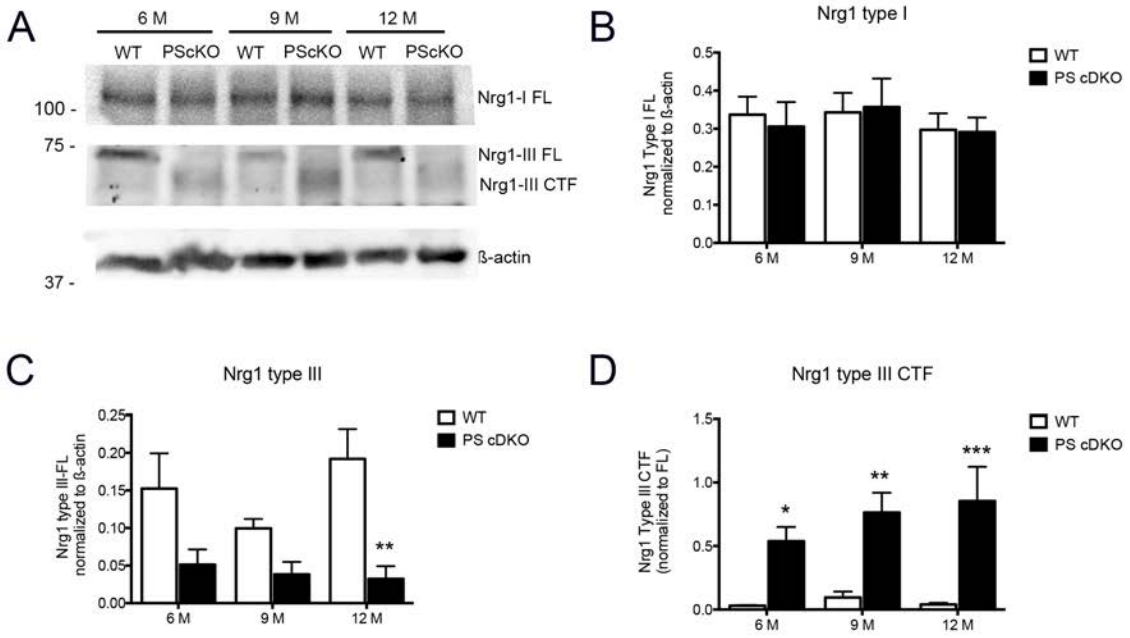

Figure 45. PS/γ-secretase activity is responsible of Nrg1 proteolysis. A) Biochemical analysis of cortical lysates of *PS* cDKO mice at 6-12 months of age. **B)** Quantification of Nrg1 type I show non-significant changes in total protein levels of full-length Nrg1 type I (115 kDa) relative to ß-actin. **C)** Quantification of Nrg1 type III (75 kDa) relative to ß-actin show a genotype-dependent effect (***p < 0.001). **D)** By contrast, Nrg1 CTFs (~65 kDa) are increased in the cortex of *PS* cDKO mice (genotype effect: ****p < 0.0001). Values represent mean SEM (n= 3-4 mice/group). Statistics was

tested by two-way ANOVA followed by Bonferroni *post hoc* test. *$p < 0.05$ compared to WT mice at the indicated age.

Similarly, the PS/γ-secretase-dependent processing of ErbB4 results in the generation of ErbB4 ICD that translocates to the nucleus and regulates the transcription of genes involved in neuronal development (Lee et al., 2002). Accordingly, biochemical analyses revealed unchanged ErbB4/β-actin levels during aging in *PS* cDKO mice (**Fig. 46A,B**). We also found the presence of an ErbB4 CTF of ~75 kDa (CTF) and ~40 kDa (ICD) in both WT and *PS* cDKO cortical lysates (**Fig. 46A,C**). Interestingly, levels of ICD, with a molecular weight likely corresponding to the ErbB4 intracellular domain, were significantly reduced in cortical lysates of *PS* cDKO mice at all ages (genotype effect; ****$p < 0.0001$; **Fig. 46A,D**).

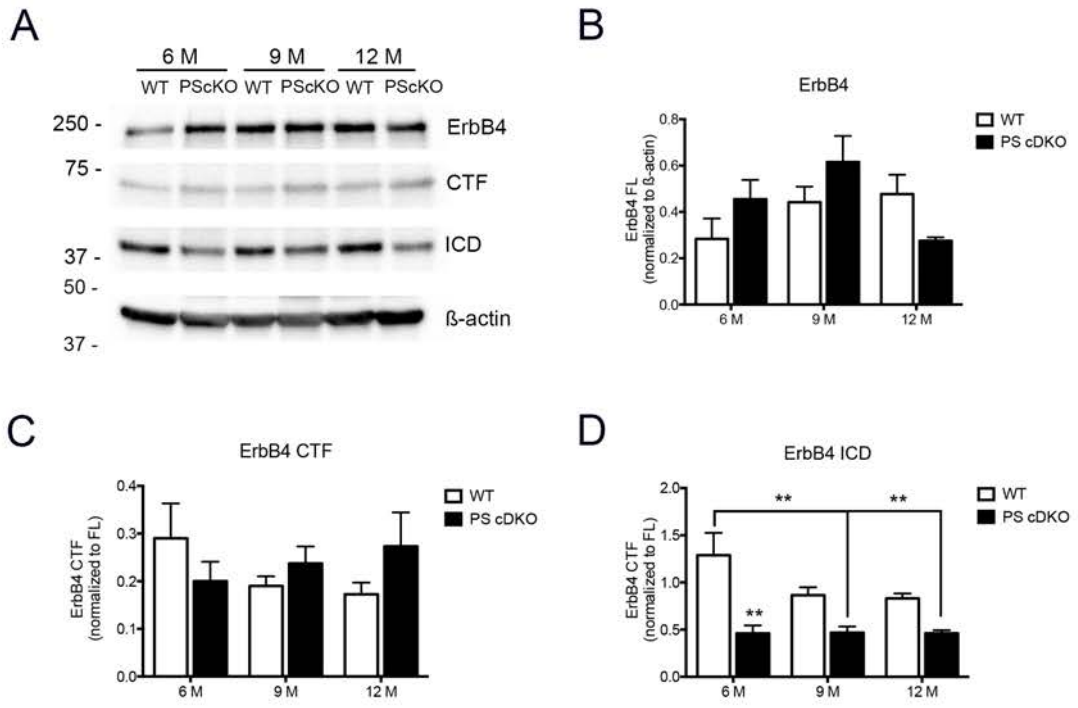

Figure 46. ErbB4 processing is altered in PS cDKO mice A) Biochemical analysis of ErbB4 receptor of cortical lysates of PS cDKO mice at 6-12 months of age. **B)** Quantification of ErbB4/ß-actin levels remains unchanged in WT and PS cDKO mice at all analyzed ages. **C)** Quantification of ErbB4 CTF accumulation (CTF/FL) show no statistical differences between aging nor genotypes. **D)** By contrast, quantification of ErbB4 ICD generation (ICD/FL) is reduced decrease in PS cDKO mice (*** $p < 0.001$). Values represent mean SEM (n= 3-4 mice/group). Statistics was tested by two-way ANOVA followed by Bonferroni *post hoc* test. **$p < 0.01$ as indicated.

1.2. ErbB4 phosphorylation at Y1284 is altered in *PS* cDKO mice

Binding of Nrg1 to ErbB4 leads the dimerization resulting in the autophosphorylation and activation of the receptor (Carpenter, 2003). Specifically, the activated ErbB4 Y1284 interacts with Shc leading to MAPK activation (Cohen, Green, & Fell, H. P, 1996). Since expression and/or processing of Nrg1 type III and its receptor ErbB4 are regulated by PS/γ-secretase, it is possible that Nrg1-ErbB4 signaling could be also regulated by PS. Interestingly, Western blot analysis revealed the accumulation of a ~50 kDa (**p < 0.01) and reduced ~75 kDa phosphorylated (Y1284) ErbB4 fragments (*p < 0.05) in the cortex of *PS* cDKO mice (**Fig. 47**). This result suggests that PS regulates Nrg1-ErbB4 signaling.

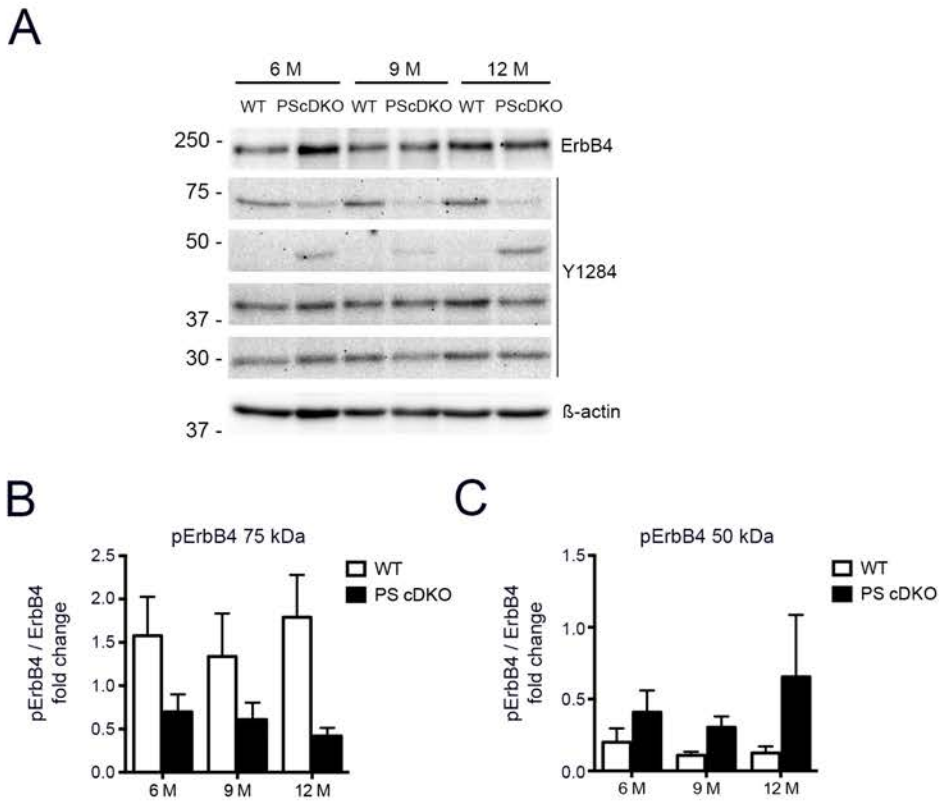

Figure 47. ErbB4 phosphorylation is altered in *PS* cDKO mice. A) Western blot analysis of ErbB4 phosphorylation in cortical lysates of *PS* cDKO mice at 6-12 months. **B)** Phosphorylated (Y1284) ErbB4 CTF (~75 kDa) levels are significant reduced in *PS* cDKO mice (**p < 0.01). **C)** Quantification of pErbB4-CTF-50 reveals a statistical significant accumulation in *PS* cDKO mice (*p < 0.05). Values represent mean SEM (n= 3-4 mice/group). Statistics was tested by two-way ANOVA.

Next, we examined the nuclear localization of the ErbB4 fragments. Western blot analysis of cortical homogenates and nuclear fractions from WT and *PS* cDKO mice revealed the presence of several ErbB4 protein bands. Interestingly, biochemical analysis of the nuclear fraction confirmed the accumulation of the 50 kDa phosphorylated ErbB4 in *PS* cDKO mice of 6 months of age **(Fig. 48)**. The results also show the presence of a ~60 and ~70 kDa phosphorylated ErbB4 bands that remained unchanged. Thus, we also observed an abundant ~75 kDa band of ErbB4 in the nuclear fraction that seems to reduced in *PS* cDKO mice compared to controls, although the differences are not statistically significant. This result suggests that the processing of ErbB4 by PS/γ-secretase decreases the accumulation of a phosphorylated ErbB4 fragment in the nucleus, although its physiological role is unclear.

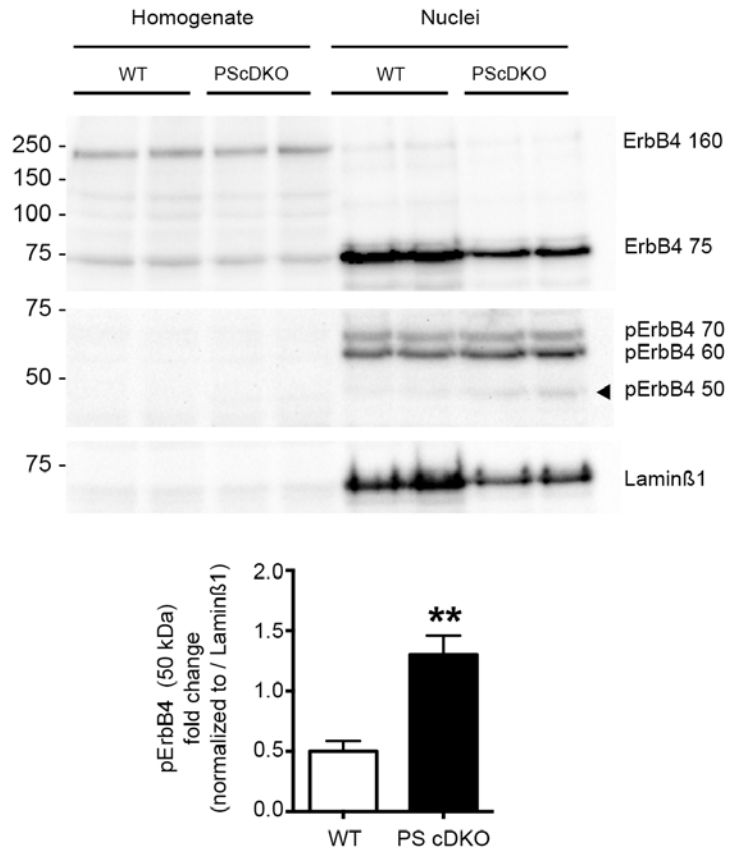

Figure 48. Effect of PS inactivation in nuclear phosphorylated ErbB4 fragment levels. Detection of ErbB4 phosphorylated fragments in homogenate and nuclear fractions in the cortex of PS cKO mice at 6 months (above). Western blot quantification (below) shows that of ErbB4 protein levels remain unchanged both in homogenate and nuclear fractions of PS cKO mice at 6 months, whereas a phosphorylated fragment of ~50 kDa CTF in the nuclear fraction is increased in PS cDKO mice (**p* < 0.05). Values represent mean SEM (n= 4 mice/group).

2. Role of Nrg1 in synaptogenesis of glutamatergic neurons

2.1. Neuronal activity alters ErbB4 phosphorylated protein levels in cortical neurons

Previous studies showed that neuronal activity regulates differentially the expression of some *Nrg1* isoforms, as in the case of *Nrg1 type I*, which expression results increased (Liu et al., 2011). First, we examined if those changes in *Nrg1 type I* expression were also maintained after mRNA transcription. Analysis by Western blotting showed that that neuronal activity triggered by KCl depolarization increases Nrg1 type I protein amounts in cortical neurons although the quantification is not statistical significant (**Fig. 49A**). We also analysed the phosphorylated and total ErbB4 levels after induction of neuronal activity by KCl-depolarization. Interestingly, biochemical analysis shows that protein amount of phospho-ErbB4 are reduced after KCl-depolarization, whereas total ErbB4 and their derived fragments remained unchanged (**Fig. 50B**). Taken together, these results suggest that Nrg1/ErbB4 signaling is altered by neuronal activity.

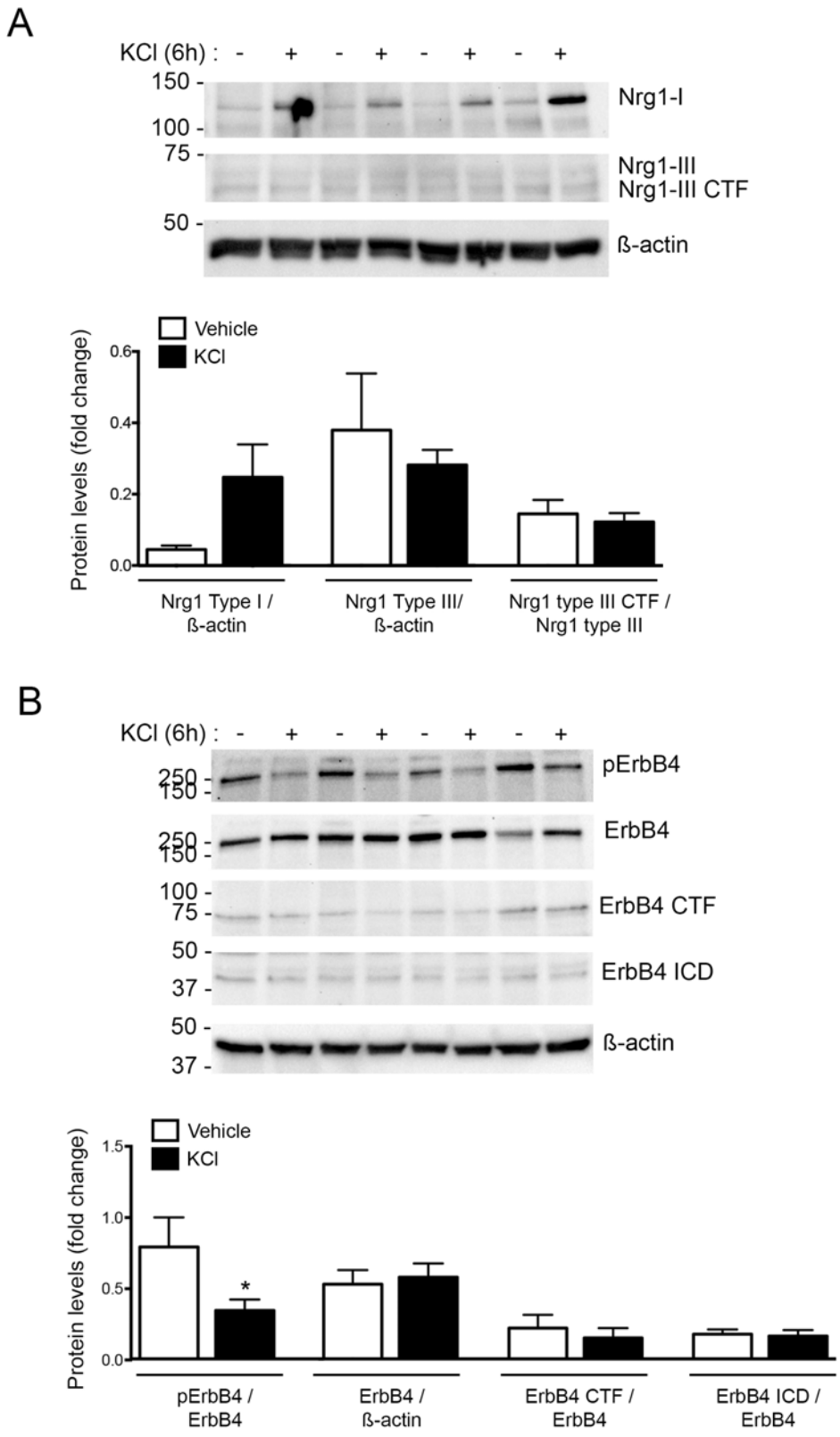

Figure 49. Neuronal activity regulates ErbB4 phosphorylation in cultured neurons. Cortical neurons were cultured for 12 DIV and treated with KCl (50 mM) 6 h before cell lysis. **A)** Western blot analysis showing the effect KCl depolarization over Nrg1 protein levels. Although qualitative

analysis indicated that Nrg1 protein levels are increased by KCl treatment (A), quantitative analysis show that differences are not statistical significant (*p = 0.1277).* Nrg1 type III and Nrg1 type III CTF protein levels remain unchanged. Values represent mean ± SEM (n=4). **B)** Western blot analysis showing the effect KCl depolarization over total and phosphorylated ErbB4 protein levels. Quantitative analysis (below) shows that protein levels of phosphorylated ErbB4 are reduced by KCl treatment (50 mM). Protein levels of ErbB4 and CTF-derived fragments remain unchanged. Values represent mean ± SEM (n=4 experiments); Unpaired two-tailed Student's *t* test; **p* < 0.05 as indicated.

2.2. Contextual learning induces changes in ErbB4 protein levels in PS cDKO mice

So far, we have found that Nrg1/ErbB4 signaling is disrupted in PS cDKO mice and that neuronal activity also affects this signaling. Next, we decided to test if neuronal activity underlying memory encoding could modify the Nrg1/ErbB4 signaling in PS cDKO mice.

The contextual fear-conditioning (CFC) test associates an aversive stimulus (electric foot-shock) with the context allowing the investigation of long-term memory encoding events. In this case, rodents were subjected to the aversive unconditioned stimulus (US) after exposure of a conditioning chamber and the amount of freezing behaviour was quantified after the re-exposure to the context 2h hours later. Western blot results show that the WT trained mice have reduced protein amounts of Nrg1 type III CTF compared to non-trained mice whereas the levels of pro-Nrg1, Nrg1 type I and Nrg1 type III remained unchanged (**Fig. 50A**). On the other hand, we also examined total and phosphorylated ErbB4 protein levels. We did not found any differences in phosphor-ErbB4, total ErbB4 neither ErbB4-derived fragments between trained and non-trained WT mice (**Fig. 50B**).

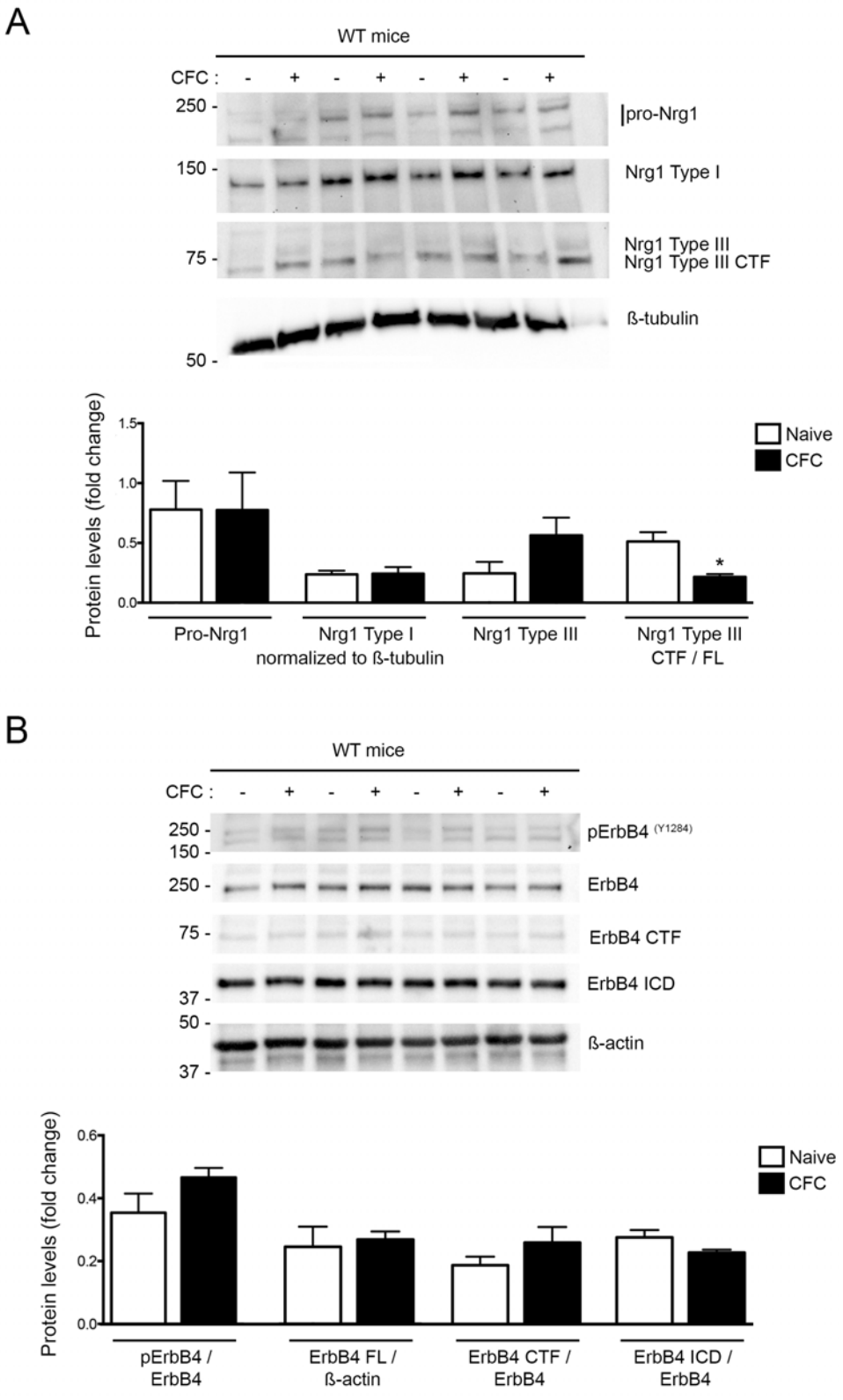

Figure 50. Neuronal activity regulates Nrg1 protein levels in WT mice. A) Biochemical analyses of Nrg1 and their derived-fragments in cortex of naïve and trained WT mice. **B)** Biochemical analyses of phosphor-ErbB4, total ErbB4 and their derived-fragments in cortex of naïve and trained WT mice. Values represent mean of fold changes ± SEM (n=4 animals/group).

Statistics was tested by two-way ANOVA followed by Bonferroni *post hoc* test. *$p < 0.05$, as indicated.

Then, we tested whether the inactivation of PS1 and PS2 could modify the amounts of protein of Nrg1 and ErbB4 in naïve or CTF-trained mice. Western blot results show that Nrg1 protein levels remained unchanged in WT trained, PS1 cKO trained and PS cDKO trained mice, compared to WT non-trained mice (**Fig. 51A**). We were not able to detect the reduction in the Nrg1 type III CTF protein levels in WT trained mice compared to the naïve (**Fig. 51A**), probably due to the variability among the animals. Similarly, the amount of phosphorylated ErbB4 neither total ErbB4 did change between trained mice (**Fig. 51B**). Interestingly, the amount of ErbB4 ICD fragment, resulting from ErbB4 PS/γ-secretase processing was reduced in trained PS cDKO mice compared to WT naïve mice (**Fig. 12B**). However, this reduction in the amount of ErbB4 ICD is the same reduction as the observed in non-trained mice (**Fig. 46**). In order to postulate that the neuronal activity may alter the PS/γ-secretase-dependent processing of ErbB4 in PS cDKO mice, we should include a non-trained mice group in this experiment.

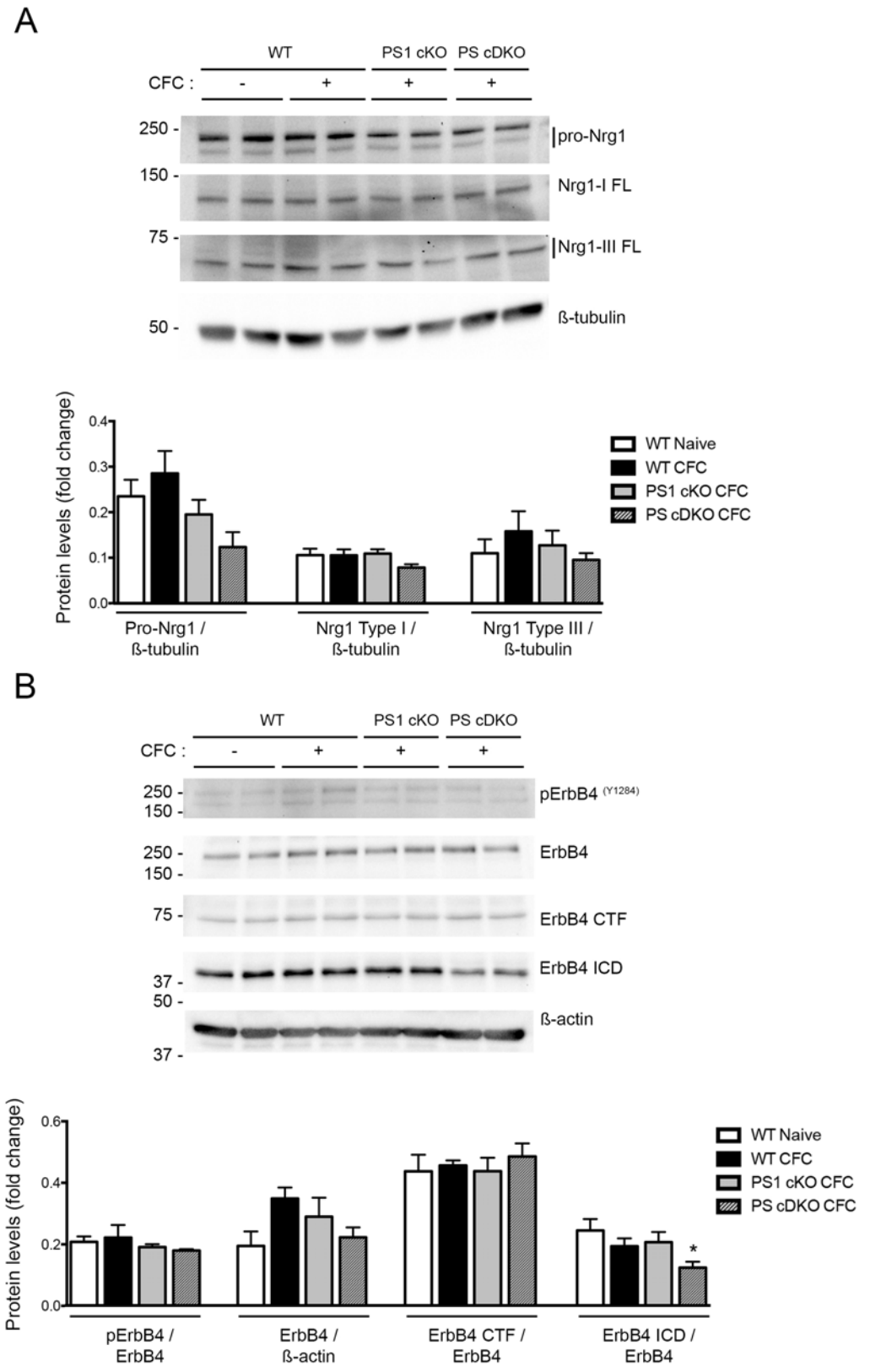

Figure 51. Neuronal activity disrupt ErbB4 processing in PS cDKO mice. Biochemical analyses of Nrg1 and their derived-fragments in cortex of naïve and memory trained control (WT) and PS cDKO mice. **B)** Biochemical analyses of phosphor-ErbB4, total ErbB4 and their derived-

fragments in cortex of naïve and trained control (WT) and PS cDKO mice. Values represent mean of fold changes ± SEM (n=4 animals/group). Statistics was tested by two-way ANOVA followed by Bonferroni *post hoc* test. *$p < 0.05$ compared with WT naïve mice.

2.3. Differential regulation of synaptogenesis by Nrg1 in physiological and pathological conditions

Next, we studied the potential role of Nrg1/ErbB4 signaling in synaptogenesis in in cultured neurons in a neurodegenerative context (i.e. PS1 inactivation). Immunocytochemical analysis shows that $PS1^{-/-}$ neurons have no reduction in the number of functional synapses (considered as the overlapping of synaptophysin and PSD95 stainings) (**Fig. 52A,B**). Interestingly, we found an increased density of both post-synaptic (PSD95) and pre-synaptic (synaptophysin) markers in $PS1^{-/-}$ neurons (*$p < 0.05$ and **$p < 0.01$, respectively) (**Fig. 52A,C**). Moreover, the activation of Nrg1/ErbB4 signaling by rhNRG1 treatment induces a reduction in the synaptophysin density in $PS1^{+/+}$ (ΔCre-transduced) neurons whereas in the $PS1^{-/-}$ (Cre-transduced) neurons remained unchanged (**Fig. 52A,C**). These results suggest that Nrg1 could be playing an opposite role in physiological and pathological conditions.

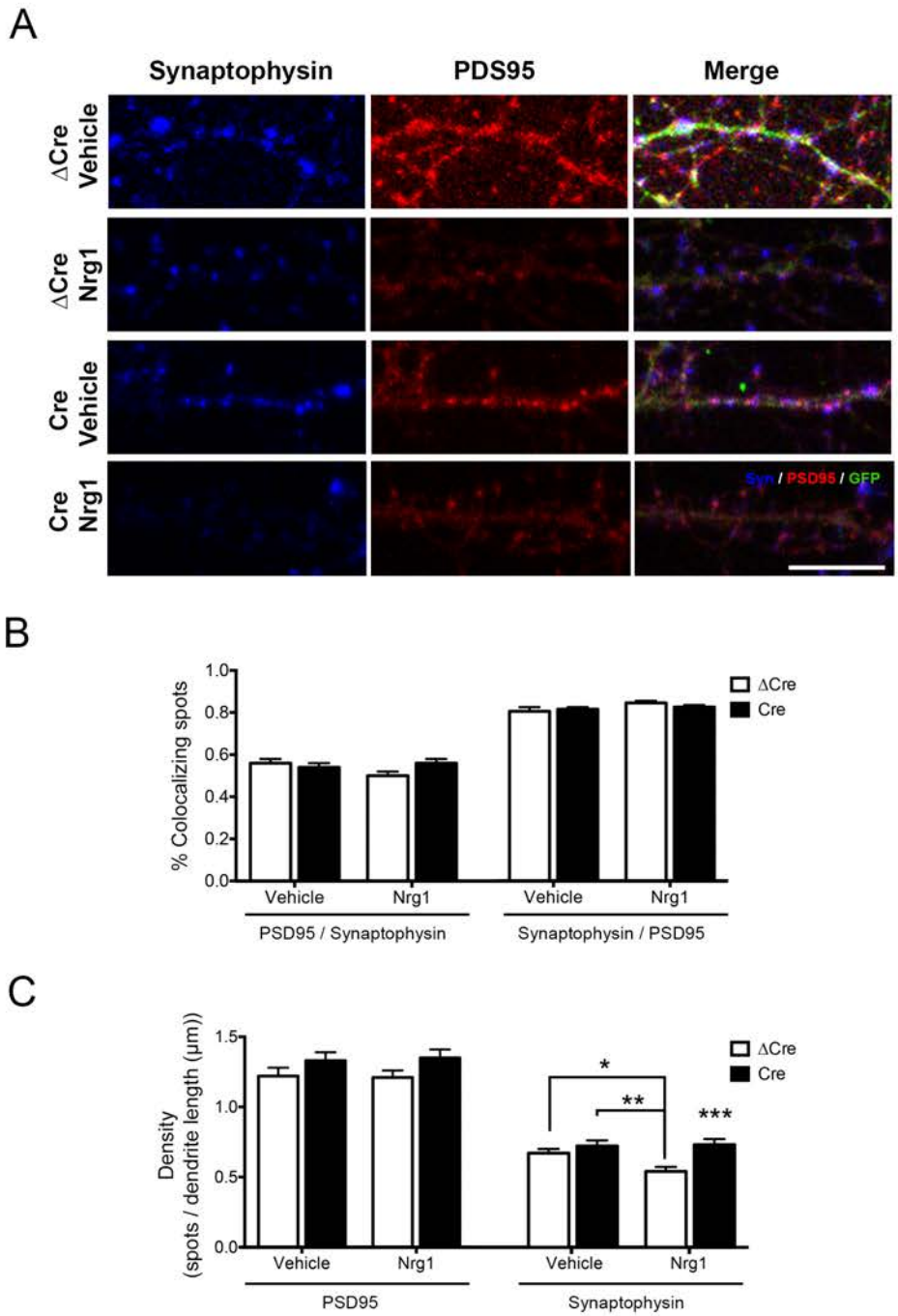

Figure 52. Nrg1 treatment increases the density of synaptophysin in PS1-lacking neurons. Cultured hippocampal neurons were transduced with ΔCre (control) or Cre-containing lentivirus at 5 DIV. Neurons were treated at 6 DIV and 11 DIV with rhNRG1 (100 ng/ml). **A)** Cultured neurons were fixed and stained with GFP (green), Synaptophysin (blue) and PSD-95 (red) at 16 DIV. **B)** Colocalization analysis show neither the rhNRG1 treatment or lentivirus transduction reduces the number of functional synapses. **C)** Quantitative analyses show that PS1-deficient neurons (previously transduced with Cre lentivirus) have an increased density of the post-synaptic marker PSD95 (*$p < 0.05$; Cre-transduction effect) and the presynaptic marker Synaptophysin (**$p < 0.01$; Cre-transduction effect). Thus, Nrg1 treatment has a negative impact on Synaptophysin density in WT neurons (ΔCre transduction). Values represent mean SEM (n= 29-40 neurons/condition; two

independent experiments). Statistics was tested by two-way ANOVA followed by Tukey *post hoc* test. *$p < 0.05$, **$p < 0.01$ and ***$p < 0.001$ as indicated.

DISCUSSION

Presenilins are the catalytic subunits of γ-secretase, an enzymatic complex that cleaves type I proteins within the transmembrane domain. The cleavage by PS/γ-secretase requires an initial shedding by a metalloprotease that generates a C-terminal fragment (CTF) that once proteolyzed by PS/γ-secretase releases a soluble intracellular domain fragment (ICD). The function of the generated ICD of the majority of substrates is in most cases unknown. Recent evidence indicates that autosomal dominant mutations in the *PS* genes linked to FAD cause a reduction of the γ-secretase cleavage of multiple substrates, suggesting a loss-of-function PS mechanism in the pathology of FAD (De Strooper, 2007; Shen & Kelleher, 2007). In support of this idea, genetic inactivation of both *PS* in the brain of mice causes defects in synaptic plasticity and memory and neurodegeneration (Saura et al., 2004). In addition, genetic inactivation of *PS1* during embryogenesis leads to brain and skeletal morphological defects although the underlying molecular mechanisms involved are still unknown (Handler, Yang, & Shen, 2000). In this line, our study provides the first evidence for a novel PS/γ-secretase-regulated mechanism involved in axon growth of hippocampal neurons in the developing brain. According to our results, PS/γ-secretase promotes axon growth by mediating the intramembrane processing of EphA3 independently of the classical ephrin/EphA3 signaling (**Fig. 30**). Second, our results indicate that PS/γ-secretase is required for *Nrg1 type III* expression, mediates Nrg1 type III and ErbB4 processing and regulates negatively synaptogenesis through Nrg1. Together, the results of this doctoral thesis indicate that PS participate in the proteolysis of signaling molecules, including EphA3 and ErbB4, involved in key mechanisms of nervous system development and neurodegeneration, suggesting that these novel signaling mechanisms may contribute to neurodegenerative diseases.

PS/γ-secretase regulates axon growth by regulating actin-myosin filaments

It is well established that PS1 regulates brain development during embryogenesis. $PS1^{-/-}$ embryos develop deficits in axonal length, neuronal migration and cortical lamination during brain development [(Handler et al., 2000); this study]. Specifically, axon guidance defects have been attributed to the truncation of PS-dependent processing of DCC that results in the alteration of Netrin/DCC and Slit/Robo signaling (Bai et al., 2011). In agreement, loss-of-function mutations in *PS* genes disrupt Notch signaling leading to neurite morphology defects in *C. elegans* (Wittenburg et al., 2000). Of interest, our results indicate that PS/γ-secretase activity regulates axon length *in vivo* and *in vitro* (**Figs. 28, 30**). Indeed,

PS1$^{-/-}$ embryos show a reduction in axon length compared to controls (**Fig. 28)**. Interestingly, a recent study showed that familial-AD linked PS1 mutations promote neurite outgrowth by increasing APP intracellular fragments and activating CREB signaling (Carole Deyts et al., 2016). In earlier studies they also show that pharmacological inhibition of γ-secretase produces the accumulation of APP CTFs leading to neurite outgrowth (C. Deyts et al., 2012). Despite the involvement of PS/γ-secretase in neurite outgrowth, the PS1/γ-secretase-dependent mechanisms affecting cytoskeleton rearrangement during axon growth are still unknown. Our results suggest that PS/γ-secretase activity stimulates the phosphorylation of non-muscle myosin IIA (**Fig. 35**) and actin/NMIIA colocalization (**Fig. 37**). Indeed, PS1/γ-secretase mediates axon elongation through the processing of EphA3 that results in the generation of an ICD fragment that: 1) regulates negatively RhoA, 2) interact with NMIIA, and 3) increases the phosphorylation (S1943) of NMIIA. All these mechanisms seem to converge to regulate filament disassembly leading to axon growth (**Fig. 50**). In support of this idea, PS1/γ-secretase-deficient neurons show: reduced EphA3 ICD levels, increased RhoA activity, which is reduced by EphA3 ICD, and reduced phosphorylated (S1943) NMIIA resulting in axon elongation deficits.

One of our first key result is the finding that EphA3 is a novel PS/γ-secretase substrate, as demonstrated by the accumulation of EphA3 CTFs in HEK293T cells treated with the γ-secretase inhibitor DAPT and in PS1$^{-/-}$ brains **(Fig. 19)**. This is in agreement with the accumulation of CTF-derived fragments due to the inhibition of γ-secretase complex in multiple PS/γ-secretase substrates as APP, EphB2, N-cadherin, Notch, p75-NTR (Litterst et al., 2007; Saura, 2011). We also detected the generation of NTF and the ICD resulting from the cleavage of EphA3 FL and CTF by PS/γ-secretase, respectively (**Figs. 21, 22**). We used proteomic approaches to verify that PS/γ-secretase-dependent EphA3 cleavage occurs at one specific cleavage site in EphA3, that is aminoacid Tyr560 (**Fig. 24**). Despite there is no consensus cleavage sequence between the substrates of γ-secretase complex, bioinformatics analysis reveals that EphA3 cleavage site was analogous to the EphB2 (**Fig. 23**) (Litterst et al., 2007). In both cases, these cleavage sites are in agreement to the ε-cleavage sites found in several PS/γ-secretase substrates (Sastre et al., 2001; Weidemann et al., 2002; Wolfe, 2006). Interestingly, biochemical analysis indicated that EphA3 processing is not apparently affected by ephrin-A5 ligand or deletion of the EphA3 ligand binding domain (**Figs. 26 and 27**), suggesting that this cleavage is

not dependent on ligand binding. Indeed, this domain, which is not processed by PS1, is supposed to be localized at the intracellular side being responsible of receptor-receptor interactions and auto-phosphorylation. In support of this, ephrin-A5 does not affect the accumulation of EphA3 CTF caused by the pharmacological inhibition of γ-secretase (**Fig. 26)**. Moreover, the EphA3 phosphorylation induced by ephrin-A5 is not affected by DAPT treatment (**Fig. 26)**. These results strongly indicate that PS1/γ-secretase-dependent processing of EphA3 is ligand-independent. In contrast to these results, the PS1/γ-secretase-dependent processing of other known substrates (i.e. EphB2 and EphA4) depends on ligand binding and neuronal activity (Inoue et al., 2009; Litterst et al., 2007). The implications of a ligand-independent EphA3 signaling mechanism may have enormous cellular implications. Many EphA3 cancer mutations disrupt ephrin binding indicating that ephrin/EphA3 signaling may play a role as a tumour suppressor (Forse et al., 2015) (Lisabeth, Fernandez, & Pasquale, 2012). Moreover, the presence of some EphA3 mutations, as S46F or G187R, may affect the membrane localization of the receptor, causing defects in EphA3 endocytosis and/or turnover (Lisabeth et al., 2012). Therefore, the discovery of a ligand-independent EphA3 signaling may enable new insights in the mechanisms underlying development of several cancers and their therapies. Although the role of specific EphA3 structural domains on regulation of axon growth is still unclear, it would be interesting to study how these genetic mutations affect ligand-independent EphA3 signaling.

The PS1/γ-secretase-dependent cleavage of EphA3 generates an ICD fragment that mediates prevention of growth cone collapse and axon elongation. A previous study showed that the inactivation of *EphA3* reduces the number and projections of callosal axons without affecting their growth (Nishikimi, Oishi, Tabata, Torii, & Nakajima, 2011). In contrast, genetic EphA3 inactivation reduces axon growth in cultured hippocampal neurons (Martín, 2013). Indeed, EphA3 ICD rescues axon length defects in PS1/γ-secretase-deficient neurons, whereas expression of the full-length receptor and removal of intracellular domain (EphA3 ΔICD) impair recovery of axon length in these neurons (**Fig. 30**), suggesting that EphA3 cleavage would occur *in vivo*. Indeed, we were able to detect the presence of EphA3 CTFs in $PS1^{-/-}$ cultured neurons and embryonic brain, indicating that EphA3 is processed by endogenous PS1/γ-secretase. Interestingly, the generation of EphA3 ICD promotes the non-collapsed morphology of growth cones (**Fig. 32**). This 'active motile' morphology corresponds with a higher ability of growth cones

to search for substrates and to grow. In contrast, when the axon has already elongated, the growth cone collapses. Our results suggest that PS1/γ-secretase mediates axon elongation by avoiding growth cone collapsed through EphA3 ICD. Several compounds targeting γ-secretase complex are currently in clinical trial since they have demonstrated efficacy reducing Aß plaques (Kumar et al., 2018). However, our results should be considered when evaluating the side effects of these γ-secretase inhibitors treatments.

The family of Rho GTPases play an essential role in the regulation of axon growth. Inhibition of the Rho-associated kinase ROCK promotes axon growth (Borisoff et al., 2003; Fournier, Takizawa, & Strittmatter, 2003; Martín, 2013; Moore et al., 2008). Ligand dependent ephrin-A5/EphA3 signaling mediates growth cone collapse through a mechanism involving the activation of RhoA signaling (Lawrenson et al., 2002; Wahl, Barth, Ciossek, Aktories, & Mueller, 2000). In contrast, a constitutive active RhoA mutant prevents EphA3 ICD-mediated recovery of axon growth, suggesting that EphA ICD regulates negatively RhoA (**Fig. 31**). Indeed, previous studies in our lab demonstrated that pharmacological RhoA inhibition reverses axon growth deficits in $PS1^{-/-}$ neurons (unpublished). Although the potential interactions between EphA3 and cytoskeletal proteins are largely unclear, some studies suggest that they are related to actomyosin polymerisation events (Krupke & Burke, 2014). Of interest, we found that PS/γ-secretase/EphA3-dependent axon elongation may involve the rearrangement of the cytoskeleton through the physical interaction between EphA3 ICD and NMIIA heavy chain. Proteomic and biochemical assays revealed that EphA3 ICD interacts with NMIIA heavy chain (**Table 3-4**; **Fig. 33**). NMIIA is a cytoskeleton protein that acts downstream of RhoA and mediates neurite retraction (Gallo, 2006; Kubo et al., 2008; Wylie & Chantler, 2003). Noteworthy, CKII-mediated phosphorylation of NMIIA (S1943) stimulates cell migration by mediating the dissociation of NMIIA filaments into monomers or preventing filament assembly (Breckenridge, Dulyaninova, & Egelhoff, 2009; Dulyaninova & Bresnick, 2013; Dulyaninova, House, Betapudi, & Bresnick, 2007). Interestingly, genetic and pharmacologic inactivation of *PS1*/γ-secretase causes a reduction of NMIIA phosphorylation (Ser1943), which presumably would result in filament assembly in neurons (**Figs. 35-36**). By

contrast EphA3 ICD increases phosphorylation of NMIIA heavy chain and enhances NMIIA/actin colocalization in PS-deficient axons **(Figs. 34-35, 37**). This result indicates that EphA3 ICD/NMIIA interaction promotes disassembly or inhibits assembly of NMIIA/actin filaments, resulting in axon growth. Proteomic results also show a possible interaction between EphA3 ICD and clathrin, suggesting the endocytosis of EphA3. Accordingly, the endocytosis of other ephrin/Eph molecules has been related to clathrin-mediated vesicles (Parker et al., 2004; Yoo, Shin, & Park, 2010).

These results suggest that PS1/γ-secretase may regulate the filament turnover (depolymerization/depolymerization) of NMIIA, inhibiting the formation of stable filaments that interact with F-actin and would lead to axon growth and elongation. Indeed, a positive effect on extension of filopodia due to the attenuation of retrograde F-actin flow has been previously reported (Lin, Espreafico, Mooseker, & Forscher, 1996). According to this idea, inactivation of NMIIA and the phosphorylation in its heavy chain (S1943) have similar effects on axon growth. Indeed, pharmacological inhibition of NMII by blebbistatin, which maintains NMII in an actin-detached state (Yu, Santiago, Katagiri, & Geller, 2012), reverses axon growth defects in PS/γ-secretase-deficient neurons, without causing additional effects in the presence of EphA3 ICD (**Fig. 38**). In support of this idea, all identified myosin-II binding partners also promote unassembled NMII forms (Dulyaninova & Bresnick, 2013). Since the axon growth effects caused by blebbistatin are not specific of NMIIA, we cannot rule out the possibility that other NMII isoforms participate in the regulation of axon elongation. The discovery that NMIIA is regulated by PS/γ-secretase-dependent cleavage of EphA3 may have tremendous impact in human diseases. Indeed, actomyosin contractibility is strongly regulated during cell division and migration. Since, EphA3 ICD deregulates the formation of NMIIA/actin filaments it may be involved in the acquisition of an invasive phenotype cells during cancer development. In conclusion, we report here a novel EphA3 mechanism independent of ligand and dependent of PS1/γ-secretase that mediates axon growth through the disassociation and/or prevention of assembly of NMIIA/actin filaments in axons (**Figure 50**).

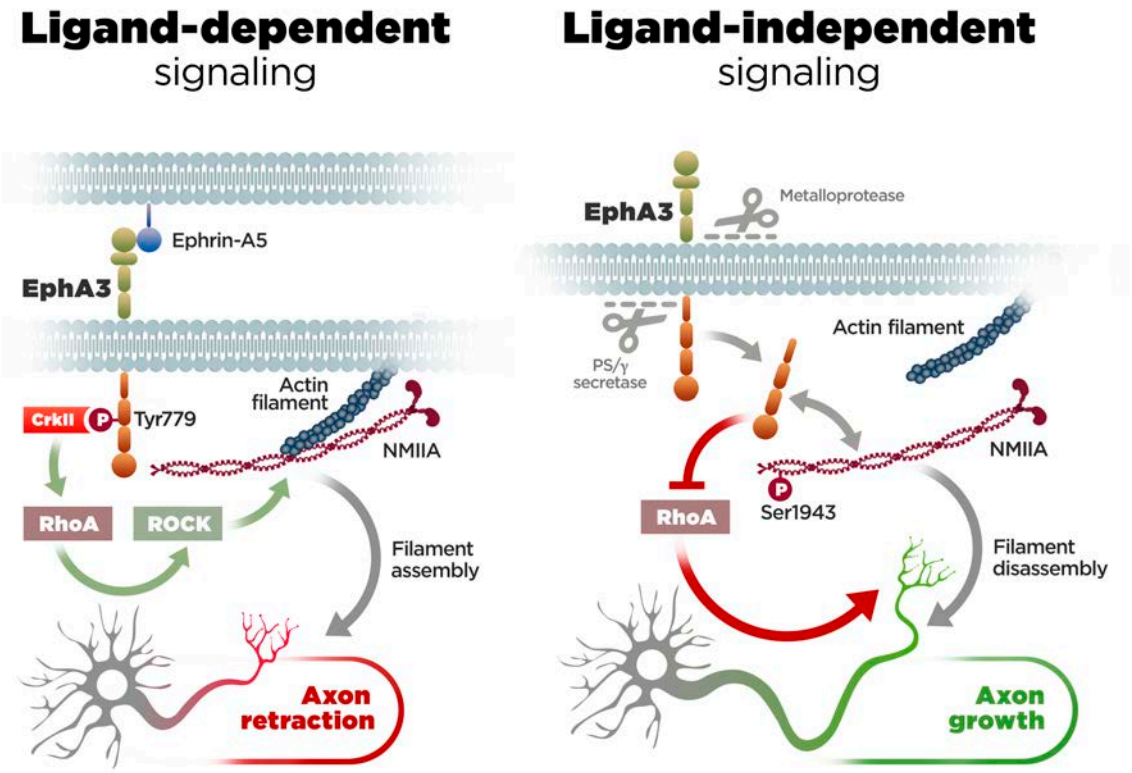

Figure 50. Proposed model of ephrin-dependent and -independent EphA3 signaling regulating axon growth in neurons. Left: Classical ligand-dependent EphA3 signaling inhibiting axon growth. Ephrin-A5 binding to EphA3 receptor results in EphA3 phosphorylation (Y779) and binding of CrkII and activation of RhoA signaling, inducing axon retraction by promoting actin/NMIIA filament assembly in hippocampal neurons. Right: Novel ligand-independent EphA3 signaling promoting axon growth. PS/γ-secretase dependent processing of EphA3 results in generation of an EphA3 intracellular domain fragment that inhibits RhoA and increases the phosphorylation (S1943) of NMIIA heavy chain, leading to actin/NMIIA filament disassembly and axon growth.

PS/γ-secretase regulates Nrg1/ErbB4 signaling in the adult brain

Several studies demonstrate that PS/γ-secretase regulates Nrg1/ErbB4 signaling by mediating the processing of Nrg1 and its receptor ErbB4 (Fleck et al., 2013; Willem, 2016). Of interest, BACE1-dependent proteolysis of Nrg1, which occurs before the γ-secretase cleavage, is critical for signaling functions during synaptic plasticity (Hu, Fan, Hou, & Yan, 2016). Since Nrg1/ErbB4 signaling regulates neuronal development and synaptogenesis, alterations in this signaling pathway are thought to contribute to neuron development and degeneration (Chaudhury et al., 2003). Importantly, some Nrg1 SNPs increase the risk of psychosis in AD (Go

et al., 2005), whereas Nrg1 protects against synapse loss in an AD mouse model (Xu et al., 2016). Moreover, the amount and the distribution of ErbB4 are altered in AD brains compared to controls (Chaudhury et al., 2003; Woo, Lee, Yu, Song, & Baik, 2011). At the beginning of this doctoral thesis the mechanisms by which PS/γ-secretase regulates Nrg1/ErbB4 signaling during neurodegeneration were unknown. To investigate this issue, we first examined Nrg1/ErbB4 signaling in PS cDKO mice of 6-12 months of age. PS cDKO mice, in which inactivation of both *PS* is restricted to excitatory neurons of the postnatal forebrain, develop memory and synaptic plasticity impairments followed by age dependent neurodegeneration (Saura et al., 2004).

First, our expression analysis indicate that mRNA levels of *Nrg1 type I* are unchanged, whereas *Nrg1 type III*, which mediates glutamatergic synaptic transmission (Jiang, Emmetsberger, Talmage, & Role, 2013; Zhong et al., 2008), was significantly reduced in the frontal cortex of PS cDKO (**Fig. 41**). These results suggest that *PS* are required for basal *Nrg1 type III* neuronal expression. Biochemical analysis showed that Nrg1 type III FL is reduced and the Nrg1 C-terminal fragment derived from the γ-secretase processing is increased in the cortex of PS cDKO mice (**Fig. 42**). The biochemical assays also revealed that the amount of ErbB4 protein and the C-terminal derived fragment (ErbB4 CTF; ~78 kDa) remained unchanged in PS cDKO mice compared to controls, whereas the generation of a possible intracellular fragment (ErbB4 ICD; ~50 kDa) is reduced **(Fig. 43)**. Interestingly, Western blot analysis also shows that PS1 inactivation increases the accumulation of ~50 kDa phosphorylated ErbB4 fragment whereas reduces a ~75 kDa phospho-ErbB4 fragment (Y1284) (**Fig. 44**). This phosphorylation results from the binding of Nrg1 to ErbB4 that leads to the dimerization and autophosphorylation of the receptor, which is essential for signal transduction (Carpenter, 2003). Interestingly, a cellular fractionation assay indicates that the ~50 kDa phosphorylated ErbB4 fragment that accumulates in the cortex of PS cDKO mice was localized in the nucleus (**Fig. 45**). Taken together, these results indicate that Nrg1/ErbB4 processing and signaling are impaired in the cortex of PS cDKO mice during aging.

Importantly, recent evidences indicate that the expression of some Nrg1 isoforms is regulated by neuronal activity (Liu et al., 2011). In agreement, KCl-induced neuronal activity increases specifically protein levels of Nrg1 type I but not type III, and reduces phosphorylated ErbB4 receptor without affecting total ErbB4 and CTFs in cultured neurons (**Fig. 46**). *In vivo,* we found a reduction in ErbB4 ICD in CFC trained PS cDKO mice compared to WT naïve mice, 2 h after CFC (**Fig. 48**). Since, PS cDKO show hippocampal-dependent memory deficits in the CFC (Saura et al., 2004), these results suggest that the Nrg1/ErbB4 signalling pathway can contribute to the neurodegeneration process observed in PS cDKO mice. However, this reduction in ErbB4 ICD was also present in non-trained PS cDKO (**Fig. 27**). To postulate whether this reduction is caused by neuronal activity, it would be interesting to include a non-trained PS cDKO mice group to see whether the alteration in the PS/γ-secretase-dependent processing of ErbB4 is due to the memory training or the genotype.

The alteration of Nrg1/ErbB4 and memory deficits present in PS cDKO mice, suggest that PS/γ-secretase may regulate Nrg1/ErbB4 signaling during neurodegeneration. To test this hypothesis, cultured hippocampal neurons from *PS1* floxed/floxed embryos were transduced with lentivirus containing Cre-recombinase or ΔCre-recombinase to inactivate or not PS1, respectively, and then treated with recombinant Nrg1 (rhNRG1). Interestingly, our results indicate that activation of Nrg1/ErbB4 signaling by rhNRG1 treatment reduced the number of pre-synaptic buttons in cultured control neurons but not in PS1-deficient neurons (**Fig. 49**). It seems that PS1 promotes Nrg-1-mediated loss of synapses, whereas the absence of PS1 abolish the negative effect of Nrg-1 in synapse loss. Therefore, it seems that synaptogenesis can be differentially regulated by the presence or absence of PS1.

Taken together our results show that PS/γ-secretase regulates axon growth and synaptogenesis by regulating non-classical EphA3 signalling and Nrg1/ErbB4 processing/signalling. These findings pave the way for exploring new relationships between neurodevelopment and neurodegeneration that can be useful potential targets in clinical therapies for nerve regeneration and to combat neurodegeneration and cancer.

CONCLUSIONS

The experimental work of this doctoral thesis allowed us to reach the following conclusions:

- PS/γ-secretase is required for axon growth *in vitro* and *in vivo*
- PS/γ-secretase cleaves EphA3 at Tyr560 independently of ephrin ligands
- PS/γ-secretase mediates through EphA3 axon growth and growth cone collapse
- EphA3 mediates PS/γ-secretase-dependent axon growth by interacting with non-muscle myosin IIA
- EphA3 ICD interacts with non-muscle myosin IIA and regulates its phosphorylation, causing a reorganization of the actin cytoskeleton
- PS-dependent Nrg1/ErbB4 signaling affects synaptogenesis and is altered in neurodegenerative conditions in the adult brain

REFERENCES

A

Abate, G., Colazingari, S., Accoto, A., Conversi, D., & Bevilacqua, A. (2018). Dendritic spine density and EphrinB2 levels of hippocampal and anterior cingulate cortex neurons increase sequentially during formation of recent and remote fear memory in the mouse. *Behavioural Brain Research*, *344*, 120–131.

AD&FTD Mutation Database. (n.d.). Retrieved November 4, 2018, from http://www.molgen.ua.ac.be/ADmutations/

Aguayo-Ortiz, R., Straub, J. E., & Dominguez, L. (2018). Influence of membrane lipid composition on the structure and activity of γ-secretase. *Physical Chemistry Chemical Physics*.

Ahn, K., Shelton, C. C., Tian, Y., Zhang, X., Gilchrist, M. L., Sisodia, S. S., & Li, Y.-M. (2010). Activation and intrinsic γ-secretase activity of presenilin. *Proceedings of the National Academy of Sciences*, *107*, 21435–21440.

Akaneya, Y., Sohya, K., Kitamura, A., Kimura, F., Washburn, C., Zhou, R., Ninan, Y., Tsumoto, T., Ziff, E. B. (2010). Ephrin-A5 and EphA5 Interaction Induces Synaptogenesis during Early Hippocampal Development. *PLoS ONE*, *5*(8), e12486.

Albertinazzi, C., Gilardelli, D., Paris, S., Longhi, R., & de Curtis, I. (1998). Overexpression of a Neural-specific Rho Family GTPase, cRac1B, Selectively Induces Enhanced Neuritogenesis and Neurite Branching in Primary Neurons. *The Journal of Cell Biology*, *142*(3), 815–825.

Andersen, C. L., Jensen, J. L., & Ørntoft, T. F. (2004). Normalization of Real-Time Quantitative Reverse Transcription-PCR Data: A Model-Based Variance Estimation Approach to Identify Genes Suited for Normalization, Applied to Bladder and Colon Cancer Data Sets. *Cancer Research*, *64*(15), 5245–5250.

Anton, E. S., Marchionni, M. A., Lee, K.-F., & Rakic, P. (1997). Role of GGF/neuregulin signaling in interactions between migrating neurons and radial glia in the developing cerebral cortex. *Development*, *124*, 10.

Arasada, R. R., & Carpenter, G. (2005). Secretase-dependent Tyrosine Phosphorylation of Mdm2 by the ErbB-4 Intracellular Domain Fragment. *Journal of Biological Chemistry*, *280*(35), 30783–30787.

Arimura, N., & Kaibuchi, K. (2007). Neuronal polarity: from extracellular signals to intracellular mechanisms. *Nature Reviews Neuroscience*, *8*(3), 194–205.

Attwood, B. K., Bourgognon, J.-M., Patel, S., Mucha, M., Schiavon, E., Skrzypiec, A. E., Young, KW., Shiosaka, S., Korostynski, M., Piechota, M., Przewlocki, R., Pawlak, R. (2011). Neuropsin cleaves EphB2 in the amygdala to control anxiety. *Nature*, *473*(7347), 372–375.

B

Bai, G., Chivatakarn, O., Bonanomi, D., Lettieri, K., Franco, L., Xia, C., Stein, E., Ma L., Lewcock, JW., Pfaff, S. L. (2011). Presenilin-Dependent Receptor Processing Is Required for Axon Guidance. *Cell*, *144*(1), 106–118.

Bagnard, D., Lohrum, M., Uziel, D., Püschel, A. W., & Bolz, J. (1998). Semaphorins act as attractive and repulsive guidance signals during the development of cortical projections. *Development*, *125*, 5043–5053.

Bardelli, A. (2003). Mutational Analysis of the Tyrosine Kinome in Colorectal Cancers. *Science*, *300*(5621), 949–949.

Barnes, A. P., & Polleux, F. (2009). Establishment of Axon-Dendrite Polarity in Developing Neurons. *Annual Review of Neuroscience*, *32*(1), 347–381.

Bashaw, G. J., Kidd, T., Murray, D., Pawson, T., & Goodman, C. S. (2000). Repulsive Axon Guidance: Abelson and Enabled Play Opposing Roles Downstream of the Roundabout Receptor. *Cell*, *101*, 703–715.

Batlle, E., Bacani, J., Begthel, H., Jonkeer, S., Gregorieff, A., van de Born, M., Malats, N., Sancho, E., Boon, E., Pawson, T., Gallinger, S., Pals, S., Clevers, H. (2005). EphB receptor activity suppresses colorectal cancer progression. *Nature*, *435*(7045), 1126–1130.

Beuter, S., Ardi, Z., Horovitz, O., Wuchter, J., Keller, S., Saha, R., Tripathi, K., Anunu, R., Kehat, O., Kriebel, M., Richter-Levin, G., Volkmer, H. (2016). Receptor tyrosine kinase EphA7 is required for interneuron connectivity at specific subcellular compartments of granule cells. *Scientific Reports*, *6*(1).

Bian, S., Zhang, B., Yang, G., Song, Q., & Li, Y. (2017). EphA2, EphrinAl expression in breast cancer and its relationship with clinical pathological study. *Biomed Res*, *28*(13), 6.

Binns, K. L., Taylor, P. P., Sicheri, F., Pawson, T., & Holland, S. J. (2000). Phosphorylation of Tyrosine Residues in the Kinase Domain and Juxtamembrane

Region Regulates the Biological and Catalytic Activities of Eph Receptors. *Molecular and Cellular Biology*, *20*(13), 4791–4805.

Borisoff, J. F., Chan, C. C. ., Hiebert, G. W., Oschipok, L., Robertson, G. S., Zamboni, R., Steeves, J. D., Tetzlaff, W. (2003). Suppression of Rho-kinase activity promotes axonal growth on inhibitory CNS substrates. *Molecular and Cellular Neuroscience*, *22*(3), 405–416.

Bovolenta, P. (2000). Nervous system proteoglycans as modulators of neurite outgrowth. *Progress in Neurobiology*, *61*(2), 113–132.

Boyd, A. W., & Lackmann, M. (2001). Signals from Eph and Ephrin Proteins: A Developmental Tool Kit. *Science's STKE*, *2001*(112), 7.

Boyd, A. W., Bartlett, P. F., & Lackmann, M. (2014). Therapeutic targeting of EPH receptors and their ligands. *Nature Reviews Drug Discovery*, *13*(1), 39–62.

Breckenridge, M. T., Dulyaninova, N. G., & Egelhoff, T. T. (2009). Multiple Regulatory Steps Control Mammalian Nonmuscle Myosin II Assembly in Live Cells. *Molecular Biology of the Cell*, *20*(1), 338–347.

Brennaman, L. H., Moss, M. L., & Maness, P. F. (2014). EphrinA/EphA-induced ectodomain shedding of neural cell adhesion molecule regulates growth cone repulsion through ADAM10 metalloprotease. *Journal of Neurochemistry*, *128*(2), 267–279.

Bresler, T. (2004). Postsynaptic Density Assembly Is Fundamentally Different from Presynaptic Active Zone Assembly. *Journal of Neuroscience*, *24*(6), 1507–1520.

Briançon-Marjollet, A., Ghogha, A., Nawabi, H., Triki, I., Auziol, C., Fromont, S., Piché, C., Enslen, H., Chebli, K., Cloutier J-F., Castellani, V., Debant, A., Lamarche-Vane, N. (2008). Trio Mediates Netrin-1-Induced Rac1 Activation in Axon Outgrowth and Guidance. *Molecular and Cellular Biology*, *28*(7), 2314–2323.

Brinkmann, B. G., Agarwal, A., Sereda, M. W., Garratt, A. N., Müller, T., Wende, H., Stassart, R. M., Nawaz, S., Humml, C., Velanac, V., Radysushkin, K., Goebbels, S., Fischer, T. M., Franklin, R. J., Lai, C., Ehrenreich, H., Birchmeier, C., Schwab, M. H., Nave, K. A. (2008). Neuregulin-1/ErbB Signaling Serves Distinct Functions in Myelination of the Peripheral and Central Nervous System. *Neuron*, *59*(4), 581–595.

Brose, K., Bland, K. S., Wang, K. H., Arnott, D., Henzel, W., Goodman, C. S., Tessier-Lavigne, M., Kidd, T. (1999). Slit Proteins Bind Robo Receptors and Have an Evolutionarily Conserved Role in Repulsive Axon Guidance. *Cell*, *96*(6), 795–806.

Brose, K., & Tessier-Lavigne, M. (2000). Slit proteins: key regulators of axon guidance, axonal branching, and cell migration. *Current Opinion in Neurobiology*, *10*(1), 95–102. https://doi.org/10.1016/S0959-4388(99)00066-5

Brown, A., Yates, P. A., Burrola, P., Ortuño, D., Vaidya, A., Jessell, T. M., Pfaff, S. L., O'Leary, D. D. M., Lemke, G. (2000). Topographic Mapping from the Retina to the Midbrain Is Controlled by Relative but Not Absolute Levels of EphA Receptor Signaling. *Cell*, *102*(1), 77–88.

Brown, J., & Bridgman, P. C. (2003). Role of Myosin II in Axon Outgrowth. *Journal of Histochemistry & Cytochemistry*, *51*(4), 421–428.

Burden, S., & Yarden, Y. (1997). Neuregulins and Their Receptors: A Versatile Signaling Module in Organogenesis and Oncogenesis. *Neuron*, *18*(6), 847–855.

Busfield, S. J., Michnick, D. A., Chickering, T. W., Revett, T. L., Ma, J., Woolf, E. A., Comrack, C. A., Dussault, B. J., Woolf, J., Goodearl, A. D. J., Gearing, D. P. (1997). Characterization of a neuregulin-related gene, Don-1, that is highly expressed in restricted regions of the cerebellum and hippocampus. *Molecular and Cellular Biology*, *17*(7), 4007–4014.

Bustin, S. A., Benes, V., Garson, J. A., Hellemans, J., Huggett, J., Kubista, M., Mueller, R., Nolan, T., Pfaffl, M. W., Shipley, G. L., Vandesompele, J., Wittwer, C. T. (2009). The MIQE Guidelines: Minimum Information for Publication of Quantitative Real-Time PCR Experiments. *Clinical Chemistry*, *55*(4), 611–622.

Bustos, V., Pulina, M. V., Bispo, A., Lam, A., Flajolet, M., Gorelick, F. S., & Greengard, P. (2017). Phosphorylated Presenilin 1 decreases β-amyloid by facilitating autophagosome–lysosome fusion. *Proceedings of the National Academy of Sciences*, *114*(27), 7148–7153.

C

Cabedo, H., Luna, C., Fernández, A. M., Gallar, J., & Ferrer-Montiel, A. (2002). Molecular Determinants of the Sensory and Motor Neuron-derived Factor Insertion into Plasma Membrane. *Journal of Biological Chemistry*, *277*(22), 19905–19912.

Cahill, M. E., Remmers, C., Jones, K. A., Xie, Z., Sweet, R. A., & Penzes, P. (2013). Neuregulin1 signaling promotes dendritic spine growth through kalirin. *Journal of Neurochemistry*, *126*(5), 625–635.

Cai, Y., Biais, N., Giannone, G., Tanase, M., Jiang, G., Hofman, J. M., Wiggins, C. H., Silberzan, P., Buguin, A., Ladoux, B., Sheetz, M. P. (2006). Nonmuscle Myosin IIA-Dependent Force Inhibits Cell Spreading and Drives F-Actin Flow. *Biophysical Journal*, *91*(10), 3907–3920.

Cao, Z., Wu, X., Yen, L., Sweeney, C., & Carraway, K. L. (2007). Neuregulin-Induced ErbB3 Downregulation Is Mediated by a Protein Stability Cascade Involving the E3 Ubiquitin Ligase Nrdp1. *Molecular and Cellular Biology*, *27*(6), 2180–2188.

Carmona, M. A., Murai, K. K., Wang, L., Roberts, A. J., & Pasquale, E. B. (2009). Glial ephrin-A3 regulates hippocampal dendritic spine morphology and glutamate transport. *Proceedings of the National Academy of Sciences*, *106*(30), 12524–12529.

Carpenter, G. (2003). ErbB-4: mechanism of action and biology. *Experimental Cell Research*, *284*(1), 66–77.

Carraway III, K. L., Weber, J. L., Unger, M. J., Ledesma, J., Yu, N., Gassmann, M., & Lai, C. (1997). Neuregulin-2, a new ligand of ErbB3/ErbB4-receptor tyrosine kinases. *Nature*, *387*, 512–516.

Casey, J. P., Magalhaes, T., Conroy, J. M., Regan, R., Shah, N., Anney, R., (…) Ennis, S. (2012). A novel approach of homozygous haplotype sharing identifies candidate genes in autism spectrum disorder. *Human Genetics*, *131*(4), 565–579.

Castellani, C. A., Awamleh, Z., Melka, M. G., O'Reilly, R. L., & Singh, S. M. (2014). Copy Number Variation Distribution in Six Monozygotic Twin Pairs Discordant for Schizophrenia. *Twin Research and Human Genetics*, *17*(02), 108–120.

Chang, L.-C., Jamain, S., Lin, C.-W., Rujescu, D., Tseng, G. C., & Sibille, E. (2014). A Conserved BDNF, Glutamate- and GABA-Enriched Gene Module Related to Human Depression Identified by Coexpression Meta-Analysis and DNA Variant Genome-Wide Association Studies. *PLoS ONE*, *9*(3), e90980.

Chantler, P.D., & Wylie, S. R. (2003). Elucidation of the separate roles of myosins IIA and IIB during neurite outgrowth, adhesion and retraction. *IEE Proceedings - Nanobiotechnology*, *150*(3), 111.

Chantler, Peter D., Wylie, S. R., Wheeler-Jones, C. P., & McGonnell, I. M. (2010). Conventional myosins – unconventional functions. *Biophysical Reviews*, *2*(2), 67–82.

Charmsaz, S. (2013). Expression and Function of the Eph Receptor Family in Leukemia and Hematopoietic Malignancies: Prospects for Targeted Therapies. *Journal of Leukemia*, *01*(01).

Chaudhury, A. R., Gerecke, K. M., Wyss, J. M., Morgan, D. G., Gordon, M. N., & Carroll, S. L. (2003). Neuregulin-1 and ErbB4 Immunoreactivity Is Associated with Neuritic Plaques in Alzheimer Disease Brain and in a Transgenic Model of Alzheimer Disease. *Journal of Neuropathology & Experimental Neurology*, *62*(1), 42–54.

Chen, F., Liu, Z., Peng, W., Gao, Z., Ouyang, H., Yan, T., Songbai, D., Cai, Z., Zhao, B., Mao, L., Cao, Z. (2018). Activation of EphA4 induced by EphrinA1 exacerbates disruption of the blood-brain barrier following cerebral ischemia-reperfusion via the Rho/ROCK signaling pathway. *Experimental and Terapeutic Medicine*, 16, 2651-2658.

Chen, J., Guo, L., Peiffer, D. A., Zhou, L., Chan, O. T. M., Bibikova, M., Wickham-Garcia, E., Lu, S-H., Zhan, Q., Wang-Rodriguez, J., Jiang, W., Fan, J.-B. (2008). Genomic profiling of 766 cancer-related genes in archived esophageal normal and carcinoma tissues. *International Journal of Cancer*, *122*(10), 2249–2254.

Chen, S., Velardez, M. O., Warot, X., Yu, Z.-X., Miller, S. J., Cros, D., & Corfas, G. (2006). Neuregulin 1-erbB Signaling Is Necessary for Normal Myelination and Sensory Function. *Journal of Neuroscience*, *26*(12), 3079–3086.

Chen, Y. M., Wang, Q. J., Hu, H. S., Yu, P. C., Zhu, J., Drewes, G., Piwnica-Worms, H., Luo, Z. G. (2006). Microtubule affinity-regulating kinase 2 functions downstream of the PAR-3/PAR-6/atypical PKC complex in regulating hippocampal neuronal polarity. *Proceedings of the National Academy of Sciences*, *103*(22), 8534–8539.

Chen, Y.-J., Zhang, M., Yin, D.-M., Wen, L., Ting, A., Wang, P., Lu, Y-S., Zhu, X-H., Li, S-J., Wu, C-Y., Wang X-M., Lai, C., Xiong, W-C., Mei, L., Gao, T.-M. (2010). ErbB4 in parvalbumin-positive interneurons is critical for neuregulin 1 regulation of long-term potentiation. *Proceedings of the National Academy of Sciences*, *107*(50), 21818–21823.

Cheng, H.-J., Nakamoto, M., Bergemann, A. D., & Flanagan, J. G. (1995). Complementary gradients in expression and binding of ELF-1 and Mek4 in development of the topographic retinotectal projection map. *Cell*, *82*(3), 371–381.

Chitsaz, D., Morales, D., Law, C., & Kania, A. (2015). An Automated Strategy for Unbiased Morphometric Analyses and Classifications of Growth Cones In Vitro. *PLOS ONE*, *10*(10), e0140959.

Cissé, M., Halabisky, B., Harris, J., Devidze, N., Dubal, D. B., Sun, B., Orr, A., Lotz, G., Kim, D. H., Hamto, P., Ho, K., Yu, G-Q., Mucke, L. (2011). Reversing EphB2 depletion rescues cognitive functions in Alzheimer model. *Nature*, *469*(7328), 47–52.

Clark, K., Middelbeek, J., Lasonder, E., Dulyaninova, N. G., Morrice, N. A., Ryazanov, A. G., Bresnick., A. R., Figdor, C. G., van Leeuwen, F. N. (2008). TRPM7 Regulates Myosin IIA Filament Stability and Protein Localization by Heavy Chain Phosphorylation. *Journal of Molecular Biology*, *378*(4), 790–803.

Clifford, M. A., Athar, W., Leonard, C. E., Russo, A., Sampognaro, P. J., Van der Goes, M.-S., Burton, D. A., Zhao, X., Lalchandani, R. R., Sahin, M., Vicini, S., Donoghue, M. J. (2014). EphA7 signaling guides cortical dendritic development and spine maturation. *Proceedings of the National Academy of Sciences*, *111*(13), 4994–4999.

Cohen, B. D., Green, J. M., & Fell, H. P. (1996). HER4-mediated Biological and Biochemical Properties in NIH 3T3 Cells. *Journal of Biological Chemistry*, *271*(9), 4813–4818.

Connor, R. J., Menzel, P., & Pasquale, E. B. (1998). Expression and Tyrosine Phosphorylation of Eph Receptors Suggest Multiple Mechanisms in Patterning of the Visual System. *Developmental Biology*, *193*(1), 21–35.

Conti, M. A., Even-Ram, S., Liu, C., Yamada, K. M., & Adelstein, R. S. (2004). Defects in Cell Adhesion and the Visceral Endoderm following Ablation of Nonmuscle Myosin Heavy Chain II-A in Mice. *Journal of Biological Chemistry*, *279*(40), 41263–41266.

Conti, Mary Anne, Sellers, J. R., Adelstein, R. S., & Elzinga, M. (1991). Identification of the serine residue phosphorylated by protein kinase C in vertebrate nonmuscle myosin heavy chains. *Biochemistry*, *30*(4), 966–970.

Corfas, G., Roy, K., & Buxbaum, J. D. (2004). Neuregulin 1-erbB signaling and the molecular/cellular basis of schizophrenia. *Nature Neuroscience*, *7*(6), 575–580.

Cowan, C. A., & Henkemeyer, M. (2001). The SH2/SH3 adaptor Grb4 transduces B-ephrin reverse signals. *Nature*, *413*(6852), 174–179.

Cowan, C. W., Shao, Y. R., Sahin, M., Shamah, S. M., Lin, M. Z., Greer, P. L., Gao, S., Griffith, E. C., Brugge, J. S., Greenberg, M. E. (2005). Vav Family GEFs Link Activated Ephs to Endocytosis and Axon Guidance. *Neuron*, *46*(2), 205–217.

Crone, S. A., & Kuo-Fen, L. (2002). The Bound Leading the Bound: Target-Derived Receptors Act as Guidance cues. *Neuron*, *36*, 333–343.

Crone, S. A., & Lee, K.-F. (2002). Gene Targeting Reveals Multiple Essential Functions of the Neuregulin Signaling System during Development of the

Neuroendocrine and Nervous Systems. *Annals of the New York Academy of Sciences*, *971*(1), 547–553.

D

Da Silva, J. S., & Dotti, C. G. (2002). Breaking the neuronal sphere: regulation of the actin cytoskeleton in neuritogenesis. *Nature Reviews Neuroscience*, *3*(9), 694–704.

Dahan, I., Yearim, A., Touboul, Y., & Ravid, S. (2012). The tumor suppressor Lgl1 regulates NMII-A cellular distribution and focal adhesion morphology to optimize cell migration. *Molecular Biology of the Cell*, *23*(4), 591–601.

Dail, M., Richter, M., Godement, P., & Pasquale, E. B. (2006). Eph receptors inactivate R-Ras through different mechanisms to achieve cell repulsion. *Journal of Cell Science*, *119*(7), 1244–1254.

Danysz, W., & Parsons, C. G. (2012). Alzheimer's disease, β-amyloid, glutamate, NMDA receptors and memantine - searching for the connections: Alzheimer's disease, β-amyloid, glutamate, NMDA receptors and memantine. *British Journal of Pharmacology*, *167*(2), 324–352.

Dash, B., Dib-Hajj, S. D., & Waxman, S. G. (2018). Multiple myosin motors interact with sodium/potassium-ATPase alpha 1 subunits. *Molecular Brain*, *11*(1).

Davis, T. L., Walker, J. R., Loppnau, P., Butler-Cole, C., Allali-Hassani, A., & Dhe-Paganon, S. (2008). Autoregulation by the Juxtamembrane Region of the Human Ephrin Receptor Tyrosine Kinase A3 (EphA3). *Structure*, *16*(6), 873–884.

Day, B. W., Stringer, B. W., Al-Ejeh, F., Ting, M. J., Wilson, J., Ensbey, K. S., Jamieson P. R., Bruce, Z. C., Liem, Y. C., Offenhäuser, C., Charmsaz, S., Cooper, L. T., Ellacott, J. K., Harding, A., Leveque, L., Inglis, P., Allan, S., Walker, D. G., Lackmann, M., Osborne, G., Khanna, K. K., Reynolds, B. A., Lickliter, J. D., Boyd, A. W. (2013). EphA3 Maintains Tumorigenicity and Is a Therapeutic Target in Glioblastoma Multiforme. *Cancer Cell*, *23*(2), 238–248.

De Strooper, B., Iwatsubo, T., & Wolfe, M. S. (2012). Presenilins and -Secretase: Structure, Function, and Role in Alzheimer Disease. *Cold Spring Harbor Perspectives in Medicine*, *2*(1), a006304–a006304.

De Strooper, B. (2007). Loss-of-function presenilin mutations in Alzheimer disease. Talking Point on the role of presenilin mutations in Alzheimer disease. *EMBO Reports*, *8*(2), 141–146.

Deininger, K., Eder, M., Kramer, E. R., Zieglgansberger, W., Dodt, H.-U., Dornmair, K., Colicelli, J., Klein, R. (2008). The Rab5 guanylate exchange factor Rin1 regulates endocytosis of the EphA4 receptor in mature excitatory neurons. *Proceedings of the National Academy of Sciences*, *105*(34), 12539–12544.

Dent, E. W., Gupton, S. L., & Gertler, F. B. (2011). The Growth Cone Cytoskeleton in Axon Outgrowth and Guidance. *Cold Spring Harbor Perspectives in Biology*, *3*(3), a001800–a001800.

Depboylu, C., Höllerhage, M., Schnurrbusch, S., Brundin, P., Oertel, W. H., Schrattenholz, A., & Höglinger, G. U. (2012). Neuregulin-1 receptor tyrosine kinase ErbB4 is upregulated in midbrain dopaminergic neurons in Parkinson disease. *Neuroscience Letters*, *531*(2), 209–214.

Deyts, C., Vetrivel, K. S., Das, S., Shepherd, Y. M., Dupre, D. J., Thinakaran, G., & Parent, A. T. (2012). Novel G S-Protein Signaling Associated with Membrane-Tethered Amyloid Precursor Protein Intracellular Domain. *Journal of Neuroscience*, *32*(5), 1714–1729.

Deyts, Carole, Clutter, M., Herrera, S., Jovanovic, N., Goddi, A., & Parent, A. T. (2016). Loss of presenilin function is associated with a selective gain of APP function. *ELife*, *5*.

Dines, M., Grinberg, S., Vassiliev, M., Ram, A., Tamir, T., & Lamprecht, R. (2015). The roles of Eph receptors in contextual fear conditioning memory formation. *Neurobiology of Learning and Memory*, *124*, 62–70.

Dotti, C., Sullivan, C., & Banker, G. (1988). The establishment of polarity by hippocampal neurons in culture. *The Journal of Neuroscience*, *8*(4), 1454–1468.

Dottori, M., Down, M., Hüttmann, A., Fitzpatrick, D. R., & Boyd, A. W. (1999). Cloning and Characterization of EphA3 (Hek) Gene Promoter: DNA Methylation Regulates Expression in Hematopoietic Tumor Cells. *Blood*, *94*, 2477–2486.

Duffy, P., Wang, X., Siegel, C. S., Tu, N., Henkemeyer, M., Cafferty, W. B. J., & Strittmatter, S. M. (2012). Myelin-derived ephrinB3 restricts axonal regeneration and recovery after adult CNS injury. *Proceedings of the National Academy of Sciences*, *109*(13), 5063–5068.

Dufour, A., Seibt, J., Passante, L., Depaepe, V., Ciossek, T., Frisén, J., Kullander, K., Flanagan, J. G., Polleux, F., Vanderhaeghen, P. (2003). Area Specificity and Topography of Thalamocortical Projections Are Controlled by ephrin/Eph Genes. *Neuron*, *39*(3), 453–465.

Duggan, S. P., & McCarthy, J. V. (2016). Beyond γ-secretase activity: The multifunctional nature of presenilins in cell signalling pathways. *Cellular Signalling*, *28*(1), 1–11.

Dulyaninova, N. G., & Bresnick, A. R. (2013). The heavy chain has its day: Regulation of myosin-II assembly. *BioArchitecture*, *3*(4), 77–85.

Dulyaninova, N. G., House, R. P., Betapudi, V., & Bresnick, A. R. (2007). Myosin-IIA Heavy-Chain Phosphorylation Regulates the Motility of MDA-MB-231 Carcinoma Cells. *Molecular Biology of the Cell*, *18*(8), 3144–3155.

Dulyaninova, N. G., Malashkevich, V. N., Almo, S. C., & Bresnick, A. R. (2005). Regulation of Myosin-IIA Assembly and Mts1 Binding by Heavy Chain Phosphorylation. *Biochemistry*, *44*(18), 6867–6876.

E

Edson, K., Weisshaar, B., & Matus, A. (1993). Actin depolymerisation induces process formation on MAP2-transfected non-neuronal cells. *Development*, *117*, 689–700.

Egea, J., & Klein, R. (2007). Bidirectional Eph–ephrin signaling during axon guidance. *Trends in Cell Biology*, *17*(5), 230–238.

Ehlers, M. D. (2003). Activity level controls postsynaptic composition and signaling via the ubiquitin-proteasome system. *Nature Neuroscience*, *6*(3), 231–242.

Esch, T., Lemmon, V., & Banker, G. (1999). Local Presentation of Substrate Molecules Directs Axon Specification by Cultured Hippocampal Neurons. *The Journal of Neuroscience*, *19*(15), 6417–6426.

Eto, K., Hommyo, A., Yonemitsu, R., & Abe, S. (2010). ErbB4 signals Neuregulin1-stimulated cell proliferation and c-fos gene expression through phosphorylation of serum response factor by mitogen-activated protein kinase cascade. *Molecular and Cellular Biochemistry*, *339*(1–2), 119–125.

Even-Ram, S., Doyle, A. D., Conti, M. A., Matsumoto, K., Adelstein, R. S., & Yamada, K. M. (2007). Myosin IIA regulates cell motility and actomyosin–microtubule crosstalk. *Nature Cell Biology*, *9*(3), 299–309.

F

Fan, X., Labrador, J. P., Hing, H., & Bashaw, G. J. (2003). Slit Stimulation Recruits Dock and Pak to the Roundabout Receptor and Increases Rac Activity to Regulate Axon Repulsion at the CNS Midline. *Neuron*, *40*(1), 113–127.

Farhy-Tselnicker, I., & Allen, N. J. (2018). Astrocytes, neurons, synapses: a tripartite view on cortical circuit development. *Neural Development*, *13*(1).

Fass, J. N., & Odde, D. J. (2003). Tensile Force-Dependent Neurite Elicitation via Anti-b1 Integrin Antibody-Coated Magnetic Beads. *Biophysical Journal*, *85*, 623–636.

Filosa, A., Paixão, S., Honsek, S. D., Carmona, M. A., Becker, L., Feddersen, B., Gaitanos, L., Rudhard, Y., Schoepfer, R., Klopstock, T., Kullander, K., Rose, C. R., Pasquale, E. B., Klein, R. (2009). Neuron-glia communication via EphA4/ephrin-A3 modulates LTP through glial glutamate transport. *Nature Neuroscience*, *12*(10), 1285–1292.

Finci, L., Zhang, Y., Meijers, R., & Wang, J.-H. (2015). Signaling mechanism of the netrin-1 receptor DCC in axon guidance. *Progress in Biophysics and Molecular Biology*, *118*(3), 153–160.

Fiore, L., Medori, M., Spelzini, G., Carreño, C. O., Carri, N. G., Sanchez, V., & Scicolone, G. (2018). Regulation of axonal EphA4 forward signaling is involved in the effect of EphA3 on chicken retinal ganglion cell axon growth during retinotectal mapping. *Experimental Eye Research*, *178*, 46–60.

Flames, N., Long, J. E., Garratt, A. N., Fischer, T. M., Gassmann, M., Birchmeier, C., Lai, C., Rubenstein, J. L. R., Marín, O. Short- and Long-Range Attraction of Cortical GABAergic Interneurons by Neuregulin-1. *Neuron*, *44*(2), 251–261.

Flanagan, J. G., & Vanderhaeghen, P. (1998). THE EPHRINS AND EPH RECEPTORS IN NEURAL DEVELOPMENT. *Annual Review of Neuroscience*, *21*(1), 309–345.

Fleck, D., van Bebber, F., Colombo, A., Galante, C., Schwenk, B. M., Rabe, L.,

Hampel, H., Novak., B., Kremmer, E., Tahirovic, S., Edbauer, D., Lichtenthaler, S. F., Schmid, B., Willem, M., Haass, C. (2013). Dual Cleavage of Neuregulin 1 Type III by BACE1 and ADAM17 Liberates Its EGF-Like Domain and Allows Paracrine Signaling. *Journal of Neuroscience*, *33*(18), 7856–7869.

Fleck, Daniel, Voss, M., Brankatschk, B., Giudici, C., Hampel, H., Schwenk, B., Edbauer, D., Fukumori, A., Steiner, H., Kremmer, E., Haug-Kröper, M., Rossner, M. J., Fluhrer, R., Willem, M., Haass, C. (2016). Proteolytic Processing of Neuregulin 1 Type III by Three Intramembrane-cleaving Proteases. *Journal of Biological Chemistry*, *291*(1), 318–333.

Fluhrer, R., Friedlein, A., Haass, C., & Walter, J. (2004). Phosphorylation of Presenilin 1 at the Caspase Recognition Site Regulates Its Proteolytic Processing and the Progression of Apoptosis. *Journal of Biological Chemistry*, *279*(3), 1585–1593.

Flynn, K. C. (2013). The cytoskeleton and neurite initiation. *BioArchitecture*, *3*(4), 86–109.

Forcet, C., Stein, E., Pays, L., Corset, V., Llambi, F., Tessier-Lavigne, M., & Mehlen, P. (2002). Netrin-1-mediated axon outgrowth requires deleted in colorectal cancer-dependent MAPK activation. *Nature*, *417*(6887), 443–447.

Forse, G. J., Uson, M. L., Nasertorabi, F., Kolatkar, A., Lamberto, I., Pasquale, E. B., & Kuhn, P. (2015). Distinctive Structure of the EphA3/Ephrin-A5 Complex Reveals a Dual Mode of Eph Receptor Interaction for Ephrin-A5. *PLOS ONE*, *10*(5), e0127081.

Fournier, A. E., Takizawa, B. T., & Strittmatter, S. M. (2003). Rho Kinase Inhibition Enhances Axonal Regeneration in the Injured CNS. *The Journal of Neuroscience*, *23*(4), 1416–1423.

Fox, B. P., Tabone, C. J., & Kandpal, R. P. (2006). Potential clinical relevance of Eph receptors and ephrin ligands expressed in prostate carcinoma cell lines. *Biochemical and Biophysical Research Communications*, *342*(4), 1263–1272.

Free, R. B., Hazelwood, L. A., & Sibley, D. R. (2009). Identifying Novel Protein-Protein Interactions Using Co-Immunoprecipitation and Mass Spectroscopy. In J. N. Crawley, C. R. Gerfen, M. A. Rogawski, D. R. Sibley, P. Skolnick, & S. Wray (Eds.), *Current Protocols in Neuroscience*. Hoboken, NJ, USA: John Wiley & Sons, Inc.

Frugier, T., Conquest, A., McLean, C., Currie, P., Moses, D., & Goldshmit, Y. (2012). Expression and Activation of EphA4 in the Human Brain After Traumatic Injury. *Journal of Neuropathology & Experimental Neurology*, *71*(3), 242–250.

Fukata, M., Nakagawa, M., & Kaibuchi, K. (2003). Roles of Rho-family GTPases in cell polarisation and directional migration. *Current Opinion in Cell Biology*, *15*(5), 590–597.

Funahashi, Y., Namba, T., Nakamuta, S., & Kaibuchi, K. (2014). Neuronal polarization in vivo: Growing in a complex environment. *Current Opinion in Neurobiology*, *27*, 215–223.

G

Gallarda, B. W., Bonanomi, D., Mu ller, D., Brown, A., Alaynick, W. A., Andrews, S. E., Lemke, G., Pfaff, S. L., Marquardt, T. (2008). Segregation of Axial Motor and Sensory Pathways via Heterotypic Trans-Axonal Signaling. *Science*, *320*(5873), 233–236.

Gallo, G. (2006). RhoA-kinase coordinates F-actin organization and myosin II activity during semaphorin-3A-induced axon retraction. *Journal of Cell Science*, *119*(16), 3413–3423.

Gao, P., Zhang, J.-H., Yokoyama, M., Racey, B., Dreyfus, C., Black, I., & Zhou, R. (1996). Regulation of topographic projection in the brain: Elf-1 in the hippocamposeptal system. *Proceedings of the National Academy of Sciences*, *93*, 11161–11166.

Gao, P.-P., Yue, Y., Zhang, J.-H., Cerretti, D. P., Levitt, P., & Zhou, R. (1998). Regulation of thalamic neurite outgrowth by the Eph ligand ephrin-A5: Implications in the development of thalamocortical projections. *Proceedings of the National Academy of Sciences*, *95*(9), 5329–5334.

Gärtner, A. (2006). Neuronal polarity is regulated by glycogen synthase kinase-3 (GSK-3) independently of Akt/PKB serine phosphorylation. *Journal of Cell Science*, *119*(19), 3927–3934.

Gassmannl, M., & Lemke, G. (1997). Neuregulins and neuregulin receptors in neural development. *Current Opinion in Neurobiology*, *7*, 87–92.

Gatto, G., Morales, D., Kania, A., & Klein, R. (2014). EphA4 Receptor Shedding Regulates Spinal Motor Axon Guidance. *Current Biology*, *24*(20), 2355–2365.

Genander, M., Halford, M. M., Xu, N.-J., Eriksson, M., Yu, Z., Qiu, Z., Martling, A., Greicius, G., Thakar, S., Catchpole, T., Chumley, M. J., Zdunek, S., Wang, C., Holm,

T., Goff, S. P., Pettersson, S., Pestell, R. G., Henkemeyer, M., Frisén, J. (2009). Dissociation of EphB2 Signaling Pathways Mediating Progenitor Cell Proliferation and Tumor Suppression. *Cell*, *139*(4), 679–692.

Georgakopoulos, A., Litterst, C., Ghersi, E., Baki, L., Xu, C., Serban, G., & Robakis, N. K. (2006). Metalloproteinase/Presenilin1 processing of ephrinB regulates EphB-induced Src phosphorylation and signaling. *The EMBO Journal*, *25*(6), 1242–1252.

Gerstmann, K., Pensold, D., Symmank, J., Khundadze, M., Hubner, C. A., Bolz, J., & Zimmer, G. (2015). Thalamic afferents influence cortical progenitors via ephrin A5-EphA4 interactions. *Development*, *142*(1), 140–150.

Go, R. C. P., Perry, R. T., Wiener, H., Bassett, S. S., Blacker, D., Devlin, B., & Sweet, R. A. (2005). Neuregulin-1 polymorphism in late onset Alzheimer's disease families with psychoses. *American Journal of Medical Genetics Part B: Neuropsychiatric Genetics*, *139B*(1), 28–32.

Goes, F. S., Sanders, L. L. O., & Potash, J. B. (2008). The genetics of psychotic bipolar disorder. *Current Psychiatry Reports*, *10*(2), 178–189.

Goldshmit, Y., & Bourne, J. (2010). Upregulation of EphA4 on Astrocytes Potentially Mediates Astrocytic Gliosis after Cortical Lesion in the Marmoset Monkey. *Journal of Neurotrauma*, *27*(7), 1321–1332.

Golomb, E., Ma, X., Jana, S. S., Preston, Y. A., Kawamoto, S., Shoham, N. G., Goldin, E., Conti, M. A., Sellers, J. R., Adelstein, R. S. (2004). Identification and Characterization of Nonmuscle Myosin II-C, a New Member of the Myosin II Family. *Journal of Biological Chemistry*, *279*(4), 2800–2808.

Gomez, T. M. (2001). Filopodial Calcium Transients Promote Substrate-Dependent Growth Cone Turning. *Science*, *291*(5510), 1983–1987.

Govek, E.-E. (2005). The role of the Rho GTPases in neuronal development. *Genes & Development*, *19*(1), 1–49.

Graus-Porta, D. (1997). ErbB-2, the preferred heterodimerization partner of all ErbB receptors, is a mediator of lateral signaling. *The EMBO Journal*, *16*(7), 1647–1655.

Gu, Y., Misonou, H., Sato, T., Dohmae, N., Takio, K., & Ihara, Y. (2001). Distinct Intramembrane Cleavage of the β-Amyloid Precursor Protein Family Resembling γ-Secretase-like Cleavage of Notch. *Journal of Biological Chemistry*, *276*(38), 35235–35238.

Gu, Z. (2005). Regulation of NMDA Receptors by Neuregulin Signaling in Prefrontal Cortex. *Journal of Neuroscience*, *25*(20), 4974–4984.

Guo, W., Jiang, H., Gray, V., Dedhar, S., & Rao, Y. (2007). Role of the integrin-linked kinase (ILK) in determining neuronal polarity. *Developmental Biology*, *306*(2), 457–468.

Guruharsha, K. G., Kankel, M. W., & Artavanis-Tsakonas, S. (2012). The Notch signalling system: recent insights into the complexity of a conserved pathway. *Nature Reviews Genetics*, *13*(9), 654–666.

Gutzman, J. H., Sahu, S. U., & Kwas, C. (2015). Non-muscle myosin IIA and IIB differentially regulate cell shape changes during zebrafish brain morphogenesis. *Developmental Biology*, *397*(1), 103–115.

H

Haapasalo, A., & Kovacs, D. M. (2011). The Many Substrates of Presenilin/γ-Secretase. *Journal of Alzheimer's Disease*, *25*(1), 3–28.

Hahn, C.-G., Wang, H.-Y., Cho, D.-S., Talbot, K., Gur, R. E., Berrettini, W. H., Bakshi, K., Kamin, J., Borgmann-Winter, K. E., Siegel, S. J., Gallop, R. J., Arnold, S. E. (2006). Altered neuregulin 1–erbB4 signaling contributes to NMDA receptor hypofunction in schizophrenia. *Nature Medicine*, *12*(7), 824–828.

Hall, A. (1994). Small GTP-Binding Proteins and the Regulation of the Actin Cytoskeleton. *Annual Review of Cell Biology*, *10*, 31–54.

Hamid, R., Kilger, E., Willem, M., Vassallo, N., Kostka, M., Bornhövd, C., Reichert, A. S., Kretzschmar, H. A., Haas, C., Herms, J. (2007). Amyloid precursor protein intracellular domain modulates cellular calcium homeostasis and ATP content. *Journal of Neurochemistry*, *102*(4), 1264–1275.

Handler, M., Yang, X., & Shen, J. (2000). Presenilin-1 regulates neuronal differentiation during neurogenesis. *Development*, *127*, 2593–2606.

Harari, D., Tzahar, E., Romano, J., Shelly, M., Pierce, J., Andrews, G., & Yarden, Y. (1999). Neuregulin-4: a novel growth factor that acts through the ErbB-4 receptor tyrosine kinase. *Oncogene*, *18*(17), 2681–2689.

Hatanaka, Y., Yamauchi, K., & Murakami, F. (2012). Formation of Axon-dendrite polarity in situ: Initiation of axons from polarized and non-polarized cells. *Development, Growth & Differentiation*, *54*(3), 398–407.

Hathaway, D. R., & Adelstein, R. S. (1979). Human platelet myosin light chain kinase requires the calcium-binding protein calmodulin for activity. *Proceedings of the National Academy of Sciences*, *76*(4), 1653–1657.

Haubensak, W., Attardo, A., Denk, W., & Huttner, W. B. (2004). Neurons arise in the basal neuroepithelium of the early mammalian telencephalon: A major site of neurogenesis. *PNAS*, *101*, 3196–3201.

He, G., Luo, W., Li, P., Remmers, C., Netzer, W. J., Hendrick, J., Bettayeb, K., Flajolet, M., Gorelick, F., Wnnogle, L. P., Greengard, P. (2010). Gamma-secretase activating protein is a therapeutic target for Alzheimer's disease. *Nature*, *467*(7311), 95–98.

Hering, H., & Sheng, M. (2001). DENDRITIC SPINES: STRUCTURE, DYNAMICS AND REGULATION. *Nature*, *2*, 880–888.

Himanen, J.-P., Chumley, M. J., Lackmann, M., Li, C., Barton, W. A., Jeffrey, P. D., Vearing, C., Geleick, D., Feldheim, D. A., Boyd, A. W., Henkemeyer, M., Nikolov, D. B. (2004). Repelling class discrimination: ephrin-A5 binds to and activates EphB2 receptor signaling. *Nature Neuroscience*, *7*(5), 501–509.

Himanen, J.-P., & Nikolov, D. B. (2003). Eph signaling: a structural view. *Trends in Neurosciences*, *26*(1), 46–51.

Holbro, T., & Hynes, N. E. (2004). ERBB RECEPTORS: Directing Key Signaling Networks Troughout Life. *Annual Review of Pharmacology and Toxicology*, *44*(1), 195–217.

Holmberg, J. (2005). Ephrin-A2 reverse signaling negatively regulates neural progenitor proliferation and neurogenesis. *Genes & Development*, *19*(4), 462–471.

Holtzman, D. M., Morris, J. C., & Goate, A. M. (2011). Alzheimer's Disease: The Challenge of the Second Century. *Science Translational Medicine*, *3*(77), 77sr1-77sr1.

Hosono, Y., Usukura, J., Yamaguchi, T., Yanagisawa, K., Suzuki, M., & Takahashi, T. (2012). MYBPH inhibits NM IIA assembly via direct interaction with NMHC IIA and reduces cell motility. *Biochemical and Biophysical Research Communications*, *428*(1), 173–178.

Hosono, Y., Yamaguchi, T., Mizutani, E., Yanagisawa, K., Arima, C., Tomida, S., Shimada, Y., Hiraoka, M., Kato, S., Yokoi, K., Suzuki, M., Takahashi, T. (2012). MYBPH, a transcriptional target of TTF-1, inhibits ROCK1, and reduces cell motility and metastasis: MYBPH inhibits ROCK1 and metastasis. *The EMBO Journal*, *31*(2), 481–493.

Howitt, J. A., Clout, N. J., & Hohenester, E. (2004). Binding site for Robo receptors revealed by dissection of the leucine-rich repeat region of Slit. *The EMBO Journal*, *23*(22), 4406–4412.

Hsieh, H., Boehm, J., Sato, C., Iwatsubo, T., Tomita, T., Sisodia, S., & Malinow, R. (2006). AMPAR Removal Underlies Aβ-Induced Synaptic Depression and Dendritic Spine Loss. *Neuron*, *52*(5), 831–843.

Hu, S., & Reichardt, L. F. (1999). From Membrane to Cytoskeleton: Enabling a Connection. *Neuron*, *22*(3), 419–422.

Hu, T., Shi, G., Larose, L., Rivera, G. M., Mayer, B. J., & Zhou, R. (2009). Regulation of Process Retraction and Cell Migration by EphA3 Is Mediated by the Adaptor Protein Nck1. *Biochemistry*, *48*(27), 6369–6378.

Hu, X., Fan, Q., Hou, H., & Yan, R. (2016). Neurological dysfunctions associated with altered BACE1-dependent Neuregulin-1 signaling. *Journal of Neurochemistry*, *136*(2), 234–249.

Huang, K.-P. (1989). The mechanism of protein kinase C activation. *Trends in Neurosciences*, *12*(11), 425–432.

Huusko, P., Ponciano-Jackson, D., Wolf, M., Kiefer, J. A., Azorsa, D. O., Tuzmen, S., (…)., Mousses, S. (2004). Nonsense-mediated decay microarray analysis identifies mutations of EPHB2 in human prostate cancer. *Nature Genetics*, *36*(9), 979–983.

I

Ikebe, M., Koretz, J., & Hartshorne, D. J. (1988). Effects of Phosphorylation of Light Chain Residues Threonine18 and Serine19 on the Properties andConformation of Smooth Muscle Myosin. *The Journal of Biological Chemistry*, *263*, 6432–6437.

Ikeuchi, T., & Sisodia, S. S. (2003). The Notch Ligands, Delta1 and Jagged2, Are Substrates for Presenilin-dependent “γ-Secretase” Cleavage. *Journal of Biological Chemistry*, *278*(10), 7751–7754.

Inoue, E., Deguchi-Tawarada, M., Togawa, A., Matsui, C., Arita, K., Katahira-Tayama, S., Sato, T., Yamauchi, E., Oda, Y., Takai, Y. (2009). Synaptic activity prompts γ-secretase–mediated cleavage of EphA4 and dendritic spine formation. *The Journal of Cell Biology*, *185*(3), 551–564.

Iwakura, Y., & Nawa, H. (2013). ErbB1-4-dependent EGF/neuregulin signals and their cross talk in the central nervous system: pathological implications in schizophrenia and Parkinson's disease. *Frontiers in Cellular Neuroscience*, *7*.

J

Janes, P. W., Saha, N., Barton, W. A., Kolev, M. V., Wimmer-Kleikamp, S. H., Nievergall, E., Blobel, C. P., Himanen, J-P., Lackmann, M., Nikolov, D. B. (2005). Adam Meets Eph: An ADAM Substrate Recognition Module Acts as a Molecular Switch for Ephrin Cleavage In trans. *Cell*, *123*(2), 291–304.

Janes, P. W., Wimmer-Kleikamp, S. H., Frangakis, A. S., Treble, K., Griesshaber, B., Sabet, O., Grabenbauer, M., Ting, A. Y., Saftig, P., Bastiaens, P. I., Lackmann, M. (2009). Cytoplasmic Relaxation of Active Eph Controls Ephrin Shedding by ADAM10. *PLoS Biology*, *7*(10), e1000215.

Jessen, K. R., & Mirsky, R. (2005). The origin and development of glial cells in peripheral nerves. *Nature Reviews Neuroscience*, *6*(9), 671–682.

Jiang, L., Emmetsberger, J., Talmage, D. A., & Role, L. W. (2013). Type III Neuregulin 1 Is Required for Multiple Forms of Excitatory Synaptic Plasticity of Mouse Cortico-Amygdala Circuits. *Journal of Neuroscience*, *33*(23), 9655–9666.

Jin, K., Mao, X. O., & Greenberg, D. A. (2006). Vascular endothelial growth factor stimulates neurite outgrowth from cerebral cortical neurons via Rho kinase signaling. *Journal of Neurobiology*, *66*(3), 236–242.

Jin, Z., & Strittmatter, S. M. (1997). Rac1 Mediates Collapsin-1-Induced Growth Cone Collapse. *The Journal of Neuroscience*, *17*(16), 6256–6263.

Junttila, T. (2000). ErbB4 and Its Isoforms Selective Regulation of Growth Factor Responses by Naturally Occurring Receptor Variants. *Trends in Cardiovascular Medicine*, *10*(7), 304–310.

K

Kageyama, R., & Ohtsuka, T. (1999). The Notch-Hes pathway in mammalian neural development. *Cell Research*, *9*(3), 179–188.

Kania, A., & Klein, R. (2016). Mechanisms of ephrin–Eph signalling in development, physiology and disease. *Nature Reviews Molecular Cell Biology*, *17*(4), 240–256.

Keino-Masu, K., Masu, M., Hinck, L., Leonardo, E., Chan, S. S-Y., Culotti, J. G., Tessier-Lavigne, M. (1996). Deleted in Colorectal Cancer (DCC) Encodes a Netrin Receptor. *Neuroscience Research*, *28*, S128–S128.

Keleman, K., & Dickson, B. J. (2001). Short- and Long-Range Repulsion by the Drosophila Unc5 Netrin Receptor. *Neuron*, *32*(4), 605–617.

Kenchappa, R. S., Zampieri, N., Chao, M. V., Barker, P. A., Teng, H. K., Hempstead, B. L., & Carter, B. D. (2006). Ligand-Dependent Cleavage of the P75 Neurotrophin Receptor Is Necessary for NRIF Nuclear Translocation and Apoptosis in Sympathetic Neurons. *Neuron*, *50*(2), 219–232.

Killeen, M., Tong, J., Krizus, A., Steven, R., Scott, I., Pawson, T., & Culotti, J. (2002). UNC-5 Function Requires Phosphorylation of Cytoplasmic Tyrosine 482, but Its UNC-40-Independent Functions also Require a Region between the ZU-5 and Death Domains. *Developmental Biology*, *251*(2), 348–366.

Kim, J., Kleizen, B., Choy, R., Thinakaran, G., Sisodia, S. S., & Schekman, R. W. (2007). Biogenesis of γ-secretase early in the secretory pathway. *The Journal of Cell Biology*, *179*(5), 951–963.

Kimura, K., Ito, M., Amano, M., Chihara, K., Fukata, Y., Nakafuku, M., Yamamori, B., Feng, J., Nakano, T., Okawa, K., Iwamatsu, A., Kaibuchi, K. (1996). Regulation of Myosin Phosphatase by Rho and Rho-Associated Kinase (Rho-Kinase). *Science*, *273*(5272), 245–248.

Kirschenbaum, F., Hsu, S.-C., Cordell, B., & McCarthy, J. V. (2001). Glycogen Synthase Kinase-3β Regulates Presenilin 1 C-terminal Fragment Levels. *Journal of Biological Chemistry*, *276*(33), 30701–30707.

Kollins, K. M., Hu, J., Bridgman, P. C., Huang, Y. Q., & Gallo, G. (2009). Myosin-II negatively regulates minor process extension and the temporal development of neuronal polarity. *Developmental Neurobiology*, *69*(5), 279–298.

Komatsu, S., & Ikebe, M. (2004). ZIP kinase is responsible for the phosphorylation of myosin II and necessary for cell motility in mammalian fibroblasts. *The Journal of Cell Biology*, *165*(2), 243–254.

Kong, Y., Janssen, B. J. C., Malinauskas, T., Vangoor, V. R., Coles, C. H., Kaufmann, R., Ni, T., Gilbert, R. J. C., Padilla-Parra, S., Pasterkamp, R. J., Jones, E. Y. (2016). Structural Basis for Plexin Activation and Regulation. *Neuron*, *91*(3), 548–560.

Kopan, R. (2012). Notch Signaling. *Cold Spring Harbor Perspectives in Biology*, *4*(10), a011213–a011213.

Kopan, Raphael, & Ilagan, M. X. G. (2009). The Canonical Notch Signaling Pathway: Unfolding the Activation Mechanism. *Cell*, *137*(2), 216–233.

Kornblum, H. I., Yanni, D. S., Easterday, M. C., & Seroogy, K. B. (2000). Expression of the EGF Receptor Family Members ErbB2, ErbB3, and ErbB4 in Germinal Zones of the Developing Brain and in Neurosphere Cultures Containing CNS Stem Cells. *Developmental Neuroscience*, *22*(1–2), 16–24.

Kovács, M., Tóth, J., Hetényi, C., Málnási-Csizmadia, A., & Sellers, J. R. (2004). Mechanism of Blebbistatin Inhibition of Myosin II. *Journal of Biological Chemistry*, *279*(34), 35557–35563.

Kriegstein, A. R., & Noctor, S. C. (2004). Patterns of neuronal migration in the embryonic cortex. *Trends in Neurosciences*, *27*(7), 392–399.

Krivosheya, D., Tapia, L., Levinson, J. N., Huang, K., Kang, Y., Hines, R., Ting, A. K., Craig, A. M., Mei, L., Bamji, S. X., El-Husseini, A. (2008). ErbB4-Neuregulin Signaling Modulates Synapse Development and Dendritic Arborization through Distinct Mechanisms. *Journal of Biological Chemistry*, *283*(47), 32944–32956.

Krupke, O. A., & Burke, R. D. (2014). Eph-Ephrin signaling and focal adhesion kinase regulate actomyosin-dependent apical constriction of ciliary band cells. *Development*, *141*(5), 1075–1084.

Kubo, T., Endo, M., Hata, K., Taniguchi, J., Kitajo, K., Tomura, S., Yamaguchi, A., Mueller, B. K., Yamashita, T. (2008). Myosin IIA is required for neurite outgrowth inhibition produced by repulsive guidance molecule. *Journal of Neurochemistry*, *105*(1), 113–126.

Kudo, C., Ajioka, I., Hirata, Y., & Nakajima, K. (2005). Expression profiles of EphA3 at both the RNA and protein level in the developing mammalian forebrain. *The Journal of Comparative Neurology*, *487*(3), 255–269.

Kumar, D., Ganeshpurkar, A., Kumar, D., Modi, G., Gupta, S. K., & Singh, S. K. (2018). Secretase inhibitors for the treatment of Alzheimer's disease: Long road ahead. *European Journal of Medicinal Chemistry*, *148*, 436–452.

Kwon, A., John, M., Ruan, Z., & Kannan, N. (2018). Coupled regulation by the juxtamembrane and sterile α motif (SAM) linker is a hallmark of ephrin tyrosine kinase evolution. *Journal of Biological Chemistry*, *293*(14), 5102–5116.

Kwon, O.-B. (2005). Neuregulin-1 Reverses Long-Term Potentiation at CA1 Hippocampal Synapses. *Journal of Neuroscience*, *25*(41), 9378–9383.

L

Lackmann, M., Oates, A. C., Dottori, M., Smith, F. M., Do, C., Power, M., Kravets, L., Boyd, A. W. (1998). Distinct Subdomains of the EphA3 Receptor Mediate Ligand Binding and Receptor Dimerization. *Journal of Biological Chemistry*, *273*(32), 20228–20237.

Lai, C., & Feng, L. (2004). Implication of γ-secretase in neuregulin-induced maturation of oligodendrocytes. *Biochemical and Biophysical Research Communications*, *314*(2), 535–542.

Lai, M.-T., Chen, E., Crouthamel, M.-C., DiMuzio-Mower, J., Xu, M., Huang, Q., (…) Li, Y.-M. (2003). Presenilin-1 and Presenilin-2 Exhibit Distinct yet Overlapping γ-Secretase Activities. *Journal of Biological Chemistry*, *278*(25), 22475–22481.

Lau, K.-F., Howlett, D. R., Kesavapany, S., Standen, C. L., Dingwall, C., McLoughlin, D. M., & Miller, C. C. J. (2002). Cyclin-Dependent Kinase-5/p35 Phosphorylates Presenilin 1 to Regulate Carboxy-Terminal Fragment Stability. *Molecular and Cellular Neuroscience*, *20*(1), 13–20.

Laudon, H., Hansson, E. M., Melén, K., Bergman, A., Farmery, M. R., Winblad, B., Lendahl, U., Von Heijne, G., Näslund, J. (2005). A Nine-transmembrane Domain Topology for Presenilin 1. *Journal of Biological Chemistry*, *280*(42), 35352–35360.

Lawrenson, I. D., Wimmer-Kleikamp, S. H., Lock, P., Schoenwaelder, S. M., Down, M., Boyd, A. W., Alewood, P. F., Lackmann, M. (2002). Ephrin-A5 induces rounding,

blebbing and de- adhesion of EphA3-expressing 293T and melanoma cells by CrkII and Rho-mediated signalling. *Journal of Cell Science*, *115*, 1059–1072.

Lebrand, C., Dent, E. W., Strasser, G. A., Lanier, L. M., Krause, M., Svitkina, T. M., Borisy, G. G., Gertler, F. B. (2004). Critical Role of Ena/VASP Proteins for Filopodia Formation in Neurons and in Function Downstream of Netrin-1. *Neuron*, *42*(1), 37–49.

Ledonne, A., Mango, D., Latagliata, E. C., Chiacchierini, G., Nobili, A., Nisticò, R., D'Amelio, M., Puglisi-Allegra, S., Mercuri, N. B. (2018). Neuregulin 1/ErbB signalling modulates hippocampal mGluRI-dependent LTD and object recognition memory. *Pharmacological Research*, *130*, 12–24.

Lee, H.-J., Jung, K.-M., Huang, Y. Z., Bennett, L. B., Lee, J. S., Mei, L., & Kim, T.-W. (2002). Presenilin-dependent γ-Secretase-like Intramembrane Cleavage of ErbB4. *Journal of Biological Chemistry*, *277*(8), 6318–6323.

Lee, M. K., Slunt, H. H., Martin, L. J., Thinakaran, G., Kim, G., Gandy, S. E., Seeger, M., Koo, E., Price, D. L., Sisodia, S. S. (1996). Expression of Presenilin 1 and 2 (PS1 and PS2) in Human and Murine Tissues. *The Journal of Neuroscience*, *16*(23), 7513–7525.

Leimeroth, R., Lobsiger, C., Lüssi, A., Taylor, V., Suter, U., & Sommer, L. (2002). Membrane-Bound Neuregulin1 Type III Actively Promotes Schwann Cell Differentiation of Multipotent Progenitor Cells. *Developmental Biology*, *246*(2), 245–258.

Leonardo, E. D., Hinck, L., Masu, M., Keino-Masu, K., Ackerman, S., & Tessier-Lavigne, M. (1997). Vertebrate homologues of C. elegans UNC-5 are candidate netrin receptors. *Nature*, *386*, 833–838.

Letourneau, P. C., Shattuck, T. A., & Ressler, A. H. (1987). “Pull” and “push” in neurite elongation: Observations on the effects of different concentrations of cytochalasin B and taxol. *Cell Motility and the Cytoskeleton*, *8*(3), 193–209.

Li, B., Woo, R.-S., Mei, L., & Malinow, R. (2007). The Neuregulin-1 Receptor ErbB4 Controls Glutamatergic Synapse Maturation and Plasticity. *Neuron*, *54*(4), 583–597.

Li, H., Chou, S.-J., Hamasaki, T., & Perez-Garcia, C. G. (2012). Neuregulin repellent signaling via ErbB4 restricts GABAergic interneurons to migratory paths from ganglionic eminence to cortical destinations, 17.

Li, S., Hong, S., Shepardson, N. E., Walsh, D. M., Shankar, G. M., & Selkoe, D. (2009). Soluble Oligomers of Amyloid β Protein Facilitate Hippocampal Long-Term Depression by Disrupting Neuronal Glutamate Uptake. *Neuron*, *62*(6), 788–801.

Li, W. (2006). FAK and Src kinases are required for netrin-induced tyrosine phosphorylation of UNC5. *Journal of Cell Science*, *119*(1), 47–55.

Li, Weiquan, Lee, J., Vikis, H. G., Lee, S.-H., Liu, G., Aurandt, J., Shen, T-L., Fearon, E. R., Guan, J-L., Han, M., Rao, Y., Hong, K., Guan, K.-L. (2004). Activation of FAK and Src are receptor-proximal events required for netrin signaling. *Nature Neuroscience*, *7*(11), 1213–1221.

Li, X., Gao, X., Liu, G., Xiong, W., Wu, J., & Rao, Y. (2008). Netrin signal transduction and the guanine nucleotide exchange factor DOCK180 in attractive signaling. *Nature Neuroscience*, *11*(1), 28–35.

Li, Z.-H., Spektor, A., Varlamova, O., & Bresnick, A. R. (2003). Mts1 Regulates the Assembly of Nonmuscle Myosin-IIA. *Biochemistry*, *42*(48), 14258–14266.

Lin, C. H., Espreafico, E. M., Mooseker, M. S., & Forscher, P. (1996). Myosin Drives Retrograde F-Actin Flow in Neuronal Growth Cones. *Neuron*, *16*, 769–782.

Lin, C.-H., & Forscher, P. (1995). Growth cone advance is inversely proportional to retrograde F-actin flow. *Neuron*, *14*(4), 763–771.

Lin, L., Lesnick, T. G., Maraganore, D. M., & Isacson, O. (2009). Axon guidance and synaptic maintenance: preclinical markers for neurodegenerative disease and therapeutics. *Trends in Neurosciences*, *32*(3), 142–149.

Lisabeth, E. M., Fernandez, C., & Pasquale, E. B. (2012). Cancer Somatic Mutations Disrupt Functions of the EphA3 Receptor Tyrosine Kinase through Multiple Mechanisms. *Biochemistry*, *51*(7), 1464–1475.

Litterst, C., Georgakopoulos, A., Shioi, J., Ghersi, E., Wisniewski, T., Wang, R., Ludwig, A., Robakis, N. K. (2007). Ligand Binding and Calcium Influx Induce Distinct Ectodomain/γ-Secretase-processing Pathways of EphB2 Receptor. *Journal of Biological Chemistry*, *282*(22), 16155–16163.

Liu, B. P., & Strittmatter, S. M. (2001). Semaphorin-mediated axonal guidance via Rho-related G proteins. *Current Opinion in Cell Biology*, *13*(5), 619–626.

Liu, G., Beggs, H., Jürgensen, C., Park, H.-T., Tang, H., Gorski, J., Jones, K. R., Reichardt, L. F., Rao, Y. (2004). Netrin requires focal adhesion kinase and Src family kinases for axon outgrowth and attraction. *Nature Neuroscience*, *7*(11), 1222–1232.

Liu, X., Bates, R., Yin, D.-M., Shen, C., Wang, F., Su, N., Kirov, S. A., Luo, Y., Wang, J-Z., Xiong, W-C., Mei, L. (2011). Specific Regulation of NRG1 Isoform Expression by Neuronal Activity. *Journal of Neuroscience*, *31*(23), 8491–8501.

Liu, Y., Ford, B., Mann, M. A., & Fischbach, G. D. (2001). Neuregulins Increase alpha7 Nicotinic Acetylcholine Receptors and Enhance Excitatory Synaptic Transmission in GABAergic Interneurons of the Hippocampus. *Journal of Neuroscience*, *21*(15), 5660–5669.

Liu, Z., Patel, K., Schmidt, H., Andrews, W., Pini, A., & Sundaresan, V. (2004). Extracellular Ig domains 1 and 2 of Robo are important for ligand (Slit) binding. *Molecular and Cellular Neuroscience*, *26*(2), 232–240.

Lleó, A., & Saura, C. A. (2011). γ-Secretase Substrates and their Implications for Drug Development in Alzheimer's Disease. *Current Topics in Medicinal Chemistry*, *11*, 1513–1527.

Logeat, F., Bessia, C., Brou, C., LeBail, O., Jarriault, S., Seidah, N. G., & Israel, A. (1998). The Notch1 receptor is cleaved constitutively by a furin-like convertase. *Proceedings of the National Academy of Sciences*, *95*(14), 8108–8112.

Louvi, A. (2004). Presenilin 1 in migration and morphogenesis in the central nervous system. *Development*, *131*(13), 3093–3105.

Louvi, Angeliki, & Artavanis-Tsakonas, S. (2006). Notch signalling in vertebrate neural development. *Nature Reviews Neuroscience*, *7*(2), 93–102.

Lowery, L. A., & Vactor, D. V. (2009). The trip of the tip: understanding the growth cone machinery. *Nature Reviews Molecular Cell Biology*, *10*(5), 332–343.

Lu, Y., Sun, X.-D., Hou, F.-Q., Bi, L.-L., Yin, D.-M., Liu, F., Chen, Y-J., Bean, J. C., Jiao, H-F., Liu, X., Li, B-M., Xiong, W-C., Gao, T-M., Mei, L. (2014). Maintenance of GABAergic Activity by Neuregulin 1-ErbB4 in Amygdala for Fear Memory. *Neuron*, *84*(4), 835–846.

Luo, Y., Raible, D., & Raper, J. A. (1993). Collapsin: A protein in brain that induces the collapse and paralysis of neuronal growth cones. *Cell*, *75*(2), 217–227.

Ly, A., Nikolaev, A., Suresh, G., Zheng, Y., Tessier-Lavigne, M., & Stein, E. (2008). DSCAM Is a Netrin Receptor that Collaborates with DCC in Mediating Turning Responses to Netrin-1. *Cell*, *133*(7), 1241–1254.

M

Mackarehtschian, K., Lau, C., Caras, I., & McConnell, S. (1999). Regional Differences in the Developing Cerebral Cortex Revealed by Ephrin-A5 Expression. *Cerebral Cortex*, *9*(6), 601–610.

Maddigan, A., Truitt, L., Arsenault, R., Freywald, T., Allonby, O., Dean, J., Narendram, A., Xiang, J., Weng, A., Napper, S., Freywald, A. (2011). EphB Receptors Trigger Akt Activation and Suppress Fas Receptor-Induced Apoptosis in Malignant T Lymphocytes. *The Journal of Immunology*, *187*(11), 5983–5994.

Maesako, M., Horlacher, J., Zoltowska, K. M., Kastanenka, K. V., Kara, E., Svirsky, S., Keller, L. J., Li, X., Hyman, B. T., Backsai, B. J., Berezovska, O. (2017). Pathogenic PS1 phosphorylation at Ser367. *ELife*, *6*, 1–23.

Malatesta, P., Appolloni, I., & Calzolari, F. (2008). Radial glia and neural stem cells. *Cell and Tissue Research*, *331*(1), 165–178.

Mansour, M., Nievergall, E., Gegenbauer, K., Llerena, C., Atapattu, L., Hallé, M., Tremblay, M. L., Janes, P. W., Lackmann, M. (2016). PTP-PEST controls EphA3 activation and ephrin-induced cytoskeletal remodelling. *Journal of Cell Science*, *129*(2), 277–289.

Marballi, K., Cruz, D., Thompson, P., & Walss-Bass, C. (2012). Differential Neuregulin 1 Cleavage in the Prefrontal Cortex and Hippocampus in Schizophrenia and Bipolar Disorder: Preliminary Findings. *PLoS ONE*, *7*(5), e36431.

Marballi, K. K., McCullumsmith, R. E., Yates, S., Escamilla, M. A., Leach, R. J., Raventos, H., & Walss-Bass, C. (2014). Global signaling effects of a schizophrenia-associated missense mutation in neuregulin 1: an exploratory study using whole genome and novel kinome approaches. *Journal of Neural Transmission*, *121*(5), 479–490.

Martín, S. M. (2013). *Regulació del creixement axonal per Presenilina-1/γ-secretasa: paper del receptor EphA3*. Universitat Autònoma de Barcelona (UAB).

Matz, A., Halamoda-Kenzaoui, B., Hamelin, R., Mosser, S., Alattia, J.-R., Dimitrov, M., Moniatte, M., Fraering, P. C. (2015). Identification of new Presenilin-1 phosphosites: implication for γ-secretase activity and Aβ production. *Journal of Neurochemistry*, *133*(3), 409–421.

Mei, L., & Nave, K.-A. (2014). Neuregulin-ERBB Signaling in the Nervous System and Neuropsychiatric Diseases. *Neuron*, *83*(1), 27–49.

Mei, L., & Xiong, W.-C. (2008). Neuregulin 1 in neural development, synaptic plasticity and schizophrenia. *Nature Reviews Neuroscience*, *9*(6), 437–452.

Meier, C., Anastasiadou, S., & Knöll, B. (2011). Ephrin-A5 Suppresses Neurotrophin Evoked Neuronal Motility, ERK Activation and Gene Expression. *PLoS ONE*, *6*(10), e26089.

Miao, H., Li, D.-Q., Mukherjee, A., Guo, H., Petty, A., Cutter, J., Basilion, J. P., Sedor, J., Wu, J., Danielpour, D., Sloan, A. E., Cohen, M. L., Wang, B. (2009). EphA2 Mediates Ligand-Dependent Inhibition and Ligand-Independent Promotion of Cell Migration and Invasion via a Reciprocal Regulatory Loop with Akt. *Cancer Cell*, *16*(1), 9–20.

Michailov, G. V. (2004). Axonal Neuregulin-1 Regulates Myelin Sheath Thickness. *Science*, *304*(5671), 700–703.

Minami, M., Koyama, T., Wakayama, Y., Fukuhara, S., & Mochizuki, N. (2011). EphrinA/EphA signal facilitates insulin-like growth factor-I–induced myogenic differentiation through suppression of the Ras/extracellular signal–regulated kinase 1/2 cascade in myoblast cell lines. *Molecular Biology of the Cell*, *22*(18), 3508–3519.

Mòdol-Caballero, G., Santos, D., Navarro, X., & Herrando-Grabulosa, M. (2018). Neuregulin 1 Reduces Motoneuron Cell Death and Promotes Neurite Growth in an in Vitro Model of Motoneuron Degeneration. *Frontiers in Cellular Neuroscience*, *11*.

Monje, P. V., Bartlett Bunge, M., & Wood, P. M. (2006). Cyclic AMP synergistically enhances neuregulin-dependent ERK and Akt activation and cell cycle progression in Schwann cells. *Glia*, *53*(6), 649–659.

Moore, S. W., Correia, J. P., Lai Wing Sun, K., Pool, M., Fournier, A. E., & Kennedy, T. E. (2008). Rho inhibition recruits DCC to the neuronal plasma membrane and enhances axon chemoattraction to netrin 1. *Development*, *135*(17), 2855–2864.

Mumm, J. S., Schroeter, E. H., Saxena, M. T., Griesemer, A., Tian, X., Pan, D. J., … Kopan, R. (2000). A Ligand-Induced Extracellular Cleavage Regulates □-Secretase-like Proteolytic Activation of Notch. *Molecular Cell*, *5*, 197–206.

Murai, K. K. (2003). 'Eph'ective signaling: forward, reverse and crosstalk. *Journal of Cell Science*, *116*(14), 2823–2832.

Murai, Keith K., & Pasquale, E. B. (2005). New Exchanges in Eph-Dependent Growth Cone Dynamics. *Neuron*, *46*(2), 161–163.

Murata-Hori, M., Suizu, F., Iwasaki, T., Kikuchi, A., & Hosoya, H. (1999). ZIP kinase identified as a novel myosin regulatory light chain kinase in HeLa cells. *FEBS Letters*, *451*(1), 81–84.

N

Namba, T., Kibe, Y., Funahashi, Y., Nakamuta, S., Takano, T., Ueno, T., (…)., Kaibuchi, K. (2014). Pioneering Axons Regulate Neuronal Polarization in the Developing Cerebral Cortex. *Neuron*, *81*(4), 814–829.

Naresh, A., Long, W., Vidal, G. A., Wimley, W. C., Marrero, L., Sartor, C. I., Tovey, S., Cooke, T. G., Bartlett, J. M. S., Jones, F. E. (2006). The ERBB4/HER4 Intracellular Domain 4ICD Is a BH3-Only Protein Promoting Apoptosis of Breast Cancer Cells. *Cancer Research*, *66*(12), 6412–6420.

Nievergall, E., Janes, P. W., Stegmayer, C., Vail, M. E., Haj, F. G., Teng, S. W., Neel, B. G., Bastiaens, P. I., Lackmann, M. (2010). PTP1B regulates Eph receptor function and trafficking. *The Journal of Cell Biology*, *191*(6), 1189–1203.

Nishikawa, M., Sellers, J. R., Adelstein, R. S., & Hidaka, H. (1984). Protein Kinase C Modulates in Vitro Phosphorylation of the Smooth Muscle Heavy Meromyosin by Myosin Light Chain Kinase. *The Journal of Biological Chemistry*, *259*, 8808–8814.

Nishikimi, M., Oishi, K., Tabata, H., Torii, K., & Nakajima, K. (2011). Segregation and Pathfinding of Callosal Axons through EphA3 Signaling. *Journal of Neuroscience*, *31*(45), 16251–16260.

Nishimura, T., Yamaguchi, T., Kato, K., Yoshizawa, M., Nabeshima, Y., Ohno, S., Hoshino, M., Kaibuchi, K. (2005). PAR-6–PAR-3 mediates Cdc42-induced Rac activation through the Rac GEFs STEF/Tiam1. *Nature Cell Biology*, *7*(3), 270–277.

Noctor, S. C., Martínez-Cerdeño, V., Ivic, L., & Kriegstein, A. R. (2004). Cortical neurons arise in symmetric and asymmetric division zones and migrate through specific phases. *Nature Neuroscience*, *7*(2), 136–144.

Noren, N. K., Lu, M., Freeman, A. L., Koolpe, M., & Pasquale, E. B. (2004). Interplay between EphB4 on tumor cells and vascular ephrin-B2 regulates tumor growth. *Proceedings of the National Academy of Sciences*, *101*(15), 5583–5588.

Noren, Nicole K., Foos, G., Hauser, C. A., & Pasquale, E. B. (2006). The EphB4 receptor suppresses breast cancer cell tumorigenicity through an Abl–Crk pathway. *Nature Cell Biology*, *8*(8), 815–825.

Norton, N., Moskvina, V., Morris, D. W., Bray, N. J., Zammit, S., Williams, N. M., (…) O'Donovan, M. C. (2006). Evidence that interaction between neuregulin 1 and its receptor erbB4 increases susceptibility to schizophrenia. *American Journal of Medical Genetics Part B: Neuropsychiatric Genetics*, *141B*(1), 96–101.

O

Oates, A. C., Lackmann, M., Power, M.-A., Brennan, C., Down, L. M., Do, C., Evans, B., Holder, N., Boyd, A. W. (1999). An early developmental role for Eph-ephrin interaction during vertebrate gastrulationq. *Mechanisms of Development*, 18.

Offenhäuser, C., Al-Ejeh, F., Puttick, S., Ensbey, K., Bruce, Z., Jamieson, P., (…) Day, B. (2018). EphA3 Pay-Loaded Antibody Therapeutics for the Treatment of Glioblastoma. *Cancers*, *10*(12), 519.

Omerovic, J., Santangelo, L., Puggioni, E. M.-R., Marrocco, J., Dall'Armi, C., Palumbo, C., Belleudi, F., Di Marcotullio, L., Frati, L., Torrisi, M-R., Cesareni, G., Gulino, A., Alimandi, M. (2007). The E3 ligase Aip4/Itch ubiquitinates and targets ErbB-4 for degradation. *The FASEB Journal*, *21*(11), 2849–2862.

O'Rourke, N. A., Sullivan, D. P., Kaznowski, C. E., Jacobs, A. A., & McConnell, S. (1995). Tangential migration of neurons in the developing cerebral cortex. *Development*, *121*, 2165–2176.

Osenkowski, P., Ye, W., Wang, R., Wolfe, M. S., & Selkoe, D. J. (2008). Direct and Potent Regulation of γ-Secretase by Its Lipid Microenvironment. *Journal of Biological Chemistry*, *283*(33), 22529–22540.

Ozaki, M., Sasner, M., Yano, R., Lu, H. S., & Buonanno, A. (1997). Neuregulin-ß induces expression of an NMDA-receptor subunit. *Nature*, *390*, 4.

P

Palmer, A., Zimmer, M., Erdmann, K. S., Eulenburg, V., Porthin, A., Heumann, R., Deutsch, U., Klein, R. (2002). EphrinB Phosphorylation and Reverse Signaling: Regulation by Src Kinases and PTP-BL Phosphatase. *Molecular Cell*, *9*, 725–737.

Parker, M., Roberts, R., Enriquez, M., Zhao, X., Takahashi, T., Pat Cerretti, D., Daniel, T., Chen, J. (2004). Reverse endocytosis of transmembrane ephrin-B ligands via a clathrin-mediated pathway. *Biochemical and Biophysical Research Communications*, *323*(1), 17–23.

Pascual, M., Pozas, E., Barallobre, M. J., Tessier-Lavigne, M., & Soriano, E. (2004). Coordinated functions of Netrin-1 and Class 3 secreted Semaphorins in the guidance of reciprocal septohippocampal connections. *Molecular and Cellular Neuroscience*, *26*(1), 24–33.

Pasquale, E. B. (2004). Eph–ephrin promiscuity is now crystal clear. *Nature Neuroscience*, *7*(5), 417–418.

Pasquale, E. B. (2005). Eph receptor signalling casts a wide net on cell behaviour. *Nature Reviews Molecular Cell Biology*, *6*(6), 462–475.

Pasterkamp, R. J., & Kolodkin, A. L. (2003). Semaphorin junction: making tracks toward neural connectivity. *Current Opinion in Neurobiology*, *13*(1), 79–89.

Pecci, A., Ma, X., Savoia, A., & Adelstein, R. S. (2018). MYH9: Structure, functions and role of non-muscle myosin IIA in human disease. *Gene*, *664*, 152–167.

Pellet-Many, C., Frankel, P., Jia, H., & Zachary, I. (2008). Neuropilins: structure, function and role in disease. *Biochemical Journal*, *411*(2), 211–226.

Placanica, L., Zhu, L., & Li, Y.-M. (2009). Gender- and Age-Dependent γ-Secretase Activity in Mouse Brain and Its Implication in Sporadic Alzheimer Disease. *PLoS ONE*, *4*(4), e5088.

Porstmann, T., Griffiths, B., Chung, Y.-L., Delpuech, O., Griffiths, J. R., Downward, J., & Schulze, A. (2005). PKB/Akt induces transcription of enzymes involved in cholesterol and fatty acid biosynthesis via activation of SREBP. *Oncogene*, *24*(43), 6465–6481.

Powell, J. C., Twomey, C., Jain, R., & McCarthy, J. V. (2009). Association between Presenilin-1 and TRAF6 modulates regulated intramembrane proteolysis of the p75 ^{NTR} neurotrophin receptor. *Journal of Neurochemistry*, *108*(1), 216–230.

Prata, D. P., Breen, G., Osborne, S., Munro, J., Clair, D. S., & Collier, D. A. (2009). An association study of the neuregulin 1 gene, bipolar affective disorder and psychosis: *Psychiatric Genetics*, *19*(3), 113–116.

R

Raulo, E., Chernousov, M. A., Carey, D. J., Nolo, R., & Rauvala, H. (1994). Isolation of a Neuronal Cell Surface Receptorof Heparin Binding Growth-associated Molecule(HB-GAM). *Journal of Biological Chemistry*, *269*(17), 12999–13004.

Ren, X., Ming, G., Xie, Y., Hong, Y., Sun, D., Zhao, Z., … Xiong, W. (2004). Focal adhesion kinase in netrin-1 signaling. *Nature Neuroscience*, *7*(11), 1204–1212.

Ren, Z., Chen, X., Yang, J., Kress, B. T., Tong, J., Liu, H., Takano, T., Zhao, Y., Nedergaard, M. (2013). Improved axonal regeneration after spinal cord injury in mice with conditional deletion of ephrin B2 under the GFAP promoter. *Neuroscience*, *241*, 89–99.

Rieff, H. I., & Corfas, G. (2006). ErbB receptor signalling regulates dendrite formation in mouse cerebellar granule cells *in vivo*. *European Journal of Neuroscience*, *23*(8), 2225–2229.

Rieff, H. I., Raetzman, L. T., Sapp, D. W., Yeh, H. H., Siegel, R. E., & Corfas, G. (1999). Neuregulin Induces GABA A Receptor Subunit Expression and Neurite Outgrowth in Cerebellar Granule Cells. *The Journal of Neuroscience*, *19*(24), 10757–10766.

Rio, C., Rieff, H. I., Qi, P., & Corfas, G. (1997). Neuregulin and erbB Receptors Play a Critical Role in Neuronal Migration. *Neuron*, *19*(1), 39–50. https://doi.org/10.1016/S0896-6273(00)80346-3

Rochlin, M. W., Itoh, K., Adelstein, R. S., & Bridgman, P. C. (1995). Localization of myosin II A and B isoforms in cultured neurons. *Journal of Cell Science*, *108*, 3661–3670.

Rohm, B., Ottemeyer, A., Lohrum, M., & Püschel, A. W. (2000). Plexin/neuropilin complexes mediate repulsion by the axonal guidance signal semaphorin 3A. *Mechanisms of Development*, *93*(1–2), 95–104.

Ross, J. S., Wang, K., Elkadi, O. R., Tarasen, A., Foulke, L., Sheehan, C. E.,

Otto, G. A., Palmer, G., Yelensky, R., Lipson, D., Chmielecki, J., Ali, S. M., Elvin, J., Morosini, D., Miller, V. A., Stephens, P. J. (2014). Next-generation sequencing reveals frequent consistent genomic alterations in small cell undifferentiated lung cancer. *Journal of Clinical Pathology*, *67*(9), 772–776.

Roy, K., Murtie, J. C., El-Khodor, B. F., Edgar, N., Sardi, S. P., Hooks, B. M., Benoit-Marand, M., Chen, C., Moore, H., O'Donnnel, P., Brunner, D., Corfas, G. (2007). Loss of erbB signaling in oligodendrocytes alters myelin and dopaminergic function, a potential mechanism for neuropsychiatric disorders. *Proceedings of the National Academy of Sciences*, *104*(19), 8131–8136.

Ruijter, J. M., Ramakers, C., Hoogaars, W. M. H., Karlen, Y., Bakker, O., van den Hoff, M. J. B., & Moorman, A. F. M. (2009). Amplification efficiency: linking baseline and bias in the analysis of quantitative PCR data. *Nucleic Acids Research*, *37*(6), e45–e45.

S

Sandrock Jr., A. W., Dryer, S. E., Rosen, K. M., Gozani, S. N., Kramer, R., Theill, L. E., & Fischback, G. D. (1997). Maintenance of Acetylcholine Receptor Number by Neuregulins at the Neuromuscular Junction in Vivo. *Science*, *276*(5312), 599–603.

Sardi, S. P., Murtie, J., Koirala, S., Patten, B. A., & Corfas, G. (2006). Presenilin-Dependent ErbB4 Nuclear Signaling Regulates the Timing of Astrogenesis in the Developing Brain. *Cell*, *127*(1), 185–197.

Sastre, M., Steiner, H., Fuchs, K., Capell, A., Multhaup, G., Condron, M. M., Teplow, D. B., Haass, C. (2001). Presenilin-dependent γ-secretase processing of β-amyloid precursor protein at a site corresponding to the S3 cleavage of Notch. *EMBO Reports*, *2*(9), 835–841.

Saura, C. A. (2011). Presenilin/γ-Secretase Regulates Neurexin Processing at Synapses. *PLoS ONE*, *6*(4), 13.

Saura, C. A., Choi, S.-Y., Beglopoulos, V., Malkani, S., Zhang, D., Rao, B. S. S., Chattarji, S., Kelleher III, R. J., Kandel, E. R., Duff, K., Kirkwood, A., Shen, J. (2004). Loss of Presenilin Function Causes Impairments of Memory and Synaptic Plasticity Followed by Age-Dependent Neurodegeneration. *Neuron*, *42*(1), 23–36.

Saura, C. A., Tomita, T., Davenport, F., Harris, C. L., Iwatsubo, T., & Thinakaran, G. (1999). Evidence That Intramolecular Associations between Presenilin Domains Are Obligatory for Endoproteolytic Processing. *Journal of Biological Chemistry*, *274*(20), 13818–13823.

Savonenko, A. V., Melnikova, T., Laird, F. M., Stewart, K.-A., Price, D. L., & Wong, P. C. (2008). Alteration of BACE1-dependent NRG1/ErbB4 signaling and schizophrenia-like phenotypes in BACE1-null mice. *Proceedings of the National Academy of Sciences*, *105*(14), 5585–5590.

Scheuner, D., Eckman, C., Jensen, M., Song, X., Citron, M., Suzuki, N., (…) Younkin, S. (1996). Secreted amyloid ß-protein similar to that in the senile plaques of Alzheimer's disease is increased in vivo by the presenilin 1 and 2 and APP mutations linked to familial Alzheimer's disease. *Nature Medicine*, *2*.

Schmucker, J., Ader, M., Brockschnieder, D., Brodarac, A., Bartsch, U., & Riethmacher, D. (2003). ErbB3 is dispensable for oligodendrocyte development in vitro and in vivo. *Glia*, *44*(1), 67–75.

Scholey, J. M., Taylor, K. A., & Kendrick-Jones, J. (1980). Regulation of non-muscle myosin assembly by calmodulin-dependent light chain kinase. *Nature*, *287*, 233–235.

Serafini, T., Kennedy, T. E., Gaiko, M. J., Mirzayan, C., Jessell, T. M., & Tessier-Lavigne, M. (1994). The netrins define a family of axon outgrowth-promoting proteins homologous to C. elegans UNC-6. *Cell*, *78*(3), 409–424.

Seroogy, K. B., Gall, C. M., Lee, D. C., & Kornblum, H. I. (1995). Proliferative zones of postnatal rat brain express epidermal growth factor receptor mRNA. *Brain Research*, *670*(1), 157–164.

Shah, S., Lee, S.-F., Tabuchi, K., Hao, Y.-H., Yu, C., LaPlant, Q., Ball, H., Dann III, C. E., Südhof, T., Yu, G. (2005). Nicastrin Functions as a γ-Secretase-Substrate Receptor. *Cell*, *122*(3), 435–447.

Shamah, S. M., Lin, M. Z., Goldberg, J. L., Estrach, S., Sahin, M., Hu, L., Bazalakova, M., Neve, R. L., Corfas, G., Deband, A., Greenberg, M. E. (2001). EphA Receptors Regulate Growth Cone Dynamics through the Novel Guanine Nucleotide Exchange Factor Ephexin. *Cell*, *105*(2), 233–244.

Shamir, A., Kwon, O.-B., Karavanova, I., Vullhorst, D., Leiva-Salcedo, E., Janssen, M. J., & Buonanno, A. (2012). The Importance of the NRG-1/ErbB4 Pathway for Synaptic Plasticity and Behaviors Associated with Psychiatric Disorders. *Journal of Neuroscience*, *32*(9), 2988–2997.

Shankar, G. M., Bloodgood, B. L., Townsend, M., Walsh, D. M., Selkoe, D. J., & Sabatini, B. L. (2007). Natural Oligomers of the Alzheimer Amyloid- Protein Induce Reversible Synapse Loss by Modulating an NMDA-Type Glutamate Receptor-Dependent Signaling Pathway. *Journal of Neuroscience*, *27*(11), 2866–2875.

Shankar, Ganesh M, Li, S., Mehta, T. H., Garcia-Munoz, A., Shepardson, N. E., Smith, I., Brett, F. M., Farrel, M. A., Rowan, M. J., Lemere C. A., Regan, C. M., Walsh, D. M., Sabatini, B. L. Selkoe, D. J. (2008). Amyloid-β protein dimers isolated directly from Alzheimer's brains impair synaptic plasticity and memory. *Nature Medicine*, *14*(8), 837–842.

Shapira, M., Zhai, R. G., Dresbach, T., Bresler, T., Torres, V. I., Gundelfinger, E. D., Ziv, N. E., Garner, C. C. (2003). Unitary Assembly of Presynaptic Active Zones from Piccolo-Bassoon Transport Vesicles. *Neuron*, *38*(2), 237–252.

Shekarabi, M. (2005). Deleted in Colorectal Cancer Binding Netrin-1 Mediates Cell Substrate Adhesion and Recruits Cdc42, Rac1, Pak1, and N-WASP into an Intracellular Signaling Complex That Promotes Growth Cone Expansion. *Journal of Neuroscience*, *25*(12), 3132–3141.

Shen, J., & Kelleher, R. J. (2007). The presenilin hypothesis of Alzheimer's disease: Evidence for a loss-of-function pathogenic mechanism. *Proceedings of the National Academy of Sciences*, *104*(2), 403–409.

Shen, J., Bronson, R. T., Chen, D. F., Xia, W., Selkoe, D. J., & Tonegawa, S. (1997). Skeletal and CNS Defects in Presenilin-1-Deficient Mice. *Cell*, *89*(1), 629–639.

Shi, G., Yue, G., & Zhou, R. (2010). EphA3 functions are regulated by collaborating phosphotyrosine residues. *Cell Research*, *20*(11), 1263–1275.

Shi, S.-H., Jan, L. Y., & Jan, Y.-N. (2003). Hippocampal Neuronal Polarity Specified by Spatially Localized mPar3/mPar6 and PI 3-Kinase Activity. *Cell*, *112*(1), 63–75.

Shirotani, K., Edbauer, D., Prokop, S., Haass, C., & Steiner, H. (2004). Identification of Distinct -Secretase Complexes with Different APH-1 Variants. *Journal of Biological Chemistry*, *279*(40), 41340–41345.

Shu, Y., Xiao, B., Wu, Q., Liu, T., Du, Y., Tang, H., Chen, S., Feng, L., Long, L., Li, Y. (2014). The Ephrin-A5/EphA4 Interaction Modulates Neurogenesis and Angiogenesis by the p-Akt and p-ERK Pathways in a Mouse Model of TLE. *Molecular Neurobiology*, *53*(1), 561–576.

Simón, A. M., de Maturana, R. L., Ricobaraza, A., Escribano, L., Schiapparelli, L., Cuadrado-Tejedor, M., Pérez-Mediavilla, A., Avila, J., Del Río, J., Frechilla, D. (2009). Early Changes in Hippocampal Eph Receptors Precede the Onset of Memory Decline in Mouse Models of Alzheimer's Disease. *Journal of Alzheimer's Disease*, *17*(4), 773–786.

Simons, M., Wang, M., McBride, O. W., Kawamoto, S., Yamakawa, K., Gdula, D., Aldestein, R. S., Weir, L. (1991). Human nonmuscle myosin heavy chains are encoded by two genes located on different chromosomes. *Circulation Research*, *69*(2), 530–539.

Singh, A. P., Bafna, S., Chaudhary, K., Venkatraman, G., Smith, L., Eudy, J. D., Johansson, S. L., Lin, M-F., Batra, S. K. (2008). Genome-wide expression profiling reveals transcriptomic variation and perturbed gene networks in androgen-dependent and androgen-independent prostate cancer cells. *Cancer Letters*, *259*(1), 28–38.

Singh, D. R., Cao, Q., King, C., Salotto, M., Ahmed, F., Zhou, X. Y., Pasquale, E. B., Hristova, K. (2015). Unliganded EphA3 dimerization promoted by the SAM domain. *Biochemical Journal*, *471*(1), 101–109.

Smith, C., Blake, J., Kadin, J., Richardson, J., & Bult, C. (n.d.). MGI-Mouse Genome Informatics-The international database resource for the laboratory mouse. Retrieved November 4, 2018, from http://www.informatics.jax.org/

Sogorb-Esteve, A., García-Ayllón, M.-S., Llansola, M., Felipo, V., Blennow, K., & Sáez-Valero, J. (2018). Inhibition of γ-Secretase Leads to an Increase in Presenilin-1. *Molecular Neurobiology*, *55*(6), 5047–5058.

Son, A. I., Hashimoto-Torii, K., Rakic, P., Levitt, P., & Torii, M. (2016). EphA4 has distinct functionality from EphA7 in the corticothalamic system during mouse brain development: Distinct Functional Features of EphA4 and EphA7. *Journal of Comparative Neurology*, *524*(10), 2080–2092.

Stassart, R. M., Fledrich, R., Velanac, V., Brinkmann, B. G., Schwab, M. H., Meijer, D., … Nave, K.-A. (2013). A role for Schwann cell–derived neuregulin-1 in remyelination. *Nature Neuroscience*, *16*(1), 48–54.

Stein, E. (2001). Binding of DCC by Netrin-1 to Mediate Axon Guidance Independent of Adenosine A2B Receptor Activation. *Science*, *291*(5510), 1976–1982.

Steiner, H., Duff, K., Capell, A., Romig, H., Grim, M. G., Lincoln, S., (…) Haass, C. (1999). A Loss of Function Mutation of Presenilin-2 Interferes with Amyloid ß-Peptide Production and Notch Signaling. *Journal of Biological Chemistry*, 6.

Stephen, L. J., Fawkes, A. L., Verhoeve, A., Lemke, G., & Brown, A. (2006). A critical role for the EphA3 receptor tyrosine kinase in heart development. *Developmental Biology*, *302*(1), 66–79.

Strooper, B. D., Annaert, W., Cupers, P., Saftig, P., Craessaerts, K., Mumm, J. S., Schroeter, E. H., Schrijvers, V., Wolfe, M. S., Ray, W. J., Goate, A., Kopan, R. (1999). A presenilin-1-dependent g-secretase-like protease mediates release of Notch intracellular domain, *398*, 5.

Sun, K. L. W., Correia, J. P., & Kennedy, T. E. (2011). Netrins: versatile extracellular cues with diverse functions. *Development*, *138*(11), 2153–2169.

Sundvall, M., Korhonen, A., Paatero, I., Gaudio, E., Melino, G., Croce, C. M., Aqeilan, R. I., Elenius, K. (2008). Isoform-specific monoubiquitination, endocytosis, and degradation of alternatively spliced ErbB4 isoforms. *Proceedings of the National Academy of Sciences*, *105*(11), 4162–4167.

Sundvall, Maria, Veikkolainen, V., Kurppa, K., Salah, Z., Tvorogov, D., van Zoelen, E. J., Aqeilan, R., Elenius, K. (2010). Cell Death or Survival Promoted by Alternative Isoforms of ErbB4. *Molecular Biology of the Cell*, *21*(23), 4275–4286.

Sussman, C. R. (2005). The ErbB4 Neuregulin Receptor Mediates Suppression of Oligodendrocyte Maturation. *Journal of Neuroscience*, *25*(24), 5757–5762.

T

Tahirovic, S., & Bradke, F. (2009). Neuronal Polarity. *Cold Spring Harbor Perspectives in Biology*, *1*(3), a001644–a001644.

Takahashi, T., & Strittmatter, S. M. (2001). PlexinA1 Autoinhibition by the Plexin Sema Domain. *Neuron*, *29*(2), 429–439.

Takahashi, Y., Fukuda, Y., Yoshimura, J., Toyoda, A., Kurppa, K., Moritoyo, H., (…) Tsuji, S. (2013). ERBB4 Mutations that Disrupt the Neuregulin-ErbB4 Pathway Cause Amyotrophic Lateral Sclerosis Type 19. *The American Journal of Human Genetics*, *93*(5), 900–905.

Takano, T., Xu, C., Funahashi, Y., Namba, T., & Kaibuchi, K. (2015). Neuronal polarization. *Development*, *142*(12), 2088–2093.

Takasugi, N., Tomita, T., Hayashi, I., Tsuruoka, M., Niimura, M., Takahashi, Y., Thinakaran, G., Iwatsubo, T. (2003). The role of presenilin cofactors in the g-secretase complex. *Nature*, *422*, 438–441.

Tamagnone, L., Artigiani, S., Chen, H., He, Z., Ming, G., Song, H., Chedotal, A., Winberg, M.L., Goodman, C. S., Poo, M-M., Tessier-Lavigne, M., Comoglio, P. M. (1999). Plexins Are a Large Family of Receptors for Transmembrane, Secreted, and GPI-Anchored Semaphorins in Vertebrates. *Cell*, *99*, 71–80.

Tan, X., & Shi, S.-H. (2013). Neocortical neurogenesis and neuronal migration. *Wiley Interdisciplinary Reviews: Developmental Biology*, *2*(4), 443–459.

Tanaka, A., Fujii, Y., Kasai, N., Okajima, T., & Nakashima, H. (2018). Regulation of neuritogenesis in hippocampal neurons using stiffness of extracellular microenvironment. *PLOS ONE*, *13*(2), e0191928.

Taveggia, C., Thaker, P., Petrylak, A., Caporaso, G. L., Toews, A., Falls, D. L., Einheber, S., Salzer, J. L. (2008). Type III neuregulin-1 promotes oligodendrocyte myelination. *Glia*, *56*(3), 284–293.

Taveggia, C., Zanazzi, G., Petrylak, A., Yano, H., Rosenbluth, J., Einheber, S., Xu, X., Esper, R. M., Loeb, J. A., Shrager, P., Chao, M. V., Falls, D. L., Role, L., Salzer, J. L. (2005). Neuregulin-1 Type III Determines the Ensheathment Fate of Axons. *Neuron*, *47*(5), 681–694.

Teng, T., Gaillard, A., Muzerelle, A., & Gaspar, P. (2017). EphrinA5 Signaling Is Required for the Distinctive Targeting of Raphe Serotonin Neurons in the Forebrain. *Eneuro*, *4*(1), ENEURO.0327-16.2017.

Thinakaran, G., Borchelt, D. R., Lee, M. K., Slunt, H. H., Spitzer, L., Kim, G., Ratovitsky, T., Davenport, F., Nordstedt, C., Seeger, M., Hardy, J., Levey, A. I., Gandy, S. E., Jenkins, N. A., Copeland, N. G., Price, D. L., Sisodia, S. S. (1996). Endoproteolysis of Presenilin 1 and Accumulation of Processed Derivatives In Vivo. *Neuron*, *17*(1), 181–190.

Thomson, P. A., Christoforou, A., Morris, S. W., Adie, E., Pickard, B. S., Porteous, D. J., Muir, W. J., Blackwood, DHR., Evans, K. L. (2007). Association of Neuregulin 1 with schizophrenia and bipolar disorder in a second cohort from the Scottish population. *Molecular Psychiatry*, *12*(1), 94–104.

Ting, A. K., Chen, Y., Wen, L., Yin, D.-M., Shen, C., Tao, Y., Liu, X., Xiong, W-C., Mei, L. (2011). Neuregulin 1 Promotes Excitatory Synapse Development and Function in GABAergic Interneurons. *Journal of Neuroscience*, *31*(1), 15–25.

Tong, J., Killeen, M., Steven, R., Binns, K. L., Culotti, J., & Pawson, T. (2001). Netrin Stimulates Tyrosine Phosphorylation of the UNC-5 Family of Netrin Receptors and Induces Shp2 Binding to the RCM Cytodomain. *Journal of Biological Chemistry*, *276*(44), 40917–40925.

Tucker, K. L., Meyer, M., & Barde, Y.-A. (2001). Neurotrophins are required for nerve growth during development. *Nature Neuroscience*, *4*(1), 29–37.

U

Udayakumar, D., Zhang, G., Ji, Z., Njauw, C.-N., Mroz, P., & Tsao, H. (2011). Epha2 is a critical oncogene in melanoma. *Oncogene*, *30*(50), 4921–4929.

Ullian, E. M., Christopherson, K. S., & Barres, B. A. (2004). Role for glia in synaptogenesis. *Glia*, *47*(3), 209–216.

Unbekandt, M., & Olson, M. F. (2014). The actin-myosin regulatory MRCK kinases: regulation, biological functions and associations with human cancer. *Journal of Molecular Medicine*, *92*(3), 217–225.

Urra, S., Escudero, C. A., Ramos, P., Lisbona, F., Allende, E., Covarrubias, P., Parraguez, J. I., Zampieri, N., Chao, M. V., Annaert, W., Bronfman, F. C. (2007). TrkA Receptor Activation by Nerve Growth Factor Induces Shedding of the p75 Neurotrophin Receptor Followed by Endosomal γ-Secretase-mediated Release of the p75 Intracellular Domain. *Journal of Biological Chemistry*, *282*(10), 7606–7615.

Usui, H., Taniguchi, M., Yokomizo, T., & Shimizu, T. (2003). Plexin-A1 and plexin-B1 specifically interact at their cytoplasmic domains. *Biochemical and Biophysical Research Communications*, *300*(4), 927–931.

V

Vail, M. E., Murone, C., Tan, A., Hii, L., Abebe, D., Janes, P. W., (…) Lackmann, M. (2014). Targeting EphA3 Inhibits Cancer Growth by Disrupting the Tumor Stromal Microenvironment. *Cancer Research*, *74*(16), 4470–4481.

Valsesia, A., Rimoldi, D., Martinet, D., Ibberson, M., Benaglio, P., Quadroni, M., (…) Stevenson, B. J. (2011). Network-Guided Analysis of Genes with Altered Somatic

Copy Number and Gene Expression Reveals Pathways Commonly Perturbed in Metastatic Melanoma. *PLoS ONE*, *6*(4), e18369.

Van Aelst, L., & Cline, H. T. (2004). Rho GTPases and activity-dependent dendrite development. *Current Opinion in Neurobiology*, *14*(3), 297–304.

Van Hoecke, A., Schoonaert, L., Lemmens, R., Timmers, M., Staats, K. A., Laird, A. S., (…) Robberecht, W. (2012). EPHA4 is a disease modifier of amyotrophic lateral sclerosis in animal models and in humans. *Nature Medicine*, *18*(9), 1418–1422.

Vearing, C., Lee, F.-T., Wimmer-Kleikamp, S., Spirkoska, V., To, C., Stylianou, C., Spanevello, M., Brechbiel, M., Boyd, A. W., Scott, A. M., Lackmann, M. (2005). Concurrent Binding of Anti-EphA3 Antibody and Ephrin-A5 Amplifies EphA3 Signaling and Downstream Responses: Potential as EphA3-Specific Tumor-Targeting Reagents. *Cancer Research*, *65*(15), 6745–6754.

Veikkolainen, V., Vaparanta, K., Halkilahti, K., Iljin, K., Sundvall, M., & Elenius, K. (2011). Function of ERBB4 is determined by alternative splicing. *Cell Cycle*, *10*(16), 2647–2657.

Vicente-Manzanares, M., Ma, X., Adelstein, R. S., & Horwitz, A. R. (2009). Non-muscle myosin II takes centre stage in cell adhesion and migration. *Nature Reviews Molecular Cell Biology*, *10*(11), 778–790.

Vidal, G. A., Naresh, A., Marrero, L., & Jones, F. E. (2005). Presenilin-dependent γ-Secretase Processing Regulates Multiple ERBB4/HER4 Activities. *Journal of Biological Chemistry*, *280*(20), 19777–19783.

Villa, J. C., Chiu, D., Brandes, A. H., Escorcia, F. E., Villa, C. H., Maguire, W. F., Hu, C-J., de Stanchina, E., Simon, M. C., Sisodia, S. S., Scheinberg, D. A., Li, Y.-M. (2014). Nontranscriptional Role of Hif-1α in Activation of γ-Secretase and Notch Signaling in Breast Cancer. *Cell Reports*, *8*(4), 1077–1092.

Vindis, C., Cerretti, D. P., Daniel, T. O., & Huynh-Do, U. (2003). EphB1 recruits c-Src and p52Shc to activate MAPK/ERK and promote chemotaxis. *The Journal of Cell Biology*, *162*(4), 661–671.

W

Wahl, S., Barth, H., Ciossek, T., Aktories, K., & Mueller, B. K. (2000). Ephrin-A5 Induces Collapse of Growth Cones by Activating Rho and Rho Kinase. *The Journal of Cell Biology*, *149*(2), 263–270.

Walsh, D. M., Klyubin, I., Fadeeva, J. V., Cullen, W. K., Anwyl, R., Wolfe, M. S., Rowan, M. J., Selkoe, D. J. (2002). Naturally secreted oligomers of amyloid b protein potently inhibit hippocampal long-term potentiation in vivo, *416*, 5.

Walsh, F. S., Skaper, S. D., & Doherty, P. (1994). Cell adhesion molecule (NCAM and N-cadherin)-dependent neurite outgrowth is modulated by gangliosides. *Progress in Brain Research*, *101*, 113–118.

Walss-Bass, C., Raventos, H., Montero, A. P., Armas, R., Dassori, A., Contreras, S., Liu, W., Medina, R., Levinson, D. F., Pereira, M., Leach, R. J., Almasy, L., Escamilla, M. A. (2006). Association analyses of the neuregulin 1 gene with schizophrenia and manic psychosis in a Hispanic population. *Acta Psychiatrica Scandinavica*, *113*(4), 314–321.

Wang, Y., Xu, Y., Liu, Q., Zhang, Y., Gao, Z., Yin, M., Jiang, N., Cao, G., Yu, B., Cao, Z., Kou, J. (2017). Myosin IIA-related Actomyosin Contractility Mediates Oxidative Stress-induced Neuronal Apoptosis. *Frontiers in Molecular Neuroscience*, *10*.

Watanabe, H., Iqbal, M., Zheng, J., Wines-Samuelson, M., & Shen, J. (2014). Partial Loss of Presenilin Impairs Age-Dependent Neuronal Survival in the Cerebral Cortex. *Journal of Neuroscience*, *34*(48), 15912–15922.

Weidemann, A., Eggert, S., Reinhard, F. B. M., Vogel, M., Paliga, K., Baier, G., … Evin, G. (2002). A Novel ε-Cleavage within the Transmembrane Domain of the Alzheimer Amyloid Precursor Protein Demonstrates Homology with Notch Processing. *Biochemistry*, *41*(8), 2825–2835.

Wen, L., Lu, Y.-S., Zhu, X.-H., Li, X.-M., Woo, R.-S., Chen, Y.-J., Yin, D-M., Lai, C., Terry, A. V., Vazdarjanova, A., Xiong, W-C., Mei, L. (2010). Neuregulin 1 regulates pyramidal neuron activity via ErbB4 in parvalbumin-positive interneurons. *Proceedings of the National Academy of Sciences*, *107*(3), 1211–1216.

Willem, M. (2016). Proteolytic processing of Neuregulin-1. *Brain Research Bulletin*, *126*, 178–182.

Williams, E. J., Furness, J., & Walsh, F. S. (1994). Activation of the FCF Receptor Underlies Neurite Outgrowth Stimulated by 11, N-CAM, and- N-Cadherin. *Neuron*, *13*, 583–594.

Willson, C. A., Irizarry-Ramírez, M., Gaskins, H. E., Cruz-Orengo, L., Figueroa, J. D., Whittemore, S. R., & Miranda, J. D. (2002). Upregulation of EphA Receptor Expression in the Injured Adult Rat Spinal Cord. *Cell Transplantation*, *11*, 229–239.

Wimmer-Kleikamp, S. H., Nievergall, E., Gegenbauer, K., Adikari, S., Mansour, M., Yeadon, T., Boyd, A. W., Patani, N. R., Lackmann, M. (2008). Elevated protein tyrosine phosphatase activity provokes Eph/ephrin-facilitated adhesion of pre-B leukemia cells. *Blood*, *112*(3), 721–732.

Wimmer-Kleikamp, Sabine H., Janes, P. W., Squire, A., Bastiaens, P. I. H., & Lackmann, M. (2004). Recruitment of Eph receptors into signaling clusters does not require ephrin contact. *The Journal of Cell Biology*, *164*(5), 661–666.

Wittenburg, N., Eimer, S., Lakowski, B., Röhrig, S., Rudolph, C., & Baumeister, R. (2000). Presenilin is required for proper morphology and function of neurons in C. elegans. *Nature*, *406*(6793), 306–309.

Wolfe, M. S. (2006). The γ-Secretase Complex: Membrane-Embedded Proteolytic Ensemble. *Biochemistry*, *45*(26), 7931–7939.

Wolfe, M. S., Xia, W., Ostaszewski, B. L., Diehl, T. S., Kimberly, W. T., & Selkoe, D. J. (1999). Two transmembrane aspartates in presenilin-1 required for presenilin endoproteolysis and g-secretase activity, *398*, 5.

Wong, K., Ren, X.-R., Huang, Y.-Z., Xie, Y., Liu, G., Saito, H., Tang, H., Wen, L., Brady-Kalnay, S. M., Mei, L., Wu, J. Y., Xiong, W-C., Rao, Y. (2001). Signal Transduction in Neuronal Migration: Roles of GTPase Activating Proteins and the Small GTPase Cdc42 in the Slit-Robo Pathway, *107*, 209–221.

Woo, R.-S., Lee, J.-H., Yu, H.-N., Song, D.-Y., & Baik, T.-K. (2011). Expression of ErbB4 in the neurons of Alzheimer's disease brain and APP/PS1 mice, a model of Alzheimer's disease. *Anatomy & Cell Biology*, *44*(2), 116.

Woo, R.-S., Lee, J-H., Yu, H-N., Song, D-Y., Baik, T-K. (2007). Neuregulin-1 Enhances Depolarization-Induced GABA Release. *Neuron*, *54*(4), 599–610.

Wu, Q., Suo, Z., Risberg, B., Karlsson, M. G., Villman, K., & Nesland, J. M. (2004). Expression of Ephb2 And Ephb4 in Breast Carcinoma. *PATHOLOGY ONCOLOGY RESEARCH*, *10*(1), 8.

Wylie, S. R., & Chantler, P. D. (2001). Separate but linked functions of conventional myosins modulate adhesion and neurite outgrowth. *Nature Cell Biology*, *3*(1), 88–92.

Wylie, S. R., & Chantler, P. D. (2003). Myosin IIA Drives Neurite Retraction. *Molecular Biology of the Cell*, *14*(11), 4654–4666.

X

Xiao, Z., Carrasco, R., Kinneer, K., Sabol, D., Jallal, B., Coats, S., & Tice, D. A. (2012). EphB4 promotes or suppresses Ras/MEK/ERK pathway in a context-dependent manner: Implications for EphB4 as a cancer target. *Cancer Biology & Therapy*, *13*(8), 630–637.

Xie, Y., Hong, Y., Ma, X.-Y., Ren, X.-R., Ackerman, S., Mei, L., & Xiong, W.-C. (2006). DCC-dependent Phospholipase C Signaling in Netrin-1-induced Neurite Elongation. *Journal of Biological Chemistry*, *281*(5), 2605–2611.

Xu, J., de Winter, F., Farrokhi, C., Rockenstein, E., Mante, M., Adame, A., Cook, J., Jin, X., Masliah, E., Lee, K.-F. (2016). Neuregulin 1 improves cognitive deficits and neuropathology in an Alzheimer's disease model. *Scientific Reports*, *6*(1).

Y

Yamashiro, S., Totsukawa, G., Yamakita, Y., Sasaki, Y., Madaule, P., Ishizaki, T., Narumiya, S., Matsumura, F. (2003). Citron Kinase, a Rho-dependent Kinase, Induces Di-phosphorylation of Regulatory Light Chain of Myosin II. *Molecular Biology of the Cell*, *14*(5), 1745–1756.

Yan, R., Farrelly, S., & McCarthy, J. V. (2013). Presenilins are novel substrates for TRAF6-mediated ubiquitination. *Cellular Signalling*, *25*(9), 1769–1779.

Yang, J. Z., Si, T. M., Ruan, Y., Ling, Y. S., Han, Y. H., Wang, X. L., Zhoy, M., Zhang, HY., Kong, QM., Liu, C., Zhang, DR., Yu, YQ., Liu, SZ., Ju, GZ., Shu, L., Ma, DL., Zhang, D. (2003). Association study of neuregulin 1 gene with schizophrenia. *Molecular Psychiatry*, *8*(7), 706–709.

Yang, N.-Y., Fernandez, C., Richter, M., Xiao, Z., Valencia, F., Tice, D. A., & Pasquale, E. B. (2011). Crosstalk of the EphA2 receptor with a serine/threonine

phosphatase suppresses the Akt-mTORC1 pathway in cancer cells. *Cellular Signalling*, *23*(1), 201–212.

Yoo, S., Shin, J., & Park, S. (2010). EphA8-ephrinA5 signaling and clathrin-mediated endocytosis is regulated by Tiam-1, a Rac-specific guanine nucleotide exchange factor. *Molecules and Cells*, *29*(6), 603–609.

Yoshimura, T., Arimura, N., Kawano, Y., Kawabata, S., Wang, S., & Kaibuchi, K. (2006). Ras regulates neuronal polarity via the PI3-kinase/Akt/GSK-3β/CRMP-2 pathway. *Biochemical and Biophysical Research Communications*, *340*(1), 62–68.

Yu, P., Santiago, L. Y., Katagiri, Y., & Geller, H. M. (2012). Myosin II activity regulates neurite outgrowth and guidance in response to chondroitin sulfate proteoglycans: Myosin II and CSPG inhibition. *Journal of Neurochemistry*, *120*, 1117–1128.

Yu, H., Saura, C. A., Choi, S.-Y., Sun, L. D., Yang, X., Handler, M., Kawarabayashi, T., Younkin, L., Fedeles, B., Wilson, M. A., Younkin, S., Kandel, E. R., Kirkwood, A., Shen, J. (2001). APP Processing and Synaptic Plasticity in Presenilin-1 Conditional Knockout Mice. *Neuron*, *31*(5), 713–726.

Yue, Y., Chen, Z.-Y., Gale, N. W., Blair-Flynn, J., Hu, T.-J., Yue, X., Cooper, M., Crockett, D. P., Yancopoulos, G. D., Tessarollo, L., Zhou, R. (2002). Mistargeting hippocampal axons by expression of a truncated Eph receptor. *Proceedings of the National Academy of Sciences*, *99*(16), 10777–10782.

Yun, M. E., Johnson, R. R., Antic, A., & Donoghue, M. J. (2003). EphA family gene expression in the developing mouse neocortex: Regional patterns reveal intrinsic programs and extrinsic influence. *The Journal of Comparative Neurology*, *456*(3), 203–216.

Z

Zeng, N., Liu, L., McCabe, M. G., Jones, D. T. W., Ichimura, K., & Collins, V. P. (2009). Real-time quantitative polymerase chain reaction (qPCR) analysis with fluorescence resonance energy transfer (FRET) probes reveals differential expression of the four *ERBB4* juxtamembrane region variants between medulloblastoma and pilocytic astrocytoma. *Neuropathology and Applied Neurobiology*, *35*(4), 353–366.

Zhang, D., Sliwkowski, M. X., Mark, M., Frantz, G., Akita, R., Sun, Y., Hillian, K., Crowley, C., Brush, J., Godowski, P. J. (1997). Neuregulin-3 (NRG3): A novel neural tissue-enriched protein that binds and activates ErbB4. *Proceedings of the National Academy of Sciences*, *94*(18), 9562–9567.

Zhang, X., Hoey, R. J., Lin, G., Koide, A., Leung, B., Ahn, K., Dolios, G., Paduch, M., Ikeuchi, T., Wang, R., Li, Y-M., Koide, S., Sisodia, S. S. (2012). Identification of a tetratricopeptide repeat-like domain in the nicastrin subunit of -secretase using synthetic antibodies. *Proceedings of the National Academy of Sciences*, *109*(22), 8534–8539.

Zhang, Xulun, Yu, C. J., & Sisodia, S. S. (2015). The topology of pen-2, a γ-secretase subunit, revisited: evidence for a reentrant loop and a single pass transmembrane domain. *Molecular Neurodegeneration*, *10*(1).

Zhang, Z., Huang, J., Shen, Y., & Li, R. (2017). BACE1-Dependent Neuregulin-1 Signaling: An Implication for Schizophrenia. *Frontiers in Molecular Neuroscience*, *10*.

Zhao, G., Mao, G., Tan, J., Dong, Y., Cui, M.-Z., Kim, S.-H., & Xu, X. (2004). Identification of a New Presenilin-dependent ζ-Cleavage Site within the Transmembrane Domain of Amyloid Precursor Protein. *Journal of Biological Chemistry*, *279*(49), 50647–50650.

Zhao, J. J., & Lemke, G. (1998). Selective disruption of neuregulin-1 function in vertebrate embryos using ribozyme-tRNA transgenes. *Development*, *125*, 1899–1907.

Zhong, C., Du, C., Hancock, M., Mertz, M., Talmage, D. A., & Role, L. W. (2008). Presynaptic Type III Neuregulin 1 Is Required for Sustained Enhancement of Hippocampal Transmission by Nicotine and for Axonal Targeting of 7 Nicotinic Acetylcholine Receptors. *Journal of Neuroscience*, *28*(37), 9111–9116.

Zhong, Chongbo, Akmentin, W., Du, C., Role, L. W., & Talmage, D. A. (2017). Axonal Type III Nrg1 Controls Glutamate Synapse Formation and GluA2 Trafficking in Hippocampal-Accumbens Connections. *Eneuro*, *4*(1), ENEURO.0232-16.2017.

Zhu, J.-M., Li, K.-X., Cao, S.-X., Chen, X.-J., Shen, C.-J., Zhang, Y., Geng, H-Y., Chen, B-Q., Lian, H., Zhang, J-M., Li, X.-M. (2017). Increased NRG1-ErbB4 signaling in human symptomatic epilepsy. *Scientific Reports*, *7*(1).

Zimmer, M., Palmer, A., Köhler, J., & Klein, R. (2003). EphB–ephrinB bi-directional endocytosis terminates adhesion allowing contact mediated repulsion. *Nature Cell Biology*, *5*(10), 869–878.

Zuliani, R., Moorhead, T. W. J., Bastin, M. E., Johnstone, E. C., Lawrie, S. M., Brambilla, P., O'Donovan, M. C., Owen, M. J., Hall, J., McIntosh, A. M. (2011). Genetic variants in the ErbB4 gene are associated with white matter integrity. *Psychiatry Research: Neuroimaging*, *191*(2), 133–137.